THESIS

MICHIGAN STATE LIBRARIES
3 1293 01826 4790

LIBRARY
Michigan State
University

This is to certify that the

dissertation entitled

Coordination Chemistry of Chelating Phosphines: Stabilizationof Metalloradicals and the Elaboration of Extended Structures

presented by

Calvin E. Uzelmeier, III

has been accepted towards fulfillment
of the requirements for

Ph.D. degree in chemistry

Kim R. Dunbar
Major professor

Date 12/11/98

MSU is an Affirmative Action/Equal Opportunity Institution

O-12771

PLACE IN RETURN BOX to remove this checkout from your record.
TO AVOID FINES return on or before date due.
MAY BE RECALLED with earlier due date if requested.

DATE DUE	DATE DUE	DATE DUE

1/98 c:/CIRC/DateDue.p65-p.14

COORDIN

SPHINES:

AND THE E

in par

COORDINATION CHEMISTRY OF CHELATING PHOSPHINES: STABILIZATION OF METALLORADICALS AND THE ELABORATION OF EXTENDED ARRAYS

By

Calvin Edward Uzelmeier, III

A DISSERTATION

Submitted to
Michigan State University
in partial fulfillment of the requirements
for the degree of

DOCTOR OF PHILOSOPHY

Department of Chemistry
1998

ABSTRACT

COORDINATION CHEMISTRY OF CHELATING : STABILIZATION OF METALLORADICALS AND THE ELABORATION OF EXTENDED ARRAYS

By

Calvin Edward Uzelmeier, III

Tertiary phosphine are one of the most versatile ligands in coordination and organometallic chemistry. Their cooperative σ-donor, π-acceptor bonding allows for the stabilization of complexes with metals in a wide range of oxidation states. Furthermore, they allow for tuning of the electronic and steric properties of the resulting metal-phosphine complexes by changes in the R groups. Modifications of the electronic and steric properties tertiary phosphines is well-documented in homogeneous catalysis to be a convenient method for altering the rates of reactions and stereoselectivity of the desired product.

Tris(2,4,6-trimethoxyphenyl)phosphine (TMPP) is an excellent ligand for stabilizing reactive metal radicals and coordinatively unsaturated, electron deficient complexes. In addition to the phosphorus atom, the metal

...ciate to eth...

...ular modes.

...al in the stab...

...ples Pt TMPP...

...mixtures. Sub...

...plexes yield...

...Pt = P C6H5...

...mparison of t...

...ed by the isol...

...Pt...(BF4)...

...he temperat...

...ET is a mech...

...of inorganic c...

...nuclear complex...

...ethyl-3',4'-t...

...ion character...

...ion of compl...

...ion of mono- a...

...ion. The ...

...compounds ...

...he o-Pt2 com...

...for the ...

can coordinate to ether functionalities, resulting in mono-, bi-, or tridentate coordination modes. The combination of steric bulk and chelating ability allowed for the stabilization of the unusual series of homoleptic TMPP complexes, $[Rh(TMPP)_2][BF_4]_n$ (n = 1, 2, 3) which span the (I), (II), and (III) oxidation states. Subsequent dealkylation of the coordinated methoxy groups by nucleophiles yields metal complexes with the phosphino-phenoxide ligand (TMPP-*O* = $[P\{C_6H_2(OMe)_3\}_2(C_6H_2(OMe)_2O]^{1-}$). This ligand is very useful for the preparation of heterobimetallic as well as much larger clusters as evidenced by the isolation and X-ray studies of $[Co^{II}_3(\mu^2\text{-}OH)_3(\mu^3\text{-}OH)\{Co^{II}(\eta^3\text{-}TMPP\text{-}O)_2\}_3][BF_4]$.

The incorporation of PPh_2 groups as functional groups on the organic donor TTF, is a method for incorporating redox active organic molecules into "hybrid" inorganic/organic arrays with metal complexes. Indeed, the mononuclear complexes, $[M(o\text{-}P2)_2][BF_4]_2$ (M = Ni, Co, Pd, Pt, Fe), where *o*-P2 = 3,4-dimethyl-3',4'-bis(diphenylphosphino)tetrathiafulvalane, exhibit redox properties characteristic of both the ligand and metal components. Stepwise formation of complexes that contain *cis*-MCl_2 moieties allows for the formation of mono- and dinuclear complexes that contain one, two, or three TTF units. The reactivity of these phosphine ligands with metal-metal bonded compounds has also been investigated.

The *o*-P2 complexes may be viewed as models for extended arrays that contain the tetradentate ligand tetrakis(diphenylphosphino)-

tetrathiafulvalene (P4). A series of soluble products, formulated as $[M(P4)]_n[BF_4]_{2n}$ (M = Ni, Co, Pd, Pt, Fe) and $[M(P4)]_n[BF_4]_n$ (M = Rh), have been prepared and characterized by $^{31}P\{^1H\}$ NMR spectroscopy, and cyclic voltammetry, among other methods. The combined results of the studies are in accord with the formulation of these products as cyclic oligomers.

In memory of my grandfathers:

Calvin E. Uzelmeier, Sr. and Donald A. Ottinger.

This work would
... first and fore
... guidance
... teacher, and m
... express my
... and the chair
... of my comm
... throughout m
... the Dunbar
... big-sister
... his first
... keep things
... Maine
... part of the
... at Mich
... tion and
... experience.
... Department
... for their
... through
... like to ac

ACKNOWLEDGEMENTS

This work would not have been possible if not for the help and support of many people. First and foremost I would like to thank my advisor, Prof. Kim R. Dunbar. Through her guidance and example I have learned much of what it means to be a scientist, teacher, and mentor. I will always cherish her advice and friendship. I would also like to express my appreciation to Dr.s Marc Fourmigué and Patrick Batail for all their help, and the chance to work with such wonderful compounds. Thank you to the members of my committee, all of which lent their advice and support on numerous occasions throughout my graduate carrier. I would like to thank all the past and present members of the Dunbar group for their friendship and partnership in science. A special thanks to my "big-sister" Jui-Sui Sun (Alice), for her patience in helping this over-zealous rookie through his first years of research, and my lab twin, Kemal Catalan, who always helped me keep things in perspective. Much of the research reported here is due to the efforts of Julia Meinershagen and Gulio Grandinetti. I am grateful for the opportunity to be a small part of the development of these two scientists. I have truly been spoiled by my comrades at Michigan State, and will be hard-pressed to find a place where I have such admiration and respect for my co-workers. They made graduate school a truly enjoyable experience, and I pray to maintain their friendships for decades to come. To the entire Department of Chemistry at Michigan State University I express my deepest appreciation for their support during the times when it looked as though I would not reach this day. It is through difficult times such as those that we realize how much people care. I would also like to acknowledge the University's Herbert T. Graham Memorial, Margaret

[illegible] and Ca[illegible]

[illegible] research grant for[illegible]

[illegible] a more person[illegible]

[illegible] over these last [illegible]

[illegible] especially gradua[illegible]

[illegible] what I would like[illegible]

[illegible] quite literall[illegible]

[illegible] that I thought I [illegible]

[illegible] an example of [illegible]

[illegible] that I have [illegible]

[illegible] thing, I wou[illegible]

[illegible] means that we a[illegible]

[illegible] of the world a[illegible]

Yates Memorial, and Carl H. Brubaker Endowed Fellowships and a Sigma Xi graduate student research grant for partial funding of this work.

On a more personal note, I would like to thank Rebecca Marcus for her love and support over these last two years. She was the glue that held me together through the final stages of my graduate career. To my family: this is because of you. Without my fan club at home, I could have never succeeded. I would like to thank my parents for staying by my side, quite literally, through all the highs and lows of the past 6 years. There were times when I thought I couldn't take another step, but you encouraged me to try. You have set an example of love before me that you cannot comprehend. Finally, I thank God for the gifts that I have been given, and the chance to use them in new ways every day.

In closing, I would like to share something a young 1st grade girl told me once. It is the reason that we all satisfy our curiosities through research, and continue to try and understand the world around us: "Science is Cool!" Never forget that!

LIST OF TABLES

LIST OF FIGURES

LIST OF SYMBOLS

LIST OF COMPOUN

CHAPTER I.

1. Functional
Complexe

2. The Chem

3. The Desig
Ligands ..

(1) The

(2) Dep
Te

4. The Deve
Tetrathia

List of Refere

CHAPTER II.

1. Introduct

2. Experimen

TABLE OF CONTENTS

Page

LIST OF TABLES xix

LIST OF FIGURES xxi

LIST OF SYMBOLS AND ABBREVIATIONS xxv

LIST OF COMPOUNDS xxix

CHAPTER I. INTRODUCTION 1

A. Fuctionalized Phosphines as Ligands in Transition Metal Complexes 2

B. The Chemistry of Tris(2, 4, 6-trimethoxyphenyl)phosphine 7

C. The Design of Molecule-Based Materials with Phosphine Ligands 14

(1) The Use of Organic Acceptors in Molecular Materials 17

(2) Derivative Chemistry of the Organic Donor, Tetrathiafulvalene 18

D. The Development of Phosphine-Fuctionalized Tetrathiafulvalenes 22

List of References 28

CHAPTER II. COORDINATION CHEMISTRY OF TRIS(2,4,6-TRIMETHOXYPHENYL)PHOSPHINE WITH PLATINUM GROUP TRANSITION METALS 37

1. Introduction 38

2. Experimental 40

A. Syn

B. X-r

Results an

A. Re
Ef

B. Cr

C. Re

A. Synthesis....40
(1) Preparation of $[Rh^{I}(TMPP)_2][BF_4]$ (**3**)....40
(i) Reduction of $[Rh^{II}(\eta^3\text{-}TMPP)_2][BF_4]_2$ with $CoCp_2$....40
(ii) Reduction of $[Rh^{II}(\eta^3\text{-}TMPP)_2][BF_4]_2$ with Zn (s)....41
(2) Dealkylation of $[Rh^{I}(TMPP)_2][BF_4]$ (**3**): Formation of $Rh^{I}(TMPP)(TMPP\text{-}O)$ (**4**)....42
(3) Dealkylation of *ax*-$[Rh^{III}(TMPP)(TMPP\text{-}O)][BF_4]_2$: Formation of *ax,ax*-$[Rh^{III}(TMPP\text{-}O)_2][BF_4]$ (**5**)....43
(4) Reaction of $Co^{II}(TMPP\text{-}O)_2$ with $Pt^{II}Cl_2(NC_7H_5)_2$....43
(5) Reaction of $Co^{II}(TMPP\text{-}O)_2$ with $[Mn(NCCH_3)_4][BF_4]_2$....44

B. X-ray Crystallography....44
(1) $[Rh^{I}(\eta^2\text{-}MPP)_2][BF_4]\bullet[Rh^{II}(\eta^3\text{-}TMPP][BF_4]_2$ (**3**•$[Rh^{II}(\eta^3\text{-}TMPP)_2][BF_4]_2$)....46
(i) Data Collection and Reduction....46
(ii) Structure Solution and Refinement....46
(2) $[Co^{II}_3(\mu^3\text{-}OH)(\mu\text{-}OH)_3\{Co^{II}(\mu\text{-}\eta^3\text{-}TMPP\text{-}O)_2\}_3][BF_4]_2\bullet[CH_3\text{-}TMPP][BF_4]\bullet CH_3CH_2)_2O\bullet(CH_2)_2CO$ (**6**•$[CH_3\text{-}TMPP][BF_4]\bullet(CH_3CH_2)_2O\bullet(CH_2)_2CO$)....47
(i) Data Collection and Reduction....47
(ii) Structure Solution and Refinement....48
(3) $Pd(TMPP\text{-}O)_2\bullet 3.73CH_2Cl_2\bullet H_2O$ (**7**•$3.73CH_2Cl_2\bullet H_2O$)....49
(i) Data Collection and Reduction....49
(ii) Structure Solution and Refinement....49

3. Results and Discussion....51

A. Reduction of $[Rh^{II}(TMPP)_2][BF_4]_2$: Formation of $[Rh^{I}(TMPP)_2][BF_4]$ (**3**)....51
(1) NMR Spectroscopic Studies....52

B. Crystal Structure of $[Rh^{I}(TMPP)_2][BF_4]$ (**3**)....56

C. Reactivity of $[Rh^{I}(TMPP)_2][BF_4]$ (**3**)....61
(1) Decomposition of $[Rh^{I}(TMPP)_2][BF_4]$ (**3**)....61
(2) Dealkylation of $[Rh^{I}(TMPP)_2][BF_4]$ (**3**)....61
(i) Synthesis and spectroscopic characterization of $Rh^{I}(TMPP)$-$(TMPP\text{-}O)$ (**4**)....62

D. Pre
Th
E. Ra
C
F. F
O
G. C
4 Conclusion
ist of Refer
PTER III.
1 Introduct
2 Experime
A. Sy
B. X-r

(ii) Decomposition of Rh^{I}(TMPP)(TMPP-*O*) (**4**) 63

D. Preparation and Spectroscopic Studies of *ax,ax*-$[Rh^{III}(TMPP\text{-}O)_2][BF_4]$ (**5**) 64

E. Reactions of $Co^{II}(TMPP\text{-}O)_2$ with Reactive Metal Complexes 65
(1) $Pt^{II}Cl_2(NC_7H_5)_2$ 65
(2) $[Mn^{II}(NCCH_3)_4][BF_4]_2$ 66

F. Formation and Crystal Structure of $[Co^{II}_3(\mu^3\text{-}OH)(\mu\text{-}OH)_3\{Co^{II}(\mu\text{-}\eta^3\text{-}TMPP\text{-}O)_2\}_3][BF_4]_2$ (**6**) 67
(1) Crystal Structure 68
(2) EPR Spectroscopy 73

G. Crystal Structure of $Pd(TMPP\text{-}O)_2$ (**7**) 73

4. Concluding Remarks 73

List of References 79

CHAPTER III. SYNTHESIS AND REACTIVITY OF $[M(o\text{-}P2)_2]\text{-}[BF_4]_x$ (M = Fe, Co, Ni, Pd, Pt, x = 2; M = Rh, x = 1) 83

1. Introduction 84

2. Experimental 85

A. Synthesis 85
(1) Preparation of $[M(o\text{-}P2)_2][BF_4]_2$ 87
(i) $[Ni(o\text{-}P2)_2][BF_4]_2$ (**8**) 87
(ii) $[Co(o\text{-}P2)_2][BF_4]_2$ (**9**) 88
(iii) $[Pd(o\text{-}P2)_2][BF_4]_2$ (**10**) 89
(iv) $[Pt(o\text{-}P2)_2][BF_4]_2$ (**11**) 89
(v) $[Fe(o\text{-}P2)_2][BF_4]_2$ (**12**) 90
(2) Reactions of $M(CF_3SO_3)_2$ with *o*-P2 (**1**) 90
(i) Preparation of $[Ni(o\text{-}P2)_2][CF_3SO_3]_2$ (**13**) 90
(ii) Reaction of $Fe(CF_3SO_3)_2$ with *o*-P2 (**1**) 91
(3) Oxidation of $[Rh^{I}(o\text{-}P2)_2][BF_4]$ with $NOBF_4$: Preparation of $[Rh^{I}(o\text{-}P2)_2][BF_4]_3$ (**14**) 91
(4) Reaction of $[Rh^{I}(o\text{-}P2)_2][BF_4]$ with [Li][TCNQ] 92

B. X-ray Crystallography 92

(1) $[Ni(o\text{-}P2)_2][BF_4]_2 \cdot C_7H_8 \cdot CH_3CN$ (**8**$\cdot C_7H_8 \cdot CH_3CN$) 94
(i) Data Collection and Reduction 94
(ii) Structure Solution and Refinement 94
(2) $[Pt(o\text{-}P2)_2][BF_4]_2 \cdot C_7H_8 \cdot CH_3CN$ (**11**$\cdot C_7H_8 \cdot CH_3CN$) 96
(i) Data Collection and Reduction. 96
(ii) Structure Solution and Refinement 96

3. Results and Discussion 97

A. Preparation of $[M(o\text{-}P2)_2][BF_4]_2$ (M = Ni, Co, Pd, Pt, Fe) 98

B. Spectrosopic Characterization of $[M(o\text{-}P2)_2][BF_4]_2$ (M = Ni, Co, Pd, Pt, Fe) 99
(1) NMR Spectroscopic Studies of $[M(o\text{-}P2)_2][BF_4]_2$ (**8-12**) 99
(i) ^1H and $^{31}P\{^1H\}$ NMR 99
(ii) Variable Temperature ^{19}F and $^{31}P\{^1H\}$ NMR of $[Fe(o\text{-}P2)_2][BF_4]_2$ (**12**) 101
(2) Infrared and Electronic Absorbance Spectroscopy 102
(3) FAB-MS of $[M(o\text{-}P2)_2][BF_4]_2$ (M = Ni, Co, Pd, Pt, Fe) (**8-12**) 102

C. Crystal Structures of $[M(o\text{-}P2)_2][BF_4]_2$ (M = Ni (**8**), Pt (**11**)) 103

D. Magnetic Studies of $[Co(o\text{-}P2)_2][BF_4]_2$ (**9**) 109
(1) Variable Temperature Magnetic Susceptibility 109
(2) EPR Spectroscopic Studies 109

E. Electrochemistry of $[M(o\text{-}P2)_2][BF_4]_x$ (M = Ni, Pd, Pt, = 2; M = Rh, x = 1) 114
(1) Redox Properties of $[M(o\text{-}P2)_2][BF_4]_2$ (M = Ni, Pd, Pt) 114
(2) Oxidation of $[Rh(o\text{-}P2)_2][BF_4]$ 117

F. Reactivity of $M(CF_3SO_3)_2$ with *o*-P2 (M = Ni, Fe) 119

G. Metathesis of $[Rh(o\text{-}P2)_2][BF_4]$ with [Li][TCNQ] 120

4. Concluding Remarks 120

List of References 124

CHAPTER IV R
C
F

I. Introduction

II. Experimen

A. Syn

B. X-r

III. Results a

A. Rea

B. Prep
Re

CHAPTER IV REACTIVITY OF METAL-METAL BONDED COMPLEXES WITH PHOSPHINE-FUNCTIONALIZED TETRATHIAFULVALENE 127

1. Introduction 128

2. Experimental 130

A. Synthesis.....130
(1) Reaction of $[Rh_2(NCCH_3)_{10}][BF_4]_4$ and $(Ph_2P)Me_3TTF$ to form (**15**) 131
(2) Reaction of $[Re_2(NCCH_3)_{10}][BF_4]_4$ and $(Ph_2P)_2Me_2TTF$ 131
(3) Reactions of $[Bu_4]_2[Re_2Cl_8]$ with *o*-P2 132
(i) Synthesis of $[ReCl_2(o\text{-}P2)_2][Re_2Cl_6(o\text{-}P2)]$ (**17**•**18**) for short reaction times.....132
(ii) Reaction time of 2 hours.....133
(4) Reduction of $[ReCl_2(o\text{-}P2)_2][Re_2Cl_6(o\text{-}P2)]$ (**16**• **17**) to yield $ReCl_2(o\text{-}P2)_2$ (**18**).....133
(5) Oxidation of $ReCl_2(o\text{-}P2)_2$ (**18**) 134
(i) Preparation of $[ReCl_2(o\text{-}P2)_2][Cl]$ (**16**•[Cl]) 134
(ii) Preparation of $[ReCl_2(o\text{-}P2)_2][BF_4]$ (**16**•$[BF_4]$).....134
(6) Reaction of $Mo_2Cl_4(SMe_2)_4$ with *o*-P2 135
(i) In CH_3CN.....135
(ii) In CH_2Cl_2 under aerobic conditions. Preparation of $MoCl_2O_2(o\text{-}P2O_2)$ (**19**).....135

B. X-ray Crystallography.....136
(1) $[ReCl_2(o\text{-}P2)_2][Re_2Cl_6(o\text{-}P2)]$•4 CH_2Cl_2 (**16**• **17**•4 CH_2Cl_2).....136
(i) Data Collection and Reduction. 136
(ii) Structure Solution and Refinement.....139
(2) $MoCl_2O_2(o\text{-}P2O_2)$ (**19**).....140
(i) Data Collection and Reduction. 140
(ii) Structure Solution and Refinement.....140

3. Results and Discussion.....142

A. Reactions with $[M_2(NCCH_3)_{10}][BF_4]_4$ (M= Rh, Re).....142

B. Preparation, Characterization and Reactivity of $[ReCl_2(o\text{-}P2)_2][Re_2Cl_6(o\text{-}P2)]$ (**16**• **17**).....145
(1) Reactivity of $[(n\text{-}Bu)_4N]_2[Re_2Cl_8]$ with *o*-P2 (1).....145

C. Rea

4 Concludi

List of Refer

ER V

1 Introduc

2 Experime

A. Sy

(2) Crystal Structure of $[ReCl_2(o\text{-}P2)_2]$ $[Re_2Cl_6(o\text{-}P2)]$ (**16•17**) 147
(3) Spectroscopic Characterization of $[ReCl_2(o\text{-}P2)_2][Re_2Cl_6(o\text{-}P2)]$ (**16•17**) 154
(4) Isolation of $[ReCl_2(o\text{-}P2)_2]^+$ (**16**) 155
(i) Reduction of $[ReCl_2(o\text{-}P2)_2][Re_2(o\text{-}P2)Cl_6]$ (**16•17**) 155
(ii) Oxidation of $ReCl_2(o\text{-}P2)_2$ (**18**) 155
(5) Electrochemical Studies 156
(6) Magnetic Studies 159
(i) $[ReCl_2(o\text{-}P2)_2][Re_2Cl_6(o\text{-}P2)]$ (**16•17**) 159
(a) Magnetic susceptibility. 159
(b) EPR Spectroscopy 161
(ii) $[ReCl_2(o\text{-}P2)_2][BF_4]$ (**16**•$[BF_4]$) 161
(iii) $ReCl_2(o\text{-}P2)_2$ (**18**) 161

C. Reactions of $Mo_2[S(CH_3)_2]_4Cl_4$ with *o*-P2 165
(1) Synthethesis 165
(2) Crystal Structure of $MoCl_2O_2(o\text{-}P2O_2)$ (**19**) 167
(3) Spectrocscopic Characterization of $MoCl_2O_2(o\text{-}P2O_2)$ (**19**) 170

4. Concluding Remarks 173

List of References 175

CHAPTER V STEP-WISE SYNTHESIS OF METAL CONTAINING ARRAYS WITH BI- AND TETRADENTATE TETRATHIAFULVALENE-PHOSPHINE LIGANDS 179

1. Introduction 180

2. Experimental 182

A. Synthesis 182
(1) Preparation of $PtCl_2(o\text{-}P2)$ (**20**) 182
(2) Preparation of $[Pt(o\text{-}P2)(NCCH_3)_2][BF_4]_2$ (**21**) 183
(3) Preparation of $Pt_2Cl_4(P4)$ (**22**) 183
(4) Preparation of $[Pt_2(P4)(NCCH_3)_4][BF_4]_4$ (**23**) 184
(5) Preparation of $[Pt_2(P4)(o\text{-}P2)_2][BF_4]_4$ (**24**) 184
(i) Reaction of $[Pt(o\text{-}P2)(NCCH_3)_2][BF_4]_2$ (**21**) with P4 (**2**) 184
(ii) Reaction of $[Pt_2(P4)(NCCH_3)_4][BF_4]_4$ (**23**) with *o*-P2 (**1**) 185

(6) Preparation of $PdCl_2$(*o*-P2) (**25**) 185
(7) Preparation of $[Pd(o\text{-}P2)(NCCH_3)_2][BF_4]_2$ (**26**) 186
(8) Preparation of Pd_2Cl_4(P4) (**27**) 187
(9) Preparation of $[Pd_2(P4)(NCCH_3)_4][BF_4]_4$ (**28**) 187
(10) Preparation of Ni_2Cl_4(P4) (**29**) 187

B. X-ray Crystallography 188
(1) $PtCl_2(o\text{-}P2)\cdot CH_3CN$ (**20**$\cdot CH_3CN$) 188
(i) Data Collection and Reduction. 188
(ii) Structure Solution and Refinement. 190
(2) Pt_2Cl_4(P4)$\cdot 3CH_3CN$ (**22**$\cdot 3CH_3CN$) 190
(i) Data Collection and Reduction. 190
(ii) Structure Solution and Refinement. 191

3. Results and Discussion 192

A. Preparation, Spectroscopy, and Redox Properties of MCl_2(*o*-P2) [M = Pt (**20**), Pd (**23**)] 193
(1) Synthesis 193
(2) ^1H and $^{31}P\{^1H\}$ NMR Spectroscopic Studies 194
(3) Infrared and Electronic Absorbance Spectroscopy 196
(4) Electrochemistry 200
B. Crystal Structure of $PtCl_2$(*o*-P2) (**20**) 200

C. Preparation and Spectroscopic Properties of M_2Cl_4(P4) (M = Pt (**22**), Pd (**27**), Ni (**29**)) 207

D. Crystal Structure of Pt_2Cl_4(P4) (**22**) 208

E. Reactioins of MCl_2(*o*-P2) and M_2Cl_4(P4) (M = Pt, Pd, Ni) with $AgBF_4$ 211
(1) Synthesis 211
(2) Spectroscopic Studies 212
(3) ^1H and $^{31}P\{^1H\}$ NMR Spectroscopic Studies 213

F. Synthesis and Characterization of $[Pt_2(o\text{-}P2)_2(P4)][BF_4]_4$ (**24**) 215
(1) Synthesis 215
(2) Spectroscopic Characterization 215
(3) ^1H and $^{31}P\{^1H\}$ NMR Spectroscopic Studies 216
(4) Electrochemistry 217

4. Concluding Remarks 218

List of References 224

CHAPTER VI ASSEMBLY OF OLIGOMERIC SYSTEMS FROM HOMOLEPTIC PLATINUM GROUP NITRILE COMPLEXES AND TETRAKIS(DIPHENYLPHOSPHINO)TETRATHIAFULVALENE (P4) 226

1. Introduction 227

2. Experimental 228

A. Synthesis 228
(1) Reaction of $[Rh_2(NCCH_3)_{10}][BF_4]_4$ with P4: Formation of $[Rh(P4)][BF_4]$ (**30**) 228
(2) Reaction of $[M^{II}(NCCH_3)_n][BF_4]_2$ (M = Pt, n = 4; M = Pd, Co, Fe, Ni, n = 6) with P4 229
(i) Formation of $[Pt(P4)]_n[BF_4]_{2n}$ (**31**). 229
(ii) Formation of $[Pd(P4)]_n[BF_4]_{2n}$ (**32**) 229
(iii) Formation of $[Co(P4)]_n[BF_4]_{2n}$ (**33**) 230
(iv) Formation of $[Fe(P4)]_n[BF_4]_{2n}$ (**34**) 231
(v) Formation of $[Ni(P4)]_n[BF_4]_{2n}$ (**35**) 231
(3) Reactions with excess P4 232
(i) $[Rh_2(NCCH_3)_{10}][BF_4]_4$ 232
(ii) $[Pd^{II}(NCCH_3)_6][BF_4]_2$ 232

3. Results and Discussion 233

A. Preparation and Characterization of $[M(P4)]_n[BF_4]_{xn}$ (M = Rh, x = 1; M = Pt, Pd, Co, Fe, Ni, x = 2) (**30-35**) 233
(1) Synthesis 234
(2) Spectrosopic Characterization 234
(i) NMR Spectroscopic Studies 234
(ii) Infrared and UV-Visible Spectroscopy 238
(iii) Magnetic Susceptibility and EPR Spectroscopic Studies of $[Co(P4)]_n[BF_4]_{2n}$ (**33**) 239
(iv) Electrochemistry of $[Rh(P4)]_n[BF_4]_n$ (**30**) 241
(v) Fast Atom Bombardment Mass Spectrometry 241
(3) Proposed Cyclic Oligomers 242
(i) Molecular Visualization 243
(ii) Gel Permeation Chromatography 243
(iii) Variable Temperature ^1H NMR Spectrscopy 245

B Re
T
4 Conclusion
List of Refer
CHAPTER IX
List of Refer
CHAPTER X
CHAPTER X A
CHAPTER X B
1 Introduct
2 Experimen
A. X-r
3 Results a
A. M
B. M
C. M
4 Conclusion
List of Refer

B. Reactivity of $[Rh_2(NCCH_3)_{10}][BF_4]_4$ and $[Pd^{II}(NCCH_3)_6][BF_4]_2$ with excess P4 245

4. Concluding Remarks 246

List of References 248

CHAPTER IX CONCLUSION 250

List of References 255

APPENDIX 256

APPENDIX A PHYSICAL MEASUREMENTS 257

APPENDIX B STRUCTURAL ANALYSIS OF FUNCTIONALIZED TETRATHIAFULVALENES 261

1. Introduction 262

2. Experimental 263

A. X-ray Crystallography 263
(1) *ortho*-$(CH_3)_2$TTF (**36**) 263
(i) Preparation, Data Collection and Reduction. 263
(ii) Structure Solution and Refinement 264
(2) *ortho*-$(CH_3)_2[(C_6H_5)_2P]_2$TTF (**1**) 264
(i) Preparation, Data Collection and Reduction. 264
(ii) Structure Solution and Refinement 265
(3) $[(C_6H_5)_2P]_4$TTF (**2**) 266
(i) Data Collection and Reduction. 266
(ii) Structure Solution and Refinement 266

3. Results and Discussion 268

A. Molecular Structure of *ortho*-$(CH_3)_2$TTF (**36**) 268

B. Molecular Structure of *ortho*-$(CH_3)_2[(C_6H_5)_2P]_2$TTF (**1**) 273

C. Molecular Structure of $[(C_6H_5)_2P]_4$TTF (**2**) 277

4. Concluding Remarks 282

List of References 283

APPENDIX C

1 Introduction

2 Experimental

A. Sy

3 Results a

A. Pr

E

4 Conclusio

List of Refer

APPENDIX D

1 Introduc

2 Experim

A. Sy

3 Results a

A

P

4 Conclusio

List of Refer

APPENDIX E

APPENDIX C SYNTHESIS OF $[Bu_4N]_2[Re_2Cl_8]$ FROM RHENIUM-CONTAINING LABORATORY RESIDUES 284

1. Introduction 285

2. Experimental 286

A. Synthesis....286
(1) Preparation of $KReO_4$ from Rhenium-Containing Residue 286
(2) Metathesis of $KReO_4$ to form $[(n\text{-}Bu)_4N]_2[ReO_4]$ 289
(3) Synthesis of $[(n\text{-}Bu)_4N]_2[Re_2Cl_8]$ 289

3. Results and Discussion....290

A. Preparation and Characterization of $[(n\text{-}Bu)_4N]_2[Re_2Cl_8]$ from Rhenium Residues 290

4. Concluding Remarks 292

List of References....295

APPENDIX D $^{31}P\{^1H\}$ NMR ANALYSIS OF PtCl(TMPP)-(TMPP-*O*)....296

1. Introduction 297

2. Experimental 298

A. Synthesis and Physical Methods 298

3. Results and Discussion....298

A. $^{31}P\{^1H\}$ NMR Simulation and Interpretation for PtCl(TMPP)(TMPP-*O*) (**37**) 298

4. Conclusing Remarks....299

List of References....302

APPENDIX E COMPILATION OF ^{31}P NMR SPECTRAL DATA 304

Crystallogr
[MPP][BF
[H
[CH
[MMPP-C
Selected B
[MPP][BF
Selected B
[H
Selected bo
Summary o
[MC-H
Selected B
[][BF
Electrochem
[][BF
Summary o
[CH
Summary o
[CH
Summary o
[

LIST OF TABLES

Page

1. Crystallographic Data for $[Rh^{I}(\eta^2\text{-TMPP})_2][BF_4]\cdot[Rh^{II}(\eta^3\text{-TMPP}][BF_4]_2$ (**3**•$[Rh^{II}(\eta^3\text{-TMPP}]\text{-}[BF_4]_2$),$[Co^{II}{}_3(\mu^3\text{-OH})(\mu\text{-OH})_3\{Co^{II}(\text{TMPP-}O)_2\}_3][BF_4]_2\cdot[CH_3\text{-TMPP}][BF_4]\cdot(CH_3CH_2)_2O\cdot 2(CH_2)_2CO$ (**6**• $[CH_3\text{-TMPP}][BF_4]\cdot(CH_3CH_2)_2O\cdot 2(CH_2)_2CO$), and $Pd(\text{TMPP-}O)_2\cdot 3.73CH_2Cl_2\cdot H_2O$, (**7**•$3.73CH_2Cl_2\cdot H_2O$) 45

2. Selected Bond Distances (Å) and Angles (deg.) for $[Rh^{I}(\eta^2\text{-TMPP})_2][BF_4]$ (**3**).....57

3. Selected Bond Distances (Å) and Angles (deg.) for $[Co^{II}{}_3(\mu^3\text{-OH})(\mu\text{-OH})_3\{Co^{II}(\mu\text{-}\eta^3\text{-TMPP-}O)_2\}_3][BF_4]_2$ (**6**).....69

4. Selected bond distances (Å) and angles (deg.) $Pd(\text{TMPP-}O)_2$ (**7**).....74

5. Summary of crystallographic data for $[Ni(o\text{-P2})_2][BF_4]_2\cdot 2C_7H_8$ (**8**•$2C_7H_8$) and $[Pt(o\text{-P2})_2][BF_4]_2\cdot 2C_7H_8$ (**11**•$2C_7H_8$).....93

6. Selected Bond Distances (Å) and Angles (deg.) for $[Ni(o\text{-P2})_2][BF_4]_2$ (**8**) and $[Pt(o\text{-P2})_2][BF_4]_2$ (**11**).....104

7. Electrochemical data (in V vs Ag/AgCl) for **8**-**11**, *o*-P2, and $[Rh(o\text{-P2})_2][BF_4]$, in 0.2 M $TBABF_4/CH_2Cl_2$ solutions, at 200 mV/s.....115

8. Summary of crystal data for $[ReCl_2(o\text{-P2})_2][Re_2Cl_6(o\text{-P2})]\cdot 4CH_2Cl_2$ (**16**·**17**•$4CH_2Cl_2$).....137

9. Summary of crystal data for $MoCl_2O_2(o\text{-P2O}_2)\cdot CH_2Cl_2$ (**19**•CH_2Cl_2).....138

10. Summary of bond distances (Å) and angles (deg) for the cation $[ReCl_2(o\text{-P2})_2]^+$ (**16**), in **16**•**17**.....148

11. Summary of bond distances (Å) and angles (deg) for the anion $[Re_2Cl_6(o\text{-}P2)]^-$ (**17**), in **16•17**. 150

12. Possible redox reactions for the salt $[Re^{III}Cl_2(o\text{-}P2)_2]$-$[Re_2^{II,III}Cl_6(o\text{-}P2)]$ (**16•17**). 156

13. Summary of bond distances (Å) and angles (deg) for $MoCl_2O_2(o\text{-}P2O_2) \cdot CH_2Cl_2$ (**19**$\cdot CH_2Cl_2$) 168

14. Summary of crystallographic data for $PtCl_2(o\text{-}P2)\cdot CH_3CN$ (**20**$\cdot CH_3CN$) and $Pt_2Cl_4(P4)\cdot 3CH_3CN$ (**22**$\cdot 3CH_3CN$). 189

15. Summary of NMR spectrosopic data for compounds **20-29**. 197

16. Summary of cyclic voltammetry, electronic absorbance and infrared spectroscopy data for compounds **20-29**. 199

17. Selected Bond Distances (Å) and Angles (deg) for $PtCl_2(o\text{-}P2)$ (**20**) and $Pt_2Cl_24(P4)$ (**22**) 202

Appendix

18. Crystallographic data for *ortho*-$(CH_3)_2TTF$ (**36**), *ortho*-$(CH_3)_2[(C_6H_5)_2P]_2TTF$ (**1**), and $[(C_6H_5)_2P]_4TTF\cdot$toluene, (**2**•toluene).. 267

19. Selected bond distances (Å) and angles (deg.) for *ortho*-$(CH_3)_2TTF$ (**36**) and *ortho*-$(CH_3)_2[(C_6H_5)_2P]_2TTF$ (**1**). 269

20. Selected bond distances (Å) and angles (deg.) for $[(C_6H_5)_2P]_4TTF$ (**2**). 279

a Schema
ellipsoids

Schematic
binding m

Schematic
binding m

Ball and st
hexagons o

ORTEP rep

Extended s
dimensiona
ribbon or sh
structure...

Schematic
Pt and te

Variable T
BF_4 3 in

PLUTO re
mixed salt

PLUTO re
disorder in
PPP_4TB

ORTEP re
O_4BF_4
and labels

LIST OF FIGURES

Page

1. (a) Schematic drawing and (b) ORTEP representation with 50% ellipsoids of tris(2, 4, 6-trimethoxyphenyl)phosphine (TMPP).....8

2. Schematics depicting the crystallographically determined binding modes for TMPP bound to a single metal center.....10

3. Schematics depicting the crystallographically determined binding modes for $[P\{C_6H_2(OMe)_3\}_2(C_6H_2(OMe)_2O]^{2-}$ (TMPP-*O*).....11

4. Ball and stick representation of the interlocking $Mn^{II}_6Cu^{II}_6$ hexagons of $(rad)_2Mn_2[Cu(opda)]_3(DMSO)_2 \cdot 2H_2O$..... 16

5. ORTEP representation of the stacked salt, [TTF][TCNQ]. 20

6. Extended structures proposed by Hoffman *et. al.*: (a) two dimensional slab structure, (b) zig-zag layered structure, (c) ribbon or sheet polymers, and (d) two-dimensional layer structure.....23

7. Schematics of the monodentate (P1), bidentate (*o*-P2, *E*-P2, *Z*-P2), and tetradentate (P4) phosphine ligands.....25

8. Variable Temperature ^1H NMR spectra of $[Rh^I(\eta^2\text{-TMPP})_2]$-$[BF_4]$ (**3**) in d_6-acetone. 54

9. PLUTO representation of $[Rh^I(\eta^2\text{-TMPP})_2][BF_4]$ (**3**) from the mixed salt $[Rh^I(\eta^2\text{-TMPP})_2][BF_4] \bullet [Rh^{II}(\eta^3\text{-TMPP})_2][BF_4]_2$.....58

10. PLUTO representation of the unique atoms, showing the disorder in the molecular structure of $[Rh^I(\eta^2\text{-TMPP})_2][BF_4] \bullet [Rh^{II}(\eta^3\text{-TMPP})_2][BF_4]_2$. 59

11. ORTEP representation of $[Co^{II}_3(\mu^3\text{-OH})(\mu\text{-OH})_3\{Co^{II}(\mu\text{-}\eta^3\text{-TMPP-}O)_2\}_3][BF_4]_2$ (**6**) with 50% probability ellipsoids. Hydrogen atoms and labels have been removed for clarity.. 70

ORTEP rep
ent meta
6 with 50
mmed for
ORTEP rep
rawed.....
Interconver
ORTEP rep
ip and b
ORTEP rep
ellipsoids w
Packing di
ORTEP rep
ellipsoids w
Plot of [Re
Re...BF4]
EPR spectr
at 107 K...
EPR spectr
Cyclic volt
in CH2Cl2
EPR spectr
at 45 K....
Schematic
4-bis di
dimethyl-
EPR spectr
Re(NCC
Thermal
hydrogen

12. ORTEP representation of the immediate coordination sphere for each metal in $[Co^{II}_3(\mu^3\text{-}OH)(\mu\text{-}OH)_3\{Co^{II}(\mu\text{-}\eta^3\text{-}TMPP\text{-}O)_2\}_3][BF_4]_2$ (**6**) with 50% probablility ellipsoids. All other atoms have been removed for clarity....71

13. ORTEP representation of Pd(TMPP-*O*)$_2$ (**7**) with 50% ellipsoids viewed....75

14. Interconversion pathways of the Rh-TMPP complexes 78

15. ORTEP representation of [Rh(*o*-P2)$_2$][BF$_4$] viewed from the (a) top and (b) side with 50% probability ellpsoids....87

16. ORTEP representation of [Ni(*o*-P2)$_2$][BF$_4$]$_2$ (**8**) with 50% ellipsoids viewed from the (a) top and (b) side.. 105

17. Packing diagram of [Ni(*o*-P2)$_2$][BF$_4$]$_2$ (**8**).. 106

18. ORTEP representation of [Pt(*o*-P2)$_2$][BF$_4$]$_2$ (**11**) with 50% ellipsoids viewed from the (a) top and (b) side 107

19. Plot of μ_{eff} (μ_B) and χ_{mol} (emu/mol) vs. temperature (K) of [Co(*o*-P2)$_2$][BF$_4$]$_2$ (**9**)....110

20. EPR spectrum of [Co(*o*-P2)$_2$][BF$_4$]$_2$ (**13**) in 50:50 CH$_3$CN:Toluene at 107 K.. 112

21. EPR spectrum of [Co(*o*-P2)$_2$][BF$_4$]$_2$ (**9**) as a solid sample at 4 K.....113

22. Cyclic voltammogram of [Pt(*o*-P2)$_2$][BF$_4$]$_2$ (**11**) in 0.2 M TBABF$_4$ in CH$_2$Cl$_2$.....116

23. EPR spectrum of [Rh(*o*-P2)$_2$][BF$_4$]$_3$ (**13**) in 50:50 CH$_3$CN:Toluene at 95 K.....118

24. Schematic drawings of the proposed ligands (a) 3,4 dimethyl-3',4'-bis(dimethylphosphino)tetrathiafulvalene and (b) 3,4 dimethyl-3',4'-bis-(phospholyl)tetrathiafulvalene.. 123

25. EPR spectrum of green paramagnetic solid from [Rh$_2$(NCCH$_3$)$_{10}$][BF$_4$]$_4$ + P1 in a toluene/CH$_3$CN glass at 133 K.. 143

26. Thermal ellipsoid plot of the cation [Re(*o*-P2)$_2$Cl$_4$]$^+$ (**16**) with non-hydrogen atoms represented by their 50% probability ellipsoids.. 149

Thermal el
anhydrou
dipyridi

Packing dia

Cyclic voltam
and b. [Re(C
at a Pt disk

Magnetic da
3 and χm
eff vs te
slope of χm

EPR spectru
chloro CH2

Plots of a
χT emu
16•[PF6]

Plot of the
P... 18

PLUTO rep

Correlation
X-ray C-L
NMR chem

Cyclic volta
[Re2Cl8

ORTEP rep
viewed fro

Packing di

ORTEP rep
viewed fro

Packing di

27. Thermal ellipsoid plot of the anion $[Re_2Cl_6(o\text{-}P2)]^-$ (**17**) with non-hydrogen atoms represented by their 50% probability ellipsoids.....151

28. Packing diagram of $[ReCl_2(o\text{-}P2)_2][Re_2Cl_6(o\text{-}P2)]$ (**16•17**).....152

29. Cyclic voltammogram of (a) $[ReCl_2(o\text{-}P2)_2][Re_2Cl_6(o\text{-}P2)]$ (**16•17**) and (b) $[ReCl_2(o\text{-}P2)_2][BF_4]$ in 0.1 M $TBABF_4/CH_2Cl_2$ vs Ag/AgCl at a Pt disk electrode.....157

30. Magnetic data for $[ReCl_2(o\text{-}P2)_2][Re_2Cl_6(o\text{-}P2)]$ (**16•17**): (a) μ_{eff} (μB) and χ_{mol} (emu/mol) vs. temperature (K) and (b) χT (emu K mol^{-1}) vs. temperature (K) fit to the Curie-Weiss law with a slope of χ_{TIP}.....160

31. EPR spectrum of $[ReCl_2(o\text{-}P2)_2][Re_2Cl_6(o\text{-}P2)]$ (**16•17**) in a 1:1 toluene/CH_2Cl_2 glass at 4 K.....162

32. Plots of (a) μ_{eff} (μB) and χ_{mol} (emu/mol) vs. temperature (K) and (b) χT (emu K mol^{-1}) vs. temperature of $[Re(o\text{-}P2)_2Cl_2][BF_4]$ (**16•[BF_4]**).....163

33. Plot of μ_{eff} (μB) and χ_{mol} (emu) vs. temperature (K) of $ReCl_2(o\text{-}P2)_2$ (**18**).....164

34. PLUTO representation of $MoCl_2O_2(o\text{-}P2O_2)$ (**19**).....169

35. Correlation of ^{31}P NMR coordination chemical shift $\Delta\delta^{31}P$ in MCl_2(L-L) (M = Ni, Pd, Pt) complexes with the free ligand ^{31}P NMR chemical shift $\delta^{31}P$.....195

36. Cyclic voltammogram of $PdCl_2(o\text{-}P2)$ (**25**) in 0.2 M $TBABF_4$ in CH_2Cl_2.....201

37. ORTEP representation of $PtCl_2(o\text{-}P2)$ (**20**) with 50% ellipsoids viewed from the (a) top and (b) side.....203

38. Packing diagram of $PtCl_2(o\text{-}P2)$ (**20**).....204

39. ORTEP representation of Pt_2Cl_4(P4) (**22**) with 50% ellipsoids viewed from the (a) top and (b) side.....209

40. Packing diagram of Pt_2Cl_4(P4) (**22**) viewed down the a-axis.....210

Fig. P4.15 ...

Schematic ...
1.1 × 10...

Plot of ...
Fig. P4.15 ...

Molecular ...

...ction

...MDEP rep...
...ligands

Packing d...
...ers .....

...2.0 re...

Packing d...
...the a-axis

...MDEP rep...
...ligands...

Packing d...

Traced sp...
recovery o...
region is s...

Traced sp...
recovery o...
region is s...

Calculated ...
NOE spec...
...e 1.0 sa...
...incidence...

Illustration ...

41. Reaction scheme depicting the step-wise synthesis of $[M_2(o\text{-}P2)_2(P4)][BF_4]_4$ (M = Ni, Pd, Pt (**24**)) 219

42. Schematic showing the potential coordination of $[TCNQ]^{n-}$ (n = 0, 1) to "$[Co_2(o\text{-}P2)_2(P4)]^{m+}$" (m = 4, 6, 7). 223

43. Plot of μ_{eff} (μ_B) and χ_{mol} (emu/mol) vs. temperature (K) of $[Co(P4)]_n[BF_4]_{2n}$ (**33**). 240

44. Molecular model of the proposed cyclic hexamer $[Ni(P4)_6]^{12+}$ 244

Appendix

45. ORTEP representation of *ortho*-$(CH_3)_2$TTF (**36**) with 50% ellipsoids 270

46. Packing diagram of *ortho*-$(CH_3)_2$TTF (**36**) viewed down the a-axis 272

47. PLUTO representation of *ortho*-$[(C_6H_5)_2P]_2(CH_3)_2$TTF (**1**) 274

48. Packing diagram of *ortho*-$[(C_6H_5)_2P]_2(CH_3)_2$TTF(**1**) viewed down the a-axis 275

49. ORTEP representation of $[(C_6H_5)_2P]_4$TTF (**2**) with 50% ellipsoids 280

50. Packing diagram of $[(C_6H_5)_2P]_4$TTF (**2**) 281

51. Infrared spectrum of impure [K][ReO_4] obtained from the recovery of rhenium-containing residues. The far-infrared region is shown in the inset 291

52. Infrared spectrum of impure TBAReO_4 obtained from the recovery of rhenium-containing residues. The far-infrared region is shown in the inset 293

53. Calculated (a) and experimental (b) room temperature $^{31}P\{^1H\}$ NMR spectra of PtCl(TMPP)(TMPP-*O*) (**40**) in acetonitrile-d_3. The 1:3 satellite:parent intensity ratio resulting from the 33% abundance of ^{195}Pt is not drawn to scale in spectrum (a). 300

54. Illustration of PtCl(TMPP(TMPP-*O*) (**37**) 301

LI

Cl
H
S
S
S

LIST OF SYMBOLS AND ABBREVIATIONS

Å	Ångström
Ag/AgCl	silver-silver chloride reference electrode
BEDT-TTF	bis(ethylenedithio)tetrathiafulvalene
br	broad
ca.	circa, about
cm	centimeter
cm^{-1}	wavenumber
cod	1,5-cyclooctadiene
CV	cyclic voltammetry
°C	degree centigrade
d	doublet (NMR), day, deuterated
δ	parts per million (ppm)
dd	doublet of doublets
depe	bis(diethylphosphino)ethane
dippb	bis(diisopropylphosphino)benzene
dmit	4,5-dimecapto-1,3-dithiole-2-thione
dppa	bis(diphenylphosphino)amine
dppb	bis(diphenylphosphino)benzene
dppe	bis(diphenylphosphino)ethane
dppee	bis(diphenylphosphino)ethene
dppm	bis(diphenylphosphino)methane
dtpe	bis(ditolylphosphino)ethane
$E_{p,a}$	anodic peak potential
$E_{p,c}$	cathodic peak potential
EPR	electron paramagnetic resonance
emu	electromagnetic unit
esd	estimated standard deviation
ES-MS	electrospray mass spectrometry
Et	ethyl
EtOH	ethanol
Et_2O	diethyl ether

ES

FAB-MS

MEL

MALDI

Me

MeCN

MeOH

B. M.

EP2

EP2

EtS	Ethylthio-
ε	molar extinction coefficient
FAB-MS	Fast Atom Bombardment Mass Spectrometry
g	epr g-value, gram
G	Gauss
h	hour
MHz	MegaHertz
IR	infrared
K	Kelvin
λ	wavelength
m	medium
M	molar
MALDI	Matrix Assisted Laser Desorption Ionization
Me	methyl
MeCN	acetonitrile
MeOH	methanol
mg	milligram
min.	minute
mL	milliliter
mmol	millimole
mult	multiplet
μ	bridging ligand
μ_B or B. M.	Bohr magneton
μL	microliter
nm	nanometer
ν	frequency
NBA	3-nitrobenzyl alcohol
NMR	nuclear magnetic resonance
OTf^-	triflate anion
ox	oxidation
P1	trimethyl-diphenylphosphino-tetrathiafulvalene
E-P2	(*E*)-dimethyl-bis(diphenylphosphino)-tetrathiafulvalene
o-P2	3,4-dimethyl-3',4'-bis(diphenylphosphino)-tetrathiafulvalene

Fc

FeO

H

Hz

K

L

M

m

n

NCMe

Nu

BF_4

CN

$CNBF_4$

Ph

PP

PPP-O

PPP-CH_2

PPP-CH_2

PS

PSH

R

s

T

t

V

w

o-P2O_2	3,4-dimethyl-3',4'-bis(diphenylphosphino)dioxide-tetrathiafulvalene
P4	tetrakis(diphenylphosphino)-tetrathiafulvalene
P4O_2	tetrakis(diphenylphosphino)-(*Z*)-dioxide-tetrathiafulvalene
ppm	parts per million
Pr^i	isopropyl
red	reduction
r.t.	room temperature
s	singlet (NMR), strong (IR)
sh	shoulder
SQUID	Superconducting Quantum Interference Device
t	triplet
TBA	tetra-*n*-butylammonium
$TBABF_4$	tetra-*n*-butylammonium tetrafluoroborate
TCNQ	7,7,8,8-tetracyanoquinonedimethane
$TCNQF_4$	2,3,5,6-tetrafluoro-7,7,8,8-tetracyanoquinodimethane
tppb	tetra(diphenylphosphino)benzene
THF	tetrahydrofuran
TMPP	tris(2,4,6-trimethoxyphenyl)phosphine
TMPP-*O*	$P[\{C_6H_2(CH_3O)_3\}_2\{C_6H_2CH_3O)_2O\}]^-$
$[TMPP\text{-}CH_3]^+$	tris(2,4,6-trimethoxyphenyl)methyl phosphonium
$[TMPP\text{-}CH_2Cl]^+$	tris(2,4,6-trimethoxyphenyl)chloromethyl phosphonium
TMS	tetramethylsilane
TMTSF	tetramethyltetraselenofulvalene
TSF	tetraselenofulvalene
TTF	tetrathiafulvaene
UV	ultraviolet
V	Volt
vs	versus, very strong

w	weak
X	halide ligand
Z-P2	(*Z*)-dimethyl-(diphenylphosphino)-tetrathiafulvalene

LIST OF COMPOUNDS

(1) ---------- *o*-P2

(2) ---------- P4

(3) ---------- $[Rh^{I}(TMPP)_2][BF_4]$

(4) ---------- Rh^{I} TMPP)(TMPP-*O*)

(5) ---------- *ax,ax*-$[Rh^{III}(\eta^3\text{-TMPP-}O)_2][BF_4]$

(6) ---------- $[Co^{II}{}_3(OH)_4\{Co^{II}(TMPP\text{-}O)_2\}_3][BF_4]_2$

(7) ---------- $Pd^{II}(\eta^3\text{-TMPP-}O)_2$

(8) ---------- $[Ni^{II}(o\text{-P2})_2][BF_4]_2$

(9) ---------- $[Co^{II}(o\text{-P2})_2][BF_4]_2$

(10) ---------- $[Pd^{II}(o\text{-P2})_2][BF_4]_2$

(11) ---------- $[Pt^{II}(o\text{-P2})_2][BF_4]_2$

(12) ---------- $[Fe^{II}(o\text{-P2})_2][BF_4]_2$

(13) ---------- $[Ni^{II}(o\text{-P2})_2][CF_3SO_3]_2$

(14) ---------- $[Rh^{I}(o\text{-P2})_2][BF_4]_3$

(15) ---------- $[Rh^{II,\,II}{}_2(NCCH_3)_{10}][BF_4]_4$ + 4 P1

(16) ---------- $[Re^{III}Cl_2(o\text{-P2})_2]^+$

(17) ---------- $[Re_2{}^{II,\,III}Cl_6(o\text{-P2})]^-$

(18) ---------- $Re^{II}Cl_2(o\text{-P2})_2$

(19) ---------- $Mo^{IV}Cl_2O_2(o\text{-P2O}_2)$

(20) ---------- $Pt^{II}Cl_2(o\text{-P2})$

(21) ---------- $[Pt^{II}(o\text{-P2})(NCCH_3)_2][BF_4]_2$

(22) ---------- $Pt_2^{II,\,II}Cl_4(P4)$

(23) ---------- $[Pt_2^{II}(P4)(NCCH_3)_4][BF_4]_4$

(24) ---------- $[Pt_2^{II,\,II}(P4)(o\text{-}P2)_2][BF_4]_4$

(25) ---------- $Pd^{II}Cl_2(o\text{-}P2)$

(26) ---------- $[Pd^{II}(o\text{-}P2)(NCCH_3)_2][BF_4]_2$

(27) ---------- $Pd_2^{II,\,II}Cl_4(P4)$

(28) ---------- $[Pt^{II,\,II}{}_2(P4)(NCCH_3)_4][BF_4]_4$

(29) ---------- $Ni_2^{II,II}Cl_4(P4)$

(30) ---------- $[Rh^{I}(P4)]_n[BF_4]_n$

(31) ---------- $[Pt^{II}(P4)]_n[BF_4]_{2n}$

(32) ---------- $[Pd^{II}(P4)]_n[BF_4]_{2n}$

(33) ---------- $[Ni^{II}(P4)]_n[BF_4]_{2n}$

(34) ---------- $[Fe^{II}(P4)]_n[BF_4]_{2n}$

(35) ---------- $[Co^{II}(P4)]_n[BF_4]_{2n}$

(36) ---------- *ortho*-$(CH_3)_2$TTF

(37) ---------- $Pt^{II}Cl$(TMPP)(TMPP-*O*)

CHAPTER I

INTRODUCTION

; Functiona

Complexe

Ternary p

em coordina

ently as a

milarly thi

entially imp

ethylation

rmation o

ron metal

ains stoich

lency of pho

d oxidatio

ing interact

ey they allo

ges in the R

and one ca

ct product.

enzymic re

ases.

Bailey pho

demonstra

A. Functionalized Phosphines as Ligands in Transition Metal Complexes

Tertiary phosphines have played an important role in the history of modern coordination and organometallic chemistry due to their extraordinary versatility as ancillary ligands.[1] Transition metal-phosphine complexes, particularly those of the later transition metals catalyze a wide range of industrially important organic processes from olefin hydrogenation, hydroformylation, hydrosilation and hydrocyanation to polymerization and oligomerization of olefins and acetylenes.[2] In addition to catalytic processes, transition metal phosphine complexes are also capable of performing numerous stoichiometric organic transformations.[3] One reason for the popularity of phosphines is their ability to stabilize transition metals in a range of oxidation states,[4] a consequence of cooperative σ-donor, π-acceptor bonding interactions.[5] Another reason for the widespread use of PR_3 ligands is that they allow for electronic and steric tuning of metal complexes with changes in the R groups. By modifying the electronic and steric properties of the ligand one can, in turn, affect the reactivity and stereoselectivity of the desired product. Tertiary phosphines act as leaving groups in stoichiometric and catalytic reactions and stabilize polynuclear as well as mononuclear structures.

Bulky phosphine complexes of low valent, early transition metals, have been demonstrated to bind small molecules such as dinitrogen and

ganated org

ubstrate the

ome different

xcellent exa

ated coordi

ith trans-

ffuse comp

organ wh

ifuses for th

although

ining num

ffuse ligan

ng deficit

ts have be

ffuses. In

ther substra

ffuse ligan

fusion and

homogeneous

ts with e

ion. The use

ffuse elu

unsaturated organic molecules.[6] The steric influence of the phosphine ligands force the metal to adopt a coordinatively unsaturated geometry. This electron deficient metal center is activated towards small molecule addition. An excellent example comes from the research of Kubas and co-workers, who prepared coordinatively unsaturated Mo^0 and W^0 complexes of general formula *trans*-$M(CO)_3(PR_3)_2$ (R = cyclohexyl, isopropyl).[7] These five-coordinate complexes have been found to bind small molecules such as dihydrogen which hints at the possibility of using phosphine-stabilized complexes for the activation of other σ-bonded molecules, *e.g.* methane.

Although they have been studied for many years, there is an increasing number of transition-metal complexes containing tertiary phosphine ligands being reported in the literature, including examples of varying denticity and functionality.[3] Over the years a myriad of functional groups have been added to phosphine ligands in order to effect specific properties. In response to the need for a good, leaving group to use as a pendent substituent on a phosphorus atom, researchers have explored ether-phosphine ligands (P,O) that participate in a strong metal-phosphorus interaction and weak metal-oxygen interaction(s). The use of (P,O) ligands for homogeneous catalysis has been extensively explored by Lindner and co-workers,[8] with earlier work being carried out by Anderson,[9] Rauchfuss[10] and Shaw.[11] The usefulness of ether-phosphines was demonstrated by the ability to stabilize elusive species such as mononuclear Rh^{2+} and Ir^{2+} via the

MeO

formation of five-membered metallacycles as depicted in (scheme 1). Specific ligand modifications have been found to affect the reactivity and stereoselectivity of the desired product, producing an unusual selectivity effect in catalysis.[8,12]

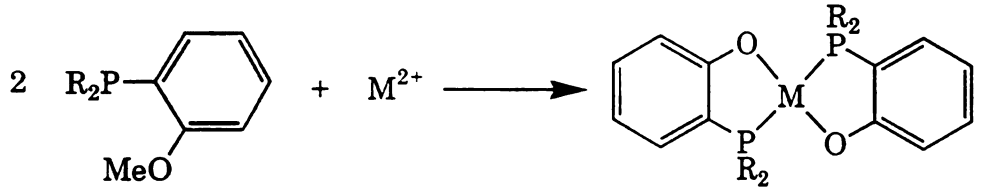

(1)

R = Me, ^{t}Bu M = Rh, Ir

Research in our laboratories has focused on changes in the R group of tertiary phosphines that affect the denticity. In the case of (P,O) ligands, the presence of both phosphorus and oxygen atoms with lone pairs available for coordination allows the ligand to be potentially multidentate. Ether-phosphines and phosphinoenolates can vary from mono- to tridentate, depending on the number and location of the oxygen substituents.[8u] Braunstein and coworkers showed that α-phosphinoenolates such as $[PPh_2CH{\cdots}C({\cdots}O)R]^-$ (R = Ph, Me, *p*-C_6H_4Me) form homoleptic complexes with Co^{III} , Ni^{II}, Pd^{II}, and Pt^{II}.[13] The Ni complex can function as a four-electron donor by chelating to CoI_2 through *cis*-oxygen atoms to form

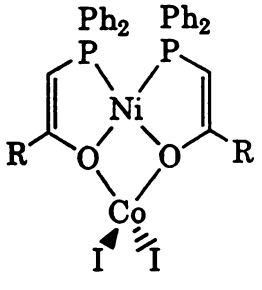

R = Ph, *p*-C_6H_4Me, Me

heterobimetallic complexes.[13a] Other examples of multidentate phosphines of this type include thio- (e.g. $P(C_6H_4\text{-}o\text{-}SH)_3$ and $Ph_{3-n}P(C_2H_4SH)_n$ n = 1, 2),[14] amino- (e.g. $Ph_2P(C_6H_4\text{-}o\text{-}NHEt)$),[15] seleno-ether (e.g. $Ph_2P(C_6H_4\text{-}o\text{-}SeMe)$,[16] arseno-ether (e.g. $Ph_2P(C_6H_4\text{-}o\text{-}AsPh_2)$,[17] and telluro-ether phosphines ($Ph_2P(C_6H_4\text{-}o\text{-}TePh)$.[18]

Besides monophosphines there are a number of polydentate phosphines, including diphosphine ligands that posses heteroatom functional groups. Chelating diphosphines such as bis(diphenylphosphino)ethane (dppe), -amine (dppa), -ethene (dppee) and their relatives are commonly used because of their ability to stabilize metal complexes through the formation of five-membered (chelating), and six-membered (bridging) rings.[19] Such diphosphine ligands have been used extensively in the preparation of metal-metal bonded complexes and cluster complexes in general.[20] In particular,

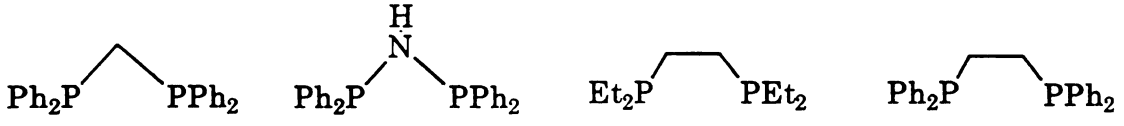

dppm dppa depe dppe

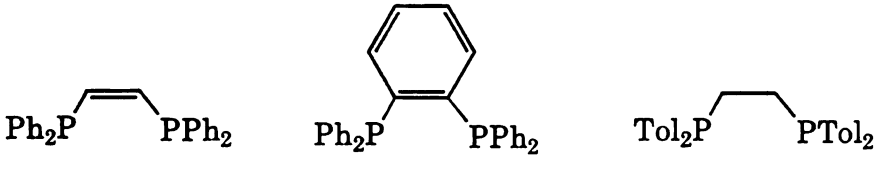

dppee dppb dtpe

diphosphine molecules with a single bridgehead atom separating the phosphorous atoms, e.g. dppm and dppa, act as excellent binucleating ligands for metal-metal bonded complexes due to the formation of a stable

remembered

ionably att

Transition m

Changes

ne hydrosph

ving metal

e apples

Types

d cleavage

destructive e

ne type is r

This redu

ne makes

ounds w

ctor influen

immediate

ctivity at the

five-membered ring.[21] The diphosphines with a ethene backbone are particularly attractive due to their tendency to form interactions with nearly all transition metals,[22] even metals in high oxidation states.[23]

Changes in bite angle (defined as the P-M-P angle upon complexation) of the diphosphine ligand lead to dramatic differences in the reactivity of the resulting metal complex.[24] A diphosphine that exhibits one of the larger bite angles is bis(diphenylphosphino)ferrocene (dppf) (95.28(2)° - 104.2(7)°).[25,26] Dppf has proven to be a useful ligand for metal mediated C-S bond cleavage,[27] the preparation of Fischer-type carbyne complexes,[28] and the reductive elimination of cyclooctatetraene.[22d] In addition to the large bite angle, dppf is redox active, exhibiting a reversible oxidation couple at 0.183 V.[29] This redox behavior, combined with the ability of the Cp rings to freely rotate, makes dppf a desirable ligand for di- and polynuclear metal compounds.[30] It has been suggested that changes in the oxidation state of the dppf influence the electron density of the central metal without changing the immediate coordination sphere, thus allowing for better control over the reactivity at the metal center.[30j]

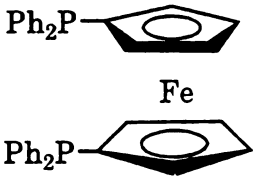

dppf

B. The Chemistry of Tris(2, 4, 6-trimethoxyphenyl)phosphine

Research in our laboratories has revealed interesting and novel coordination chemistry for the phosphine ligand tris(2,4,6-trimethoxyphenyl)phosphine (TMPP).[31] TMPP was first prepared by Protopopov *et al.* from the reaction of PCl_3 and 1,3,5-trimethoxybenzene in the presence of $ZnCl_2$.[32a-b] The phosphine was later prepared by Wada *et al.*, by an alternate route involving lithiation of 1,3,5-trimethoxybenzene, followed by coupling with triphenylphosphite.[32c-d] This procedure was further modified in our laboratories (scheme 2), and the X-ray structure of

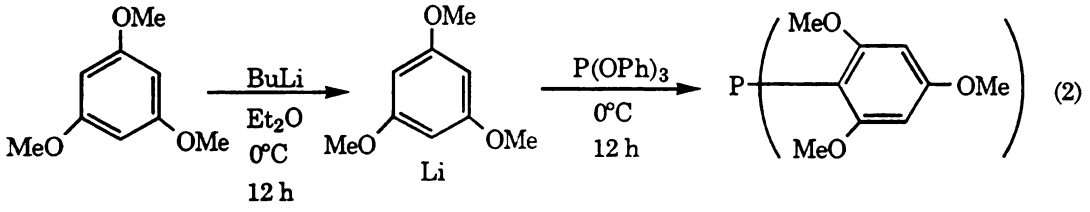

(2)

the compound was reported was determined by Haefner and Dunbar in 1994.[33]

The unusually large steric bulk (cone angle = 184°) of this ligand combined with its high basicity (pK_a of $[HTMPP]^+$ = 11.2) allow TMPP to be quite versatile in its ability to stabilize a wide range of oxidation states, and for stabilizing coordinatively unsaturated, electron deficient complexes. The basicity and bulk of TMPP are consequences of the presence of *ortho* and *para* methoxy groups on the phenyl rings. As a result of the mesomeric effect on

a

ure 1. a
el

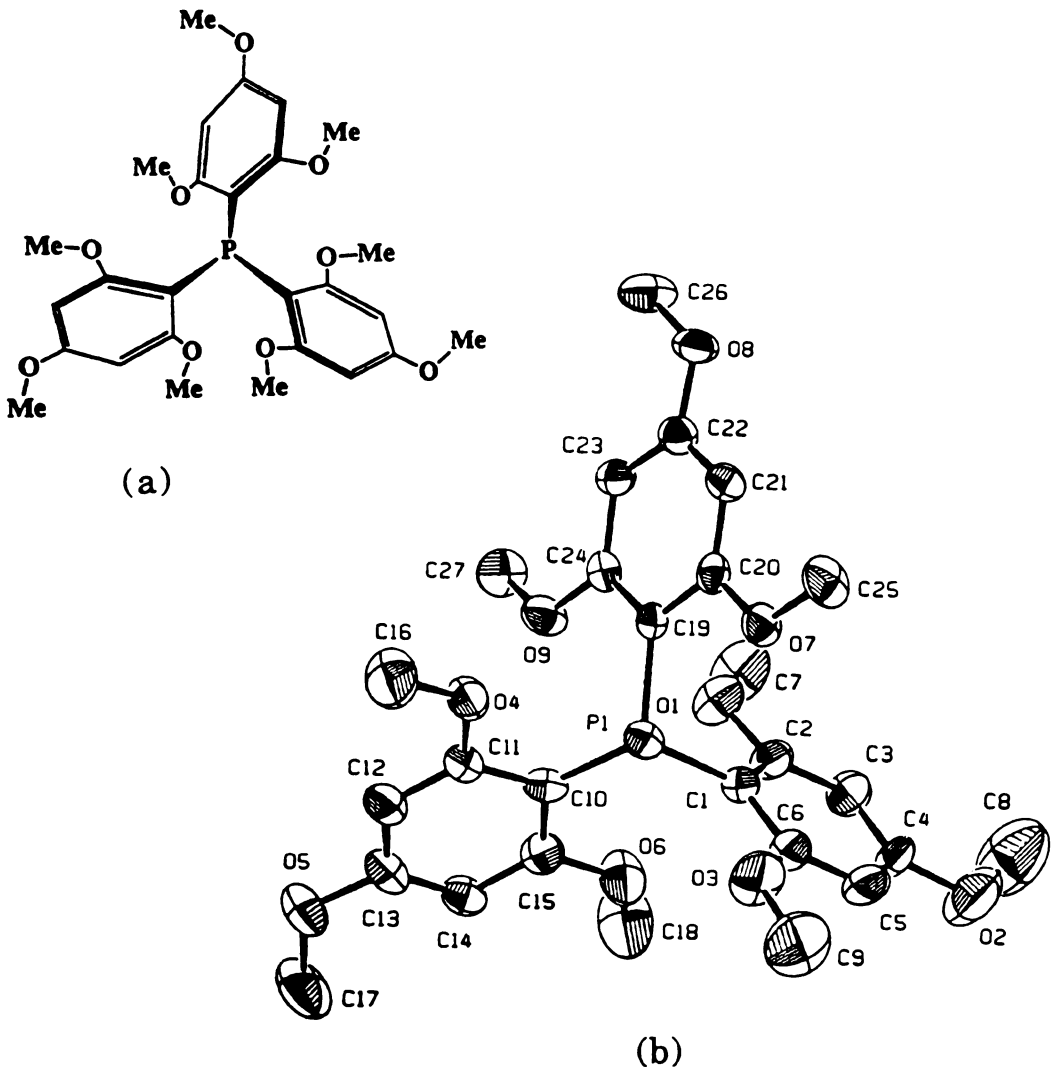

Figure 1. (a) Schematic drawing and (b) ORTEP representation with 50% ellipsoids of tris(2, 4, 6-trimethoxyphenyl)phosphine (TMPP).

the phenyl ring, the methoxy groups donate extra electron density to the lone pair of the phosphorus, serving to increase its basicity. There is, however, an opposing effect of the bulky groups which can hinder the ability of the lone pair to strongly bind to the metal. This tends to render TMPP rather labile, but the chelate effect involving bonding the ether substituents precludes the high reactivities observed for PPh_3, as for example in Wilkinson's catalyst.

The ligation of the *ortho*-methoxy substituents is an important facet of the chemistry of TMPP. The presence of two such groups on each ring allows TMPP to act as a mono-, bi-, or even tri-dentate ligand (Figures 2 and 3). The tridentate mode was first observed in the metalloradical $[Rh(\eta^3\text{-}TMPP)_2][BF_4]_2$ reported by Dunbar and Haefner.[31a] Apart from Co(II) and to a lesser degree Ni(III), little is known regarding the chemistry of d^7 metal ions such as Rh(II), since these species are highly reactive, and appear only as short-lived intermediates or impurities in the chemistry of d^6 and d^8 metal complexes. It is of considerable interest, then, to design d^7 complexes and study their reactivity in stoichiometric and catalytic reactions of the late transition elements. This is especially true for Rh^{II}, whose presence has been detected in reactions involving Wilkinson's catalyst, but whose potential role in the chemistry is not known.[34] Metalloradicals exhibit promise for undergoing reversible reactions with important molecules such as CO and O_2 since they bind much less tightly to substrates than their d^8 counterparts. For these reasons, and for the general purpose of delineating reaction

R
P
R
R

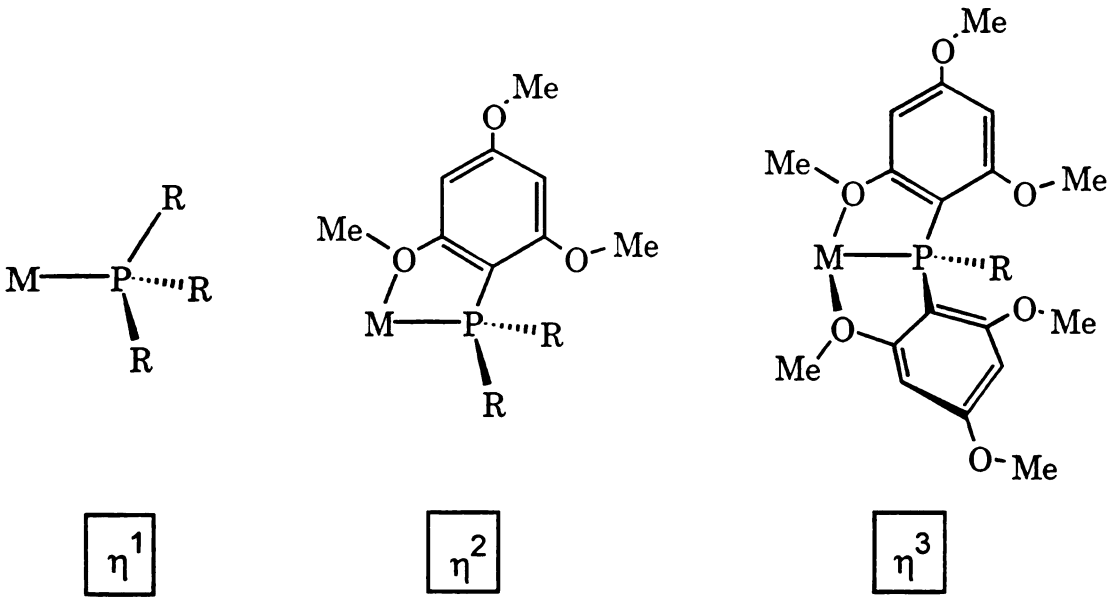

Figure 2. Schematics depicting the crystallographically determined binding modes for TMPP bound to a single metal center.

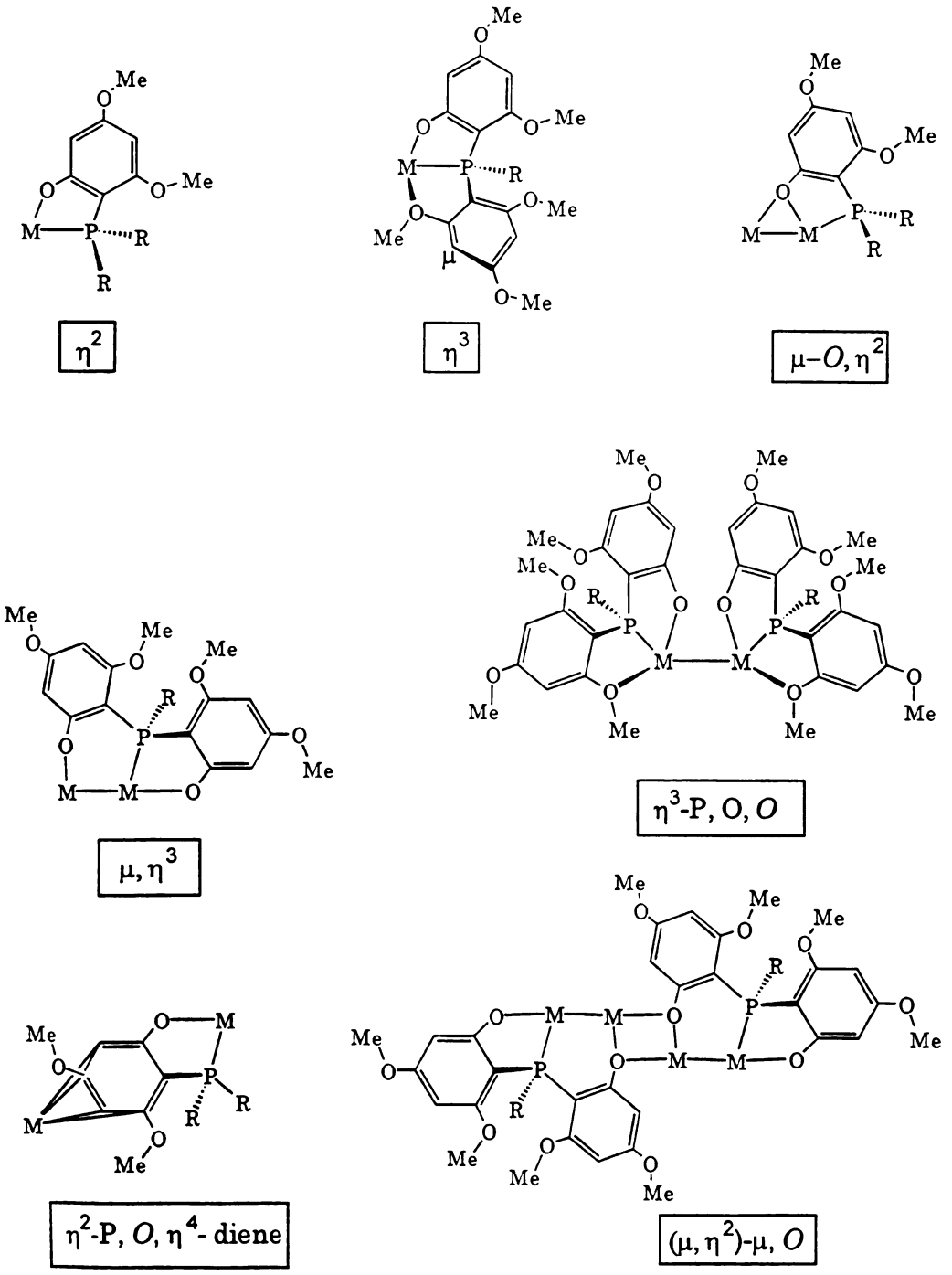

Figure 3. Schematics depicting the crystallographically determined binding modes for $[P\{C_6H_2(OMe)_3\}_2(C_6H_2(OMe)_2O)]^{1-}$ (TMPP-*O*).

pathways for elusive metalloradicals, we have been engaged in efforts to design mononuclear d^7 complexes of the platinum group metals *e.g.*, Co(II), Ni(III), Rh(II), with the goal of engendering stability in the solid-state by

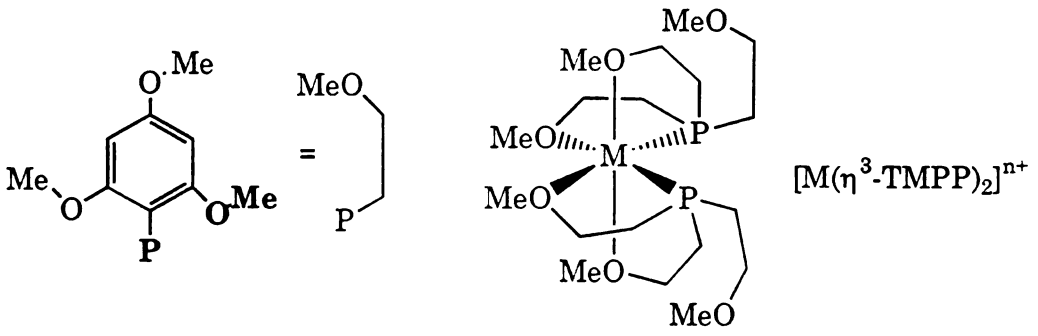

using a bulky ligand that possesses pendent ether groups that are easily displaced in solution.

The remarkably stable compound $[Rh(\eta^3\text{-TMPP})_2][BF_4]_2$, which contains two tri-dentate phosphine ligands, has been shown to exhibit reversible reactions with CO and to undergo non-redox substitution reactions with isocyanides RCN (R = ^{t}Bu, ^{i}Pr, Cy).[31b,c,e] One of the products of the CO reaction is $[Rh(TMPP)_2CO]^+$, which possesses one TMPP ligand acting as a bidentate ligand, with the second phosphine being bound only through the phosphorus atom. The overall trigonal bipyramidal geometry is completed by the CO ligand. This molecule nicely illustrates TMPP's ability to flexibly alter its coordination geometry to accommodate the electronic and geometric requirements of a given metal center.

A reaction that can complicate the chemistry of the TMPP ligand is demethylation of one or more of the coordinating methoxy groups. The

aking phen

ee groups. W

ressingly la

ed complex

hline pair

also be la

human an

ylases of N

does such a

Chapter

II and C

of the s

ERPP pl

ylases in

ylases of

ecies the

ylation o

Assembly

ERPs

ssembly

s also be d

resulting phenoxide ligands are more strongly bound to the metal than the ether groups, which causes any remaining coordinated methoxy groups to be increasingly labile. The presence of the phosphino-phenoxide ligand allows metal complexes of this ligand to act as "ligands" themselves by the donation of a lone pair on the phenoxide oxygen atom to a second metal center. They can also be labile and allow for binding of small molecules as shown by Braunstein and coworkers who demonstrated that α-phosphino-enolate complexes of Ni, Pd, and Pt react with organic isocyanates, CO_2, or activated alkynes such as $MeO_2CC{\equiv}CCO_2Me$ via formation of a carbon-carbon bond.[35]

Chapter II of this thesis describes the isolation and reactivity of Rh(I), Rh(III), and Co(II) complexes of TMPP. The frst section of the chapter deals with the synthesis and reactivity of the homoleptic complexes, $[Rh^{I}(TMPP)_2][BF_4]$ and [*ax*, *ax*-Rh^{III}(TMPP-*O*)$_2$][BF_4]. The role of these complexes in the interconversion of d^6, d^7, and d^8 homoleptic TMPP complexes of Rh will also be presented. The second part of Chapter II describes the use of Co(TMPP-*O*)$_2$ as an inorganic "ligand" for the deliberate preparation of bi-, heterobi- and heterotrimetallic complexes, as well as for the assembly of the hexanuclear cluster $[Co^{II}_3(\mu\text{-}OH)_3(\mu^3\text{-}OH)\{Co^{II}(\eta^3\text{-}TMPP\text{-}O)_2\}_3][BF_4]$. The properties of these complexes, including the magnetic susceptibility and EPR spectral properties of the paramagnetic complexes will also be discussed.

C. The Design of Molecule-Based Materials with Phosphine Ligands

The design of molecule-based materials with tunable conducting, magnetic or optical properties is the focus of much research activity in synthetic organic and inorganic chemistry.[36,37] The deliberate assembly of molecular building blocks into two- and three-dimensional structures is, in principle, a way to control molecular orientation and the overall architecture. The long-range orbital overlap created by controlled assembly determines electronic band structure, local magnetic interactions, and polarizability, which are at the core of the electrical conductivity, bulk magnetism, and optical nonlinearity properties exhibited by organic, inorganic, and polymeric materials. In this vein, the rational preparation of materials using individual organic and inorganic components is an approach of considerable current interest.[38] In particular, the introduction of transition metal ions into a conjugated polymer chain could lead to partially filled bands with significant intrinsic conductivity.[38]

In order to prepare conductive materials from molecular organic/inorganic units, two criteria must be met.[39] First, the redox-active centers (inorganic, organic, or a combination of the two) must be oriented to permit strong interactions, often requiring close spatial proximity and similar crystallographic and electronic environments for the units. Second, the polymers must be partially oxidized or reduced (forming mixed-valence species) to permit free charge transfer along the chain.[40]

In a m

ounds dep

ks that ca

ed coordin

n hexadiyl

rrangemet

, and Cu

ounce

mpleted by b

ained inter

ounce with

a spanned

, namely

ctadiyndi

octatetryle

hain-link

In the

ntent di

ause of op

the electr

ntech et

ed hexad

ter M = C

In a more general sense, the design of molecular inorganic/organic materials depends on the accessibility of specifically engineered building blocks that can be assembled in solution. Products of this strategy include metal coordination polymers of tetrathiooxalate,[41] dihydroxybenzoquinone,[42] and benzodithiolene.[43] In other work, Kahn and coworkers prepared ferrimagnetically coupled bimetallic chains, consisting of alternating Mn (S = 5/2) and Cu (S = 1/2) metals linked by oxamato bridges.[44] In the crystal structure of $MnCu(pbaOH)(H_2O)_2$ (pbaOH = 2-hydroxy-1,3-propanediylbisoxamato), the ferrimagnetic chains are aligned such that the shortest interchain separations are Mn···Cu which creates a two dimensional structure with a ferrimagnetic ordering (T_c = 30 K). The same laboratory has also reported a three-dimensional compound that is ferromagnetic below 22.5 K, namely $(rad)_2Mn_2[Cu(opda)]_3(DMSO)_2 \cdot 2H_2O$ (rad = 2-(4-N-methylpyridinium)-4,4,5,5-tetramethylimidazoline-1-oxyl-3-oxide; opda = *ortho*-phenylene-bisoxamato) in which $Mn^{II}_6Cu^{II}_6$ hexagons are interlocked in a "chain-link" motif (see Figure 4).[45]

In the previous examples, the organic portions of the materials were "innocent" diamagnetic molecules. Recently, emphasis has been placed on the use of open-shell bridging ligands that also contribute to the magnetic and/or electronic properties of the molecular or ionic solids. For example, Gatteschi *et al.* synthesized one-dimensional magnetic chains consisting of metal hexafluoroacetonates $M(hfac)_2$ linked by nitronyl nitroxides (NITR) where M = Cu, Ni, Co, and Mn. The result is a material that undergoes

Q.2

ure 4.

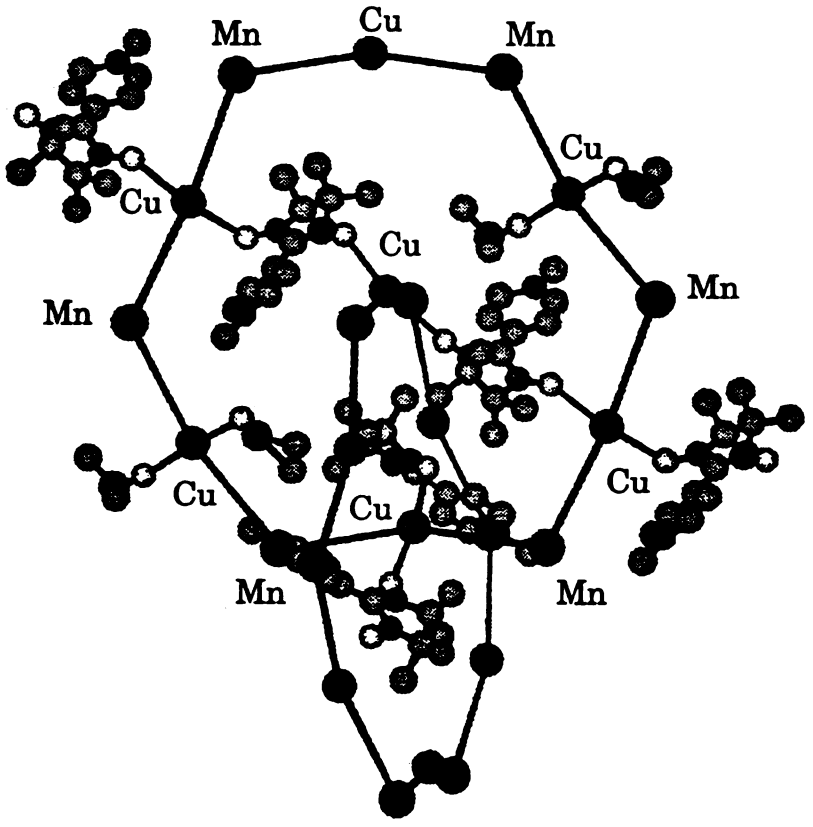

Figure 4. Ball and stick representation of the interlocking $Mn^{II}_6Cu^{II}_6$ hexagons of $(rad)_2Mn_2[Cu(opda)]_3(DMSO)_2 \cdot 2H_2O$.

ferrimagnetic ordering at T_c = 7.6 K, in the case of M = Mn and R = ^{i}Pr, as a result of the non-cancellation of alternating spins of S = 5/2 and 1/2.[46]

(1) The Use of Organic Acceptors in Molecular Materials

Semiquinone radicals such as the organic acceptors $[TCNQ]^{-\bullet}$ (7,7,8,8-tetracyanoquinodimethanide), and DCNQI's (N,N'-dicyanoquinonediimides) have recently been employed as bridges via σ-coordination to metal centers

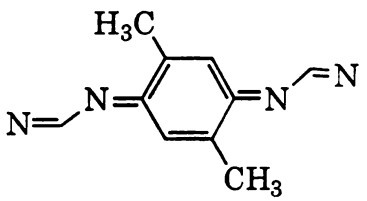

DM-DCNQI

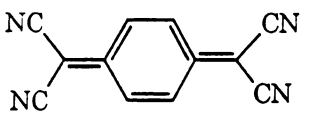

TCNQ

through the nitrile groups. Although it has been almost nearly four decades since researchers at Dupont discovered that products of general formula M(TCNQ) and $M(TCNQ)_2$ can be isolated,[47] it has not been until recently that structures of these materials have been elucidated in our laboratories.[48] A related compound, $Cu(DM\text{-}DCNQI)_2$, is a three-dimensional network solid that exhibits unusually high conductivities that persist even at low temperatures.[49] Another organic acceptor, TCNE (tetracyanoethene) was shown by Miller *et. al.* to form a room temperature ferromagnet formulated as $V(TCNE)_2 \cdot 1/2(CH_2Cl_2)$.[50] The direct coordination of organic radicals and metal ions offers the potential for achieving new pathways for electronic coupling through pπ-dπ overlap in addition to the usual pπ overlap found in

organic donor/acceptor salts. It has been proposed that with the proper energy match of metal and organic orbitals, it may be possible to achieve an interplay between superexchange and charge-transport pathways, perhaps even leading to a synergistic state wherein superconductivity and ferromagnetism co-exist.[51]

(2) Derivative Chemistry of the Organic Donor, Tetrathiafulvalene

Another approach to preparing materials with paramagnetic metal centers in the same structural framework as open-shell π-organic radical cations is the formation of salts from organic donors and high-moment metal cluster anions. The most widely used organic donors are derivatives of tetrathiafulvalene (TTF). Since its synthesis in 1970, TTF and its derivatives have played a key role in the preparation of conducting and superconducting charge-transfer complexes.[52] One example of their use in hybrid inorganic/organic systems is their incorporation into salts with polychalcogenide, halide and mixed chalcogenide/halide cluster anions of Re. The clusters exhibit remarkable variations in properties, differences that have been attributed to changes in the size, shape and redox properties of the organic donor and inorganic acceptors.[53]

Tetrathiafulvalene contains four sulfur atoms that participate in the molecule's π-system. The molecule readily undergoes a one-electron oxidation to form a stable radical cation which packs in parallel stacks with extended π-overlap occurring above and below the molecular planes through

ynthesis of
charge-tra
minimum
unaccepto
lunar cry
ith Orbm
epared m
rmen stab
ibrator
mum of eq
mem the d
epared sta
ther* Th
conductiv
epared st
ermon be
ilize and
In atte
ed to us
easement
Rademach
ncreased

p_z orbitals.[54] The electrons in these systems are delocalized, thereby allowing for charge-transport along the stack, but allowing only a minimum of inter-stack communication. Cowan *et al.* first reported the synthesis of the organic donor-acceptor salt, TTF-TCNQ in 1973.[55] The salt was the first example of a molecular crystal exhibiting metallic conductivity (σ_{RT} = ~500 $\Omega^{-1}cm^{-1}$,[54] σ_{max} = 10^4 $\Omega^{-1}cm^{-1}$ at 66 K[55]). The TTF-TCNQ salt forms one-dimensional segregated molecular stacks with intermolecular S···S contacts of 3.47 Å between stacked TTF cations, as opposed to 3.62 Å for the neutral molecule.[56,57] This stacking phenomenon is an important factor in the formation of conducting solids and can occur one of two ways: in mixed stacks wherein the donors and acceptors stack alternatively within a given stack, or segregated stacks where donors and acceptors stack independently of one another.[58] The majority of molecular compounds with mixed stacks are not very conductive because of electron localization on the acceptor species, but segregated stacks such as TTF-TCNQ exhibit a strong charge-transfer interaction between stacked molecules causing the unpaired electrons to delocalize and enhance the conduction in that direction.

In attempts to improve the conductivity of TTF salts, researchers have turned to using derivatives of TTF.[59] Early modifications involved the replacement of sulfur atoms with larger selenium atoms to make tetraselenathiafulvalene, TSF.[60] The more diffuse orbitals of selenium leads to increased stacking interactions for the TSF-TCNQ and a two-fold increase

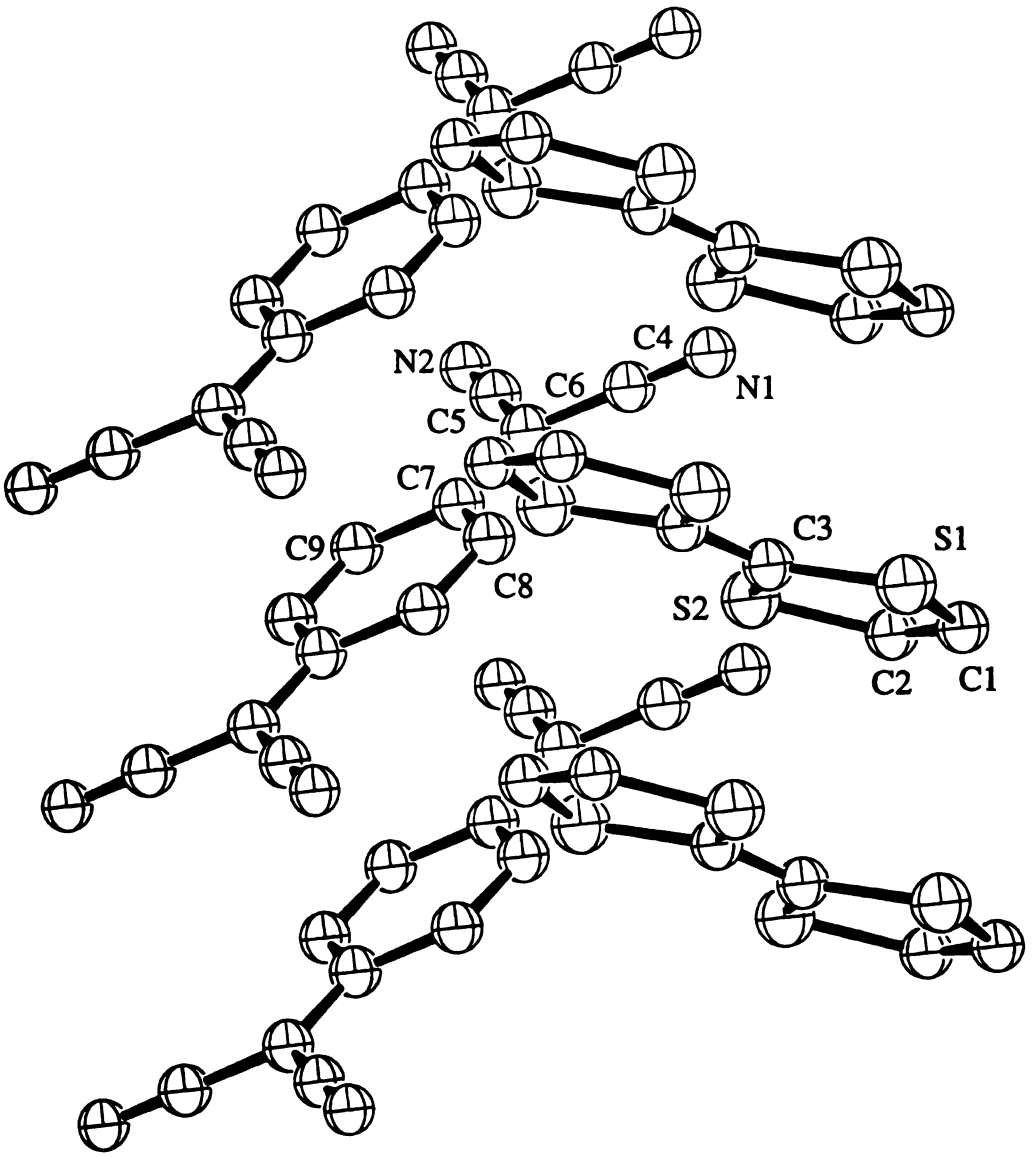

Figure 5. ORTEP representation of the stacked salt, [TTF][TCNQ].

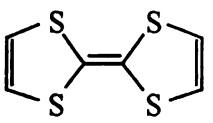

TTF

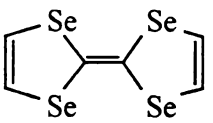

TSF

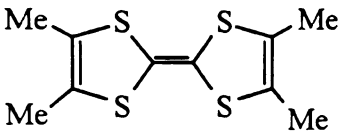

TMTTF

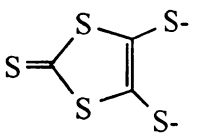

DMIT

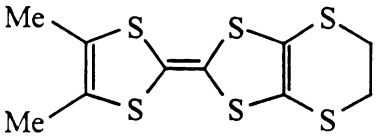

DMET

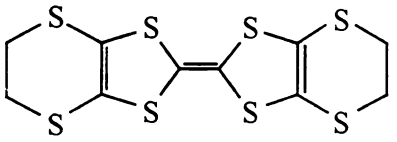

BEDT-TTF

in the electrical conductivity. Bechgaard and co-workers advanced this notion further by preparing tetramethylselenafulvalene (TMTSF).[61] At lowtemperatures (~1 K) and high pressure (8-10 kbar), salts (now known as "Bechgaard salts") of $[TMTSF]^+$ with monovalent inorganic anions such as $[PF_6]^-$, $[ReO_4]^-$, and $[BF_4]^-$ were found to be the first molecular organic compounds to behave as superconductors. $[TMTSF]_2[ClO_4]$ is the first example of a superconducting material (T_c = 1.3 K) at ambient pressure.[62] More recently, salts of $[BEDT\text{-}TTF]^+$ have been found to be superconducting at much higher temperatures (10-11 K).[63]

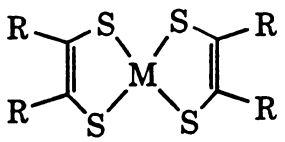

Classic Metal Dithiolate

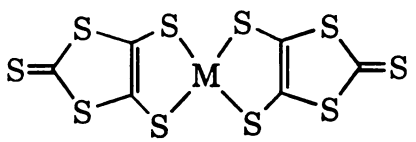

Classic Metal "DMIT"

Early work by Interrante, Miller and Epstein on the use of bisdithiolenes for the development of electronic materials paved the way for TTF derivatives to be used as ligands.[64] While most bisdithiolenes are semiconductors, some salts such as [TTF][Ni(dmit)$_2$]$_2$ have been found to exhibit metallic behavior down to 4 K,[65] while other M(dmit)$_2$ salts have been found to be superconductors under pressure.[66] More recently, Underhill and co-workers prepared homoleptic Hg^{II} and Ni^{II} complexes with *cis*-[S$_2$TTF(SR)$_2$]$^{n-}$ (n = 0, 2) units that are involved in intermolecular stacking at c.a. 3.4 Å and S···S contacts of 3.51(2) Å.[67] Related work by McCullough and Belot led to the preparation of homoleptic tetrathiafulvalene-tetrathiolate complexes with TiCp$_2$, TiCp$_2$*, and Pt(PPh$_3$)$_2$,[68] wherein the tetradentate ligand bridges two metal centers to yield dinuclear species. These dinuclear compounds are reminiscent of extended structures proposed by Hoffman *et. al.* in 1985,[69] who suggested that the ribbons, stacked, two-dimensional layers, and zig-zag layers shown in Figure 6 would make for very interesting properties. The unfortunate reality of these structures is that, in all likelihood, they will produce insoluble products that would pose serious characterization problems.[70]

D. The Development of Phosphine-Fuctionalized Tetrathia-fulvalenes

Much of the research being conducted in the field of TTF-metal coordination chemistry involves TTF-sulfur derivatives, but it is attractive to

ure 6.

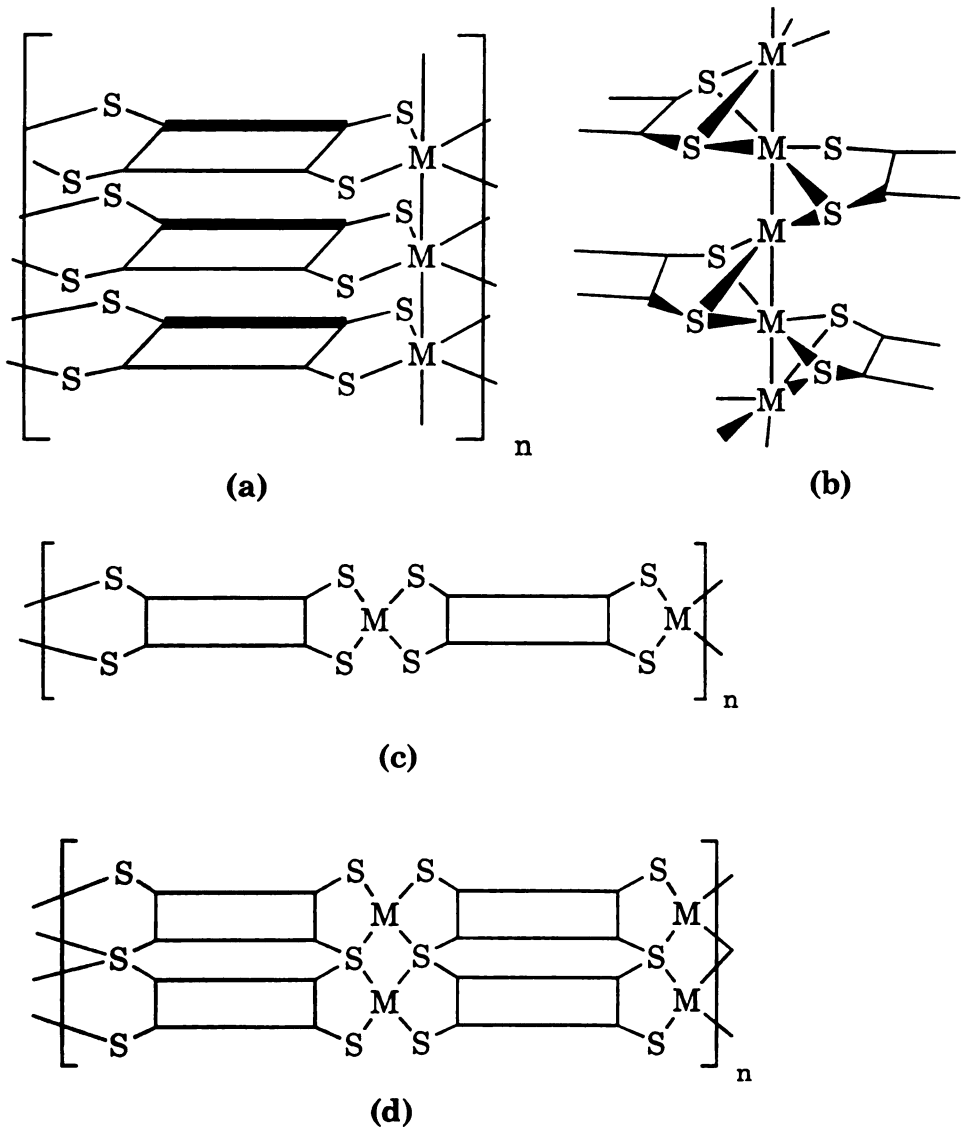

Figure 6. Extended structures proposed by Hoffman *et. al.*: (a) two dimensional slab structure, (b) zig-zag layered structure, (c) ribbon or sheet polymers, and (d) two-dimensional layer structure.

consider the potential for incorporating *non-chalcogenide* linking groups. Inconsidering candidates for functional groups it is important to retain the redox functionality of the TTF, but to include the capability for engendering strong metal-ligand interactions through chelation. The tetrathiafulvalene-based phosphorus ligands depicted in Figure 7 fit these criteria quite well. The groups of Batail and Fourmigué *et al.*, first demonstrated in 1992 that the molecules 3,4-dimethyl-3',4'-bis(diphenylphosphino)tetrathiafulvalene (*o*-P2) and tetrakis(diphenyl-phosphino)tetrathiafulvalene (P4) can be synthesized from the appropriate TTF precursors.[71] More recently the *E* and *Z* isomers of the diphosphine ligand were also prepared.[72] These ligands are similar to the ethylene-bridged ligands bis(diphenylphospohino)ethene (dppee) and -benzene (dppb).

The availability of monodentate (P1), bidentate (P2) and tetradentate (P4) ligands allows for a wide range of structural possibilities. In order to be able to build polymeric structures two ingredients are required: (i) a bridging diphosphine or tetraphosphine, and (ii) a metal center capable of coordinating two phosphines or two diphosphine ligands. The *E*-P2 or P4 ligands meet these ligand requirements. The chelating ability of the TTF diphosphines was first demonstrated by the isolation of NiX_2(*o*-P2) (X = Cl, Br).[71a] More recently the structure of the homoleptic phosphine cation $[Rh(o\text{-}P2)_2]^+$ was determined as its $[BF_4]^-$.[72]

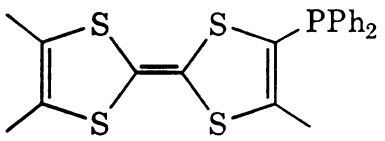

P1

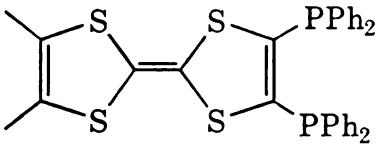

***o*-P2**

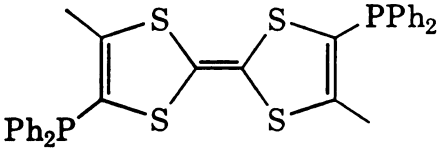

***E*-P2**

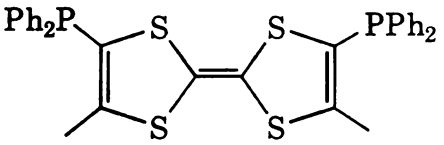

***Z*-P2**

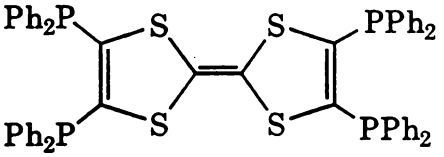

P4

Figure 7. Schematics of the monodentate (P1), bidentate (*o*-P2, *E*-P2, *Z*-P2), and tetradentate (P4) phosphine ligands.

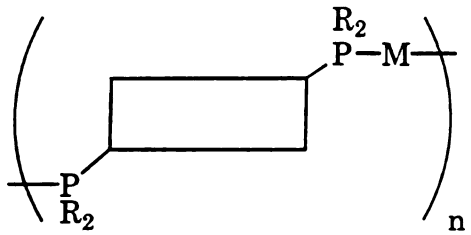

E- P2

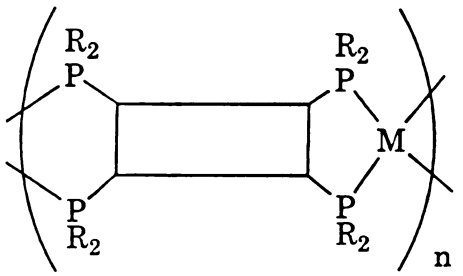

P4

Chapter III of this thesis reports the synthesis and characterization of a series of mononuclear o-P2 complexes of formula $[M(o\text{-}P2)_2][BF_4]_2$ (M = Ni, Co, Pd, Pt, Fe). These complexes serve as models for the extended molecules that contain the tetradentate ligand, P4. Oxidation of the previously reported $[Rh(o\text{-}P2)_2][BF_4]$ to $[Rh(o\text{-}P2)_2][BF_4]_3$, and metathesis of $[Rh(o\text{-}P2)_2][BF_4]$ with LiTCNQ are also described. Chapter IV details the reactivity of the TTF-phosphine ligand with metal-metal bonded compounds. The similarities between these new phosphines and the well-known diphos ligand (dppe) render them attractive candidates for exploiting their ability to act as both chelating and bridging ligands. Reactivity of *o*-P2 with $[Re_2Cl_8]^{2-}$ results in the formation of a mixed-nuclearity salt, $[ReCl_2(o\text{-}P2)_2][Re_2Cl_6(o\text{-}P2)]$, which includes the first example of an α-M_2X_6(L-L) complex, where α is the chelating mode. The chemistry of *o*-P2 is further described in Chapter V, where the stepwise build-up of extended arrays is outlined. The use of *cis*-MCl_2 moieties with *o*-P2 and P4 ligands allows for the preparation of mono- and dinuclear metal complexes that contain one, two, or three TTF units. The use of the tetradentate P4 complex to form high nuclearity extended

materials is reported in Chapter VI. reaction of the solvated cations, $[Rh_2(NCCH_3)_{10}][BF_4]_4$ and $[M(NCCH_3)_n][BF_4]_2$ (M = Pt, n = 4; M = Ni, Co, Pd, Fe, n = 6) led to the formation of phosphine bound complexes formulated as $[M(P4)]_n[BF_4]_{2n}$ for M = Ni, Co, Pd, Pt, Fe and $[M(P4)]_n[BF_4]_n$ for M = Rh. These products are highly soluble and do not exhibit $^{31}P\{^1H\}$ NMR spectral properties expected for straight chain oligomers.[40] Various experiments designed to elucidate the identity of these complexes are discussed.

List of References

1. (a) Stelzer, O. In *Topics in Phosphorus Chemistry*, Eds. Grayson, M.; Griffith, E. J. Wiley & Sons: New York, **1980**, *10*, 193. (b) Fluck, E. In *Topics in Phosphorus Chemistry*, Eds. Grayson, M.; Griffith, E. J. Wiley & Sons: New York, **1977**, *9*, 1. (c) *Homogeneous Catalysis with Metal Phosphine Complexes*, Ed. Pignolet, L. H. Plenum Press: New York, **1983**.

2. a) Parshall, G. W. *Homogeneous Catalysis: The Applications and Chemistry of Catalysis by Soluble Transition Metal Complexes*; Wiley: New York, **1980**. (b) Cornils, B. In *New Syntheses with Carbon Monoxide*; Falbe, J., ed.; Springer-Verlag: Berlin, **1980**. (c) *Catalytic Aspects of Metal Phosphine Complexes, Advances in Chemistry Series 196*; Alyea, E. C.; Meek, D. W. Eds.; American Chemical Society: Washington, D. C. **1982**. (d) Hughes, R. P. in *Comprehensive Organometallic Chemistry*; Wilkinson, G.; Stone, F. G. A.; Abel, E. W., eds.; Pergamon: New York, **1982**; vol. 5, p 228.

3. Collman, J. P.; Hegedus, L. S.; Norton, J. R.; Finke, R. G. *Principles and Applications of Organotransition Metal Chemistry*; University Science Books: Mill Valley, Ca. **1987**, and references therein.

4. McAuliffe, C. A. In *Comprehensive Coordination Chemistry;* Wilkinson, G.; Gillard, R. D.; McCleverty, J. A., eds.; Pergamon: Oxford, **1987**, chapter 14, p 989.

5. (a) Cruickshank, D. W. J. *J. Mol. Struct.*, **1985**, *130*, 1771. (b) Beach, D. B.; Jolly, W. L. *Inorg. Chem.* **1984**, *23*, 4774.

6. Kubas, G. *J. Acc. Chem. Res.* **1988**, *12*,120.

7. Kubas, G. J.; Unker, C. J.; Swanson, B. F.; Fukushima, E. *J. Am. Chem. Soc.* **1986**, *108*, 7000.

8. (a) Lindner, E.; Reber, J. P.; Wegner, P. *Z. Naturforsch.* **1988**, *43b*, 1268. (b) Lindner, E.; Sickinger, A.; Wegner, P. *J. Organomet. Chem.* **1988**, *349*, 75. (c) Lindner, E.; Schrober, U.; Glaser, E.; Norz, H.; Wegner, P. *Z. Naturforsch.* **1987**, *42b*, 1527. (d) Lindner, E.; Mayer, H. A.; Wegner, P. *Chem. Ber.***1986**, *119*, 2616. (e) Lindner, E.; Sickinger, A.; Wegner, P. *J. Organomet. Chem.* **1986**, *312*, C37. (f) Lindner, E.; Raudeler, H ; Scheytt, C.; Mayer, H. A.; Hiller, W.; Fawzi, R.; Wegner, P. *Z. Naturforsch.* **1984**, *39b*, 632. (g) Lindner, E.; Scheytt, C. *Z. Naturforsch.* **1986**, *41b*, 10. (h) Lindner, E.; Scheytt, C.; Wegner, P. *J.*

Organomet. Chem. **1986**, *308*, 311. (i) Lindner, E.; Fawzi, R.; Mayer, H. A.; Eichele, K.; Pohmer, K. *J. Organomet. Chem.* **1990**, *386*, 63. (j) Lindner, E.; Schober, U.; Fawzi, R.; Hiller, W.; Englert, U.; Wegner, P. *Chem. Ber.* **1987**, *120*, 1621. (k) Lindner, E.; Karle, B. *Chem. Ber.* **1990**,*123*, 1464. (l) Lindner, E.; Karle, B. *Z. Naturforsch.* **1990**, *45b*, 1108. (m) Lindner, E.; Schober, U. *Inorg. Chem.* **1988**, *27*, 212. (n) Lindner, E.; Andres, B. *Chem. Ber.* **1987**, *120*, 761. (o) Lindner, E.; Andres, B. *Chem. Ber.* **1988**, *121*, 829. (p) Lindner, E.; Norz, H. *Chem. Ber.* **1990**, *123*, 459. (q) Lindner, E.; Norz, H. *Z. Naturforsch.* **1989**, *44b*, 1493. (r) Lindner, E.; Meyer, S. *J. Organomet. Chem.* **1988**, *339*, 193. (s) Lindner, E.; Andres, B. *Z. Naturforsch.* **1988**, *43b*, 369. (t) Lindner, E.; Speidel, R. *Z. Naturforsch.* **1989**, *44b*, 437. (u) Bader, A.; Lindner, E. *Coord. Chem. Rev.* **1991**, *108*, 27. (v) Lindner, E.; Rothfuß, H.; Fawzi, R.; Hiller, W. *Chem. Ber.* **1992**, *125*, 541. (w) Lindner, E.; Bader, A.; Mayer, H. A. *Z. Anorg. Allg. Chem.* **1991**, *598/599*, 235. (x) Lindner, E.; Dettinger, J.; Möckel, A. *Z. Naturforsch.* **1991**, *46b*, 1519. (y) Lindner, E.; Scheiber, R.; Kemmler, M.; Mayer, H. A.; Fawzi, R.; Steimann, M. *Anorg. Allg. Chem.* **1993**, *619*, 202. (z) Lindner, E.; Schreiber, R.; Kemmler, Schneller, T.; Mayer, H. A. *Chem. Mater.*, **1995**, *7*, 951. (aa) Lindner, E.; Haustein, M.; Mayer, H. A.; Gierling, K.; Fawzi, R.; Steimann, M. *Organometallics*, **1995**, *14*, 2246. (bb) Lindner, Kemmler, M.; Schneller, T.; Mayer, H. A. *Inorg. Chem.*, **1995**, *34*, 5489, (cc) Lindner, E.; Geprags, M.; Gierling, K.; Fawzi, R.; Steimann, M. *Inorg. Chem.*, **1995**, *34*, 6106. (dd) Lindner, E.; Schreiber, R.; Schneller, T.; Wegner, P.; Mayer, H. A.; Gopel, W.; Ziegler, C. *Inorg. Chem.*, **1996**, *35*, 514. (ee) Lindner, E.; Pautz, S.; Haustein, M. *J. Organomet. Chem.*, **1996**, *509*, 215. (ff) Lindner, E.; Keppeler, B.; Mayer, H. A.; Gierling, K. *J. Organomet. Chem.*, **1996**, *515*, 139. (gg) Lindner, E.; Yin, Y. C.; Geprags, M; Yih, K. H.; Fawzi, R.; Steimann, M. *J. Organomet. Chem.*, **1996**, *512*, 101. (hh) Lindner, E.; Pautz, S.; Haustein, M. *Coord. Chem. Rev.*, **1996**, *155*, 145. (ii) Lindner, E.; Keppler, B.; Mayer, H. A.; Gierling, K.; Fawzi, R.;, Steimann, M. *J. Organomet. Chem.*, **1996**, *526*, 175. (jj) Lindner, E.; Jager, A.; Schneller, T; Mayer, H. A. *Chem Mater.*, **1997**, *9*, 81. (kk) Lindner, E.; Jager, A.; Kemmler, M.; Auer, F.; Wegner, P.; Mayer, H. A.; Benez, A; Piles, E. *Inorg. Chem.*, **1997**, *36*, 862. (ll) Lindner, E.; Keppeler, B.; Wegner, P. *Inorg. Chim. Acta* **1997**, *258*, 97. (mm) Lindner, E.; Schneller, T.; Mayer, H. A.; Bertagnolli, H.; Ertel, T. S.; Horner, W. *Chem. Mater.*, **1997**, *9*, 1524. (nn) Lindner, E.; Gierling, K.; Keppeler, B.; Mayer, H. A. *Organometallics*, **1997**, *16*, 3531. (oo) Lindner, E.; Gierling, K.; Fawzi, R.; Steimann, M. *Inorg. Chim. Acta*, **1998**, *269*, 13. (pp) Lindner, E.; Jager, A.; Auer, F.; Wegner, P.; Mayer, H. A.; Benez, A.; Adam, D.; Plies, E. *Chem. Mater.*, **1998**, *10*, 217.

9. (a) Anderson, G. K.; Kumar, R. *Inorg. Chem.* **1984**, *23*, 4064. (b) Anderson, G. K.; Corey, E. R.; Kumar, R. *Inorg. Chem.* **1987**, *26*, 97. (c) Anderson, G. K.; Kumar, R. *Inorg. Chim. Acta* **1988**, *146*, 89. (d) Anderson, G. K.; Lumetta, G. J.; Siria, J. W. *Organomet. Chem.* **1992**, *434*, 253.

10. (a) Rauchfuss, T. B.; Patino, F. T.; Roundhill, D. M. *Inorg. Chem.* **1975**, *14*, 652. (b) Jeffrey, J. C; Rauchfuss, T. B. *Inorg. Chem.* **1979**, *18*, 2658.

11. (a) Mason, R.; Thomas, K. M.; Empsall, H. D.; Fletcher, S. R.; Heys, P. N.; Hyde, E. M.; Jones, C. E.; Shaw, B. L. *J. Chem. Soc., Chem. Commun.* **1974**, 612. (b) Jones, C. E.; Shaw, B. L.; Turtle, B. L. *J. Chem. Soc., Dalton Trans.* **1974**, 992. (c) Empsall, H. D.; Heys, P. N.; Shaw, B. L. *J. Chem. Soc., Dalton Trans.* **1978**, 257.

12. (a)Keim, W. *Chem. Ing. Techn.* **1984**, *56*, 850. (b) Reber, J. -P., Ph. D. Dissertation, Universität Tübingen, **1991**. (c) Knowles, W. S. *Acc. Chem. Res.* **1983**, *16*, 106. (d) Brunner, H. *Angew. Chem. Int, Ed. Engl.* **1983**, *22*, 897. (e) Brown, J. M.; Cook, S. J.; Khan, R. *Tetrahedron* **1986**, *42*, 5105.

13. (a) Andrieu, J.; Braunstein, P.; Tiripicchio, A.; Ugozzoli, F. *Inorg. Chem.*, **1996**, *35*, 5975. (b) Braunstein, P.; Kelley, D. G.; Tiripicchio, A.; Ugozzoli, F. *Inorg. Chem.*, **1993**, *32*, 4845. (c) Braunstein, P.; Kelley, D. G.; Dusausoy, Y.; Bayeul, D.; Lanfranchi, M.; Tiripicchio, A. *Inorg. Chem.*, **1994**, *32*, 233. (d) Andrieu, J.; Braunstein, P.; Drillon, M.; Dusausoy, Y.; Ingold, F.; Rabu, P.; Tiripicchio, A.; Ugozzoli, F. *Inorg. Chem.*, **1996**, *35*, 5986.

14. (a) Nicholson, T.; Cook, J.; Davison, A.; Jones, A. G. *Inorg. Chim. Acta* **1994**, *218*, 97. (b) Chatt, J.; Dilworth, J. R.; Schmutz, J. A.; Zubieta, J. A. *J. Chem. Soc., Dalton Trans.* **1979**, 1595. (c) Geigy, J. R., F. P. 1,401,930/1965.

15. (a) Fryzuk, M. D.; Montgomery, C. D. *Coord. Chem. Rev.* **1989**, *95*, 1. (b) Farnetti, E.; Nardin, G.; Granziani, M. *J. Organomet. Chem.*, **1991**, *417*, 163. (c) Park, S.; Hedden, DD.; Roundhill, D. M. *Organometallics*, **1986**, *5*, 336.

16. Harborn, S. K.; Higgins, S. J.; Hope, E. G.; Kemmitt, T.; Levanson, W. *Inorg. Chim. Acta* **1987**, *130*, 43.

17. (a) Meek, D. W.; Nicpon, P. E.; Meek, V. I. *J. Am. Chem. Soc.* **1970**, *92*, 5351. (b) Nicpon, P.; Meek, D. W. *Inorg. Chem.* **1967**, *6*, 145.

18. Gysling, H. J.; Luss, H. R. *Organometallics*, **1984**, *3*, 596.

19. Cotton, F. A.; Hong, B. *Prog. Inorg. Chem.*, **1992**, *40*, 179.

20. Cotton, F. A.; Walton, R. A. *Multiple Bonds Between Metal Atoms, 2nd Ed.*, Clarendon Press: Oxford, **1993**, and references therein.

21. Puddephatt, R. J. *Chem. Soc. Rev.* **1983**, 99.

22. (a) Higgins, S. J.; Levanson, W. J. *J. Chem. Soc., Dalton Trans.* **1986**, 317. (b) Gray, L. R.; Higgins, S. J.; Levanson, W. J.; Webster, M. J. *J. Chem. Soc., Dalton Trans.* **1984**, 1433. (c) Fox, M. A.; Chaudler, D. A. *NATO ASI Ser. C.* **1987**, *214*, 405. (d) Gray, L. R.; Gulliver, D. J.; Levanson, W. J.; Webster, M. J. *J. Chem. Soc., Dalton Trans.* **1983**, 133. (e) Warren, L. F.; Bennett, M. A. *Inorg. Chem.* **1976**, *15*, 3126.

23. (a) Mahadevan, C.; Seshasayee, M.; Ramakrishna, B. L.; Manoharon, P. T. *Acta Crystallogr., Sect. C* **1985**, *41*, 38. (b) Bennett, M. A.; Robertson, G. B.; Rosalky, J. M.; Warren, L. F. *Acta Crystallogr., Sect. A* **1975**, *31*, S136.

24. (a) Oberhauser, W.; Bachmann, C.; Brüggeller, P. *Inorg. Chim. Acta* **1995**, *238*, 35. (b) Miedaner, A.; Haltiwanger, R. C.; DuBois, D. L. *Inorg. Chem.* **1991**, *30*, 417. (c) Liu, S.-T.; Chen, J.-T.; Peng, S.-M.; Hsiao, Y.-L.; Cheng, M.-C. *Inorg. Chem.* **1990**, *29*, 1169. (d) Brown, J. M.; Guiry, P. J. *Inorg. Chim. Acta*, **1994**, *220*, 249.

25. Housecroft, C. E.; Owen, S. M.; Raithby, P. R.; Shaykh, A. M. *Organometallics*, **1990**, *9*, 1617.

26. Butler, I. R.; Cullen, W. R.; Kim, T.-J.; Rettig, S. J.; Trotter, J. *Organometallics*, **1985**, *4*, 972.

27. Smith, C. M.; Aplin, R. T.; Brown, J. M.; Hursthouse, M. B.; Karalulov, A. I.; Abul Malik, K. M.; Cooley, N. A. *J. Am. Chem. Soc.* **1994**, *116*, 5180.

28. Sekino, M.; Sato, M.; Nagasawa, A.; Kikuchi, K. *Organometallics*, **1994**, *13*, 1451.

29. Pilloni, G.; Longato, B.; Corain, B. *J. Organomet. Chem.* **1991**, *420*, 57.

30. (a) Hayashi, T.; Konishi, M.; Kobari, Y.; Kumada, <.; Higuchi, T.; Hirotsu, K. *J. Am. Chem. Soc.* **1984**, *106*, 158. (b) Cullen, W. R.; Kim, T.; Einstein, F. W. B.; Jones, T. *Organometallics*, **1985**, *4*, 346. (c) Butler, I. R.; Cullen, W. R.; Kim, T.; Rettig, S. J.; Trotter, J. *Organometallics*, **1985**, *4*, 972. (d) Onaka, S. *Bull. Chem. Soc. Jpn.* **1986**, *59*, 2359. (e) Miller, T. M.; Kazi, J. A.; Wrighton, M. S. *Inorg. Chem.*, **1989**, *28*, 2347. (f) Hill, D. T.; Girard, G. R.; McCabe, F. L.; Johnson, R. K.; Stupik, P. D.; Zhang,. H.; Reiff, W. M.; Eggleston, D. S. *Inorg. Chem.*, **1989**, *28*, 3529. (g) Casellato, U.; Corain, R.; Graiani, R.; Longato, B.; Pilloni, G. *Inorg. Chem.*, **1990**, *29*, 1193. (h) Longato, B.; Pilloni, G.; Graziani, R.; Casellato, U. *J. Organomet. Chem.*, **1991**, *407*, 369. (i) Pilloni, G.; Graziani, R.; Longato, B.; Corain, B. *Inorg. Chim. Acta*, **1991**, *190*, 165. (j) Pilloni, G.; Longato, B. *Inorg. Chim. Acta*, **1993**, *208*, 17.

31. (a) Dunbar, K. R.; Haefner, S. C.; Pence, L. E. *J. Am. Chem. Soc.* **1989**, *111*, 5504. (b) Dunbar, K. R.; Haefner, S. C.; Bender, C. *J. Am. Chem. Soc.* **1991**, *113*, 9540. (c) Dunbar, K. R.; Haefner, S. C.; Swepston, P. N. *J. Chem. Soc., Chem. Commun.* **1991**, 640. (d) Chen, S.-J.; Dunbar, K. R. *Inorg. Chem.*, **1991**, *30*, 2918. (e) Dunbar, K. R.; Haefner, S. C. *Organometallics* **1992**, *11*, 0000. (f) Dulebohn, J. I.; Haefner, S. C.; Bergland, K. A.; Dunbar, K. R. *Chem. of Mat.*, **1992**, *4*, 506. (g) Dunbar, K. R.; Quillevéré, A. *Organometallics*, **1993**, *12*, 618. (h) Dunbar, K. R.; Matonic, J. H.; Saharan, V. *Inorg. Chem.*, **1994**, *33*, 25. (i) Dunbar, K. R.; Quillevéré, A.; Sun, J.-S. *Inorg. Chem.*, **1994**, *33*, 2598. (j) Dunbar, K. R.; Sun, J.-S. *J. Chem. Soc. Chem. Comm.*, **1994**, *2387*. (k) Dunbar, K. R.; Haefner, S. C.; Uzelmeier, C. E.; Howard, A. *Inorg. Chim. Acta.*, **1995**, *240*, 527.

32. (a) Protopopov, I. S.; Kraft, M. Ya. *Med. Prom. USSR* **1959**, *13*,5. (b) Protopopov, I. S.; Kraft, M. Ya. *Zhurnal Obshchei Khimii* **1963**, *33*, 3050. (c) Wada, M.; Higashizaki, S. *J. Chem. Soc., Chem. Commun.* **1984**, 482. (d) Wada, M. *J. Chem. Res.* **1985**, (S), 38; (M), 0467.

33. (a) Dunbar, K. R.; Haefner, S. C. *Polyhedron*, **1994**, *13*, 727.

34. (a) Osborn, J. A.; Jardine, F. H.; Wilkinson, G. *J. Chem. Soc. (A)* **1966**, 1712. (b) Taqui-Khan, M. M.; Samad, S. A.; Siddiqui, M. R. H.; Bajaj, H. C.; Ramachandraiah, G. *Polyhedron* **1991**, *10*, 2729. (c) Howe, J. P.; Lung, R.; Nile, T. A. *J. Organomet. Chem.* **1981**, *208*, 401.

35. (a) Braunstein, P.; Matt, D.; Dusausoy, Y.; Fischer, J.; Miyschler, A.; Ricard, L. *J. Am. Chem. Soc.* **1981**, *103*, 5115. (b) Braunstein, P.; Matt, D.; Nobel, D. *Chem. Rev.*, **1988**, *88*, 747. (c) Bouaoud, S.-E.; Braunstein, P.; Grandjean, D; Matt, D.; Nobel, D. *J. Chem. Soc., Chem.*

Commun. **1987**, 488. (d) Bouaoud, S.-E.; Braunstein, P.; Grandjean, D; Matt, D.; Nobel, D. *Inorg. Chem.* **1988**, *27*, 2279. (e) Braunstein, P.; Nobel, D. *Chem. Rev.* **1989**, *89*, 1927. (f) Balegroune, F.; Braunstein, P.; Gomes Carneiro, T. M.; Grandjean, D.; Matt, D. *J. Che. Soc., Chem. Commun.* **1989**, 582. (g) Braunstein, P.; Gomes Carneiro, T. M.; Balegroune, F.; Grandjean, D. *Organometallics*, **1989**, *8*, 1737.

36. (a) Manriquez, J. M.; Yee, G. T.; McLean, S.; Epstein, A. J.; Miller, J. S. *Science* **1991**, *252*, 1415-1417. (b) Pei, Y.; Kahn, O.; Nakatani, K.; Codjovi, E.; Mathonière, C.; Sletten, J. *J. Am. Chem. Soc.* **1991**, *113*, 6558-6564. (c) Cornelissen, J. P.; LeLoux, R.; Jansen, J.; Haasnoot, J.G.; Reedijk, J.; Horn, E.; Spek, A.L.; Pomarède, B.; Legros, J.; Reefman, D. *J. Chem. Soc. Dalton Trans.* **1992**, 2911-2921. (d) Serroni, S.; Denti, G.; Campagna, S.; Juris, A.; Ciano, M.; Balzani, V. *Angew. Chem. Int. Ed. Engl.* **1992**, *31*, 1493-1495. (e) Kollmar, C.; Kahn, O. *Acc. Chem. Res.* **1993**, *26* , 259-265. (f) Miller, J.; Epstein, A. *Angew. Chem. Int. Ed. Engl.* **1994**, *33*, 385-415. (g) *Molecular Magnetism*, Kahn, O. VCH, **1993**. (h) Pomarède, B.; Garreau, B.; Malfant, I.; Valade, L.; Cassoux, P.; Legros, J.; Audouard, A.; Brossard, L.; Ulmet, J.; Doublet, M.; Canadell, E. *Inorg. Chem.* **1994**, *33*, 3401-3414. (i) Stumpf, H. O.; Pei, Y.: Michaut, C.; Kahn, O.; Renard, J.; Ouahab, L. *Chem. of Mater.* **1994**, *6*, 257-259. (j) Miller, J.; Epstein, A. *Angew. Chem. Int. Ed. Engl.* **1994**, *33*, 385-415.

37. (a) Saito, G.S; Kagoshima, S. Eds, *The Physics and Chemistry of Organic Superconductors* Springer: Berlin, **1990**. (b) Wudl, F. *Acc. Chem. Res.* **1984**, *17*, 227-232. (c) Saito, G.S.; Kagoshima, S. Eds, *The Physics and Chemistry of Organic Superconductors*; Springer: Berlin, **1990**. (d) Williams, J. M.; Wang, . H.; Emge, T. J.; Geiser, U.; Beno, M.A.; Leung, P. C. W.; Carlson, K. D.; Thorn, R. J.; Schultz, A. J.; Whangbo, H. H. In *Progress in Inorganic Chemistry* Lippard, S. J.; Ed; Wiley: New York **1987**; *35*, 51-218.

38. (a) Day. P. *Philos. Trans. R. Soc. London Ser., A* **1985**, *A314*, 145. (b) Ogawa, M. Y.; Hoffman, B. M.; Lee, S.; Yudkowsky, M.; Halperin, W. P. *Phys. Rev. Lett.* **1986**, *57*, 1177. (c) Kurmoo, M.; Graham, A. W.; Day, P.; Coles, S. J.; Hursthouse, M. B.; Caulfield, J. L.; Singleton, J.; Pratt, F. L.; Hayes, W.; Ducrtasse, L.; Guionneau, P. *J. Am. Chem. Soc.* **1995**, *117*, 12209.

39. Marks, T. J. *Angew. Chem., Int. Ed. Engl.* **1990**, *29*, 857.

40. Wang, P.-W.; Fox, M. A. *Inorg. Chem.* **1994**, *33*, 2938.

41. Reynolds, J. R.; Lillya, C. P.; Chien, J. C. W. *Macromolecules* **1987**, *20*, 1184.

42. Wrobleski, J. T.; Brown, D. B. *Inorg. Chem.* **1979**, *18*, 2738.

43. Dirk, C. W.; Bousseau, M.; Barrett, P. H.; Moraes, F.; Wudl, F.; Heeger, A. J. *Macromolecules* **1986**, *19*, 266.

44. (a) Nakatani, K.; Bergerat, P.; Codojovi, E.; Mathoniére, C.; Pei, Y.; Kahn, O. *Inorg. Chem.* **1991**, *30*, 3977. (b) van Koningsbruggen, P. J.; Kahn, O.; Nakatani, K.; Pei, Y.; Renard, J. P.; Drillon, M.; Legroll, P. *Inorg. Chem.* **1990**, *29*, 3325. (c) Pei, Y.; Nakatani, K.; Kahn, O.; Sletten, J.; Renard, J. P. *Inorg. Chem.* **1989**, *28*, 3170. (d) Kahn, O.; Pei, Y.; Verdaguer, M.; Renard, J. P.; Sletten, J. *Inorg. Chem.* **1988**, *110*, 782. (e) Lloret, F.; Nakatani, K.; Journaux, Y.; Kahn, O.; Pei, Y.; Renard, J. P. *J. Chem. Soc., Chem. Commun.* **1988**, 642. (f) Pei, Y.; Verdaguer, M.; Kahn, O.; Sletten, J.; Renard, J. P. *Inorg. Chem.* **1987**, *26*, 138.

45. Stumpf, H. O.; Ouahab, L.; Pei, Y.; Grandjean, D.; Kahn, O. *Science* **1993**, *261*, 447.

46. (a) Caneschi, A.; Gatteschi, D.; Renard, J. P.; Rey, P.; Sessoli, R. *Inorg. Chem.* **1989**, *28*, 3314. (b) Caneschi, A.; Gatteschi, D.; Sessoli, R. *Acc. Chem. Res.* **1989**, *22*, 392. (c) Caneschi, A.; Gatteschi, D.; Renard, J. P.; Rey, P.; Sessoli, R. *Inorg. Chem.* **1989**, *28*, 1976. (d) Caneschi, A.; Gatteschi, D.; Rey, P.; Sessoli, R. *Inorg. Chem.* **1988**, *27*, 1756.

47. (a) Middelton, W. J.; Little, E. L.; Coffman, D. D.; Englehardt, V. A. *J. Am. Chem. Soc.*, **1958**, *80*, 2795. (b) Webster, O. W.; Mahler, W.; Benson, R. E. *J. Am. Chem. Soc.*, **1962**, *84*, 3678. (c) Melby, L. R.; Harder, R. J.; Hertler, W. R.; Mahler, W.; Benson, R. E.; Mochel, W. E. *J. Am. Chem. Soc.*, **1962**, *84*, 3374.

48. (a) Zhao, H.; Heintz, R. A.; Rogers, R. D.; Dunbar, K. R. *J. Am. Chem. Soc.*, **1996**, *118*, 12844. (b) Zhao, H.; Cowen, J. A.; Ouyang, X.; Grandinetti, G.; Heintz, R. A.; Dunbar, K. R. manuscript in preparation. (c) Dunbar, K. R.; Heintz, R. A.; Zhao, H.; Ouyang, X.; Rogers, R. D. manuscript in preparation. (d) Ouyang, X., Ph. D. Dissertation, Michigan State University, **1998**.

49. (a) Amüller, A; Hünig, S. *Liebigs Ann. Chem.* **1986**, 142. (b) Sinzger, K.; Hünig, S.; Jopp, M.; Bauer, D.; Bietsch, W.; von Schütz, J. U.; Wolf, H. C.; Kremer, R. K.; Metzenthin, T.; Bau, R.; Khan, S. I.; Lindbaum, A.; Lengauer, C. L.; Tillmanns, E. *J. Am. Chem. Soc.*, **1993**, *115*, 7696.

(c) Kato, R.; Kobayashi, H.; Kobayashi, A. *J. Am. Chem. Soc.*, **1989**, *111*, 5224.

50. Manriquez, J. M.; Yee, G. T.; McLean, R. S.; Epstein, A. J.; Miller, J. S. *Science*, **1991**, *252*, 1415.

51. Dunbar, K. R. *Angew. Chem., Int. Ed. Engl.* **1996**, *35*, 1659.

52. Wudl, F.; Smith, G. M.; Hufnagel, E. J. *J. Chem. Soc., Chem. Commun.* **1970**, 1453.

53. (a) Davidson, A.; Boubekeur, K.; Pénicaud, A.; Auban, P.; Lenoir, C.; Batail, P.; Hervé, G. *J. Chem. Soc. Chem. Commun.* **1989**, 1373-1374. (b) Pénicaud, A.; Boubekeur, K.; Batail, P.; Canadell, E.; Auban-Senzier, P.; Jérome *J. Am. Chem. Soc.* **1993**, *115*, 4101-4112. (c) Coulon, C.; Livage, C.; Gonzalvez, L.; Boubekeur, K.; Batail, P. *J. Phys. I France* **1993**, *3*, 1. (d) Coronado, E.; Gómez-Garcia, C. J. *Comments Inorg.Chem.*, **1995**, *17*, 255. (e) Gómez-Garcia, C. J.; Giménez-Saiz, Triki, S.; Coronado, E.; Magueres, P. L.; Ouahab, L.; Ducasse, L.; Sourisseau, C.; Delhaes, P. *Inorg, Chem.*, **1995**, *34*, 4139.

54. Ferraro, J. R.; Williams, J. M. *Introduction to Synthetic Electric Materials*. Academic Press: Orlando, Florida, **1987**.

55. (a) Ferraris, J.; Cowan, D. O.; Walatka, V. V.; Perstein, J. H. *J. Am. Chem. Soc.* **1973**, *95*, 948. (b) Coleman, L. B.; Cohen, M. J.; Sandman, D. J.; Yamagishi, F. G.; Garito, A. F.; Heeger, A. J. *Solid State Commun.* **1973**, *12*, 1135.

56. Kistenmacher, T. J.; Phillips, T. E.; Cowan, D. O. *Acta. Cryst., B* **1974**, *B30*, 763.

57. Phillips, T. E.; Kistenmacher, T. J.; Ferris, J. P.; Cowan, D. O. *Chem. Commun.* **1973**, 471.

58. Torrance, J. B. *Mol. Cryst. Liq. Cryst.* **1985**, *126*, 55.

59. (a) Becker, J. Y., In *International Symposium on New Organic Materials*, Seoane, C.; Martin, N., Organizers, **1994**, 37. (b) Rovira, C.; Veciana, J.; Tarrés, J.; Santaló, In *International Symposium on New Organic Materials*, Seoane, C.; Martin, N., Organizers, **1994**, 58. (c) Garín, J., In *International Symposium on New Organic Materials*, Seoane, C.; Martin, N., Organizers, **1994**, 72.

60. Engler, W.; Patel, V. V. *J. Am. Chem. Soc.*, **1974**, *96*, 7376.

61. Bechgaard, K.; Jacobsen, C. S.; Anderson, N. H. *Solid State Commun.* **1980**, *25*, 875.

62. Bechgaard, K.; Carneiro, K.; Rasmussen, F. B.; Olsen, H.; Rindorf, G. Jacobsen, C. S.; Pederson, H.; Scott, J. E. *J. Am. Chem. Soc.* **1981**, *103*, 2440.

63. (a) Williams, J. M.; Beno, M. A.; Wang, H. H.; Leung, P. C. W.; Emge, Y. J.; Geiser, U.; Carlson, K. D. *Acc. Chem. Res.*, **1985**, *18*, 261. (b) Urayama, H.; Yamochi, H.; Sato, G.; Nozawa, K.; Sugano, T.; Kinoshita, M.; Osgima, K.; Kawamoto, A.; Tanaka, J. *Chem. Lett.* **1988**, 55. (b) Nuzawa, K.; Sugano, T.; Urayama, H.; Yamochi, H.; Sato, G.; Kinishita, M. *Chem. Lett.* **1988**, 617.

64. (a) Interrante, L. V.; Browall, K. W.; Hart, H. R.; Jacobs, I. S.; Watkins, G. D.; Lee, S. H. *J. Am. Chem. Soc.* **1975**, *97*, 889. (b) Bray, J. W.; Hart, H. R., Jr.; Interrante, L. V.; Jacobs, I. S.; Kasper, J. S.; Piacente, P. A.; Watkins, G. D. *Phys. Rev. B.* **1977**, *16*, 1359.

65. Bousseau, M.; Valade, L.; Legros, J.-P.; Cassoux, P.; Garbaukas, M.; Interrante, L. V. *J. Am. Chem. Soc.* **1986**, *108*, 1908.

66. Bryce, M. R. *Chem. Soc. Rev.* **1991**, *20*, 355 and references therein.

67. Le Narvor, N.; Robertson, N.; Weyland, T.; Kilburn, J. D.; Underhill, A. E.; Webster, M.; Svenstrup, N.; Becher, J. *Chem. Commun.* **1996**, 1363.

68. McCullouch, R. D.; Belot, J. A. *Chem. Mater.* **1994**, *6*, 11396.

69. Alvarez, S.; Vicente, R.; Hoffman, R. *J. Am. Chem. Soc.* **1985**, *107*, 6253.

70. (a) Rivera, N. M.; Engler, E. M. *J. Chem. Soc., Chem. Commun.* **1979**, 184. (b) Poleschner, H.; John, E.; Hoppe, F.; Fanghanel, E. *J. Prakt. Chem.* **1983**, *325*, 957.

71. (a) Fourmigué, M.; Batail, P. *Bull. Soc. Chim. Fr.* **1992**, *129*, 829-836. (b) Jarchow, S.; Fourmigué, M.; Batail, P. *Acta Cryst.* **1993**, *C49*, 1936. (c) Fourmigué, M.; Huang, Y.-S. Organometallics, **1993**, *12*, 797. (d) Gerson, F.; Lamprecht, A.; Fourmigué, M. *J. Chem. Soc., Perkin Trans. 2*, **1996**, 1.

72. Fourmigué, M.; Uzelmeier, C. E.; Boubekeur, K.; Bartley, S. L.; Dunbar, K. R., *J. Organomet. Chem.*, **1997**, *529*, 343.

CHAPTER II

COORDINATION CHEMISTRY OF TRIS(2,4,6-TRIMETHOXYPHENYL)PHOSPHINE WITH PLATINUM GROUP TRANSITION METALS

1. Introduction

A considerable quantity of research in our laboratories has involved the use of the bulky and basic ligand tris(2,4,6-trimethoxyphenyl)phosphine (TMPP) in organometallic and transition metal coordination chemistry.[1] Several years ago Haefner and Dunbar reported the successful stabilization of an unusual paramagnetic, homoleptic Rh^{II} complex with TMPP.[1a] The metalloradical, $[Rh(\eta^3\text{-TMPP})_2][BF_4]_2$, was shown to exhibit a rich and reversible chemistry with CO and non-redox substitution reactions with isocyanides RCN (R = ^{t}Bu, ^{i}Pr, Cy).[1b,c,e] Results indicate that the use of a bulky, yet flexible ligand allows for the kinetic stabilization of ordinarily unstable intermediates, and renders possible the monitoring of reactions by NMR and infrared spectroscopy. Very often, ligands with large cone angles form complexes that are too sterically congested to undergo further reactions,[2] a situation that is not the case with the TMPP ligand. Mixed-donor ligands such as TMPP with its nine methoxy substituents, may be envisioned as possessing "built-in" solvent molecules in the form of weak ether interactions with the metal center. These prove to be sufficiently labile in solution and even in the solid-state,[3] thereby providing requisite vacant coordination sites. Such properties of ether-phosphine ligands have been referred to as hemi-labile, with the complexes themselves being labeled as "incipiently coordinatively unsaturated".[4] The properties and catalytic applications of ether-phosphines have recently been extensively reviewed.[5]

More recently our laboratories have reported the synthesis of bis(phosphino-phenoxide) ligands derived from TMPP with Ni,[1i] where the ligand is in it's demethylated form (TMPP-*O*). While the phenoxides positions in the Ni^{II} complex are *trans* to one another, evidence for a *cis* conformation has been observed with Rh^{III}.[6] The ability to form phenoxides that are *cis* to each other opens up the possibility for preparing heterobimetallic complexes via bridging phenoxides. The possibility of preparing early-late and late-late transition metal combinations occurred to us, given that the ligand possesses both "soft" and "hard" O-donors. There are several reports in the literature by Wolczanski and co-workers of these types of complexes (*e.g.* $Cp^*Zr(\mu\text{-}OCH_2Ph_2P)_2RhMe$).[7] Darensbourg *et al.* have utilized a similar approach to form bi- and heterometallic compounds from square-planar Ni^{II} complexes possessing a N_2S_2 environment.[8] Of most relevance to our work is that of Braunstein and co-workers who synthesized a series of *cis*-coordinated phosphino-enolate complexes with nickel(II), palladium(II), and platinum(II).[9] The nickel compound of this series was demonstrated to act as a metalloligand toward CoI_2 and $AlMe_2$ units; in the latter case the compound exhibits reactivity as an ethylene polymerization catalyst.[10]

In order to ascertain whether it was feasible to use a basic tertiary phosphine such as TMPP to stabilize 3d metals, we set out to investigate the chemistry of this ligand with Co^{II}. The successful use of the solvated

dirhodium(II,II) species, $[Rh_2(NCCH_3)_{10}][BF_4]_4$,[1a] in earlier studies prompted us to make use of $[Co(NCCH_3)_6]^{2+}$ as the starting material for these reactions.

2. Experimental

A. Synthesis

Starting Materials and Reaction Procedures. $[Rh^{II}(TMPP)_2][BF_4]_2$,[1b] $[Rh^{III}(TMPP)(TMPP\text{-}O)][BF_4]_2$,[1b] $Co(TMPP\text{-}O)_2$,[1o] $PtCl_2(NCC_6H_5)_2$,[11] $[Mn(NCCH_3)_4][BF_4]_2$[12] and $Pd(TMPP\text{-}O)_2$[1j] were prepared according to previously reported procedures. $[Me_3O][BF_4]$ and $[(C_4H_9)_4N][I]$ were purchased from Aldrich Chemical Co. and $CoCp_2$ was purchased from Strem Chemical Co. All three reagents were used as received. Zn (s) pellets were purchased from Fisher Scientific, activated with HCl and washed with diethyl ether prior to use. Acetone was distilled over 3 Å molecular sieves. Diethyl ether, tetrahydrofuran, and hexanes were distilled over sodium-potassium/benzophenone. Unless otherwise specified, all reactions were carried out under an argon atmosphere by using standard Schlenk-line techniques.

(1) Preparation of $[Rh^{I}(TMPP)_2][BF_4]$ (3)

(i) Reduction of $[Rh^{II}(\eta^3\text{-}TMPP)_2][BF_4]_2$ with $CoCp_2$. Solutions of $[Rh^{II}(TMPP)_2][BF_4]_2$, (0.107 g, 0.080 mmol) $Co(C_5H_5)_2$ (0.028 g, 0.148 mmol), and $[Me_3O][BF_4]$ (0.022 g, 0.149 mmol), were prepared separately by dissolving the respective solids in 10 mL of acetone. The cobaltocene and trimethyloxonium solutions were then simultaneously added to the Rh(II) complex dropwise, with stirring, resulting in a color change from purple to

brown after 1 h. The solvent was removed by vacuum and the brown residue was washed with 3 x 10 mL of THF, producing a yellow solution, indicative of $[Rh^{III}(TMPP)(TMPP\text{-}O)][BF_4]_2$. The residue was finally washed with copious amounts of Et_2O, and dried *in vacuo;* yield 0.048 g (mixture of **3** and $[CoCp_2][BF_4]$) ^1H NMR: (d_6-acetone) δ ppm: $-OCH_3$, 3.63 (b), 3.86 (s) (27H combined); *m* -H, 6.25 (b, 6H); $[CoCp_2]^+$, 5.91 (s, 10H). $^{31}P\{^1H\}$ NMR (d_6-acetone) δ ppm: +17.9 ppm (d, $^1J_{Rh\text{-}P}$ = 158.1 Hz). After ~ 1h the solution changed color to yellow-orange: ^1H NMR: (d_6-acetone) δ ppm: $-OCH_3$, 3.04 (s), 3.15 (s), 3.31 (s), 3.45 (s), 3.55 (s), 3.59 (s), 3.65 (s), 3.67 (s), 3.72 (s), 3.79 (s), 3.87 (s), 3.89 (s), 3.91 (s), 3.92 (s), 3.93 (s), 3.95 (s), 4.35 (s), 4.44 (s), 4.67 (s); *m* -H, 5.69 (dd), 5.75 (dd), 5.82 (dd), 6.04 (dd), 6.12 (dd), 6.17 (dd), 6.24 (dd), 6.36 (dd), 6.41 (dd), 6.45 (dd), 6.68 (dd), 6.84 (dd), 7.05 (dd); $[CoCp_2]^+$, 5.94. $^{31}P\{^1H\}$ NMR (d_6-acetone) δ ppm: +38.23 (dd, $^1J_{Rh\text{-}P}$ = 139.2 Hz, $^2J_{P\text{-}P}$ = 13.3 Hz), +32.31 (dd, $^1J_{Rh\text{-}P}$ = 41.6 Hz, $^2J_{P\text{-}P}$ = 13.3 Hz).

(ii) Reduction of $[Rh^{II}(\eta^3\text{-}TMPP)_2][BF_4]_2$ with Zn (s). $[Rh^{II}(TMPP)_2][BF_4]_2$ (0.103 g, 0.077 mmol) and 0.024 g (0.162 mmol) of $[Me_3O][BF_4]$ were dissolved in 10 mL and 5 mL of acetone respectively. The two solutions were then simultaneously added, with stirring, to a Schlenk flask containing an excess of activated Zn pellets (4-5 pellets). The stirring was discontinued and the flask was allowed to sit for ~24 h, during which time a subtle color change from dark purple to red-brown became evident. The solution was transferred by cannula to a Schlenk tube, and the solvent was removed by

vacuum, leaving a rose-colored residue. The residue was washed with THF to remove demethylated impurities, followed by copious amounts of Et_2O, and finally dried *in vacuo*; yield 0.067 g (70%). Slow diffusion of hexanes into an acetone solution of the solid yielded red-brown crystals suitable for X-ray diffraction. Red-brown crystals: ^1H NMR: (d_6-acetone) δ ppm: -OCH_3, 3.54 (b), 3.86 (s) (27H combined); *m* -H, 6.16 (b, 6H). $^{31}P\{^1H\}$ NMR (d_6-acetone) δ ppm: 17.8 (d, $^1J_{Rh\text{-}P}$ = 158.7 Hz), 17.9 (d, $^1J_{Rh\text{-}P}$ = 158.7 Hz). EPR (50:50 acetone/toluene, 110 K) g_{xx} = 2.24, g_{yy} = 2.30, g_{zz} = 2.00.

(2) Dealkylation of $[Rh^I(TMPP)_2][BF_4]$ (3): Formation of $Rh^I(TMPP)$-(TMPP-*O*) (4)

A flask containing 0.108 g (0.086 mmol) of $[Rh^I(TMPP)_2][BF_4]$ (3) and 0.030 g (0.081 mmol) of [*n*-Bu_4N][I] was cooled to -40°C and treated with 10 mL of acetone, after which time the flask was allowed to slowly warm to room temperature. After 1 h, the color of the solution changed to a darker shade of brown. The solvent was removed and the residue was dissolved in 10 mL of THF. The solvent was removed under vacuum, and the tan residue was washed with *copious* amounts of hexanes; yield 0.784 g. ^1H NMR: (d_6-acetone) δ ppm: -OCH_3, 3.56 (s), 3.40 (s), 3.42, (s), 3.46 (s), 3.47 (s), 3.62 (s), 3.66 (s), 3.80 (s), 3.83 (s); *m* -H, 5.50 (dd), 5.83 (dd), 5.88 (m), 5.91 (d), 6.06 (br), 6.23 (br); 6.15 (t). $^{31}P\{^1H\}$ NMR (d_6-acetone) δ ppm: 4, +20.0 (dd, $^1J_{Rh\text{-}P}$ = 164.0 Hz, $^1J_{P\text{-}P}$ = 21.8 Hz), +10.3 (dd, $^1J_{Rh\text{-}P}$ = 135.5 Hz, $^2J_{P\text{-}P}$ = 21.8 Hz); +15.4 (d, $^1J_{Rh\text{-}P}$ = 146.4 Hz); 5, +35.7 (d, $^1J_{Rh\text{-}P}$ = 152.5 Hz).

(3) Dealkylation of *ax*-[Rh^{III}(TMPP)(TMPP-*O*)][BF_4]$_2$: Formation of *ax,ax*-[Rh^{III}(TMPP-*O*)$_2$][BF_4] (5)

A mixture of *ax*-[Rh(TMPP)(TMPP-*O*)][BF_4]$_2$ (0.103 g, 0.078 mmol) and [TBA][I] (0.032 g, 0.087 mmol) was dissolved in 10 mL of acetone and exposed to a brief vacuum before being stirred for 3 h. During this time no color change was observed. The solvent was removed under vacuum, and the solid was washed with copious amounts of Et_2O before being dried under vacuum; yield 0.063 g (66%). ^{1}H NMR: (d_6-acetone) δ ppm: -OCH_3, 3.11 (s, 6H), 3.34 (s ,6H), 3.39 (s, 6H), 3.45 (s, 6H), 3.65 (s, 6H), 3.85 (s, 6H), 4.27 (s, 6H); *m* -H, 5.49 (br, 2H), 5.63 (br, 2H), 5.85 (br, 2H), 5.95 (br, 2H), 6.27 (br, 2H), 6.72 (br, 2H). ^{31}P{^{1}H} NMR (d_6-acetone) δ ppm: 35.5 (dd, $^1J_{Rh\text{-}P}$ = 153.4 Hz). FAB-MS (m/z): 1137 (M^+).

(4) Reaction of Co^{II}(TMPP-*O*)$_2$ with $Pt^{II}Cl_2(NC_7H_5)_2$

A quantity of $PtCl_2(NCC_6H_5)_2$ (0.0416 g, 0.088 mmol) Co(TMPP-*O*)$_2$ and (0.099 g, 0.091 mmol) were dissolved in 10 mL of acetone and stirred for 12 h. After this time the solution was reduced to a residue, washed 3 times with 20 mL of Et_2O and dried *in vacuo*; yield 0.089 g (74% for Cl_2PtCo(TMPP-*O*)$_2$). IR (Nujol, cm^{-1}): 329 ($\nu_{Pt\text{-}Cl}$), 480 ($\nu_{C..C}$), 1032 (ν_{COC}), 1228 ($\nu_{as\text{-}COC}$), 1579 (vs, $\nu_{C..C}$ + $\nu_{C..C}$), 1595 (vs, $\nu_{C..C}$ + $\nu_{C..O}$). FAB-MS (m/z): 1093 ([Co(TMPP-*O*)$_2$]$^+$).

(5) Reaction of Co^{II}(TMPP-*O*)$_2$ with $[Mn^{II}(NCCH_3)_4][BF_4]_2$

A solid mixture of Co(TMPP-*O*)$_2$ (0.202 g, 0.185 mmol)) and $[Mn(NCCH_3)_4][BF_4]_2$ (0.037 g, 0.094 mmol) were dissolved in 15 mL of acetone, and stirred at 40°C for .5 h. The dark green solution was then allowed to stir for 12 h while it cooled to ambient temperature. At that time the solution was reduced to a residue, washed 3 times 20 mL of Et_2O and dried *in vacuo*; yield: 0.181 g (81% for $[Mn\{Co(TMPP\text{-}O)_2\}_2][BF_4]_2$). IR (Nujol, cm^{-1}): 481 (ν_{C_C}), 1098 (vs, $\nu_{B\text{-}F}$), 1232 ($\nu_{as\text{-}COC}$), 1578 (vs, $\nu_{C_C} + \nu_{C_O}$) + 1599 (vs, $\nu_{C_C} + \nu_{C_O}$), FAB-MS (m/z): 1093 ($[Co(TMPP\text{-}O)_2]^+$), 576 ($[MnCo(TMPP\text{-}OH)_2]^{2+}$) .

B. X-ray Crystallography

The structures of complexes **3**, **6**, and **7** were determined by applications of general procedures described elsewhere.[13] Geometric and intensity data were collected on a Bruker SMART diffractometer for compounds **3** and **6**, and on a Rigaku AFC6S diffractometer for compound **7**; both are equipped with graphite monochromated MoK_α (λ_α = 0.71069 Å and 0.71071 Å, respectively) radiation. The data were corrected for Lorentz and polarization effects. Computing for **3**, **6** and **7** was performed on a Silicon Graphics Indigo II workstation using the Texsan and SHELXTL[14] software systems. Crystal parameters and basic information pertaining to data collection and structure refinement for compounds **3**, **6**, and **7** are summarized in Table 1.

[redacted]

Table 1. Crystallographic Data for $[Rh^{I}(\eta^2\text{-TMPP})_2][BF_4]\cdot[Rh^{II}(\eta^3\text{-TMPP}][BF_4]_2$ (**3**·$[Rh^{II}(\eta^3\text{-TMPP}][BF_4]_2$), $[Co^{II}_3(\mu^3\text{-OH})(\mu\text{-OH})_3\{Co^{II}(TMPP\text{-}O)_2\}_3][BF_4]_2\cdot[CH_3\text{-TMPP}][BF_4]\cdot(CH_3CH_2)_2O\cdot 2(CH_2)_2CO$ (**6**·$[CH_3\text{-TMPP}][BF_4]\cdot(CH_3CH_2)_2O\cdot 2(CH_2)_2CO$), and $Pd(TMPP\text{-}O)_2\cdot 3.73CH_2Cl_2\cdot H_2O$, (**7**·$3.73CH_2Cl_2\cdot H_2O$).

	3·$RhC_{54}H_{66}O_{18}P_2B_2F_8$	**6**·$C_{28}H_{36}O_9PBF_4\cdot C_4H_{10}O\cdot C_6H_8O_2$	**7**·$C_{3.7}H_{7.5}Cl_{7.5}\cdot H_2O$
Formula	$Rh_2C_{108}H_{132}O_{36}P_4B_3F_{12}$	$Co_6C_{232}H_{288}O_{78}P_8B_3F_{12}$	$PdC_{55.7}H_{69.5}O_{19}P_2Cl_{7.5}$
Space group	Aba2	R3c	Pbcn
a, Å	14.9687(6)	22.7188(5)	20.162 (9)
b, Å	20.9487(8)	22.7188(5)	24.62 (2)
c, Å	19.2004(8)	76.651(3)	24.326 (11)
α, deg	90.00	90.00	90.00
β, deg	90.00	90.00	90.00
γ, deg	90.00	120.00	90.00
V, Å3	6020.(4)	34262(2)	12566 (11)
Z	4	8	8
Data col. range, 2θ, deg.	4-57	3- 57	4-47
No. unique data,	6846	65724	9199
R1[a]	0.060	0.089	0.1065
wR2[b]	0.132	0.229	0.2598
Quality-of-fit indicator[c]	0.98	1.03	1.030

[a] $R1 = \sum||F_o| - |F_c||/\sum|F_o|$. [b] $wR2 = [\sum[w(F_o^2-F_c^2)^2]/\sum[w(F_o^2)^2]]^{1/2}$; $w = 1/\sigma^2(|F_o|)$.

[c] quality-of-fit = $[\sum w(|F_o|-|F_c|)^2/(N_{obs}-N_{parameter})]^{1/2}$

(1) $[Rh^{I}(\eta^3\text{-TMPP})_2][BF_4]\cdot[Rh^{II}(\eta^3\text{-TMPP}][BF_4]_2$ ($3\cdot[Rh^{II}(\eta^3\text{-TMPP})_2]$-$[BF_4]_2$).

(i) Data Collection and Reduction. Single crystals of $3\cdot[Rh^{II}(\eta^3\text{-TMPP})_2][BF_4]_2$ were grown by slow diffusion of diethyl ether into an acetone solution of the complex. A red-brown crystal of dimensions 0.21 x 0.18 x 0.11 mm^3 was secured on the tip of a glass fiber with Dow Corning silicone grease and placed in a cold N_2(g) stream at –123 ± 1 °C. Least-squares refinement using 21 well-centered reflections in the range $25 \leq 2\theta \leq 35°$ indicated an orthorhombic crystal system. The data were collected in a θ range of 1.94 to 28.28°. Of the 18047 reflections that were collected, 6846 reflections were used for F^2 refinement, and 4323 data were observed with $I > 2.00\sigma(I)$. The data were corrected for Lorentz polarization effects and an empirical absorption correction based on azimuthal ψ-scans near $\chi = 90°$ was applied.

(ii) Structure Solution and Refinement. The space group was determined to be Aba2 based on the observed systematic absences. The structure was solved by the SHELXTL program.[14] The metal center was found to reside on a center of inversion, rendering half the molecule unique. Rh(1), P(1), and the trimethoxyphenyl rings defined by C(1) through C(6) and C(19) through C(24) were refined anisotropically with occupancies of 1.0. The third trimethoxyphenyl ring was found to be disordered as two fully resolved rings, defined by C(10) through C(15) and C(10A) through C(15A). Each disordered ring was refined isotropically, with free variables resulting in

occupancies of ~0.50 for each. The disordered rings were constrained to the calculated positions of a normal phenyl ring. The $[BF_4]^-$ anion was found to exhibit a rotational disorder and was refined as two independent molecules with the B(1) and F(1) atoms in the same positions. The common atoms were refined with free variables resulting in occupancies of 1.0. The flourine atoms F(2)/(2A), F(3)/(3A), and F(4)/(4A) were such that the summed occupancies of the two representations equaled the ocupancies of B(1) and F(1). All atoms associated with the anion were refined anisotropically. Restraints were used on all F···F distances associated with a given molecule. F^2 refinement of 452 parameters resulted in residuals of R1 = 0.061 and wR2 = 0.131. The goodness-of-fit index was 0.982, and the maximum shift in the final difference map was 0.483 Å associated with H(14B') (symmetry code (') - x, 1-y, z). The mean shift/esd was 0.072 and the highest peak in the difference Fourier map is 0.49 $e^-/Å^3$ which is associated with C(14).

(2) $[Co^{III}_3(\mu^3\text{-}OH)(\mu\text{-}OH)_3\{Co^{II}(\mu\text{-}\eta^3\text{-}TMPP\text{-}O)_2\}_3][BF_4]_2 \cdot [CH_3\text{-}TMPP][BF_4] \cdot (CH_3CH_2)_2O \cdot (CH_2)_2CO$ ($7 \cdot [CH_3TMPP][BF_4] \cdot (CH_3CH_2)_2O \cdot CH_2)_2CO$).

(i) Data Collection and Reduction. A dark green crystal of approximate dimensions 0.37 x 0.26 x 0.23 mm^3 was selected and mounted at the end of a glass fiber with silicon grease and placed in a N_2 cold stream at –123 ± 1°C. Initial data indicated a monoclinic system, but subsequent solution and successful refinement of the structure was carried out in the rhombahedral

space group R3c. The data were collected in a θ range of 1.48 to 28.28°. Of the 65724 reflections that were collected, 17871 reflections were used for F^2 refinement, and 9352 data were observed with $I > 2.00\sigma(I)$. The data were corrected for Lorentz polarization effects and an empirical absorption correction based on azimuthal ψ-scans near $\chi = 90°$ was applied.

(ii) Structure Solution and Refinement. The structure was solved using the SHELXTL program.[14] Due to the size of the structure, initial least squares cycles were run using the Kennert-Hendrickson conjugate-gradient algorithm,[15] with the final cycles run using blocked refinement. The methoxy methyl groups associated with C(39) was found to be disordered, and was refined isotropically as three methyl groups, A, B and C, with a combined occupancy of 1.0 and with restraints on C-O. All other non-hydrogen atoms were refined anisotropically, except for $[BF_4]^-$ and solvent molecules. The $[BF_4]^-$ anion was found to undergo a rotational disorder and was refined as three molecules sharing the B(11) and F(13) atoms, which were refined anisotropically. The flourine atoms F(n1), F(n2), and F(n4) (n = 1,2,3) were refined isotropically with free variables such that the summed occupancies of the three representations equaled 1.0. Restraints were used on all F(n)···F(n) and F(n)···F(13) distances. The acetone molecule was refined isotropically with restraints on C(1/3)···O(4). The oxygen atom of the diethyl ether molecule was refined isotropically with restraints on O(96)-C(91/95). All hydrogen atoms are located at calculated positions.

Final full-matrix least-squares refinement was based on 17871 reflections that were used to fit 957 parameters with 83 restraints to give R1 = 0.089 and wR2 = 0.189. The goodness-of-fit index was 1.034, and the maximum shift in the final difference map was 0.195 Å associated with H(38C). The mean shift/esd was 0.032, and the highest peak in the difference Fourier map is 0.95 $e^-/Å^3$ which is associated with H(38C). The structure was additionally solved in the lower symmetry space groups Cc (#9) and P-1 (#1) with no improvement in the final refinement.

(3) Pd(TMPP-*O*)$_2$•3.73CH_2Cl_2•H_2O (7)•3.73CH_2Cl_2•H_2O.

(i) Data Collection and Reduction. Single crystals of **7** were grown by slow diffusion of diethyl ether into a CH_2Cl_2 solution of compound **7**. An orange crystal of dimensions 0.40 x 0.98 x 0.22 mm^3 was secured on the tip of a glass fiber with Dow Corning silicone grease and placed in a cold N_2(g) stream. Least-squares refinement using 25 well-centered reflections in the range $15.0 \leq 2\theta \leq 22.3°$ indicated that the crystal is consistent with an orthorhombic crystal system. The data were collected at - 85 ± 1 °C using the ω-2θ scan technique to a maximum 2θ value of 47°. Of the 10169 reflections that were collected, 815 were systematically absent. An empirical absorption correction based on azimuthal scans of three reflections with χ near 90° was applied which resulted in transmission factors ranging from 0.55-1.00.

(ii) Structure Solution and Refinement. The data were corrected for Lorentz and polarization effects. The structure was solved in the space group

Pbcn using the MITHRIL[16] and DIRDIF[17] structure solution programs and refined by full-matrix least-squares refinement on F^2.[18] Methoxy methyl groups associated with atoms C39, C47, and C48 were found to be disordered, and each was refined isotropically in two orientations, A and B, with a combined occupancy of 1.0 and with restraints on the C-O and C···C distances. All other non-hydrogen atoms were refined anisotropically, except for the solvent molecules. Treatment of the dichloromethane molecules is described in the following section. The final full-matrix least-squares refinement was based on 9199 reflections that were used to fit 774 parameters with 540 restraints to give R1 = 0.1065 and wR2 = 0.2598. The goodness-of-fit index was 1.030, and the maximum shift in the final difference map was 0.002 Å associated with Cl(73). After convergence, the mean shift/esd was 0.006 and the highest peak in the difference Fourier map was 1.16 $e^-/Å^3$ which is associated with the solvent molecule containing Cl(72).

Dichloromethane molecules were located using electron density difference maps generated using the SHELXTL software package.[14] The disordered CH_2Cl_2 molecules were modeled with restraints on the C-Cl and Cl···Cl distances. All C-Cl bond distances were constrained to 1.79 Å. Occupancies were also refined, resulting in a total of 3.73 dichloromethane molecules per Pd atom. An additional isolated atom was added as the oxygen of a water molecule and refined isotropically.

3. Results and Discussion

A. Reduction of $[Rh^{II}(TMPP)_2][BF_4]_2$: Formation of $[Rh^{I}(TMPP)_2][BF_4]$ (3).

The unstable d^8 complex, $[Rh^{I}(TMPP)_2][BF_4]$ (**3**), was prepared by two different reduction methods, neither of which yielded an analytically pure product. The inability to isolate the product from the cobaltacene reaction is due to similarities in the solubility of **3** and the byproduct, $[CoCp_2][BF_4]$. Preliminary $^{31}P\{^1H\}$ and ^1H NMR results reported by Dunbar and Haefner involving the reduction of $[Rh^{II}(TMPP)_2][BF_4]_2$ by $CoCp_2$ support the formation of minor quantities of $[TMPP\text{-}CH_3]^+$ salts and an extremely unstable dealkylated species.[19] In light of this, a methylating agent was added in order to prevent dealkylation of the reduction product, and to allow for a complex with two neutral TMPP ligands to be isolated. An excess (1.4 equivalents) of reducing agent appears to be necessary, as reactions using 1:1 equivalents of $CoCp_2$ produced no color change or new $^{31}P\{^1H\}$ NMR signals. This may be explained by the decomposition chemistry of **3**, which will be discussed later.

The reaction with $CoCp_2$ appears to be considerably faster, producing an immediately visible color change, whereas reduction with Zn (s) requires extended reaction times and is accompanied by a very subtle color change that is difficult to detect.

(1) NMR Spectroscopic Studies

The ^{31}P NMR spectra of the product of the cobaltocene reduction shows a doublet that is shifted +83.9 ppm downfield from the free phosphine,[20] indicating the presence of equivalent phosphorus nuclei with Rh-P coupling. This signal is shifted upfield relative to $[Rh^{III}(TMPP)_2][BF_4]_3$, which is understood in terms of increased shielding of the phosphorus nuclei due to increased electron density about the metal center. Curiously, the NMR spectra for the cobaltocene product and the crystalline product from zinc are slightly different. The product from the reduction by cobaltocene, and the crystals formed from the reduction by Zn contain the same doublet pattern in the their ^{31}P NMR spectra, but the latter, from which the crystals were formed, occasionally show a doublet of doublets centered at +17.73 ppm. This pattern of only one doublet of doublets cannot be reconciled with magnetically inequivalent phosphorus atoms, as two doublets of doublets should occur as a result of coupling first to the Rh center, and then to the other P nucleus. It was then thought that the pattern may be the result of two overlapping doublets (+17.78 ppm, +17.67 ppm), caused by two distinct isomers. To verify this a ^{31}P NMR spectrum was taken of the same sample on both a 300 MHz and a 500 MHz NMR spectrometer. This was performed to check if the doublet positions would shift relative to one another when the field was varried. The results revealed the true pattern to be two doublets centered at 17.8 ppm (^1J = 158.7 Hz) and 17.7 ppm (^1J = 158.7 Hz). Both signals are extremely close to that observed for the product of the

metallocene reaction, with nearly identical $^1J_{X\text{-}P}$ coupling constants. A pattern such as this must arise from at least two separate species in solution.

^{1}H NMR studies of $[Rh(TMPP)_2][BF_4]$ (3) in acetone-d_6 indicate that the TMPP ligands are involved in a highly fluxional process similar to the previously reported Pd^{II} analog.[1j] The room temperature ^{1}H NMR spectrum of **3** from $CoCp_2$ contains a broad resonance at 6.16 ppm due to the *m*-protons of the phenyl rings, a sharp resonance at 3.86 ppm assigned to the equivalent *para*-methoxy substituents and a broad signal at 3.54 ppm due to the *ortho*-methoxy substituents. The broad resonances in the *meta*-hydrogen and *ortho*-methoxy regions of the ^{1}H spectrum support the fluxionality of the ligand, probably due to an on-off binding interaction of methoxy groups at the axial positions. This type of fluxional behavior is not uncommon for these types of complexes.[21] An added feature of the spectrum is a singlet at δ = 5.91 ppm due to the ring protons of the metallocinium ion.

The ^{1}H NMR spectrum from the Zn(s) reduction, shown in Figure 8, reveals the same resonances, with an absence of the singlet at δ = 5.91 ppm. Upon cooling the sample from to 20°C, two additional broad resonances appear at δ = 3.49 and 6.34 ppm, respectively. At -40°C the intense signal at 3.86 ppm has shifted slightly upfield to 3.83 ppm, but is otherwise unchanged. The broad signals shift and sharpen slightly, but not sufficiently enough to reveal additional peaks. Continued cooling to -80°C leads to broadening of the resonances at 6.34 and 3.95 ppm and the appearance of an

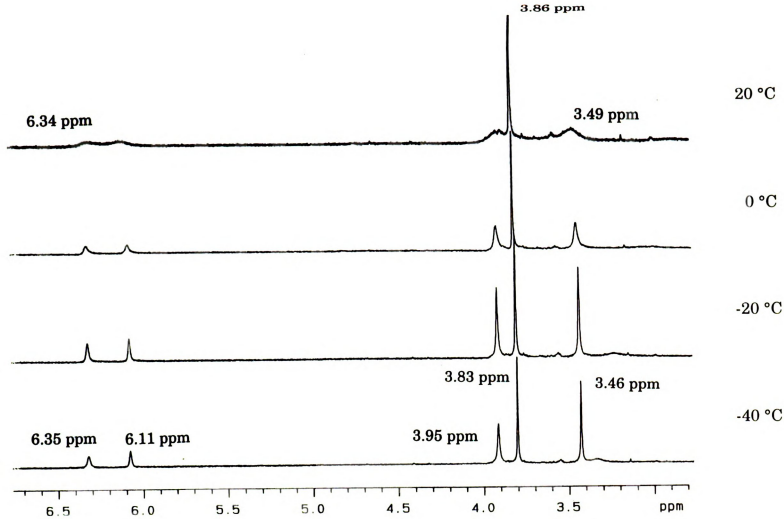

Figure 8. Variable Temperature ^1H NMR spectra of $[Rh^I(TMPP)_2][BF_4]$ (**3**) in d_6-acetone.

additional peak at 3.68 ppm. The formation of two broad resonances in both the *meta*-proton and *ortho*-methoxy positions supports the theory that two species are present in solution. The resolution of two 1:1 singlets in the *m*-H region, and three 1:1:1 singlets in the methoxy region at -40 °C can be explained by the presence of two different species in a nearly 1:1 ratio. The three different methoxy resonances would be caused by one *o*-OCH_3 for each compound, and a *p*-OCH_3 resonance common to both. This is supported by the 1:1 integration of the two doublets in the ^{31}P NMR spectrum. The identity of the second species is undetermined. One possibility is the formation of a the *trans*-$[Rh(TMPP)_2][BF_4]$ isomer. This would explain the NMR data, but is unusual given the only *trans*-TMPP complex reported to date is Ni(TMPP-*O*)$_2$,[1i] where both ligands have undergone demethylation. Furthermore, the observed 1:1 ratio of species is cause for suspicion, as an exact 50:50 mixture of *cis* and *trans* isomers is highly unlikely. A second possibility that we considered is the coordination of TMPP to the Zn ions. Given the similarities between the reactivities of Zn^{II} and Cd^{II},[22] it is not without reason to expect that the formation of $[Zn(TMPP)_2][BF_4]_2$ would be favored. However, the $[Zn(TMPP)_2][BF_4]_2$ would not account for either NMR spectrum based on the fact that $[Cd(TMPP)_2][BF_4]_2$ exhibits a singlet in its ^{31}P NMR spectrum, and symmetrical η^1-coordinated TMPP in its ^1H NMR spectrum.[10] Deliberate methods to prepare the Zn complex have thus far

been unsuccessful. Clearly, further studies are needed to identify the second product that occurrs from reduction of the Rh^{II} compound with Zn (s).

B. Crystal Structure of $[Rh^{I}(TMPP)_2][BF_4]$ (3).

X-ray quality single crystals of $[Rh^{I}(TMPP)_2][BF_4]$ (**3**) were grown by slow diffusion of diethyl ether into an acetone solution of the compound. A PLUTO representation of the molecular cation as well as selected bond distances and angles for **3** are provided in Figure 9 and Table 2. The crystal structure displays a very unusual disorder as a result of two separate Rh species having co-crystallized in the sample. The two species are the salts $[Rh^{II}(\eta^3\text{-TMPP})_2][BF_4]_2$ and the reduction product $[Rh^{I}(\eta^2\text{-TMPP})_2][BF_4]$. The Rh atom in the divalent species resides at the center of an octahedron defined by two phosphorus atoms (P(1), P(1')), two ether-oxygen atoms (O(1), O(1')) in an equatorial arrangement, and two ether oxygen atoms O4 and O4' at the axial positions. The distortion of the equatorial positions away from planarity is easily understood in terms of the requirements of the five-membered metallacycles Rh(1)-P(1)-C(1)-C(2)-O(1) and Rh(1)-P(2)-C(19)-C(20)-O(10) that involve acute angles (P(1)-Rh(1)-O(1) = 77.71 (11)°, and P(2)-Rh(1)-O(10) = 78.1 (2)°). The $Rh\text{-}O_{axial}$ distance of 2.405(12) Å in the Rh(II) complex is comparable to the previously reported value of 2.398(5) Å.[1b] The Rh(I) center is coordinated in a square-planar environment, also defined by atoms (P(1), P(1')), O(1), and O(1'), but with a much more elongated O_{axial} distance of 2.812 Å (defined by O(4A) and O(4A)'). The elongated axial

Table 2. Selected Bond Distances (Å) and Angles (deg.) for $[Rh^{I}(\eta^{2}\text{-}TMPP)_2][BF_4]$ (**3**).

Atom 1	Atom 2		3
Rh(1)	P(1)		2.209(2)
Rh(1)	O(1)		2.219(4)
Rh(1)	O(4)		2.405(12)
Rh(1)	O(4A)		2.812(7)
P(1)	C(1)		1.819(6)
P(1)	C(10)		1.838(10)
P(1)	C(10A)		1.838(10)
P(1)	C(19)		1.788(6)
O(4)	C(11)		1.39(2)
O(4A)	C(11A)		1.35(2)
Atom 1	**Atom 2**	**Atom 3**	**3**
P(1)	Rh(1)	P(1)'	106.44(8)
P(1)	Rh(1)	O(1)	77.71(11)
O(1)	Rh(1)	O(1)	100.0(2)
Rh(1)	O(4)	C(11)	114.5(7)
P(1)	C(1)	C(2)	114.5(5)
P(1)	C(1)	C(2)	122.2(5)

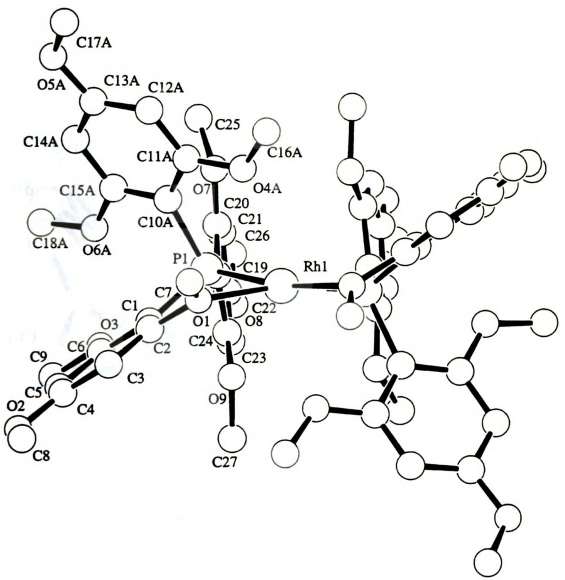

Figure 9. PLUTO representation of $[Rh^{I}(\eta^{2}\text{-TMPP})_2][BF_4]$ (**3**) from the mixed salt, $[Rh^{I}(\eta^{2}\text{-TMPP})_2][BF_4] \cdot [Rh^{II}(\eta^{3}\text{-TMPP})_2][BF_4]_2$.

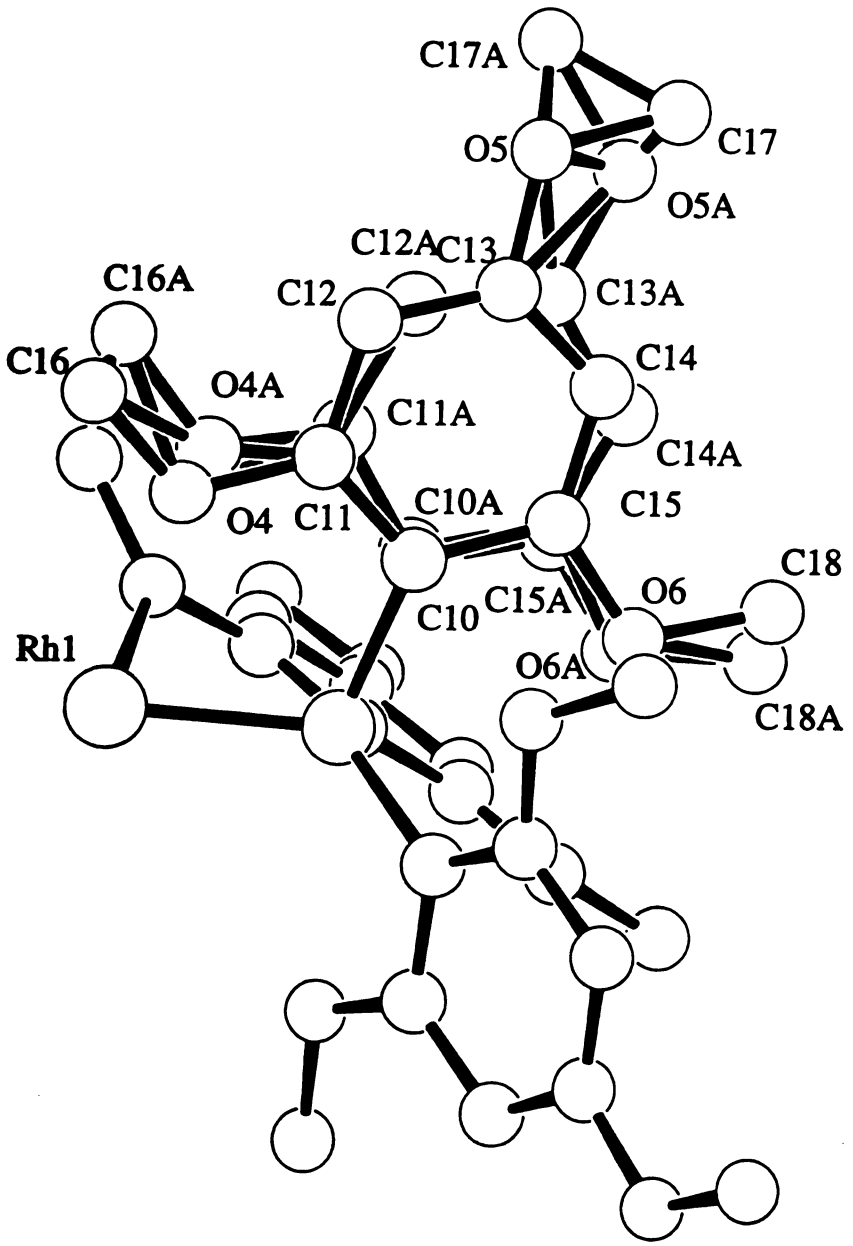

Figure 10. PLUTO representation of the unique atoms, showing the disorder in the molecular structure of $[Rh^{I}(\eta^{2}\text{-}TMPP)_2][BF_4] \cdot [Rh^{II}(\eta^{3}\text{-}TMPP)_2][BF_4]_2$.

distance arises from distortion of the ligand, resulting in two, fully resolved phenyl rings with an angle between the rings (planes defined as C(10)-C(15) and C(10A)-C(15A)) of 0.7°. The geometry of the square plane for **3**•$[Rh^{II}(\eta^3\text{-}TMPP)_2][BF_4]_2$ is very similar to that found in the bona fide Rh(II) structure, with Rh-P distances of 2.029(2) Å versus 2.16(2) Å and P- Rh-P angles of 106.44(8) versus 105.2(1). Attempts to model the $[BF_4]^-$ groups to account for the 2:1 ratio of counterions in the Rh(II) vs. Rh(I) complexes were unsuccessful.

Due to the close similarities of the above structure with that of our earlier X-ray study of $[Rh^{II}(\eta^3\text{-}TMPP)_2][BF_4]_2$, it became necessary to verify that the structure was not merely a result of disorder in the structure of $[Rh^{II}(\eta^3\text{-}TMPP)_2][BF_4]_2$. Accordingly, ^1H and ^{31}P NMR spectra were measured on microcrystals of $[Rh^{II}(\eta^3\text{-}TMPP)_2][BF_4]_2$, grown from slow diffusion of E_2O into a concentrated acetone solution of the complex. The resulting ^1H NMR spectrum was broad and unresolved with no observable ^{31}P NMR signals, supporting that only the paramagnetic Rh(II) is present. After reduction of this Rh(II) sample with Zn (s), EPR measurements of the resulting crystals in a 1:1 acetone/toluene glass were taken at 110 K. The observed signal was identical to that reported for $[Rh^{II}(\eta^3\text{-}TMPP)_2][BF_4]_2$, confirming that it is present in crystals representative of the one used in the X-ray investigation. ^1H and ^{31}P NMR spectral studies on representative samples from the same crystal "batch" exhibited the spectra discussed

previously for the proposed Rh(I) complex These combined results indicate that the sample is not composed entirely of Rh(II), but that it also contains a diamagnetic species. This is also supported by the noticeable color difference between the two crystals (purple for Rh(II) versus red-brown for the one that contains both Rh(I) and Rh(II)).

C. Reactivity of $[Rh^{I}(TMPP)_2][BF_4]$ (3).

(1) Decomposition of $[Rh^{I}(TMPP)_2][BF_4]$ (3).

The yellow-orange solution which eventually results from solutions of **3** can be identified by ^{31}P NMR spectroscopy as $[Rh^{III}(TMPP)(TMPP\text{-}O)][BF_4]_2$, which supports the conclusion that there must have been two TMPP ligands on the metal originally. This is a result of oxidation of the Rh(I) complex with concomitant dealkylation of a methoxy group. At the present time the pathway for the demethylation/oxidation of this compound is unknown. The only clue that is available is the gradual appearance of a peak at 2.85 ppm in the ^{1}H NMR spectrum. This resonance has not yet been assigned, but grows over time along with the resonances for the Rh^{III} product.

(2) Dealkylation of $[Rh^{I}(TMPP)_2][BF_4]$ (3).

(i) Synthesis and spectroscopic characterization of Rh^{I}(TMPP)-(TMPP-*O*) (4). A solution of $[Rh^{I}(TMPP)_2][BF_4]$ was cooled to -40°C, and reacted with 1 equivalent of [TBA][I]. No reaction was observed until the temperature was allowed to warm to room temperature, after which time the color of the solution darkened slightly. The resulting product is soluble in THF which tends to be the case for all Rh-TMPP complexes with at least one

demethylated TMPP ligand.[1b,19] In contrast, all complexes with both TMPP ligands in their neutral form are invariably insoluble in THF.[1b] This solubility change indicates the formation of the highly reactive d^8 species Rh^I(TMPP)(TMPP-*O*) (4).

The ^1H NMR spectrum of 4 is very complicated owing to the presence of several different species in solution, which causes the ^{31}P NMR spectrum to be the most reliable tool for analysis of the product(s). The twin doublet of doublets at 20.0 ($^1J_{Rh\text{-}P}$ = 164.0 Hz, $^1J_{PA\text{-}PB}$ =21.8 Hz) and 10.3 ppm ($^1J_{Rh\text{-}P}$ =135.5 Hz, $^2J_{PA\text{-}PB}$ =21.8 Hz) indicate a species containing inequivalent phosphorus nuclei where the observed couplings are due to Rh-P, and P-P coupling. This pattern is typical for a mono-demethylated Rh-TMPP complex , but is further upfield than any pattern previously observed for Rh TMPP complexes, which supports that there is increased electron density at the metal center.

The resonance patterns exhibited in the ^{31}P NMR spectrum of 4 suggests the presence of several different complexes, due to its instability in solution. The doublet located furthest downfield (35.7 ppm, $^1J_{Rh\text{-}P}$ = 152.5 Hz) in the $^{31}P\{^1H\}$ NMR spectrum was identified as the previously characterized compound *ax,ax*-[Rh^{III}(TMPP-*O*)$_2$][BF_4].[19] The upfield doublet at 15.4 ppm ($^1J_{X\text{-}P}$ =146.4 Hz) is still unidentified, with a possible candidate being the bis-demethylated [Rh^I(TMPP-*O*)$_2$]$^-$. This assignment would explain the pattern, and its upfield position relative to the [Rh^I(TMPP)$_2$]$^+$ cation.

However, this is a highly unlikely formulation given it is doubtful the metal center could support the increased electron density of this anionic complex. This instability of the Rh(TMPP)(TMPP-*O*) compound caused further characterization, specifically by elemental analysis, impossible.

(ii) Decomposition of Rh^{I}(TMPP)(TMPP-*O*) (4). Exposure of **4** to air results in an instantaneous color change from brown to yellow. Room temperature acetone solutions of **4** kept under rigorously anaerobic conditions produces identical results over a period of several minutes. ^{1}H and ^{31}P NMR spectra of the resulting solutions confirmed complete conversion to *ax,ax*-[Rh^{III}(TMPP-*O*)$_2$][BF_4], without evidence for the formation of [CH_3-TMPP]$^+$ salts. This observation is consistent with dealkylation resulting from attack by [BF_4]$^-$.[23] Several examples of transition metal complexes that activate [BF_4]$^-$ have been reported,[24] and this mechanism has been proposed for the solid-state decomposition of [Rh(TMPP)$_2$][BF_4]$_3$ to [Rh(TMPP)(TMPP-*O*)][BF_4]$_2$.[19]

D. Preparation and Spectroscopic Studies of *ax,ax*-[Rh^{III}(TMPP-*O*)$_2$][BF_4] (5).

Previous work by Steven Haefner led to the identification of two isomers from the addition of 1 equivalent of TMPP to [Rh^{III}(TMPP)(TMPP-*O*)][BF_4]$_2$.[19] These isomers were assigned on the basis of their ^{31}P NMR spectra as *ax, ax*-[Rh^{III}(TMPP-*O*)$_2$][BF_4] , and *ax, eq*- [Rh^{III}(TMPP-*O*)$_2$][BF_4] in a 59:41 ratio. The isomers occur due to the availability of two possible sites

for the second dealkylation reaction to occur; namely in the equatorial plane, *trans* to the neutral TMPP ligand or in the axial position, *trans* to the phenoxide group. The two isomers are distinguishable from each other due to the presence of a doublet at +35.7 ppm (CD_3CN, $^1J_{Rh\text{-}P}$=152.5 Hz) for the *ax*, *ax*, and two doublet of doublets at +47.1 ppm (CD_3CN, $^1J_{Rh\text{-}P}$=152.5 Hz, $^2J_{P\text{-}P}$=16.7 Hz) and +19.9 ppm (CD_3CN, $^1J_{Rh\text{-}P}$=122.9 Hz, $^2J_{P\text{-}P}$=16.7 Hz) respectively for the *ax*, *eq* isomer. Although subsequent attempts to isolate either pure isomer had proved unsuccessful, an *in situ* NMR reaction revealed that reaction of the mono-demethylated Rh(III) with an alkyl ammonium salt may preferentially form the *ax*, *ax* isomer.

Reaction of $[Rh^{III}(TMPP)(TMPP\text{-}O)][BF_4]_2$ with an equimolar amount of tetra-n-butyl ammonium iodide ([TBA][I]), was shown by ^{31}P NMR spectroscopy to form exclusively *ax*, *ax*- $[Rh^{III}(TMPP\text{-}O)_2][BF_4]$. No evidence for the formation of the *ax*, *eq* isomer was found. The product is a yellow solid that is nearly identical in appearance to its mono-demethylated precursor. The ^1H NMR spectrum shows six doublets of doublets of equal intensity in the *meta*-proton region between δ = 5.4 and 6.8 ppm, and seven equal resonances in the methoxy region between δ = 3.1 and 3.9 ppm. This supports the presence of two magnetically equivalent demethylated-TMPP ligands. The presence of the $TBABF_4$ byproduct was also detected.

E. Reactions of $Co^{II}(TMPP\text{-}O)_2$ with Unsaturated Metal Complexes.

Our successful isolation of $Cl_2MCo(TMPP\text{-}O)_2$ (M = Co, Mn) from

reactions of the high spin d^7 complex, Co(TMPP-*O*)$_2$ with the appropriate metal chloride sparked our interest in the assembly of early-late transition metal heterobimetallic complexes. There are several reports in the literature of these types of complexes, *e.g.* *trans*-$Me_2RTa(\mu\text{-}CH_2)(\mu\text{-}OCMe_2\text{-}CH_2Ph_2P)_2PtMe$,[25] and $Cp^*Zr(\mu\text{-}OCH_2Ph_2P)RhMe_2$.[26] An interesting twist on these types of compounds is the combination of magnetic centers to form high spin-count complexes which may exhibit interesting properties by virtue of communication through the phenoxide bridge.

(1) $Pt^{II}Cl_2(NC_7H_5)_2$

The reaction of stoichiometric amounts of $PtCl_2(NC_7H_5)_2$ with Co(TMPP-*O*)$_2$ does not lead to a discernible color change from the original green color. This is not surprising given that the *O*-metallated complex *cis*-$Pt(Ph_2PCHC\text{-}OPh)_2$ is white,[27] and the color of Co(TMPP-*O*)$_2$ would be expected to dominate. ^1H and ^{31}P NMR spectral studies of the resulting green solid exhibits broadening properties typical of a paramagnetic species in solution. The infrared spectrum exhibits modes attributable to the $\nu_{Pt\text{-}Cl}$ stretching frequency, but without vibrations characteristic of nitriles. The presence of absorption associated with the [ν(C⋯C) + ν(C⋯O)] vibrations at 1579 and 1595 cm^{-1} are in the range reported to be an indication of chelation to a second metal center by *cis*-oriented phosphino-enolate ligands.[10a] FAB-MS analysis reveals a base peak of m/z = 1093 for the $[Co(TMPP\text{-}O)_2]^+$ ion, with the detection of several higher mass peaks that have yet to be identified

(up to m/z = 1349, 7% of base). These data support the presence of an intact Co(TMPP-*O*)$_2$ moiety with the phenoxide groups acting as a bridge between two metal centers, possibly forming Cl_2PtCo(TMPP-*O*)$_2$.

(2) $[Mn^{II}(NCCH_3)_4][BF_4]_2$

The reaction of $[Mn(NCCH_3)_4][BF_4]_2$ with two equivalents of Co(TMPP-*O*)$_2$ results in the eventual isolation of an emerald green product. ^1H and ^{31}P NMR spectral studies of this solid indicate the presence of a paramagnetic species in solution. The infrared spectrum exhibits an intense feature at 1098 cm^{-1} attributable to the ν_{B-F} stretching frequency. The absence of any modes characteristic of bound nitriles supports complete ligand substitution around the Mn(II) ion. Modes at 1578 and 1599 cm^{-1} [ν(C⋯C) + ν(C⋯O)] support chelation of a second metal center by the phenoxide groups of Co(TMPP-*O*)$_2$.[10a] The FAB-MS spectrum contains a base peak of m/z = 1093 for the $[Co(TMPP\text{-}O)_2]^+$ ion, with the detection of a peak at m/z = 576 that can be formulated as $[MnCo(TMPP\text{-}OH)_2]^{2+}$, resulting from loss of a Co(TMPP-*O*)$_2$ with protonation of the phenoxide groups. Such a mass ion would require reduction of one of the metal centers by two electrons. This protonantion of a bound phenoxide group has been previously demonstrated by reaction of $[Rh^{III}(TMPP)(TMPP\text{-}O)][BF_4]_2$ with HBF_4.[19] These data support coordination of two Co(TMPP-*O*)$_2$ "ligands" to the Mn center, resulting in the heterotrinuclear moiety, $[Mn\{Co(TMPP\text{-}O)_2\}_2]^{2+}$. Both octahedral and tetrahedral complexes are known for Mn(II). Although acetonitrile was not

detected in the I.R. spectrum, we cannot rule out the possibility of axial coordination to the manganese center.

F. Formation and Crystal Structure of $[Co^{II}_3(\mu^3\text{-}OH)(\mu\text{-}OH)_3\{Co^{II}(\mu\text{-}\eta^3\text{-}TMPP\text{-}O)_2\}_3][BF_4]_2$ (6)

It has been noted that the compound Co(TMPP-*O*)$_2$ is highly moisture-sensitive.[1n] This has been illustrated by our isolation of $[Co_3(\mu^3\text{-}OH)(\mu^2\text{-}OH)_3\{Co(TMPP\text{-}O)_2\}_2][BF_4]_2$ (**6**) from the slow diffusion of diethyl ether or hexanes into acetone solutions of Co(TMPP-*O*)$_2$. This is presumed to be a result of hydrolysis caused by residual amounts of water in the system. The formation of partial cubanes such as **6** has been previously reported in the chemistry of Re, Mo, and Cr in aqueous media.[28] A similar core, $[Co_3(\mu^3\text{-}O)(\mu^2\text{-}OH)_3]^{4+}$, was reported by Christou and Ama to be present in different compounds.[29] The triply bridging hydroxide is not unprecedented in Co chemistry, having been reported previously for the complex $[(py)_5Co_3(\mu^3\text{-}OH)(OAc)_3(cat)]$.[30] In the cases of the above Co(III) complexes, reactions were carried out in aqueous media with the addition of H_2O_2, but the paramagnetic Co(II) complex containing the μ^3-OH was prepared by the addition of Et_4NOH to $Co(OAc)_2 \cdot 4H_2O$ in ethanol. Coucouvanis and co-workers found that substitution of μ^3-OMe for OH could be achieved by the use of NaOMe in "strictly nonaqueous" solutions.[30]

(1) Crystal Structure

An ORTEP representation of **6** is shown in Fig. 11 and important bond distances and angles are listed in Table 3. The structure of **6** contains a partial cubane core of $[Co_3(\mu^3\text{-}OH)(\mu^2\text{-}OH)_3]^{2+}$, with each metal within the core ligated to a Co(TMPP-*O*)$_2$ moiety through the *cis*-phenoxides in a $\mu\text{-}\eta^2$-fashion. The triply bridging hydroxide, O(3), is situated on a special position of three-fold symmetry. The molecular structure of the Co(TMPP-*O*)$_2$ fragment in **6** is essentially the same as that found in the dinuclear compound Cl_2Co_2(TMPP-*O*)$_2$.[1n] The coordination sphere about Co(1) in **6** is nearly equivalent to the octahedral Co environments in Cl_2M(CoTMPP-*O*)$_2$ (M = Co, Mn) with the largest difference occurring in the wider O(32)-Co(1)-O(26) and tighter P(1)-Co(1)-P(2) angles of **6** versus the dinuclear complexes (81.3(2) and 108.35(9)° versus 79.5(2) for Co and 110.10(9)° for Mn). The Co atoms within the partial cubane core lie within a distorted trigonal bipyramidal coordination sphere. The atoms O(1) and O(32) can be considered to be the axial ligands, with an O(1)-Co(2)-O(32) angle of 175.6(2)°, where O(26), O(2) and O(2)' occupy the equatorial positions. The μ_2-OH oxygen atoms deviate from 90°, towards the μ^3-OH, with O(2)-Co(2)-O(1) angles of 78.9(2) and 79.2(2)°. The Co-O distances for the μ^2-OH groups are 1.947(5) Å and 1.961(5 Å, with the μ^3-OH bonds being slightly longer, at 2.191(4) Å. These values are in good agreement with previously reported Co(μ^2-OH) and Co(μ^3-OH) distances of 1.971(5)-2.03(1) Å and 2.09(1)-2.13(1)

Table 3

Table 3. Selected Bond Distances (Å) and Angles (deg.) for $[Co^{II}_3(\mu^3\text{-}OH)(\mu\text{-}OH)_3\{Co^{II}(\mu\text{-}\eta^3\text{-}TMPP\text{-}O)_2\}_3][BF_4]_2$ (**6**).

Atom 1	Atom 2	6
Co(1)	O(32)	1.938(5)
Co(1)	O(26)	1.958(5)
Co(1)	P(1)	2.187(2)
Co(1)	P(2)	2.194(2)
Co(1)	O(46)	2.284(5)
Co(1)	O(56)	2.320(5)
Co(2)	O(2')	1.947(5)
Co(2)	O(2)	1.961(5)
Co(2)	O(26)	2.027(5)
Co(2)	O(32)	2.111(5)
Co(2)	O(1)	2.191(4)

Atom 1	Atom 2	Atom 3	6
O(32)	Co1)	O(26)	81.3(2)
O(26)	Co(1)	P(1)	166.6(2)
P(1)	Co(1)	P(2)	108.35(9)
P(1)	Co(1)	O(56)	78.17(15)
O(46)	Co(1)	O(56)	177.1(2)
O(2)	Co(2)	O(2')	113.7(3)
O(26)	Co(2)	O(32)	75.6 (2)
O(2)	Co(2)	O(1')	79.2(2)
O(2)	Co(2)	O(1)	78.9(2)

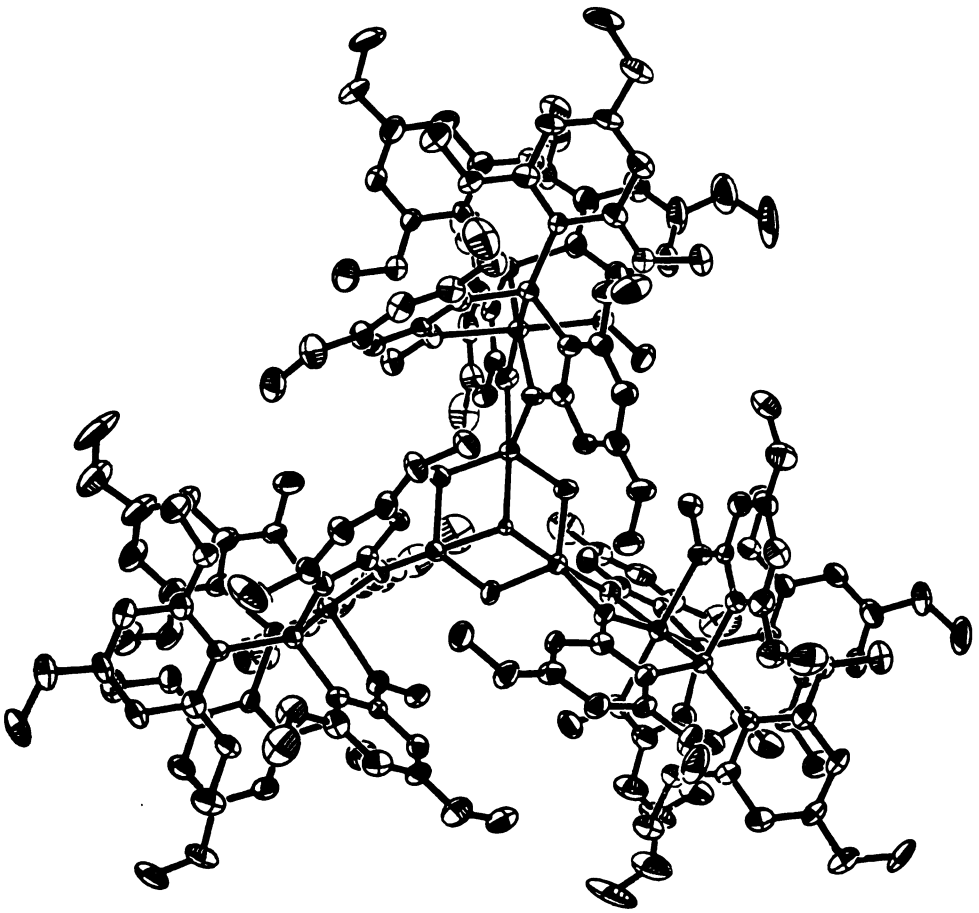

Figure 11. ORTEP representation of $[Co^{II}_3(\mu^3\text{-}OH)(\mu\text{-}OH)_3\{Co^{II}(\mu\text{-}\eta^3\text{-}TMPP\text{-}O)_2\}_3][BF_4]_2$ (**6**) with 50% probability ellipsoids. Hydrogen atoms and labels have been removed for clarity.

Figure 12.

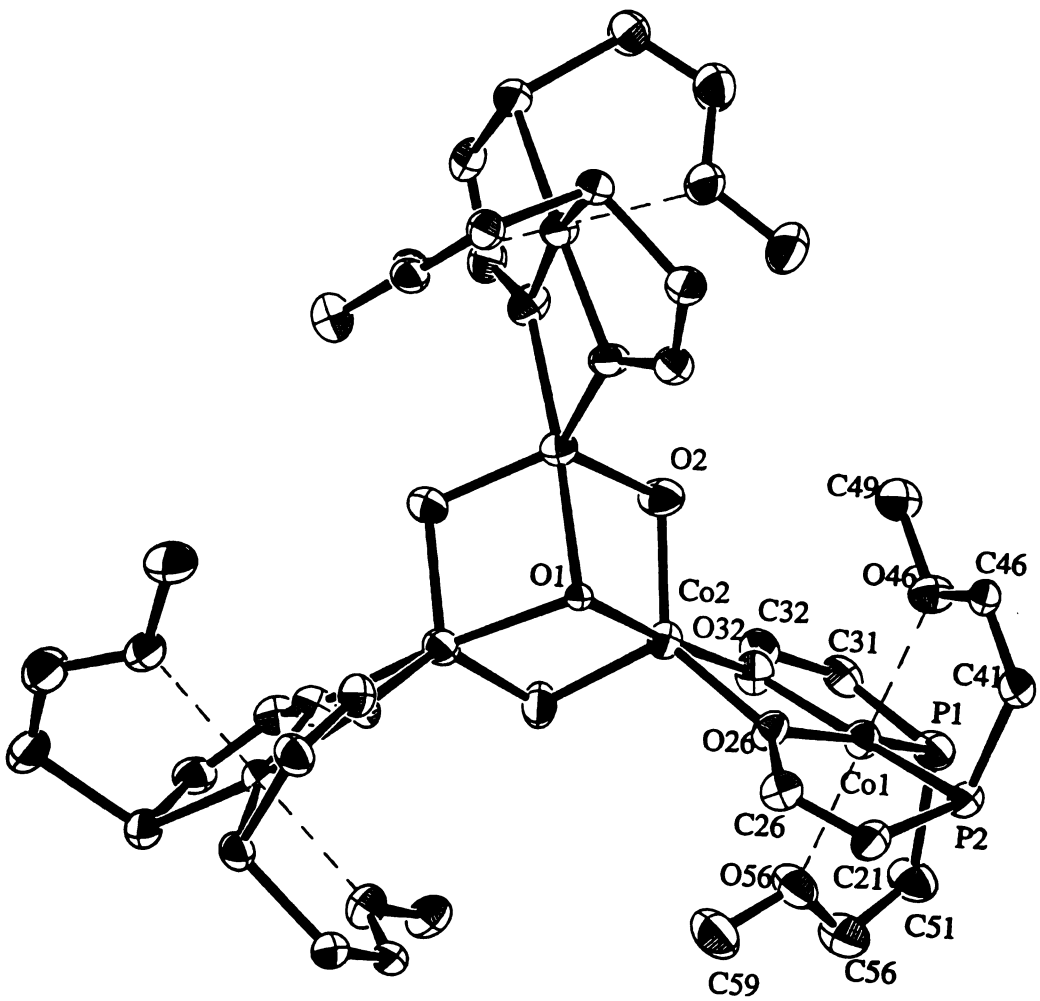

Figure 12. ORTEP representation of the immediate coordination sphere for each metal in $[Co^{II}_3(\mu^3\text{-}OH)(\mu\text{-}OH)_3\{Co^{II}(\mu\text{-}\eta^3\text{-}TMPP\text{-}O)_2\}_3][BF_4]_2$ (**6**) with 50% probablility ellipsoids. All other atoms have been removed for clarity.

Å respectively.[30,31] This elongation of the Co(2)-O(1) distance relative to Co(2)- O(2) is indicative of μ^3-OH, as μ^3-O groups have nearly identical distances to μ^2-OH groups. [29]

A recent report by Wood and Palenik examines the potential for calculating the oxidation state of Co complexes using equation 1, where rij is

$$s_{ij} = \exp[(R_o - r_{ij})/b] \quad (1)$$

the C-O bond lengths of the Co center in question, b is a constant (usually 0.37), and R_o is the constant under investigation by the authors.[32] The authors found an Ro value of 1.661 Å can be used to calculate the oxidation state of a Co atom in complexes containing only Co-O bonds with no prior assumptions. Using this value and the Co-O distances associated with the Co atoms of the partial cubane core in **6**, a bond valence sum (BVS) of 1.81 is calculated. This is significantly lower than 2.00, possibly due to the distorted geometry about the metal centers. Using R_o = 1.686 Å, the experimental value found for use with five-coordinate metal centers, a BVS = 1.94 Å is obtained. This is in good agreement with the presence of Co(II) according to the experimental errors listed by Wood and Palenik. This calculation supports our assignment of the central O in the core as a μ^3-OH group rather than μ^3-O, because the later would result in an over all charge of +1, and does not match the number of $[BF_4]^-$ ions found in the structure.

EPE

T

broad s

typical

a high

change

incre

give n

resc

G. Cr

4. C

(2) EPR Spectroscopy

The EPR spectrum of **6** in a 1:1 acetone/toluene glass exhibits a strong, broad signal with $g_1 = 4.46$, $g_2 = 2.25$, and $g_3 = 2.03$. The lowest field signal is typical for high spin six-coordinate systems, and the intensity is indicative of a high spin count. Five-coordinate high spin cobalt complexes exhibit changes in $g_{\|}$ and $g_{\perp}$ with changes in the A-Co-B angle (tetrahedral distortions).[28] The distortions evident in the molecular structure of **6** may give rise to the higher field pattern. An added complication is the second g tensor for the six-coordinate systems which should also be seen near g = 2.

G. Crystal Structure of Pd(TMPP-*O*)$_2$ (7)

An ORTEP representation of the molecular cation in **7** is displayed in Figure 13, with selected bond distances and angles provided in Table 4. The geometry about the Pd atom of **7** is square planar, consisting of a *cis* arrangement defined by P(1), P(2) and the phenoxide oxygen atoms O(22) and O(52). Ring strain in **7** is evidenced by angles of O(22)-Pd(1)-O(52) = 81.4 (3)°, O(52)-Pd(1)-P(2) = 84.6° (2), and P(2)-Pd(1)-P(1) = 109.4° (2). Axial ether-oxygen atoms O(16) and O(46) are at distances of 2.887 and 3.025 Å which are much longer than the analogous interactions in $[Pd(TMPP)_2][BF_4]_2$.[1j]

4. Concluding Remarks

The combination of both hard and soft donor groups on tris(2,4,6-trimethoxyphenyl)phosphine provides the ability to stabilize a metal atom in

Table 4. Selected bond distances (Å) and bond angles (°) for Pd(TMPP-*O*)$_2$.

Bond Distances

A	B	A-B (Å)	A	B	A-B (Å)
Pd1	P1	2.270 (4)	P1	C11	1.822 (13)
Pd1	P2	2.251 (4)	P1	C21	1.832 (12)
Pd1	O22	2.047 (7)	P1	C31	1.824 (13)
Pd1	O52	2.047 (8)	P2	C41	1.81 (2)
O22	C22	1.363 (4)	P2	C51	1.78 (2)
O52	C52	1.363 (4)	P2	C61	1.87 (2)

Bond Angles

A	B	C	A-B-C (°)
P2	Pd1	P1	109.4 (2)
O22	Pd1	P1	84.9 (2)
O52	Pd1	P1	165.2 (2)
O22	Pd1	O52	81.2 (3)
C11	P1	Pd1	118.1 (5)
C21	P1	Pd1	97.6 (4)
C11	P1	C31	111.5 (6)
C11	P1	C21	104.2 (6)
C22	O22	Pd1	121.1 (7)
C52	O52	Pd1	117.5 (8)

Figure

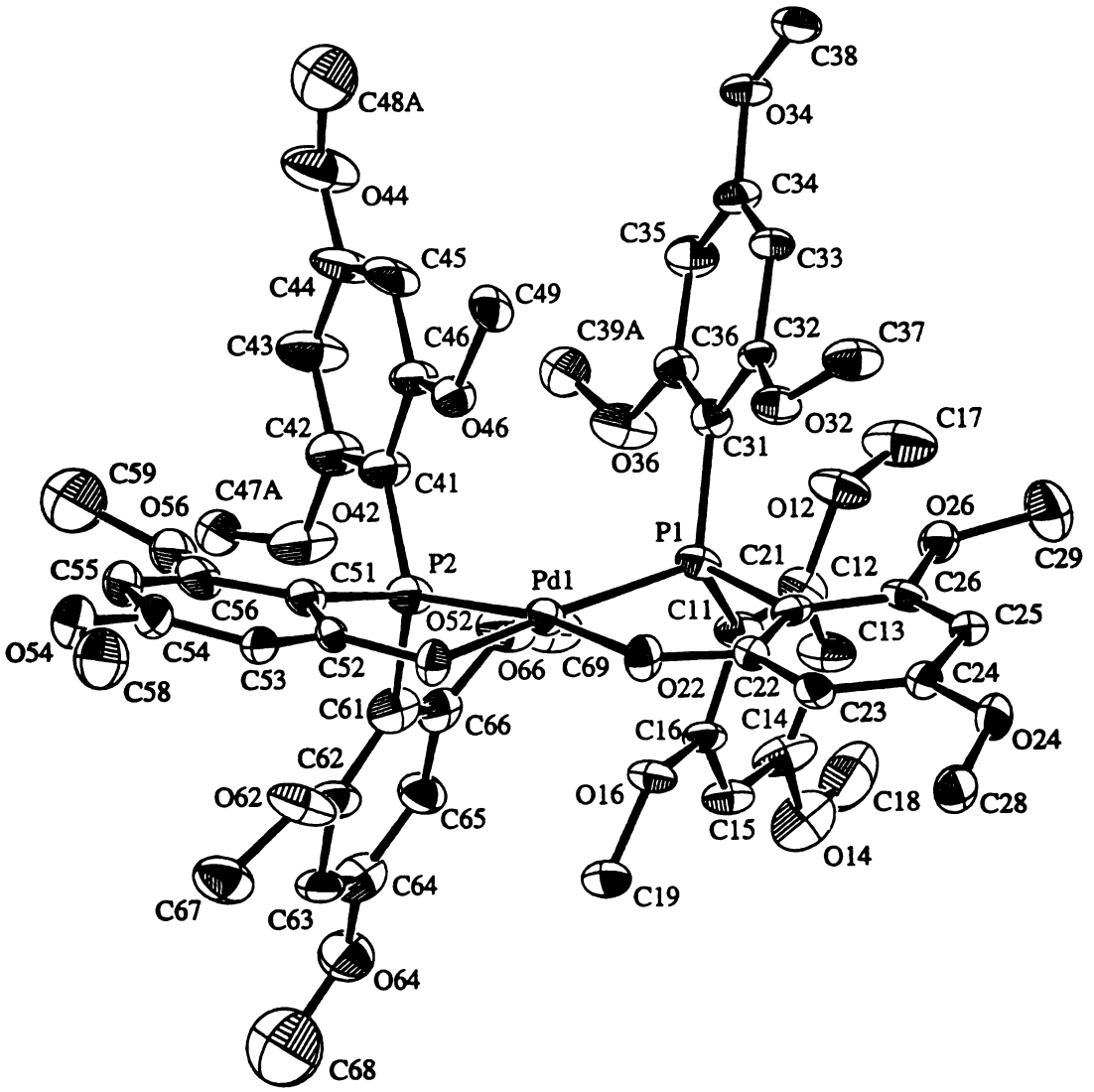

Figure 13. ORTEP representation of Pd(TMPP-*O*)$_2$ (7) with 50% ellipsoids viewed.

a variety

nsidere

inimal

mplexes

ifferent

quid set

n access

nconve

rious r

igure 1-

ordinat

ssibly ap

Dipl-T

duced.

sponse

He

operties

sters.

sters (

eterobi-

ferromagne

mpound

a variety of coordination geometries and oxidation states. Although considered sterically bulky, the ligand is quite flexible as evidenced by the fluxional and isomerization processes which have been observed for metal complexes of TMPP.[1] This flexibility has rendered it possible to access different oxidation states of the rhodium center while maintaining the same ligand set. Each of the complexes described in this study exhibit more than one accessible redox state. The most rich redox and electrochemical/chemical interconversions are found in the Rh series. Relationships between the various rhodium-TMPP complexes isolated in this study are illustrated in Figure 14. The ability of the TMPP ligand to adjust to the available coordination sites and the electronic requirements of the metal center is readily apparent when one examines the structural changes in going from $[Rh^{I}(\eta^2\text{-TMPP})_2][BF_4]$ to $[Rh^{II}(\eta^3\text{-TMPP})_2][BF_4]_2$. As the metal center is reduced, the hapticity of the phosphine ligand decreases from η^3 to η^2 in response to the decreased need for electron density at the metal center.

Heteropolymetallic molecules are of interest due to the unusual properties that can arise from electronic interactions between different metal centers. The availability of *cis*-oriented phosphine phenoxide ligands renders Co(TMPP-*O*)$_2$ an excellent "ligand" in the preparation of novel bi-, heterobi-, poly-, and heteropolymetallic complexes. The high spin d^7 parmagnetic species such as Co(TMPP-*O*)$_2$ produces paramagnetic compounds nuclearities ranging from dinuclear to hexanuclear. Such

synthons based on *cis* phenoxides should be generally useful for the deliberate preparation of clusters.

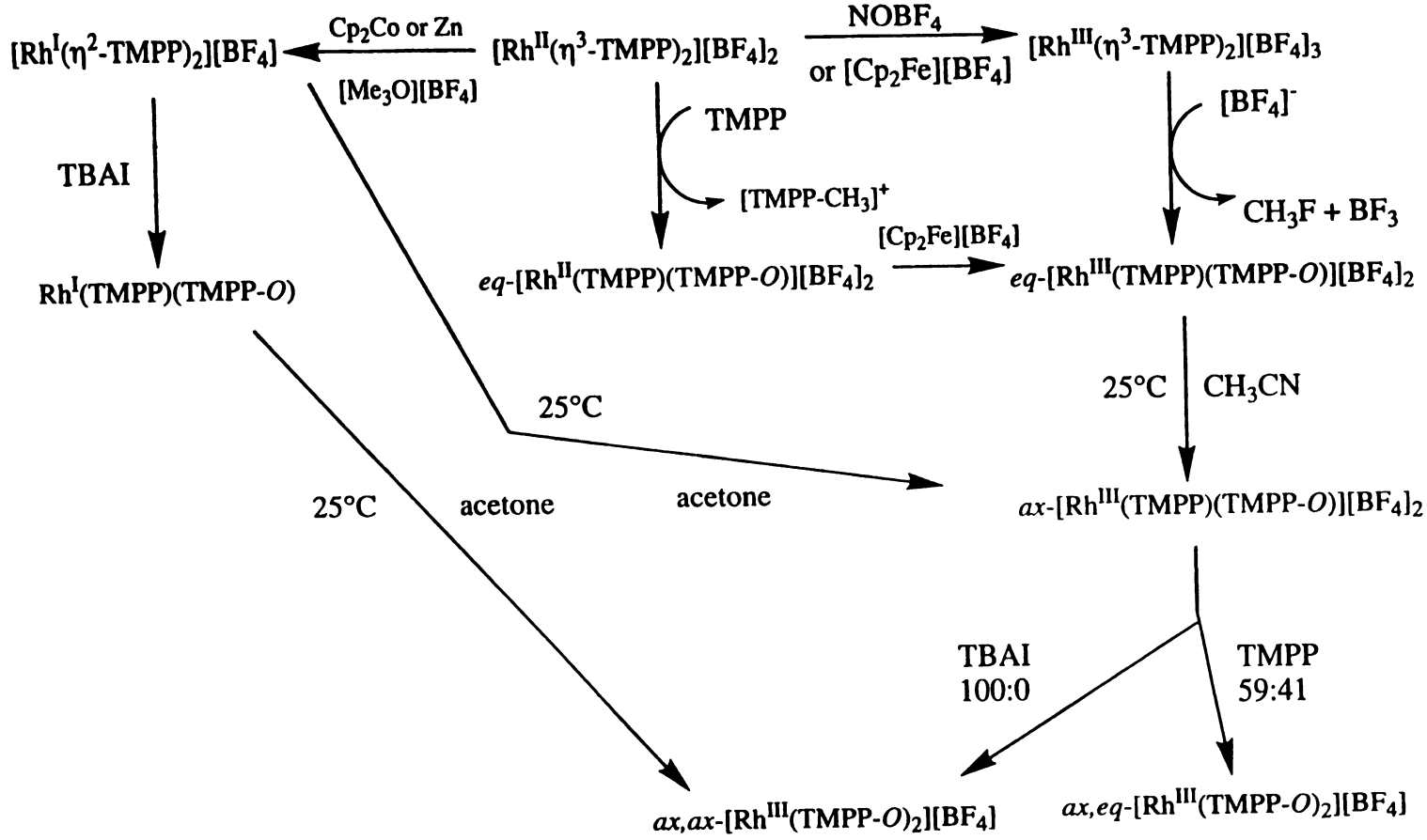

Figure 14. Interconversion pathways of the Rh-TMPP complexes.

List of References

1. (a) Dunbar, K. R.; Haefner, S. C.; Pence, L. E. *J. Am. Chem. Soc.* **1989**, *111*, 5504. (b) Dunbar, K. R.; Haefner, S. C.; Bender, C. *J. Am. Chem. Soc.* **1991**, *113*, 9540. (c) Dunbar, K. R.; Haefner, S. C.; Swepston, P. N. *J. Chem. Soc., Chem. Commun.* **1991**, 640. (d) Chen, S.-J.; Dunbar, K. R. *Inorg. Chem.*, **1991**, *30*, 2918. (e) Dunbar, K. R.; Haefner, S. C. *Organometallics* **1992**, *11*, 0000. (f) Dulebohn, J. I.; Haefner, S. C.; Bergland, K. A.; Dunbar, K. R. *Chem. of Mat.*, **1992**, *4*, 506. (g) Dunbar, K. R.; Quillevéré, A. *Organometallics*, **1993**, *12*, 618. (h) Dunbar, K. R.; Matonic, J. H.; Saharan, V. *Inorg. Chem.*, **1994**, *33*, 25. (i) Dunbar, K. R.; Quillevéré, A.; Sun, J.-S. *Inorg. Chem.*, **1994**, *33*, 2598. (j) Dunbar, K. R.; Sun, J.-S. *J. Chem. Soc. Chem. Comm.*, **1994**, *2387*. (k) Dunbar, K. R.; Haefner, S. C.; Uzelmeier, C. E.; Howard, A. *Inorg. Chim. Acta.*, **1995**, *240*, 527. (l) Quillevéré, A.; Uzelmeier, C. E.; Sun, J.-J.; Dunbar, K. R. manuscript in preparation. (m) Haefner, S. C.; Uzelmeier, C. E.; Dunbar, K. R. manuscript in preparation. (n) Quillevéré, A. Ph. D. Dissertation, Michigan State University, **1992**. (o) Sun, J.-J. Ph. D. Dissertation, Michigan State University, **1994**.

2. (a) Jones, R. A.; Lasch, J. G.; Norman, N. C.; Whittlesey, B. R.; Wright, T. C. *J. Am. Chem. Soc.* **1983**, *105*, 6184. (b) Kreter, P. E.; Meek, D. W. *Inorg. Chem.* **1983**, *22*, 319. (c) Carty, A. J. *Adv. Chem. Ser.* **1982**, *196*, 163. (d) Breen, M. J.; Geoffroy, G. L. *Organometallics* **1982**, *1*, 1437. (e) Jones, R. A.; Stuart, A. L.; Atwood, J. L.; Hunter, W. E.; Rogers, R. D. *Organometallics* **1982**, *1*, 1721. (f) Atwood, J. L.; Hunter, W. E.; Jones, R. A.; Wright, T. C. *Inorg. Chem.* **1983**, *22*, 993. (g) Jones, R. A.; Wright, T. C.; Atwood, J. L.; Hunter, W. E. *Organometallics* **1983**, *2*, 470.

3. see for example: (a) Lindner, E.; Dettinger, J. *Z. Naturforsch.* **1991**, *46b*, 432 and references therein. (b) Werner, H.; Stark, A.; Schultz, M.; Wolf, J. *Organometallics* **1992**, *11*, 1126.

4. (a) Jeffrey, J. C.; Rauchfuss, T. B. *Inorg. Chem.* **1979**, *18*, 2658. (b) Anderson, G. K.; Kumar, R. *Inorg. Chem.* **1984**, *23*, 4064. (c) Braunstein, P.; Matt, D.; Dusausay, Y. *Inorg. Chem.* **1983**, *22*, 2043. (d) Podlahová, J.; Kratochvil, B.; Langer, V. *Inorg. Chem.* **1981**, *20*, 2160. (e) Empsall, H. D.; Johnson, S.; Shaw, B. L. *J. Chem. Soc., Dalton Trans.* **1980**, 302. (f) O'Flynn, K. H. P.; Mc Donald, W. S. *Acta Cryst.* **1977**, *B33*, 194.

5. (a) Popov, L. D.; Shevts, A. A.; Kogan, V. A. *Koord. Khim.* **1989**, *15*, 1299. (b) Bader, A.; Lindner, E. *Coord. Chem. Rev.* **1991**, *108*, 27.

6. Dunbar, K. R.; Haefner, S. C.; Uzelmeier, C. E. manuscript in preparation.

7. (a) Ferguso, G. S..; Wolczanski, P.T.; Parkanyi, L.; Zonnevyle, M. C. *Organometallics*, **1988**, *7*, 1967. (b) Baxter, S.M.; Wolczanski, P.T.; Parkanyi, L.; Zonnevyle, M. C. *Organometallics*, **1990**, *9*, 2498.

8. Mills, D. K.; Hsiao, M. H.; Farmer, P. J.; Atnip, E. V.; Reibenspies, J. H.; Darensbourg, M. Y. *J. Am. Chem. Soc.* **1991**, *113*, 1421.

9. (a) Andrieu, J.; Braunstein, P.; Tiripicchio, A.; Ugozzoli, F. *Inorg. Chem.*, **1996**, *35*, 5975. (b) Braunstein, P.; Kelley, D. G.; Tiripicchio, A.; Ugozzoli, F. *Inorg. Chem.*, **1993**, *32*, 4845. (c) Braunstein, P.; Kelley, D. G.; Dusausoy, Y.; Bayeul, D.; Lanfranchi, M.; Tiripicchio, A. *Inorg. Chem.*, **1994**, *32*, 233. (d) Andrieu, J.; Braunstein, P.; Drillon, M.; Dusausoy, Y.; Ingold, F.; Rabu, P.; Tiripicchio, A.; Ugozzoli, F. *Inorg. Chem.*, **1996**, *35*, 5986.

10. (a) Andrieu, J.; Braunstein, P.; Drillon, M.; Dusausoy, Y.; Ingold, F.; Rabu, P.; Tiripicchio, A.; Ugozzoli, F., *Inorg. Chem.*, **1996**, *35*, 5986. (b) Klabunde, U.; Mulhaupt, R.; Herskovitz, T.; Janowicz, A. H.; Calabrese, J.; Ittel, S. D., *J. Polym. Sci.*, **1987**, *25*, 1989. (c) Klabunde, U.; Ittel, S. D., *J. Mol. Catal.*, **1987**, *41*, 123.

11. Uchiyana, T., *Bull. Chem. Soc. Jap.*, **1981**, *54*, 181.

12. Hathaway, B. J.; Holah, D. G.; Underhill, A. E. *J. Chem. Soc.* **1962**, 2444.

13. (a) Bino, A.; Cotton, F. A.; Fanwick, P. E. *Inorg. Chem.* **1979**, *18*, 3558. (b) Cotton, F. A.; Frenz, B. A.; Deganello, G.; Shaver, A. *J. Organomet. Chem.* **1973**, 227.

14. SHELXTL v. 5.04, G. M. Sheldrick and Siemens Analytical X-Ray Systems, Inc., **1997**, 6300 Enterprise Lane, Madison WI. 53719.

15. *Computing in Crystallography,* Diamond, R.; Ramasesham, S.; Venkatesan, K., Eds.; IUCr and the Indian Academy of Sciences, Banglore, **1980**; p.13.01.

16. MITHRIL: Integrated Direct Methods Computer Program, Gilmore, C. J. *J. Appl. Cryst.* 1984, ***17***, 42.

17. DIRDIF: Direct Methods for Difference Structure, An Automatic Procedure for Phase Extension; Refinement of Difference Structure Factors: Beurskens, R. T. Technical Report, 1984.

18. Backes, G.; Reinen, D. *Z. Anorg. Allg. Chem.* **1975**, *418*, 217.

19. Haefner, S. C. Ph. D. Dissertation, Michigan State University, **1992**.

20. Wada, M.; Higashizaki, S. *J. Chem. Soc., Chem. Commun.* **1984**, 482.

21. Boeré, R. T.; Montgomery, C. D.; Payne, N. C.; Willis, C. J. *Inorg. Chem.* 1985, ***24***, 3680.19. (a) Dimitrou, K.; Folting, K.; Streib.; Christou, G., *J. Am. Chem. Soc.*, **1993**, *115*, 6432. (b) Ama, T.; Miyazaki, J-i.; Hamada, K.; Okamoto, K-i.; Yonemura, T.; Kawaguchi, H.; Yasui, T., *Chem. Lett.*, **1995**, 267.

22. Cotton, F. A.; Wilkinson, G. *Advanced Inorganic Chemistry, 3rd Ed.* John Wiley & Sons: New York, **1972**.

23. (a) Igau, A.; Gladysz, J. A. *Polyhedron* **1991**, *10*, 1903. (b) Ferandez, J. M.; Gladysz, J. A. *Organometallics* **1989**, *8*, 207.

24. (a) Gorrel, I. B.; Parkin, G. *Inorg. Chem.* **1990**, *29*, 2452. (b) Thomas, R. R.; Chebolu, V.; Sen. A. *J. Am. Chem. Soc.* **1986**, *108*, 4096. (c) Crabtree, R. H.; Hlatky, G. G.; Holt, E. M. *J. Am. Chem. Soc.* **1983**, *105*, 7302. (d) Hitchcock, P. B.; Lappert, M. F.; Taylor, R. G. *J. Chem. Soc., Chem. Commun.* **1984**, 1082. (e) Reedijk, J. *Comments Inorg. Chem.* **1982**, *6*, 379 and references therein.

25. Baxter, S. M.; Wolczanski, P. T. *Organometallics* **1990**, *9*, 2498.

26. Ferguso, G. S.; Wolczanski, P. T; Parkanyi, L.; Zonnevylle, M. C. *Organometallics*, **1988**, *7*, 1967.

27. Carlin, R. L.; *Magnetochemistry*, Springer: New York, **1986**.

28. (a) Richens, D.T.; Guille-Photin, C. *J. Chem. Soc., Dalton Trans.*, **1990**, 407. (b) Alberto, R.; Egli, A.; Abram, U.; Hegetschweiler, K.; Gramlich, V.; Schubiger, P. A. *J. Chem. Soc., Dalton Trans.*, **1994**,

2815. (c) Speiccia, L.; Marty, W.; Giovanoli, R. *Inorg. Chem.*, **1988**, 27, 2660.

29. (a) Dimitrou, K.; Folting, K.; Streib.; Christou, G., *J. Am. Chem. Soc.*, **1993**, *115*, 6432. (b) Ama, T.; Miyazaki, J-i.; Hamada, K.; Okamoto, K-i.; Yonemura, T.; Kawaguchi, H.; Yasui, T., *Chem. Lett.*, **1995**, 267.

30. Reynolds, R.A.; Yu, W.O.; Dunham, W.R.; Coucouvanis, D., *Inorg. Chem.*, **1996**, *35*, 2721.

31. Kitajima, N.; Hikichi, S.; Tanaka, M.; Moro-oka, Y., *J. Am. Chem. Soc.*, **1993**, *115*, 5496.

32. Wood, R. M.; Palenik, G. J. *Inorg. Chem.*, **1998**, *37*, 4149.

33. Banci, L.; Bencini, A.; Benelli, C.; Gatteschi, D.; Zanchini, C. In *Structure and Bonding, Vol. 52*, Eds. Clarke, M. J.; Goodenough, J. B.; Hemmerich, P.; Ibers, J. P.; Jørgensen, C. K.; Neilands, J. B.; Reinen, S.; Weiss, R; Williams, R. J. P. Springer-Verlag: New York, **1962**, 37.

CHAPTER III

SYNTHESIS AND REACTIVITY OF $[M(o\text{-}P2)_2][BF_4]_x$

(M = Fe, Co, Ni, Pd, Pt, x = 2; M = Rh, x = 1)

1 Introd

The

backbone

n view of

pproach

ransitior

nding.

ngagate

ndustr

lymers

ave bee

the so

In

sen pla

ounde

imulta

ible

behavio

2 spi

learnin

he ger

1. Introduction

The incorporation of transition metal ions into a conjugated polymer backbone to form coordination polymers is the subject of considerable interest in view of the possible electrical and magnetic properties of such chains. One approach to *covalent* inorganic/organic materials involves the assemblies of transition metals into an organic array or polymer through direct σ/π bonding. It has been proposed that the introduction of metal ions into a conjugated chain could lead to partially-filled bands and possibly metallic conductivity.[1] In terms of paramagnetic systems, several coordination polymers with magnetic metal ions (Cu^{2+}, Mn^{3+}) bridged by organic ligands have been reported by Kahn and others to exhibit ferrimagnetic interactions in the solid state.[2]

In spite of the considerable activity in the fields, little emphasis has been placed on the use of *open-shell* ligands to bridge metal ions which could provide the linking bidentate or tetradentate functionality with a simultaneous contribution to the electronic and/or magnetic properties of the whole composite chain. For example one may anticipate ferrimagnetic behavior in composite chains formed of both metal ($S > 1/2$) and organic ($S = 1/2$) spins.

In this vein, we are investigating the reactivity of multidentate ligands bearing the extra redox functionality of a TTF core. The use of phosphorus as the central atom in connecting TTF molecules is particularly intriguing, not

nly for

potential

The mixi

xpected

ifferent

Fo

the typ

ethia

-P2. I

xcellen

odels

molep

Rho-P

the din

Prepara

-Ni C

-NiTC

2. Exp

A Syn

S

P C6H

M = P

only for engendering new radical TTF-TTF π-interactions, but for their potential as ligands in new mixed-valence mono- and polymetallic species. The mixing of dπ-pπ metal-TTF frontier orbitals in such "hybrid" systems is expected to lead to unique electronic and/or magnetic behavior that is quite different from the "all-organic" charge transfer materials.

Fourmigué *et al.* first demonstrated that phosphorus(III) compounds of the types in Figure 7 could readily be synthesized from the tetrathiafulvalenyl lithium derivatives by preparing *ortho*-$(CH_3)_2(PPh_2)_2TTF$ (*o*-P2, **1**).[3] While *o*-P2 will not form extended structures, it can act as an excellent ligand for forming mononuclear complexes which may be viewed as models for the extended structures anticipated for P4 (**2**). Precedence for homoleptic compounds containing two *o*-P2 ligands exists in the form of $[Rh(o\text{-}P2)_2][BF_4]$, prepared from the reaction of 4 equivalents of *o*-P2 (**1**) with the dinuclear complex $[Rh_2(NCCH_3)_{10}][BF_4]_4$.[4] This chapter describes the preparation and characterization of the homoleptic series $[M(o\text{-}P2)_2][BF_4]_2$ (M = Ni, Co, Pd, Pt, Fe) as well as the chemical oxidation and metathesis with [Li][TCNQ] of $[Rh(o\text{-}P2)_2][BF_4]$.

2. Experimental

A. Synthesis

Starting Materials and Reaction Procedures. *Ortho*-$[P(C_6H_5)_2]_2(CH_3)_2TTF$ (*o*-P2),[3] $[M(NCCH_3)_x][BF_4]_2$ (M = Ni, Co, Fe,[5] Pd,[6] x = 6; M = Pt,[7] x = 4), $M(CF_3SO_3)_2$ (M = Ni, Fe)[8] and $[Rh(o\text{-}P2)_2][BF_4]$[4] and

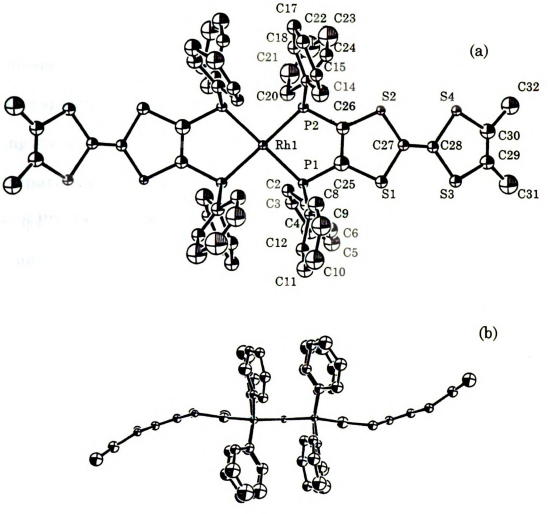

Figure 15. ORTEP representation of $[Rh(o\text{-}P2)_2][BF_4]$ viewed from the (a) top and (b) side with 50% probability ellpsoids.

[Li][TCNQ][9] were prepared according to published procedures. $NOBF_4$ was purchased from Aldrich Chemical Co. and was used as received. Acetonitrile, acetone, and CH_2Cl_2 were distilled over 3 Å molecular sieves. Diethyl ether and toluene were distilled over sodium-potassium/benzophenone. Unless otherwise specified, all reactions were carried out under an argon atmosphere by using standard Schlenk-line techniques.

(1) Preparation of $[M(o\text{-}P2)_2][BF_4]_2$.

(i) $[Ni(o\text{-}P2)_2][BF_4]_2$ (8). In separate flasks, $[Ni(MeCN)_{6.5}][BF_4]_2$ (0.040 g, 0.080 mmol) and *o*-P2 (1) (0.306 g, 0.510 mmol) were dissolved in 5 mL of acetonitrile and 15 mL of CH_2Cl_2 respectively. A 5 mL (0.170 mmol) aliquot of the orange phosphine solution was added via syringe to the blue nickel solution, prodwhich produced an immediate color change to brown. After stirring for 12 h, the solution was concentrated to a volume of 5 mL, treated with 20 mL of Et_2O to produce a red-brown solid, and filtered in air. The solid was then washed with *copious* amounts of Et_2O, and dried *in vacuo*; yield 0.098 g (85%). Single crystals were grown by slow diffusion of toluene into an CH_2Cl_2 solution of 8. ^1H NMR (CD_3CN) δ ppm: $-CH_3$, 1.82 (s); Ph-H, 7.16 (m), 7.35 (m), 7.68 (m). ^{13}C NMR (CD_3CN) δ ppm: 15.2 ($-CH_3$), 107.2 (inner C=C), 119.2 (inner C=C), 124.3 (outer C=C), 125.8 (outer C=C), 132.6 (Ph), 136.2 (Ph), 136.6 (Ph), 150.0. $^{31}P\{^1H\}$ NMR (CD_3CN) δ ppm: 42.1. IR (Nujol, cm^{-1}): 1058 (br, $\nu_{B\text{-}F}$), 691 (m, $\nu_{=C\text{-}H}$), 506 (s, $\nu_{C=C}$). C.V. (0.2 M CH_2Cl_2/$TBABF_4$, Pt electrode vs Ag/AgCl): $E_{(p,c)}$ = -0.27 V, $E_{1/2}(ox)_1$ = +0.68 V,

$E_{1/2}(ox)_2$ = +1.08 V. UV/Visible (CH_3CN) λ_{max}, nm (ε, $M^{-1}cm^{-1}$): 510 ($3.5x10^3$), 325 ($2.1x10^4$), 266 ($3.0x10^4$). FAB-MS (m/z): 630 ($M^{2+}/2$), 1260 (M^+).

(ii) $[Co(o\text{-}P2)_2][BF_4]_2$ (9). In separate flasks, 0.040 g (0.084 mmol) of $[Co(NCCH_3)_6][BF_4]_2$) was dissolved in 5 mL of acetonitrile, and 0.103 g (0.171 mmol) of *o*-P2 (1) was dissolved in 5 mL of CH_2Cl_2. The cobalt solution was added to the TTF solution, which effected a color change to dark brown, and the reaction solution was stirred for 12 h. The solution volume was reduced by ~50%, treated with 20 mL of toluene and reduced in volume to afford a brown solid that was isolated by filtration in air. The remaining solid was washed with 3 x 10 mL of toluene to remove unreacted *o*-P2, and 4 x 5 mL of Et_2O until the washings became colorless. Finally, the solid was dried *in vacuo*; yield 0.098 g (83%). *Anal.* Calcd for **8**, $CoP_4S_8C_{64}H_{52}B_2F_8$: C, 53.87; H, 3.86. Found: C, 54.65; H, 3.90. ^1H NMR (CD_3CN) δ ppm: broad and unresolved. $^{31}P\{^1H\}$ NMR (CD_3CN) δ ppm: not observed. IR (Nujol, cm^{-1}): 1058 (br, $\nu_{B\text{-}F}$), 692 (m,$\nu_{=C\text{-}H}$), 534 (s, $\nu_{C\equiv C}$). C.V. (0.1 M $CH_3CN/TBABF_4$, Pt electrode vs Ag/AgCl): $E_{(p,c)1}$ = -0.91 V, $E_{(p,c)2}$ = -1.19 V, $E_{1/2}(ox)_1$ = +0.63 V, $E_{1/2}(ox)_2$ = +1.07 V. UV/Visible (CH_3CN) λ_{max}, nm (ε, $M^{-1}cm^{-1}$): 506 ($5.0x10_3$), 326 sh($1.5x10_4$), 291 ($1.8x10_4$), 261 ($2.3x10_4$). FAB-MS (m/z): 629 ($M^{2+}/2$), 1259 (M^+). EPR (50:50 CH_3CN/toluene, 107 K) $g_\perp$ = 2.29, $g_{||}$ = 2.04 ($|A|$ = 70.7 G); (solid, 4 K) g = 4.08, $g_\perp$ = 2.22, $g_{||}$ = 2.05. Magnetic moment: μ_{eff} = 4.62 μ_B (320 K, S = 3/2), 2.51 μ_B (5 K, S' = 1/2).

(iii) $[Pd^{II}(o\text{-}P2)_2][BF_4]_2$ (10). A 5 mL aliquot (0.172 mmol) of a 15 mL stock solution of *o*-P2 (1) (0.309 g, 0.515 mmol total) in CH_2Cl_2 was added to a solution of $[Pd(NCCH_3)_6][BF_4]_2$ (0.042 g, 0.080 mmol) dissolved in 5 mL of acetonitrile, causing an immediate color change from orange to brown. The solution was stirred overnight, concentrated to ~5 mL, and treated with 20 mL of Et_2O to afford a brown precipitate. The solid was isolated by filtering in air, was washed with *copious* amounts of Et_2O, and dried under reduced pressure. ^1H NMR (CD_3CN) δ ppm: $-CH_3$, 1.83 (s); Ph-H, 7.25 (m), 7.60 (m). $^{31}P\{^1H\}$ NMR (CD_3CN) δ ppm: 43.9. IR (Nujol, cm^{-1}): 1057 (br, $\nu_{B\text{-}F}$), 690 (m, $\nu_{=C\text{-}H}$), 519 (s, $\nu_{C\equiv C}$). C.V. (0.2 M CH_2Cl_2/TBAPF$_6$, Pt electrode vs Ag/AgCl): $E_{1/2}$(red) = -0.31 V, $E_{1/2}(ox)_1$ = +0.64 V, $E_{1/2}(ox)_2$ = +1.16 V. UV/Visible (CH_3CN) λ_{max}, nm (ε, $M^{-1}cm^{-1}$): 421 ($5.7x10^3$), 332 ($8.0x10^4$), 295 sh($5.5x10^4$), 265 ($3.3x10^4$). FAB-MS (m/z): 653 ($M^{2+}/2$), 1306 (M^+).

(iv) $[Pt(o\text{-}P2)_2][BF_4]_2$ (11). $[Pt(NCCH_3)_4][BF_4]_2$ (0.046 g, 0.075 mmol) and *o*-P2 (0.109 g, 0.182 mmol) were dissolved in 10 mL of CH_2Cl_2, to give a red-orange solution, which was stirred for 12 h. The solution was then reduced to 5 mL, and 20 mL of Et_2O was added to precipitate a red-orange solid. The mixture was filtered in air, washed with 15 mL diethyl ether, and dried *in vacuo*; yield 0.078 g (67%). Single crystals were grown by slow diffusion of Et_2O into a CH_2Cl_2 solution of **11** following treatment with, and removal of, toluene. ^1H NMR (CD_3CN) δ ppm: $-CH_3$, 1.82 (s); Ph-H, 7.38 (m), 7.56 (m). $^{31}P\{^1H\}$ NMR (CD_3CN) δ ppm: 35.8 ($^2J_{Pt\text{-}P}$ = 2357 Hz). IR (Nujol, cm^{-1}): 1059

(br, ν_{B-F}), 690 (m, $\nu_{=C-H}$), 525 (s, $\nu_{C=C}$). C.V. (0.2 M CH_2Cl_2/TBAPF$_6$, Pt electrode vs Ag/AgCl): $E_{1/2}$(red) = -0.45 V, $E_{1/2}(ox)_1$ = +0.70 V, $E_{1/2}(ox)_2$ = +1.19 V. UV/Visible (CH_3CN) λ_{max}, nm (ε, $M^{-1}cm^{-1}$): 458 ($1.7x10^3$), 315 ($2.5x10^4$), 248 ($2.9x10^4$). FAB-MS (m/z): 698 ($M^{2+}/2$), 1296 (M^+).

(v) [Fe(*o*-P2)$_2$][BF$_4$]$_2$ (12). A quantity of [Fe(NCCH$_3$)$_6$][BF$_4$]$_4$ (0.041 g, 0.086 mmol) was loaded into a Schlenk flask and dissolved in 5 mL of acetonitrile. A stock solution of 0.309 g (0.515 mmol) of *o*-P2 (1) dissolved in 15 mL of CH_2Cl_2 was prepared. A 5 mL (0.172 mmol) aliquot of the phosphine stock solution was added to the metal complex and the solution was stirred for 12 h. The solution was concentrated to ~5 mL, treated with 20 mL of Et_2O, and the solution was decanted from the red solid. The solid was washed with 10 mL portions of Et_2O until the washings were clear, and dried under reduced pressure; yield 0.041 g (34%). $_1$H NMR (CD_3CN) δ ppm: Ph-H, 7.54 (m), 7.68 (m). $^{31}P\{^1H\}$ NMR (CD_3CN) δ ppm: 56.1, 75.5. ^{19}F NMR (CD_3CN) δ ppm: -503.0, -148.6. IR (Nujol, cm^{-1}): 1063 (br, ν_{B-F}), 699 (m, $\nu_{=C-H}$), 519 (s, $\nu_{C=C}$). FAB-MS (m/z): 1256 (M^+), 1275 ($[M+F]^+$).

(2) Reactions of M(CF$_3$SO$_3$)$_2$ with *o*-P2 (1).

(i) Preparation of [Ni(*o*-P2)$_2$][CF$_3$SO$_3$]$_2$ (13). In separate flasks, Ni(CF$_3$SO$_3$)$_2$ (0.040 g, 0.112 mmol) and *o*-P2 (1) (0.306 g, 0.510 mmol) were dissolved in 5 mL of acetonitrile and 15 mL of CH_2Cl_2 respectively. A 5 mL aliquot (0.170 mmol) of the orange phosphine solution was added via syringe to the blue nickel solution, producing an immediate color change to brown.

After stirring for 12 h, the solution was concentrated to a volume of 5 mL, treated with 45 mL of Et_2O, and cooled in an ice bath to precipitate a red-brown solid. The liquid was decanted, and the solid was washed 3 times with 5 mL amounts of Et_2O, and dried under reduced pressure; yield 0.098 g (85%). ^1H NMR (CD_3CN) δ ppm: $-CH_3$, 1.82 (s, 12H); Ph-H, 7.16 (m, 16H), 7.32 (m, 16H), 7.35 (br, 8H). $^{31}P\{^1H\}$ NMR (CD_3CN) δ ppm: 46.6. FAB-MS (m/z): 629 ($M^{2+}/2$), 1260 (M^+), 1409 ($[M+OTf]^+$).

(ii) Reaction of $Fe(CF_3SO_3)_2$ with *o*-P2 (1). $Fe(CF_3SO_3)_2$ (0.056 g, 0.158 mmol) was dissolved in 5 mL of acetonitrile, and *o*-P2 (1) (0.2032 g, 0.339 mmol) was dissolved in 11 mL of CH_2Cl_2. A 5.5 mL (0.169 mmol) aliquot of the phosphine stock solution was added to the metal complex and the solution was stirred several days. The solution was treated with 15 mL of toluene and concentrated under vacuum resulting in the formation of orange needles. Analysis of one such crystal by single crystal X-ray diffraction revealed its identity to be unbound *o*-P2 (1). $^{31}P\{^1H\}$ NMR (CD_2Cl_2) δ ppm: -18.1.

(3) Oxidation of $[Rh_I(o\text{-}P2)_2][BF_4]$ with $NOBF_4$: Preparation of $[Rh_I(o\text{-}P2)_2][BF_4]_3$ (14).

Quantities of $[Rh^I(o\text{-}P2)_2][BF_4]$ (0.111 g 0.080 mmol) and $NOBF_4$ (0.028 g, 0.240 mmol) were loaded into a 150 mL pear-shaped Schlenk flask, covered in aluminum foil to avoid light, cooled in an ice bath, and dissolved in 10 mL of CH_2Cl_2. The foil and cold bath were removed, the flask was briefly exposed

to a vacuum, and the dark green solution was stirred for 12 h. The solution volume was reduced to dryness under vacuum and the resulting residue redissolved in 5 mL CH_2Cl_2 and treated with 20 mL of Et_2O to afford a green precipitate. The solid was isolated by filtration through Celite, extraction with additional CH_2Cl_2, concentration of the resulting solution to ~5 mL, and treatment with 20 mL of Et_2O to re-precipitate the product. The liquid was decanted, the solid was washed 4 times with 7 mL of Et_2O, and dried *in vacuo*; yield 0.114 g (86% for $[Rh^I(o\text{-}P2)_2][BF_4]_3$). EPR (50:50 CH_3CN/toluene, 95 K) g = 2.02.

(4) Reaction of $[Rh^I(o\text{-}P2)_2][BF_4]$ with [Li][TCNQ].

An acetone solution of [Li][TCNQ] (0.019 g, 0.090 mmol, 40 mL) was filtered through a Schlenked frit to remove undissolved solid, and added to a CH_2Cl_2 solution of $[Rh(o\text{-}P2)_2][BF_4]$ (0.032 g, 0.022 mmol, 10 mL). The reaction mixture was stirred with slight warming for 3 h (to ensure dissolution of the [Li][TCNQ]), during which time a fine green precipitate formed. The mixture was filtered, the solid washed 3 times with 5 mL of acetone, and finally dried *in vacuo*; yield 0.030 g (91%). IR (Nujol, cm^{-1}): 2178 (m, ν_{C+N}), 2153 (m, ν_{C+N}), 692 (s, $\nu_{=C\text{-}H}$), 521 (s, $\nu_{C=C}$).

B. X-ray Crystallography

The structures of the compounds $[Ni(o\text{-}P2)_2][BF_4]_2$ (8) and $[Pt(o\text{-}P2)_2][BF_2]_2$ (11) were determined by application of general procedures that

Table 5. Summary of crystallographic data for $[Ni(o\text{-}P2)_2][BF_4]_2 \cdot 2C_7H_8$ ($\mathbf{8} \cdot 2C_7H_8$) and $[Pt(o\text{-}P2)_2][BF_4]_2 \cdot 2C_7H_8$ ($\mathbf{11} \cdot 2C_7H_8$).

	$\mathbf{8} \cdot 2C_7H_8$	$\mathbf{11} \cdot 2C_7H_8$
Formula	$NiS_8P_4F_8C_{98}B_2H_{52}$	$PtS_8P_4F_8C_{90}B_2H_{52}$
Formula weight	1842.1	1882.39
Space group	C2/m	C2/m
a, Å	24.677(2)	24.617(2)
b, Å	14.3220(13)	14.3476(13)
c, Å	15.4465(13)	15.5292(13)
α, deg	90	90
β, deg	127.169(10)	127.072(10)
γ, deg	90	90
V, Å^3	4350.2(6)	4376.2(6)
Z	2	2
d_{calc}, g/cm^3	1.406	1.429
μ, cm^{-1}	0.554	1.928
Temperature, °C	293 ± 2	293 ± 2
R1[a]	0.075	0.060
wR2[b]	0.195	0.162
quality-of-fit[c]	1.142	0.675

[a] $R = \sum| |$ [a] $R = \sum| |F_o| - |F_c| |/\sum|F_o|$. [b] $wR2 = [\sum [w(F_o^2-F_c^2)^2]/\sum [w(F_o^2)^2]]^{1/2}$

[c] quality-of-fit = $[\sum w(|F_o| - |F_c|)^2/(N_{obs}-N_{parameter})]^{1/2}$

have b

nforma

summa

structu

refiner

(i) [N

(i) I

P[OP

CH2Cl

U_{iso} w

Ir 8

mmol

benal

obse

Ir in

Fill v

were

Refe

Refi

(ii) S

Spec

Spec

have been fully described elsewhere.[10] Crystal parameters and basic information pertaining to data collection and structure refinement are summarized in Table 5. Structure was solved using the SHELXL 93 structure solution program and refined by full-matrix least-squares refinement on F^2.[11,12]

(1) $[Ni(o\text{-}P2)_2][BF_4]_2 \cdot 2C_7H_8$ ($8 \cdot 2C_7H_8$)

(i) Data Collection and Reduction. Single crystals of $[Ni(o\text{-}P2)_2][BF_4]_2 \cdot 2C_7H_8$ ($8 \cdot 2C_7H_8$) were grown by slow diffusion of Et_2O into an CH_2Cl_2 solution of 8. A brown platelet of dimensions 0.15 x 0.11 x 0.027 mm^3 was mounted on the tip of a glass fiber and secured with epoxy. Data for 8 were collected on a Stoe IPDS diffractometer equipped with monochromated MoKα radiation at 293+2 °C in a θ range of 1.9 to 26.0°. Initial data indicated that the crystal belonged to a monoclinic system; subsequent solution and successful refinement of the structure was carried out in the C2/m space group. Of the 21449 reflections that were collected, 4411 were unique, and 2767 data were observed with $I > 2.00\sigma(I)$. The data were corrected for Lorentz polarization effects, and an empirical absorption correction based on azimuthal ψ-scans near $\chi = 90°$ was applied which resulted in transmission factors ranging from 0.822 to 0.971.

(ii) Structure Solution and Refinement. The structure was solved by direct methods and refined by full-matrix least squares refinement. All non-hydrogen atoms, except those associated with the solvent, were refined

anisotropically. Hydrogen atoms were not included in refinement. Atoms C(51) through C(57) were found to define a toluene molecule disordered over two positions with a center of inversion relating the two solvents. The molecule was refined with restraints keeping C(52)···C(57) and C(56)···C(57) equidistant. Occupancies were refined such that the independent toluene fragments possessed an occupancy of 0.5, resulting in a sum of 1.0. A second toluene molecule defined by atoms C(21) through C(27) was located and refined with restraints on the C-C distances within the ring, as well as on the C···C distances between alternating C atoms of the ring (e.g. C(24)···C(22)). Additional restraints were added to keep C(22)-C(27) and C(26)-C(27) distances equal. Hydrogen atoms were not included with the solvent molecules.

The final refinement was based on 5000 reflections that were used to fit 261 parameters to give R1 = 0.0752 and wR2 = 0.1949. The goodness-of-fit index was 1.142, and the maximum shift in the final difference map was 0.030 Å associated with C(57) After the last least squares cycle, the mean shift/esd was 0.043 and the highest peak in the difference Fourier map was 2.15 $e^-/Å^3$ which is associated with C(22). This peak is at the center of the solvent ring defined by C(21)-C(26), and indicates additional disorder associated with the ring that must be modeled.

(2) $[Pt(o\text{-}P2)_2][BF_4]_2 \cdot 2C_7H_8$ ($11 \cdot 2C_7H_8$)

(i) Data Collection and Reduction. Single crystals of $[Pt(o\text{-}P2)_2][BF_4]_2 \cdot 2C_7H_8$ ($11 \cdot 2C_7H_8$) were grown by slow diffusion of diethyl ether into an acetonitrile solution of the compound. A red-orange platelet of dimensions 0.06 x 0.06 x 0.03 mm^3 was mounted on the tip of a glass fiber and secured with epoxy. Data for **11** were collected on a Stoe IPDS diffractometer equipped with monochromated MoKα radiation at 293+2 °C in a θ range of 1.70 to 25.9°. Initial data indicated that the crystal belonged to a monoclinic system; subsequent solution and successful refinement of the structure was carried out in the C2/m space group. Of the 21325 reflections that were collected, 4404 were unique, and 2426 data were observed with $I > 2.00\sigma(I)$. The data were corrected for Lorentz polarization effects, and an empirical absorption correction based on azimuthal ψ-scans near $\chi = 90°$ was applied which resulted in transmission factors ranging from 0.7870 to 0.9175.

(ii) Structure Solution and Refinement. The structure was solved by direct methods and refined by full-matrix least squares refinement. All non-hydrogen atoms, except those associated with the solvent, were refined anisotropically. Hydrogen atoms were not included in refinement. Atoms C(31) through C(35) were found to define a toluene molecule disordered over two positions with a center of invresion relating the two solvents. The molecule was refined with restraints keeping C(32)···C(31) and C(34)···C(31) equidistant. Occupancies were refined such that the independent toluene

fragments are at an occupancy of 0.5, resulting in a sum of 1.0. A second toluene molecule defined by atoms C(51) through C(57) was located and refined with restraints on the C-C distances within the ring, as well as on the C···C distances between alternating C atoms of the ring (e.g. C(54)···C(52)). Additional restraints were added to keep C(52)-C(57) and C(56)-C(57) distances equal. Hydrogen atoms were not included with the solvent molecules. The final refinement was based on 5000 reflections that were used to fit 266 parameters to give R1 = 0.0603 and wR2 = 0.1616. The goodness-of-fit index was 0.675, and the maximum shift in the final difference map was 0.148 Å associated with C(56). After the last least squares cycle, the mean shift/esd was 0.224 and the highest peak in the difference Fourier map was 1.79 $e^-/Å^3$ which is associated with C(58). This peak is at the center of the solvent ring defined by C(51)-C(56), with C(58) part of an unresolved solvent molecule, indicating further modeling is needed.

3. Results and Discussion

The homoleptic complexes $[M(o\text{-}P2)_2][BF_4]_2$ (M = Ni (**8**), Co (**9**), Pd (**10**), Pt (**11**), Fe (**12**)) can be prepared by reacting the appropriate acentonitrile complex, $[M(NCCH_3)_x][BF_4]_2$ (x = 4, 6), with 2 equivalents of the phosphine ligand, *o*-P2 (**1**). The complexes have been characterized by NMR, infrared, and electronic absorbance spectroscopies, as well as FAB-MS. EPR and magnetic susceptibility studies of the paramagnetic Co^{II} complex have also

been conducted, indicating a change from high spin in solution to low spin in the solid state. ^{19}F NMR spectroscopy and FAB-MS support the tendency for **12** to coordinate F-, to yield $[Fe(o\text{-}P)_2F]^+$ species. Compounds **8**, **10**, and **11** display redox chemistry which involve both the divalent metal center and the TTF groups.

The structures of **8** and **11** have been determined by single crystal X-ray diffraction methods. Crystal parameters and basic information pertaining to data collection and structure refinement are summarized in Table 5. ORTEP representations of $[Ni(o\text{-}P2)_2][BF_4]_2$ (**8**) and $[Pt(o\text{-}P2)_2][BF_4]_2$ (**11**) are depicted in Figures 16 and 18. Selected bond distances and angles for each structure are listed in Table 6.

Oxidation of $[Rh(o\text{-}P2)_2][BF_4]$ with 3 equivalents of $NOBF_4$ results in oxidation of the TTF units and formation of $[Rh(o\text{-}P2)_2][BF_4]_3$ (**13**). The organic radical, **13**, has been studied by EPR spectroscopy. Preliminary infrared anaylsis suggest that the counterion in $[Rh(o\text{-}P2)_2][BF_4]$ can be replaced with another organic radical, $[TCNQ]^-$, by metathesis with [Li][TCNQ].

A. Preparation of $[M(o\text{-}P2)_2][BF_4]_2$ (M = Ni, Co, Pd, Pt, Fe)

The reaction of $[M(NCCH_3)_x][BF_4]_2$ (M = Ni, Co, Pd, Fe, x = 6; M = Pt, x = 4) with 2 equivalents of *o*-P2 (**1**) result in the formation of the appropriate homoleptic complex, $[M(o\text{-}P)_2][BF_4]_2$ (**8-12**). The reactions were all performed with the metal complex dissolved in acetonitrile and the ligand in CH_2Cl_2,

with the exception of M = Pt, where both reactants were dissolved in CH_2Cl_2. The procedures are similar to that used in the synthesis of $[Rh(o\text{-}P2)_2][BF_4]$, but mononuclear, rather than dinuclear, solvated cations were used as starting materials. The displacement of acetonitrile for phosphine is rapid, as evidenced by the immediate color changes observed for M = Ni, Co, and Pd. The products range in color from red to brown, with the TTF chromophore dominating the perceived color. These colors indicate that the reactions occur with retention of the metal's oxidation state, as green is indicative of oxidized TTF.

The products are all air stable and relatively insensitive to light in the solid state, but **10** and **11** are prone to decomposition if exposed to light for extended periods of time in solution (> 3 days). Such photochemical sensitivity has been well documented for other complexes of both metals.[13] The decomposition of these compounds is accelerated in the presence of chlorinated solvents, most likely owing to the instability of the phosphine ligand in this medium.[14] The complexes are soluble in nitriles, chlorinated solvents, and acetone.

B. Spectrosopic Characterization of $[M(o\text{-}P2)_2][BF_4]_2$ (M = Ni, Co, Pd, Pt, Fe)

(1) NMR Spectroscopic Studies of $[M(o\text{-}P2)_2][BF_4]_2$ (8-12)

(i) ^1H and $^{31}P\{^1H\}$ NMR. The ^1H NMR spectra of **8** and **10-11** in CD_3CN exhibit a series of multiplets in the region δ = 7.2 - 7.7 ppm due to the phenyl

protons, and a singlet at δ = ~1.8 ppm due to the methyl protons. The $^{31}P\{^{1}H\}$ NMR spectra of **8** and **10** each contain a single resonance at δ = 42.1 and 43.9 ppm respectively, while **11** shows a singlet with platinum satellites at 35.8 ppm ($J_{Pt\text{-}P}$ = 2357 Hz). The downfield shift of the signal from the free phosphine at -18.8 ppm is a result of 5-coordinate ring stabilization,[3] and indicates that the phosphine chelates the metal whereas the $J_{Pt\text{-}P}$ value is indicative of *trans*-disposed chlorides.[15] Compound **9** exhibits no resonances in its $^{31}P\{^{1}H\}$ NMR spectrum, and only broad signals in the ^{1}H spectrum, indicating a paramagnetic complex.

The presence of an NMR signal for $[Fe(o\text{-}P2)_2][BF_4]_2$ (**12**) indicates a diamagnetic product, with the metal behaving as a low-spin, d^6, Fe^{II} center. A freshly isolated sample of **12** contains a singlet in its $^{31}P\{^{1}H\}$ NMR spectrum at 56.1 ppm. The downfield shift is in the range expected for coordinated *o*-P2 and supports bound phosphine atoms, while the absence of additional signals indicates one phosphorus environment. Shortly after recovery of the product a second signal can be observed at δ = 76.2 ppm. Eventually the upfield peak is completely replaced by the downfield singlet, which indicates that it is a separate species that forms over time. The signal is at considerably lower fields than the region expected for coordinated *o*-P2, a fact that may indicate the presence of coordinated fluoride.[16] The ^{1}H NMR spectrum of **12**, while containing the expected phenyl resonances between δ = 7.5 and 7.7 ppm, exhibits no observable methyl-proton resonance. This

discrepancy in the ^{1}H NMR spectrum of **12** remains unresolved and is cause for further investigation.

(ii) Variable Temperature ^{19}F and $^{31}P\{^{1}H\}$ NMR of $[Fe(o\text{-}P2)_2][BF_4]_2$ (12). The ^{19}F NMR spectrum contains singlets appearing at δ = -148.6 and -503.0 ppm. The resonance at -148 ppm falls in the range for uncoordinated $[BF_4]^-$, but some M-BF_4 complexes exhibit ^{19}F NMR signals near the position of the uncoordinated anion due to their free F atoms.[16d] The singlet at -503.0 ppm is indicative of bound fluoride, and falls into the range for both coordinated $[F]^-$ and $[BF_4]^-$.[16b,e] $^{31}P\{^{1}H\}$ NMR spectra measured at temperatures as low as -40°C revealed no splitting due to the coordinated fluoride, possibly due to fast anion exchange if the fluoride interaction is a result of coordinated $[BF_4]^-$. [16b] Additional variable temperature studies of the $^{31}P\{^{1}H\}$ NMR spectra of **12** reveal that the coordinated flouride can be affected by temperature. The room temperature $^{31}P\{^{1}H\}$ NMR spectrum of a representative sample of **12**, taken shortly after isolation, displayed a ratio of roughly 2.3:1 for the downfield:upfield shift integrations. Upon cooling to -40°C, this ratio shifts dramatically in favor of the F-coordinated peak, leaving a ratio of 3:1. At higher temperatures the opposite behavior was found, with a ratio of 1.4:1 observed at 60°C, indicating that the coordinated group can be forced outersphere with increased temperature. This "fluxionality" may indicate the bound group is $[BF_4]^-$, as coordinated $[F]^-$ would be less likely to dissociate with mild heating. These changes are

mirrored in the ^{19}F spectrum, where the resonance at -148 ppm was found to dominate at higher temperatures, supporting the partial loss of bound $[BF_4]^-$.

(2) Infrared and Electronic Absorbance Spectroscopy

The infrared spectra of **8-12** display bands at ca. 690 and 520 cm^{-1} attributable to out-of-plane bends for the phenyl rings of *o*-P2. Strong features at ca. 1058 cm^{-1} are due to the B-F stretch of the $[BF_4]^-$ groups. The absence of peaks at higher wavenumbers (c.a. 2300 cm^{-1}) supports complete displacement of acetonitrile, but is not conclusive due to the fact that the frequency and intensity of the C≡N stretching vibration can be quite variable, and in some cases be absent when coordinated nitrile is present.[17] Electronic spectra of **8-11** recorded in acetonitrile exhibit transitions attributable to the phenyl groups between 248 and 266 nm, and the TTF group at 291-332 and 421-510 nm.

(3) FAB-MS of $[M(o\text{-}P2)_2][BF_4]_2$ (M = Ni, Co, Pd, Pt, Fe) (8-12)

Fast Atom Bombardment Mass Spectrometry (FAB-MS) of **8-12** vary with the identity of the metal center. The FAB-MS spectra of compounds **8-11** contain peaks associated with the appropriate mono-cationic complex, $[M(o\text{-}P2)_2]^+$ and the di-cationic species, $[M(o\text{-}P2)_2]^{2+}$. Retention of the $[BF_4]^-$ moiety is seen in **10** and **11** through the presence of $[M(o\text{-}P2)_2][BF_4]^+$ as a medium intensity peak.[18] Compounds **8-12** all produce peaks which represent oxygen addition to the intact molecule, $[M(o\text{-}P2)_2+O]^+$. Similarly, the spectra of **9** and **12** display peaks representing $[o\text{-}P2]^+$ (m/z = 600), [*o*-

P2+O]$^+$ (m/z = 616), and [*o*-P2+2O]$^+$ (m/z = 632). This oxygen addition has been seen previously in the isolation of dioxidized P4 (*trans*-$P4O_2$).[19] The most intense peak in the FAB-MS spectrum of $[Fe(o\text{-}P2)_2][BF_4]_2$ (**12**) is m/z = 1275, which is 19 a.u. greater than the molecular cation and which fits well with the assignment [Fe(*o*-P2)$_2$+F]$^+$. The same [M(*o*-P2)$_2$+F]$^+$ ion was observed in the FAB-MS spectrum of $[Ni(o\text{-}P2)_2][BF_4]_2$ (**8**) and $[Co(o\text{-}P2)_2][BF_4]_2$ (**9**). The absence of such fluorine adducts in the spectra of $[Pd(o\text{-}P2)_2][BF_4]_2$ (**10**) and $[Pt(o\text{-}P2)_2][BF_4]_2$ (**11**) can be explained by simple hard/soft acid/base (HSAB) theory.[20] Based on HSAB theory, one would predict that the smaller, harder first row transition metals will have a stronger affinity towards fluoride than would the second and third row transition metal ions.

C. Crystal Structures of $[M(o\text{-}P2)_2][BF_4]_2$ (M = Ni (8), Pt (11))

ORTEP diagrams for compounds **8** and **11** are shown in Figures 16 and 18, respectively. The compounds, which are isostructural, consist of two *o*-P2 ligands bound to the metal center in a square planar geometry. The inclusion of toluene molecules in the lattice with **11** is thought to be a result of the samples exposure to the solvent during previous, unsuccessful, slow diffusion experiments. The bonding arrangements are identical to that observed in the Rh^I analog, $[Rh(o\text{-}P2)_2][BF_4]$.[4] Selected bond distances and angles for both structures are given in Table 2. The average Ni-P and Pt-P distances are 2.2551(13) Å and 2.342(2) Å respectively, with P(1)-M(1)-P(1)' five-ring

Table 6. Selected Bond Distances (Å) and Angles (deg.) for [Ni(*o*-P2)$_2$][BF$_4$]$_2$ (8) and [Pt(*o*-P2)$_2$][BF$_4$]$_2$ (**11**).

Atom 1	**Atom 2**	8	**11**
Ni/Pt(1)	P(1)	2.2550(13)	2.341(2)
P(1)	C(1)	1.810(6)	1.817(7)
C(1)	S(1)	1.751(5)	1.741(7)
C(2)	S(1)	1.760(4)	1.761(5)
C(2)	C(3)	1.335(11)	1.338(13)
C(3)	S(2)	1.752(4)	1.753(6)
C(4)	S(2)	1.762(7)	1.767(8)
C(4)	C(5)	1.508(10)	1.506(11)

Atom 1	**Atom 2**	**Atom 3**	8	**11**
P(1)	Ni/Pt(1)	P(1)A	93.82(7)	95.05(10)
P(1)	Ni/Pt(1)	P(1)B	86.18(7)	84.95(10
C(1)	S(1)	C(2)	92.4(3)	92.6(4)
S(1)	C(2)	S(1)B	113.0(4)	113.2(5)
S(2)	C(3)	S(2)B	113.7(4)	113.9(6)
C(4)	S(2)	C(3)	95.2(3)	95.0(4)
C(4)B `	C(4)	C(5)	128.2(5)	129.0(5)

A = 1-x, y, -z; B = 1-x, -y, -z

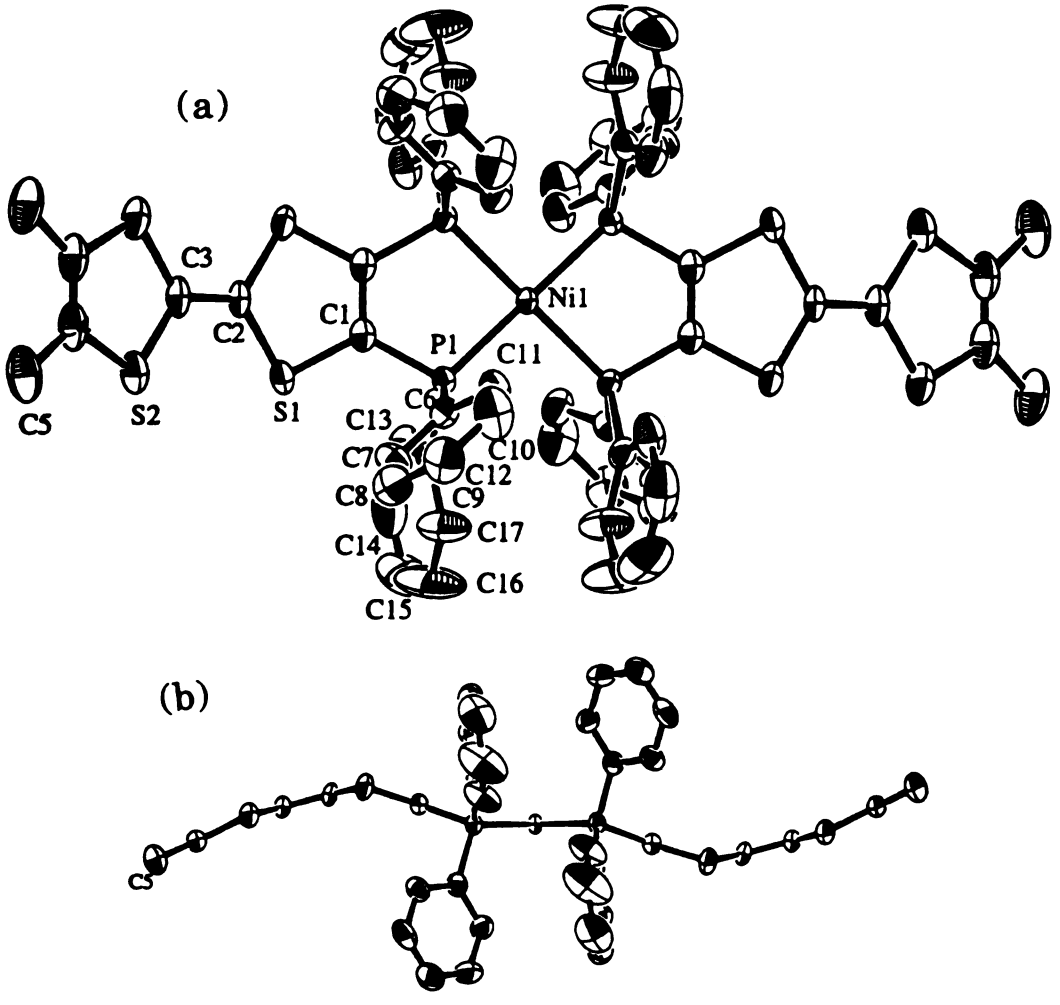

Figure 16. ORTEP representation of $[Ni(o\text{-}P2)_2][BF_4]_2$ (8) with 50% ellipsoids viewed from the (a) top and (b) side.

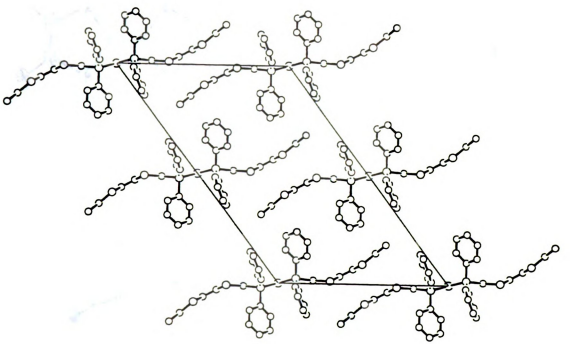

Figure 17. Packing diagram of $[Ni(o\text{-}P2)_2][BF_4]_2$ (**8**).

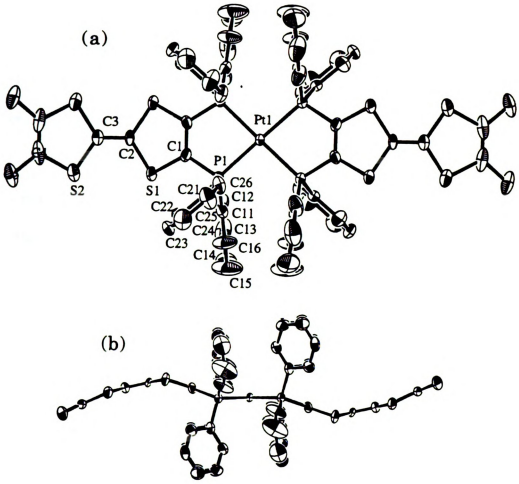

Figure 18. ORTEP representation of $[Pt(o\text{-}P2)_2][BF_4]_2$ (**11**) with 50% ellipsoids viewed from the (a) top and (b) side.

chelate angles of 93.82(7)° for Ni and 95.05(10)° for Pt. This distortion from 90° is in the range observed in the previously reported Rh^{I} complex, as well as $NiCl_2$(*o*-P2),[3] $[Ni(dppee)_2][ClO_4]_2$,[11] $[Ni(dppb)_2][PF_6]_2$,[21] $[Pt(dppee)_2][BPh_4]_2$.[15] The C(1)-C(1)' double bond distances of 1.328(12) Å in **8** and 1.354(14) Å in **11** are similar to that in the free ligand, *o*-P2 (**1**) (1.35(3) Å, see Appendix I), and within errors of 1.337(6) Å, which is expected for a standard C=C double bond, indicating no significant M-to-P π -interactions.[15] All other distances and angles within the TTF core are comparable to those found in *o*-P2 (**1**), $NiBr_2$(*o*-P2),[2] and $[Rh(o\text{-}P2)_2][BF_4]$.[4]

The TTF units are folded along the S(1)···S(1)' axis of the phosphine-functionalized dithiole ring by 31.2° in the case of $[Ni(o\text{-}P2)_2][BF_4]_2$ (**8**) and 31.6° in $[Pt(o\text{-}P2)_2][BF_4]_2$ (**11**). Although such deviations from planarity are not unusual, and have been observed in several other non-oxidized TTF derivatives,[22] the deformation in **11** is the largest out-of-plane bending reported for a non-strained TTF unit. The packing diagram of **8** is shown in Figure 17 and shows the close intermolecular interactions between the outer dithiole rings of the neighboring molecules with a plane-to-plane distance of ~3.5 Å. A packing diagram of **11** reveals the same packing motif. Similar interactions were observed in the packing of $[Rh(o\text{-}P2)_2][BF_4]$, which exhibits an out-of-plane bend of 24.2(2)° along its S(1)···S(2) axis. In a strictly planar geometry the bulky phenyl rings would prevent adequate TTF-TTF intermolecular interactions. Thus, the favored energetics of these close S···S

intermolecular contacts might be the main driving force for the bending of the TTF ligands.

D. Magnetic Studies of $[Co(o\text{-}P2)_2][BF_4]_2$ (9).

(1) Variable Temperature Magnetic Susceptibility

Figure 19 shows the experimental molar magnetic susceptibilities (c, indicated by circles), corrected for diamagnetisim, and the corresponding effective magnetic moment (μ_{eff}, indicated by squares), from 5 to 320 K for $[Co(o\text{-}P2)_2][BF_4]_2$ (**9**). Studies of the magnetic susceptibility of **9** revealed a μ_{eff} range of 4.62 μ_B at 320 K to 2.51 μ_B at 5 K; these values are in good agreement for a typical high-spin, S = 3/2 spin system, with pseudo-octahedral geometry.[23] Explanations for this behavior are identical to that presented in Chapter I for $Co(TMPP\text{-}O)_2$. The moment observed at higher temperatures is a result of the large spin-orbit contribution to the expected spin-only moment of 3.87 μ_B. The large spin-orbit coupling constant for high spin Co^{II} ($\lambda \sim -180$ cm^{-1} for free ion) is also an important contributor to zero-field splitting effects, causing the $^4T_1$ ground state to split into a set of three levels. Temperatures below 20 K result in population of the doubly-degenerate ground state and an observed S' = 1/2.

(2) EPR Spectroscopic Studies

Based on the results of the magnetism studies, an EPR signal would not be expected until very low temperatures due to fast electronic relaxation, but in fact this is not the case. EPR measurements of **9** were initially carried

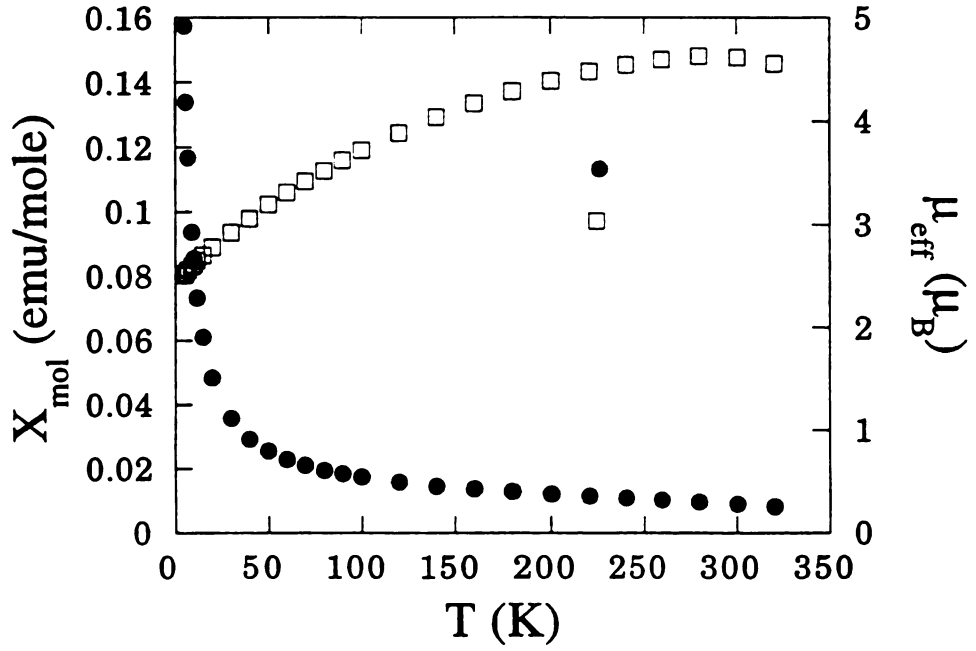

Figure 19. Plot of μ_{eff} (μ_B) and χ_{mol} (emu/mol) vs. temperature (K) of [Co(*o*-P2)$_2$][BF_4]$_2$ (**9**).

out

solve

Th

the p

such

config

in the

our in

descri

This

system

The av

40 de

approx

out in CH_3CN/toluene (1:1) glasses at 298, 107 and 4 K. Spectra of **9** in solvent media display an axial signal with $g_\perp = 2.29$ and $g_\parallel = 2.04$ (Figure 20).

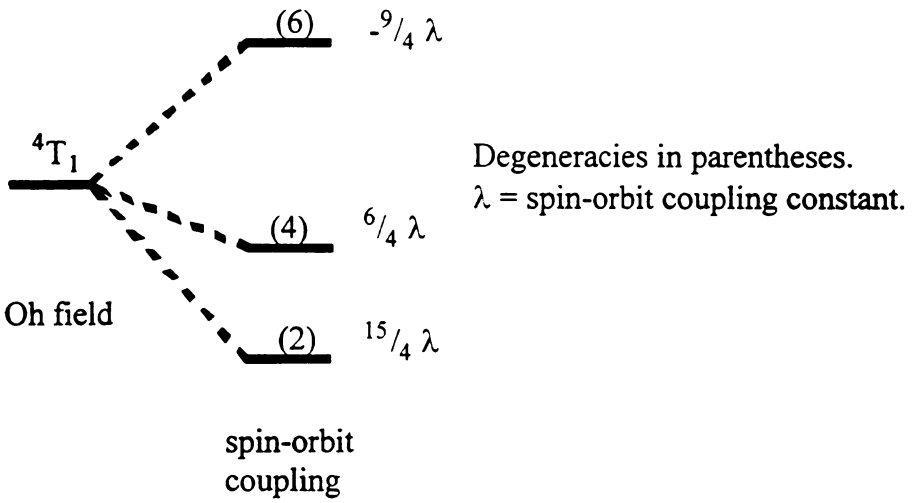

The $g_\parallel$ tensor is split into eight distinct lines ($|A_\parallel| = 3.3\text{x}10^{-3}$ cm^{-1}) due to the hyperfine interaction with the I = 7/2 nucleus of ^{59}Co. The appearance of such a signal suggests the metal center is in a four-coordinate, S = 1/2, configuration; a result in direct conflict with the observed magnetic moment in the solid state. To further probe this issue, EPR studies of **9** were carried out in the solid state at 4 K. The resulting spectrum contains the previously described axial signal, as well as a very broad signal at g = 4.84 (Figure 21). This falls in the range expected for $g_\perp$ of a six-coordinate high-spin Co^{II} system, and appears to be the result of the superposition of 2 $g_\perp$ tensors.[24] The average g value for regular octahedral complexes may range from 4.43 to 4.0 depending on the orbital reduction factor and the strong or weak field approximation which is appropriate for the particular complex. Based on this

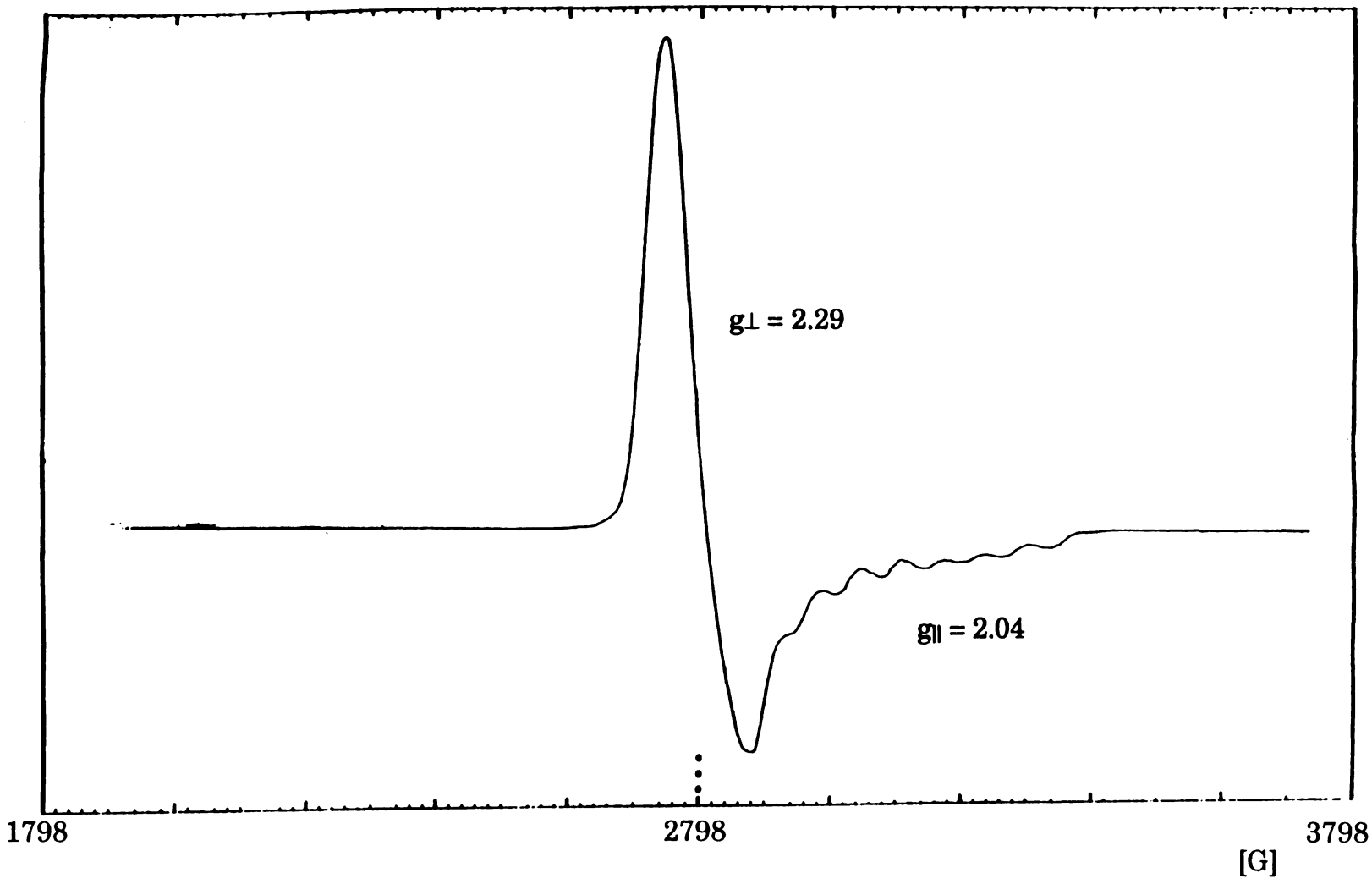

Figure 20. EPR spectrum of $[Co(o\text{-}P2)_2][BF_4]_2$ (**13**) in 50:50 CH_3CN:Toluene at 107 K.

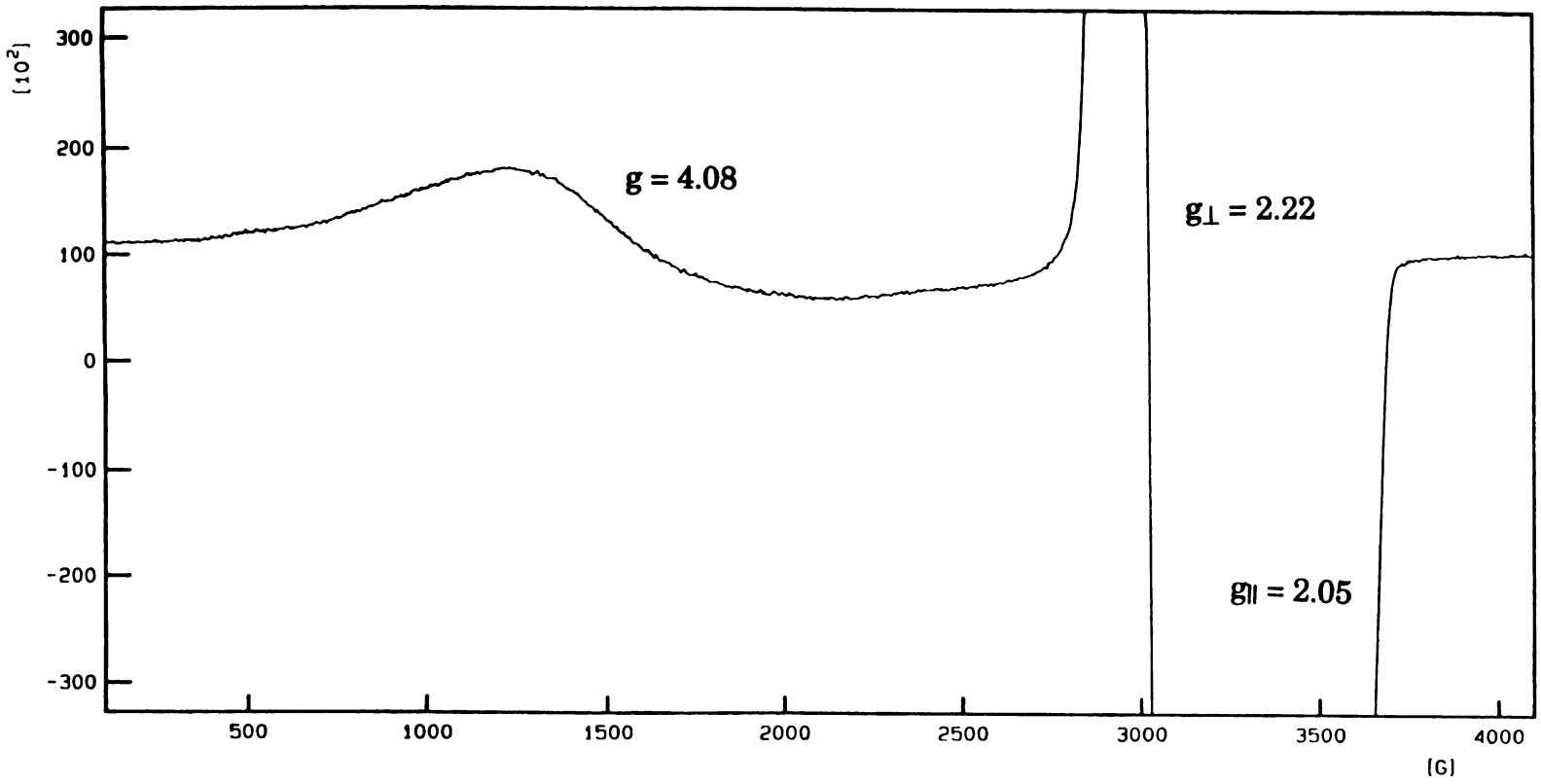

Figure 21. EPR spectrum of $[Co(o\text{-}P2)_2][BF_4]_2$ (**9**) as a solid sample at 4 K.

$g_{avg} = (g_{\perp} + g_{\perp} + g_{||})/3$, $g_{||}$ would be expected to fall in the range masked by the previously observed axial signal.

It is possible that fluxionality is occurring in the coordination sphere of the metal center, resulting in a change from six- to four-coordinate upon dissolving the solid. One possibility for this is the axial coordination of CH_3CN, resulting in $[Co(o\text{-}P)_2(NCCH_3)_2][BF_4]_2$, but this is contradictory to elemental analysis results. Thermal Gravimetric Analysis is warranted to prove/disprove the presence of solvent. Another possibility is the axial coordination of $[BF_4]^-$. This is supported by the presence of $[Co(o\text{-}P2)_2+F]^+$ (m/z = 1278) in the FAB-MS spectrum. Such coordination of $[BF_4]^-$ is not uncommon among the first-row transition metals such as cobalt.[25] but does not explain the presence of the "low-spin" signal in the solid state EPR spectrum. One explanation for this might be that the observed axial signal is only a minor impurity, thus having very little effect on the measured susceptibility. Given the traditionally greater intensity of the EPR signals for low-spin versus high spin Co^{II}, it is possible that a significantly higher spin-density is associated with the broader "high-spin" signal, although the "low-spin" signal dominates the spectrum.

E. Electrochemistry of $[M(o\text{-}P2)_2][BF_4]_x$ (M = Ni, Pd, Pt, x = 2; M = Rh, x = 1).

(1) Redox Properties of $[M(o\text{-}P2)_2][BF_4]_2$ (M = Ni, Pd, Pt)

The cyclic voltammetry data for **8-11** are presented in Table 3 and compared to that of the free phosphine, *o*-P2 (1), and $[Rh(o\text{-}P2)_2][BF_4]$. The

Table 7. Electrochemical data (in V vs Ag/AgCl) for **8-11**, *o*-P2, and $[Rh(o\text{-}P2)_2][BF_4]$, in 0.2 M $TBABF_4/CH_2Cl_2$ solutions, at 200 mV/s.

	$E_{1/2(ox)1}^{rev}$	$E_{1/2(ox)2}^{rev}$	$E_{(p,c)1}^{irr}$	$E_{(p,c)2}^{irr}$
o-P2 (**1**)	0.46	0.91	-	-
$[Ni(o\text{-}P2)_2][BF_4]_2$ (**8**)	0.68	1.08	-0.27	-
$[Co(o\text{-}P2)_2][BF_4]_2$ (**9**)[a]	0.63	1.07	-0.91	-1.19
$[Pd(o\text{-}P2)_2][BF_4]_2$ (**10**)	0.64	1.16	-0.31	-
$[Pt(o\text{-}P2)_2][BF_4]_2$ (**11**)	0.70	1.19	-0.45	-
$[Rh(o\text{-}P2)_2][BF_4]$	0.63	1.01	-	-

[a] 0.1 M CH_3CN; rev reversible, irr irreversible

first oxidation couple of the TTF unit in the metal complexes is shifted to more positive potentials as expected for coordinated versus free ligands. Shifts in the second TTF couple vary from +160 mV for **9**, to 280 mV for **11**. These potentials are within the range previously reported for $[Rh(o\text{-}P2)_2][BF_4]$ and $NiX_2(o\text{-}P2)$ (X = Cl, Br).[4,3] The presence of only two oxidation couples rather than four one-electron couples indicates that the TTF units are not in communication, and are acting as isolated redox centers. It can be surmised that each couple is the superposition of two one-electron processes, but coulometry studies are needed to be certain of this. The irreversible reduction waves are attributed to reductions of the metal centers. The first

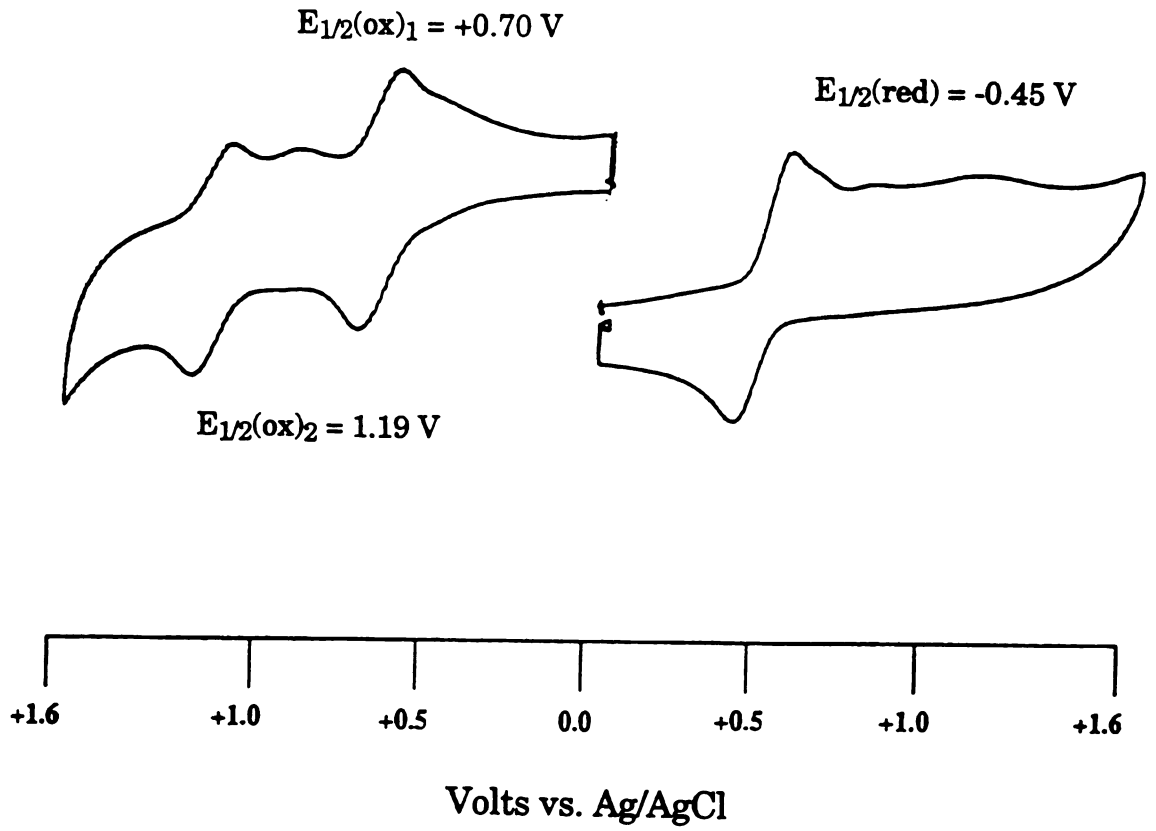

Figure 22. Cyclic voltammogram of $[Pt(o\text{-}P2)_2][BF_4]_2$ (**11**) in 0.2 M $TBABF_4$ in CH_2Cl_2.

reduction pathway is due to the M^{II}/M^{I} process for **8-11**. The two-electron M^{II}/M^{0} reduction is common in bis-diphosphine complexes of Pd and Pt, but typically occur at much more negative potentials (-0.71 to -1.07 V).[21,26] The second reduction in **9** can be assigned to the Co^{I}/Co^{0} reduction. This is most likely accompanied by substantial decomposition, although zero-valent phosphine complexes of Co are actually known (e.g. $Co(PMe_3)_4$).[13]

(2) Oxidation of [Rh(*o*-P2)$_2$][BF$_4$]

The addition of three equivalents of $NOBF_4$ to [Rh(*o*-P2)$_2$][BF$_4$] results in an immediate color change from yellow to green. Addition of one equivalent of oxidizing agent results in a brief color change that returns to the original yellow after several minutes. The color change to green is indicative of oxidized TTF. The lack of communication between the TTF cores causes them to be oxidized at the same potential, thus a mixed valence state with only one TTF moiety oxidized is not possible. Addition of less than one equivalent is expected to result in a mixture of [Rh(*o*-P2)$_2$][BF$_4$] and [Rh(*o*-P2)$_2$][BF$_4$]$_3$, while the addition of three equivalents would produce a combination of paramagnetic [Rh(*o*-P2)$_2$][BF$_4$]$_3$ (**14**) and diamagnetic [Rh(*o*-P2)$_2$][BF$_4$]$_5$. The EPR spectrum of this product in a 1:1 CH_3CN/toluene glass at 96 K exhibits a sharp signal with anisotropic g values of $g_1 = 2.08$ and $g_2 = 2.07$. The narrow line width of the signal (55 G) indicates that it is due to an organic radical, with anisotropy typical for oxidized TTF.[27]

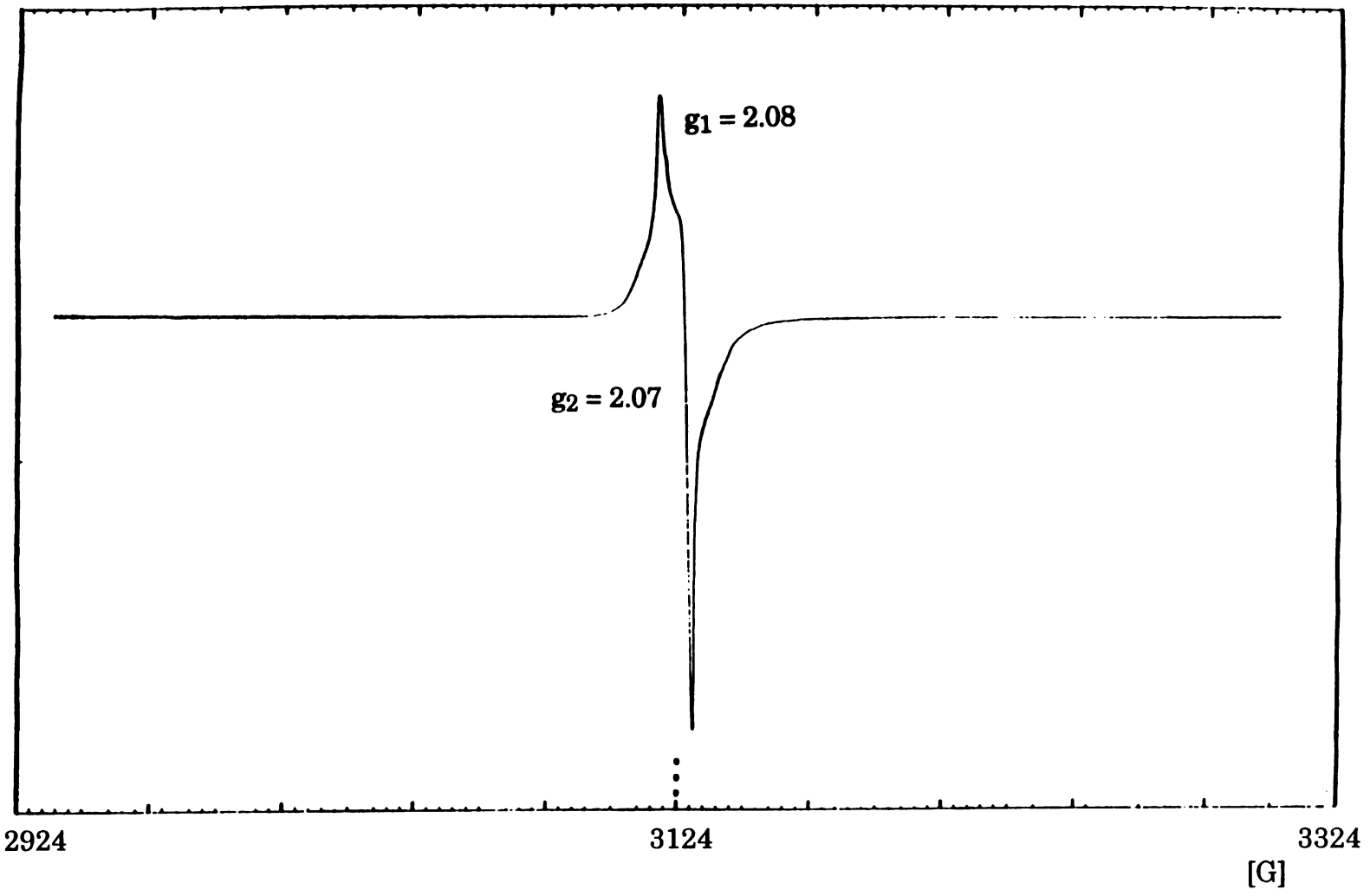

Figure 23. EPR spectrum of $[Rh(o\text{-}P2)_2][BF_4]_3$ **(13)** in 50:50 CH_3CN:Toluene at 95 K.

F. Reactivity of $M(CF_3SO_3)_2$ with *o*-P2 (M = Ni, Fe)

The addition of two equivalents of *o*-P2 to $M(CF_3SO_3)_2$ (M = Ni, Fe) produces very different results for each metal. Upon addition of phosphine to the Ni precursor, an immediate color change to brown ensues. Subsequent isolation of a product yields a green solid. The ^1H NMR spectrum in CD_3CN exhibits a series of multiplets in the region δ = 7.1 - 7.7 ppm due to the phenyl protons, and a singlet at δ = 1.82 ppm due to the methyl protons. The $^{31}P\{^1H\}$ NMR spectra contains a singlet at δ = 46.6 ppm. The downfield shift of the signal from the free phosphine at -18.8 ppm indicates metal-coordination of the phosphines to form $[Ni(o\text{-}P2)_2][CF_3SO_3]_2$ (**13**).[3] The downfield shift relative to **8** supports a decrease in the electron density about the Ni center, possibly due to axial coordination of the triflate groups. This is supported by the presence of $[Ni(o\text{-}P2)_2][CF_3SO_3]^+$ (m/z = 1409), where the equivalent $[BF_4]^-$ adduct is not seen in **8**.

The same reaction performed using the Fe complex resulted in no color change, which is not surprising given the color of **12** (red-orange) is the same as the physical mixture of *o*-P2 and $Fe(CF_3SO_3)_2$. After stirring for 12 h, a $^{31}P\{^1H\}$ NMR spectrum of the reaction mixture revealed only free *o*-P2. Continued stirring for several days affected no change in the $^{31}P\{^1H\}$ NMR spectrum, indicating no reaction had occurred. As further proof of this, single crystals of the free ligand were grown from slow evaporation (under vacuum) of CH_3CN/toluene solutions of the reaction mixture.

G. Metathesis of $[Rh(o\text{-}P2)_2][BF_4]$ with [Li][TCNQ].

Reaction of $[Rh(o\text{-}P2)_2][BF_4]$ and [Li][TCNQ] in warm acetone/CH_2Cl_2 solutions produces a finely divided green precipitate. Infrared analysis of the solid reveals nitrile stretching frequencies at 2178 and 2153 cm^{-1}. These are similar to the values obtained for $[FeCp^*_2][TCNQ]$ (2179, 2153 cm^{-1}) and $[CrCp^*_2][TCNQ\}$ (2178, 2153 cm^{-1}), but quite different from the $[Li]^+$ precursor (2200, 2114 cm^{-1}).[28] The presence of aromatic out-of-plane bending vibrations at 692 and 521 cm^{-1} support the presence of the *o*-P2 ligand. The absence of a strong band c.a. 1069 cm^{-1} supports the absence of $[BF_4]^-$.

Due to the shift to more positive potentials in the oxidation couples of the ligand after complexation, TCNQ is no longer an adequate oxidizing agent for the metal complexes. Because oxidation of *o*-P2 by TCNQ prior to reaction with the metal would introduce a competing ligand in the form of $[TCNQ]^-$, metathesis is currently the best method of forming the TCNQ salt. The more accessible reduction of 2,3,5,6-tetrafluoro-7,7,8,8-tetracyano-quinodimethane ($TCNQF_4$)[29] is more suitable for oxidations of M-(*o*-P2) complexes, and offer a different method of introducing a radical semiquinone into the formula.

4. Concluding Remarks

The TTF-phosphine complexes, $[M(o\text{-}P2)_2][BF_4]_2$ (M = Ni (**8**), Co (**9**), Pd (**10**), Pt (**11**), Fe (**12**)), can be prepared by addition of two equivalents of the free phosphine to the appropriate homoleptic mononuclear acetonitrile

complex. These complexes retain the redox functionality of the TTF unit, while introducing the redox (and magnetic in the case of Co^{II}) properties associated with the metal. The presence of two superimposed reversible oxidations associated with the two TTF moieties in the electrochemical studies of **8-11** support previous observations regarding a lack of communication through the phosphine atoms. The successful preparation of **9** illustrates the potential for incorporating magnetic metal centers into TTF structures through direct coordination. Given the success of coordination with Co^{II} and Fe^{II} (although diamagnetic), the next logical progression is the preparation of $[Mn^{II}(o\text{-}P2)_2][BF_4]_2$. The d^5 complex would exhibit magnetism associated with a S = 5/2 spin system, and characterization by EPR would be much more straight-forward given the strong signals typically associated with Mn.

The introduction of additional spins by way of TTF oxidation, the inclusion of organic acceptors, or a combination of the two, offers new strategies to access compounds with magnetic and possibly conducting properties. The oxidation of TTF is expected to lead to significant structural changes due to forced planarity of the organic core.[30] Such a change would eliminate the ability of the complexes to form S···S contacts, as the bulky phenyl groups are expected to preclude stacking interactions. For this reason, synthesis of the less bulky PMe_2 and phosphole derivatives, shown in Figure 24, are worth exploring as alternatives. An additional property of phosphole is the inclusion of the heteroatom in the ring system. This may

change the electronic effects of the functional group and allow for communication between bound TTF moieties.

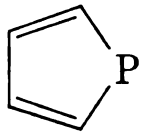

Phosphole

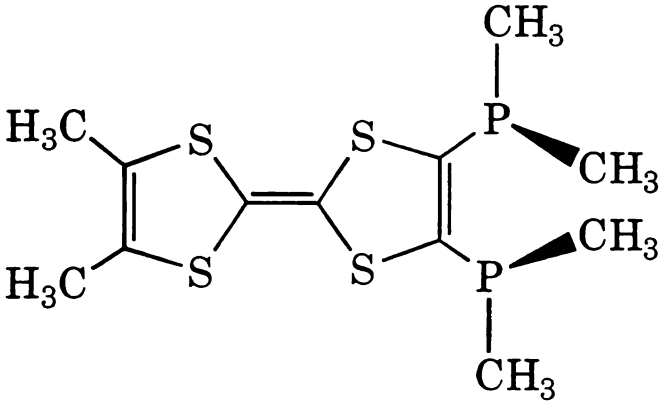

(a)

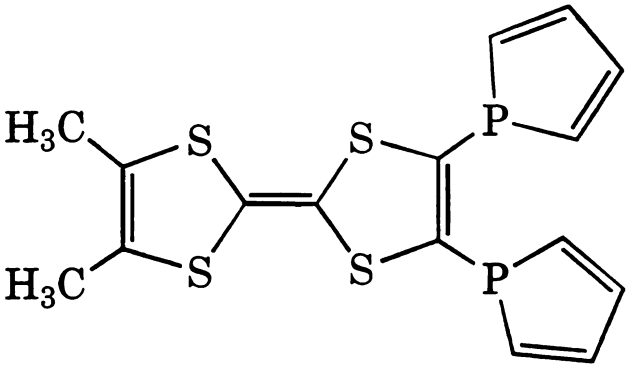

(b)

Figure 24. Schematic drawings of the proposed ligands (a) 3,4 dimethyl-3',4'-bis(dimethylphosphino)tetrathiafulvalene and (b) 3,4 dimethyl-3',4'-bis-(phospholyl)tetrathiafulvalene.

List of References

1. Fox, M. A.; Chandler, D. A. *Adv. Mater.*, **1991**, *3*, 381.

2. Kahn, O.; Pei, Y.; Verdaguer, M.; Renard, J.P.; Sletten, J. *J. Am. Chem. Soc.* **1988**, *110*, 782.

3. Fourmigué, M.; Batail, P. *Bull. Soc. Chim. Fr.* **1992**, *129*, 829.

4. Fourmigué, M.; Uzelmeier, C. E.; Boubekeur, K.; Bartley, S. L.; Dunbar, K. R., *J. Organomet. Chem.*, **1997**, *529*, 343.

5. Hathaway, B. J.; Holah, D. G.; Underhill, A. E., *J. Chem. Soc.*, **1962**, 2444.

6. Thomas, R. R.; Sen, A., Inorg. Synth., 1989, 26, 128.

7. DeRenzi, A.; Panunzi, A.; Vitagliano, A., *J. Chem. Soc., Chem. Commun.*, **1976**, 47.

8. Dixon, N. E.; Lawrance, G. A.; Lay, P. A.; Sargeson, A. M.; Taube, H. *Inorg. Chem.* **1984** *23*, 243.

9. Melby, L. R.; Harder, R. J.; Hertler, W. R.; Mahler, W.; Benson, R. E.; Mochel, W. E., *J. Am. Chem. Soc.*, **1962**, *84*, 3374.

10. (a) Bino, A.; Cotton, F. A.; Fanwick, P. E. *Inorg. Chem.* **1979**, *18*, 3558. (b) Cotton, F. A.; Frenz, B. A.; Deganello, G.; Shaver, A. *J. Organomet. Chem.* **1973**, *50*, 227.

11. North, A. C. T.; Phillips, D. C.; Mathews, F. S. *Acta Cryst.*, **1968**, *A24*, 351.

12. Sheldrick, G. M. SHELXL93. Program for the Refinement of Crystal Structures., **1993**, University of Gottingen, Germany.

13. Cotton, F.A.; Wilkinon, G., *Advanced Inorganic Chemistry, 3rd Ed.*, Wiley & Sons, New York, **1972**.

14. Fourmigué, M., personal communication.

15. Oberhauser, W.; Bachmann, C.; Brüggeller, P., *Inorg. Chim. Acta*, **1995**, *238*, 35.

16. (a) Honeychuck, R. V.; Hersh, W. H. *Inorg. Chem.* **1987**, *26*, 1826. (b) Honeychuck, R. V.; Hersh, W. H. *Inorg. Chem.* **1989**, *28*, 2869. (c) Lundquist, E. G.; Folting, K.; Hoffman, J. C.; Caulton, K. G. *Organometallics*, **1990**, *9*, 2254. (d) Fernandez, J. M.; Gladysz, J. A. *Inorg. Chem.*, **1986**, *25*, 2672.

17. Johnson, A.; Taube, H., *J. Indian. Chem. Soc.*, **1989**, *66*, 503.

18. Asara, J. M.; Uzelmeier, C. E.; Dunbar, K. R.; Allison, J. *Inorg. Chem.*, **1998**, *37*, 1833.

19. Fourmigué, M.; Jarchow, S.; Batail, P. *Phosphorus, Sulfur, Silicon Relat. Elem.* **1993**, *75*, 175.

20. Miller, J. N.; Jones, T. R.; Deacon, G. B. *Inor. Chim. Acta* **1979**, *32*, L75.

21. Miedaner, A.; Haltiwanger, R. C.; DuBois, D. L. Inorg. Chem., **1991**, *30*, 417.

22. (a) Fourmigué, M.; Batail, P. *J. Chem. Soc., Chem. Commun.*, **1991**, 1370. (b) Garreau, R. R.; de Montauzon, D.; Cassoux, P.; Legros, L.-P.; Fabre, J.-M.; Saoud, K.; Chakroune, S. *New J. Chem.*, **1995**, *19*, 161. (c) Izuoka, A.; Tachikawa, T.; Sugawara, T.; Suzuki, Y.; Konno, M.; Saito, Y.; Shinohara, H. *J. Chem. Soc., Chem. Commun.* **1992**, 1472. (d) Jørgensen, T.; Girmay, B.; Hansen, T. K.; Becher, J.; Underhill, A. E.; Hursthouse, M. B.; Harman, M. E.; Kilburn, J. D. *J. Chem. Soc., Perkin Trans.* **1992**, 2907. (e) Jørgensen, T.; Becher, J.; Hansen, T. K.; Chrisiansen, K.; Roepstorff, P.; Larsen, S.l Nygaard, A. *Adv. Mater.* **1991**, *10*, 486. (f) Endres, H. *Z. Naturforsch*, **1986**, *41b*, 1351.

23. Carlin, R. L.; van Duyneveldt, A. J. *Magnetic Properties of Transition Metal Compounds*, Springer: New York, **1977**.

24. Banci, L.; Bencini, A.; Benelli, C.; Gatteschi, D.; Zanchini, C. In *Structure and Bonding, Vol. 52*, Eds. Clarke, M. J.; Goodenough, J. B.; Hemmerich, P.; Ibers, J. P.; Jørgensen, C. K.; Neilands, J. B.; Reinen, S.; Weiss, R; Williams, R. J. P. Springer-Verlag: New York, **1962**, 37.

25. (a) Egan, J. W.; Theopold, K. H. *Acta Crystallogr., C.* **1990**, 46, 1013. (b) Shah, N.; Adak, A. K.; Data, K. M. *Synth. React. Inorg. Met.-Org.*, **1984**, *14*, 731.

26. Davies, J. A.; Staples, R. J. *Polyhedron*, **1991**, *10*, 899

27. Clérac, R. Ph. D. Dissertation, Université Bordeaux, I., **1997**.

28. (a) Melby, L. R.; Harder, R. J.; Hertler, W. R.; Mahler, W.; Benson, R. E.; Mochel, W. E. *J. Am. Chem. Soc.* **1962**, *84*, 3374. (b) Miller, J. S.; Reiff, W. M.; Zhang, J. H.; Preston, L. D.; Reis, A. H., Jr.; Gebert, E.; Extine, M.; Troup, J.; Dixon, D. A.; Epstein, A. J.; Ward, M. D. *Phys. Chem.* **1987**, *91*, 4344. (c) Broderick, W. E.; Hoffman, B. M. *J. Am. Chem. Soc.* **1991**, *113*, 6334.

29. Miller, J. S.; Dixon, D. A.; Calabrese, J. C.; *J. Phys. Chem.*, **1989**, *93*, 2284.

30. Kistenmacher, T. J.; Phillips, T. E.; Cowan, D. O. *Acta. Crystallogr. B.*, **1974**, *B30*, 763.

CHAPTER IV

REACTIVITY OF METAL-METAL BONDED COMPLEXES WITH PHOSPHINE-FUNCTIONALIZED TETRATHIAFULVALENE

1. Introduction

Chelating diphosphines such as bis(diphenylphosphino)ethane (dppe), -ethene (dppee) and their relatives are commonly used for their ability to stabilize metal complexes through the formation of five- (chelating), and six-membered (bridging) rings.[1] Diphosphine ligands have been used extensively in the preparation of metal-metal bonded complexes as well as other cluster complexes[2] due to the fact that they exhibit several characteristics applicable in multiply bonded systems; they are bidentate, the donor orbitals of the phosphorus atoms are oriented parallel to each other, and the distance between the heteroatoms is typically 2.0-2.5 Å.[2] Diphosphine molecules with a single bridgehead atom separating the phosphorous atoms, e.g. dppm and bis(diphenylphosphino)amine (dppa), are particularly useful as bridging ligands for metal-metal bonded complexes due to the formation of a stable five-membered ring.[3] The diphosphines with an ethene backbone are attractive due to their tendency to strongly coordinate to nearly all transition metals[4] and stabilize high oxidation states.[5] Several "diphos" ligands have been reported to coordinate to dinuclear metal centers in both the chelating (α) and bridging (β) modes. The structural characterization of several α- and β-$Mo_2X_4(LL)_2$ compounds, where "LL" is a diphos ligand, has led to a clearer understanding of factors that influence M-M bond distance and has prompted Cotton to suggest a mechanism for internal rotation of a M_2 unit within its ligand sphere.[6,7]

One of our early interests in pursuing TTF phosphine chemistry was to merge the redox activity of the tetrathiafulvalene functionality[8] with the extensive chemistry of metal-metal bonded compounds.[2,9] Many of these metal-metal bonded compounds have been found to exhibit fascinating photophysical properties and are known to display rich redox chemistry.[10] The use of TTF itself as a ligand for metal-metal bonded systems has witnessed little activity in the literature, with the only reported examples being the dinuclear compound $Rh_2(O_2CCH_3)_4(TTF)_2$, wherein neutral TTF ligands are bound to the axial positions through sulfur atoms.[11] More recently, $[Cu_2(\mu\text{-}Cl)_2(\mu\text{-}TMT\text{-}TTF)]_\alpha$ (TMT-TTF = tetrakis{methylthio}tetrathiafulvalene) with no direct M-M interaction was reported to contain TTF ligands bound via methylthio groups. An interesting feature of this structure are the close S···S contacts of 3.53 and 3.63 Å between layers of the 2D sheets.[12] A third structure, while not involving directly bonded TTF, is an interesting example of the use of TTF in stacking arrangements, in this instance with alternating $[Pt(dmit)_2]_3^{n-1}$ anions. In this structure, two of the $[Pt(dmit)_2]^{n/3-}$ units are connected by a Pt-Pt bond, and the TTF is present in both its neutral and oxidized forms. Crystals of this material are semiconducting from 100-300 K.[13]

The present studies of new TTF-phosphines build on the wealth of known chemistry of metal-metal bonded compounds with phosphine ligands. The reactions of the quadruply-bonded compounds $[Re_2Cl_8]^{2-}$ and

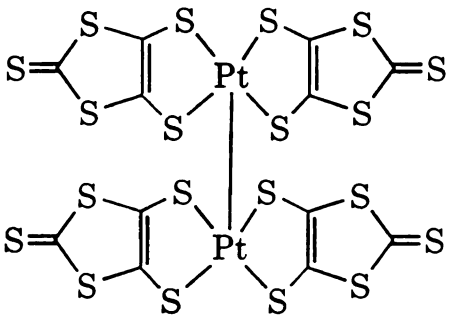

$[Pt(dmit)_2]_2$

$Mo_2Cl_4(SMe_2)_4$ with the diphosphine ligand *o*-P2 (**1**) have been explored and the products characterized by a combination of structural, spectroscopic, electrochemical and magnetic studies.

2. Experimental

A. Synthesis

Starting Materials and Reaction Procedures. *Ortho*-$[P(C_6H_5)_2]_2(CH_3)_2TTF$,[8a] $P(C_6H_5)_2(CH_3)_3TTF$,[8b] $[Rh_2(NCCH_3)_{10}][BF_4]_4$[14] $[Re_2(NCCH_3)_{10}][BF_4]_4$,[15] $[(n\text{-}Bu)_4N]_2[Re_2Cl_8]$,[16] and $Mo_2Cl_4[S(CH_3)_2]_4$[17] were prepared according to published procedures. $NOBF_4$ and CCl_4 were purchased from Aldrich Chemical Co. and was used as received. Acetone, acetonitrile, and methylene chloride were distilled over 3 Å molecular sieves, and ethanol was distilled over $Mg(OMe)_2$ under a nitrogen atmosphere. Diethyl ether and toluene were distilled over sodium-potassium/benzophenone. Unless otherwise specified, all reactions were carried out under an argon atmosphere by using standard Schlenk-line techniques.

(1) Reaction of $[Rh_2(NCCH_3)_{10}][BF_4]_4$ and $(Ph_2P)Me_3TTF$ to form (15).

Samples of $[Rh_2(NCCH_3)_{10}][BF_4]_4$ (0.026 g, 0.03 mmol) and $(Ph_2P)Me_3TTF$ (P1) (0.046 g, 0.12 mmol) were dissolved in 10 mL of acetonitrile, and stirred for 12 hours at r.t. A large excess of Et_2O (~50 mL) was then added to the dark green solution, and the reaction flask was chilled in an ice bath to allow the precipitate to settle. The mixture was filtered through Celite, and both the green solid and orange filtrate were dried under reduced pressure. The orange solid was washed with hexanes and dried by suction filtration in air; yield 0.011 g. The green solid was washed with *copious* amounts of Et_2O and dried *in vacuo*. Recovery of the green solid was complicated by its finely divided nature, making it subject to static problems. Consequently an accurate mass could not be obtained. Doubling the reaction scale did not improve the recovery of the green solid. ^1H NMR ($CDCl_3$) δ ppm: broad and unresolved. $^{31}P\{^1H\}$ NMR ($CDCl_3$) δ ppm: not observed. IR (Nujol, cm^{-1}): 475 (m), 530 (s, P1), 695 (m, P1), 720 (m), 750 (w), 890 (w), 1050 (s-br, $\nu_{B\text{-}F}$). UV-Vis. (CH_2Cl_2) λ_{max} (nm) 510, 600. EPR (T=133 K, CH_3CN/CH_2Cl_2): g = 2.00.

(2) Reaction of $[Re_2(NCCH_3)_{10}][BF_4]_4$ and $(Ph_2P)_2Me_2TTF$.

Solutions of $[Re_2(NCCH_3)_{10}][BF_4]_4$ (0.024 g, 0.02 mmol) and *o*-P2 (0.053 g, 0.14 mmol) were prepared separately by dissolving the solids in 10 mL of acetonitrile and 7 mL of dichloromethane respectively. Approximately one-half of the phosphine containing solution was added to the dirhenium

complex, resulting in a color change from orange to green. After stirring for 5 h, the reaction solution was heated to reflux and stirred for an additional 12 h. The solution was reduced to dryness by application of a dynamic vacuum, and the resulting residue washed six times with 5 mL of Et_2O, and dried *in vacuo*: Recovery was extremely difficult due to the susceptibility of the solid to static problems. Much of the product remained in the flask, and as a result the mass would be inaccurate; approximate yield 0.059 g. ^1H NMR (CD_3CN): broad and unresolved. $^{31}P\{^1H\}$ NMR (CD_3CN) δ ppm: none observed. EPR (1:1 toluene/CH_3CN, 133K): g = 2.00.

(3) Reactions of $[Bu_4]_2[Re_2Cl_8]$ with *o*-P2.

(i) Synthesis of $[ReCl_2(o\text{-}P2)_2][Re_2Cl_6(o\text{-}P2)]$ (16•17) for short reaction times. A flask charged with a mixture of $[n\text{-}Bu_4N]_2[Re_2Cl_8]$ (0.104 g, 0.091 mmol) and *o*-P2 (0.131 g, 0.219 mmol) was treated with 10 mL of ethanol and refluxed for 1 h, during which time the solution became yellow-orange with the deposition of a red solid. The mixture was filtered in air, and the solid was washed with *copious* amounts of EtOH and CH_3CN to remove unreacted starting materials, followed by ~50 mL Et_2O to dry the solid. The solid was dried *in vacuo*. Single crystals of the dichloromethane tetrasolvate were obtained by slow diffusion of CH_3CN into a dichloromethane solution of the compound; yield 0.115 g (72%). *Anal.* Calcd for **16•17•**CH_2Cl_2, $Re_3Cl_{10}S_{12}P_6C_{97}H_{80}$: C, 42.70; H, 2.95. Found: C, 42.74; H, 2.72. IR (Nujol, cm^{-1}): 329 ($\nu_{Re\text{-}Cl}$), 333 sh($\nu_{Re\text{-}Cl}$), 352 ($\nu_{Re\text{-}Cl}$), 517 ($\nu_{=C\text{-}H}$), 691 ($\nu_{C=C}$). UV-Vis.

(CH_2Cl_2) λmax (nm) (ε (M^{-1},cm^{-1})): 976 ($4.80x10^1$), 448 ($5.0x10^3$), 322 ($6.4x10^4$), 276 ($7.5x10^4$). C.V. (0.1M $TBABF_4$, CH_2Cl_2, Pt disk electrode vs Ag/AgCl): $E_{1/2}(red)_1$ = +0.03 V, $E_{(p,c)2}$ = -0.79 V, $E_{(p,c)3}$ = -1.12 V, $E_{1/2}(ox)_1$ = +0.31 V, $E_{1/2}(ox)_2$ = +0.50 V, $E_{1/2}(ox)_3$= +0.67 V, $E_{(p,a)4}$ = +1.05. FAB-MS (m/z): 1457 $ReCl_2(o\text{-}P2)_2]^+$), -1186 ($[Re_2(o\text{-}P2)Cl_6]^-$). Magnetic moment ($\mu_B$): μ_{eff} = 5.2 at 340 K (1T), μ_{eff} = 1.9 at 5 K (1T).

(ii) Reaction time of 2 hours. $[n\text{-}Bu_4N]_2[Re_2Cl_8]$ (0.031 g, 0.03 mmol) and *o*-P2 (0.069 g, 0.13 mmol) were dissolved in 10 mL of ethanol and stirred under refluxing conditions for 2 h. The yellow-orange solution was cooled to room temperature and transferred to a second flask. The solvent was removed under vacuum, the solid was washed with Et_2O, and then dried under reduced pressure to give a green solid. FAB-MS (m/z): +1457 ($[Re(o\text{-}P2)_2Cl_2]^+$).

(4) Reduction of $[ReCl_2(o\text{-}P2)_2][Re_2Cl_6(o\text{-}P2)]$ (16•17) to yield $ReCl_2(o\text{-}P2)_2$ (18).

A solution of $Co(C_5H_5)_2$ (0.01 g, 0.053 mmol) in 2 mL of CH_2Cl_2 was added to $[ReCl_2(o\text{-}P2)_2][Re_2Cl_6(o\text{-}P2)]$ (**16•17**) (0.100, 0.038 mmol) in 5 mL CH_2Cl_2 which led to an immediate color change to brown-green ensued. The reaction mixture was stirred for 12 hours, to give a yellow precipitate that was isolated by filtration, washed 3 times with 5 mL of CH_2Cl_2, and dried *in vacuo*. yield = 0.031g (56%). IR (Nujol, cm^{-1}): 330 ($\nu_{Re\text{-}Cl}$), 513 ($\nu_{\equiv C\text{-}H}$), 702 ($\nu_{C\equiv C}$). FAB-MS (m/z) = +1457 ($[ReCl_2(o\text{-}P2)_2]^+$), -1457 (very low intensity,

$[ReCl_2(o\text{-}P2)_2]^-$). Magnetic moment ($\mu_B$): μ_{eff} = 5.0 at 300 K (1T), μ_{eff} = 1.8 at 2 K (1T).

(5) Oxidation of $ReCl_2(o\text{-}P2)_2$ (18).

(i) Preparation of $[ReCl_2(o\text{-}P2)_2][Cl]$ (16•[Cl]). A small quantity of $ReCl_2(o\text{-}P2)_2$ (18) (0.020g, 0.014 mmol) was stirred in a mixture of 5 mL of CH_2Cl_2 and 10 mL of CCl_4 under refluxing conditions for 3 days. The yellow-orange solution was reduced in volume under vacuum and 30 mL of Et_2O was added to precipitate a yellow-orange solid which was washed with *copius* amounts of Et_2O and dried *in vacuo*; yield = 0.008 g (38%). IR (Nujol, cm^{-1}): 327 ($\nu_{Re\text{-}Cl}$), 518 ($\nu_{=C\text{-}H}$), 695 ($\nu_{C\text{-}C}$). FAB-MS (m/z): 1457 ($[ReCl_2(o\text{-}P2)_2]^+$)

(ii) Preparation of $[ReCl_2(o\text{-}P2)_2][BF_4]$ (16•$[BF_4]$). An aliquot (4.2 mL) of a stock solution of $NOBF_4$ (0.014 g, 0.120 mmol, 10 mL CH_2Cl_2) was slowly added to a mixture of $ReCl_2(o\text{-}P2)_2$ (18) (0.054 g, 0.037 mmol) in 5 mL of CH_2Cl_2 (a slight excess of stock solution was added due to the poor solubility of $NOBF_4$ in CH_2Cl_2). The mixture was stirred for 3 days, during which time the solution color gradually became red-brown. The reaction mixture was filtered in air to remove unreacted $ReCl_2(o\text{-}P2)_2$ (18) and treated with 30 mL of Et_2O to afford a red-brown precipitate. The resulting solid was isolated by filtration, washed with *copious* amounts of Et_2O and dried under vacuum; yield 0.035 g (61%). C.V. (0.2 M $TBABF_4$, CH_2Cl_2, Pt disk electrode vs Ag/AgCl): $E_{1/2}(ox)_1$ = +0.75 V, $E_{1/2}(ox)_2$ = +1.14 V, $E_{1/2}(red)_1$ = +0.07 V,

$E_{1/2}(red)_2$ = - 0.97 V. Magnetic moment (μ_B): μ_{eff} = 4.9 at 300 K (1T), μ_{eff} = 0.7 at 2 K (1T).

(6) Reaction of $Mo_2Cl_4(SMe_2)_4$ with *o*-P2.

(i) In CH_3CN. Solutions of $Mo_2Cl_4(SMe_2)_4$ (0.059 g, 0.137 mmol) and *o*-P2 (0.122 g, 0.202 mmol), each in 10 mL of CH_3CN, were combined and stirred for 8 h. During this time, the solution became dark brown in color, and a green precipitate was observed to have formed. The liquid was decanted and the green solid was washed 3 times with 5 mL of Et_2O before being dried under reduced pressure; yield 0.059 g. ^1H NMR (CD_3CN (integration)) δ ppm: 1.85 (s, 2.08), 1.95 (s, 3.87), 2.15 (s), 7.37 (m, 6.12). $^{31}P\{^1H\}$ (CD_3CN) δ ppm: -17.60 (s). UV-Vis. (CH_3CN) λ_{max} (nm)): 600. The addition of CH_2Cl_2 to the green solid led to a dark brown solution that was reduced to dryness under reduced pressure and washed with *copious* amounts of Et_2O. ^1H NMR (CD_3CN) δ ppm: 1.806 (s), 1.84 (s), 1.95 (s), 2.13 (s), 7.27 (br), 7.36 (br), 7.46 (m), 7.61 (m). $^{31}P\{^1H\}$ (CD_3CN) δ ppm: -0.64 (d, $J^1_{P\text{-}P}$ = 17.1 Hz), -2.72 (d, $J^1_{P\text{-}P}$ = 19.5 Hz), 40.71 (s). UV-Vis. (CH_2Cl_2) λ_{max} (nm)): 460.

(ii) In CH_2Cl_2 under aerobic conditions. Preparation of $MoCl_2O_2$(o-P2O_2) (19). A solution of *o*-P2 (0.048 g, 0.080 mmol) in 5 mL of CH_2Cl_2 was added to a solution of $Mo_2Cl_4(SMe_2)_4$ (0.023 g, 0.047 mmol) in 8 mL of CH_2Cl_2 and stirred for 8 h, thereby effecting a color change from blue to dark brown. The solution was treated with 15 mL of Et_2O to afford a brown precipitate which was collected by filtration in air. The remaining solid was washed 3

times with 5 mL of Et_2O and dried *in vacuo*; yield 0.041 g (61%). Needle-like single crystals were obtained by slow evaporation in air of a dichloromethane solution of the compound.

B. X-ray Crystallographic Studies

(1) $[ReCl_2(o\text{-}P2)_2][Re_2Cl_6(o\text{-}P2)]\cdot 4\ CH_2Cl_2$ (16•17•4 CH_2Cl_2)

(i) Data Collection and Reduction. Crystallographic data for **16•17** were collected on a Siemens SMART/CCD area detector diffractometer equipped with monochrmoated MoKα radiation. Crystallographic computing was performed using SHELXTL version 5.0.[18] Crystal parameters and basic information pertaining to data collection and structure refinement are summarized in Table 8.

Single crystals of $[ReCl_2(o\text{-}P2)_2][Re_2Cl_6(o\text{-}P2)]\cdot 4CH_2Cl_2$ (**16•17**•$4CH_2Cl_2$) were grown by slow diffusion of acetonitrile into a dichloromethane solution of the title compound. A red-orange parallelepiped of approximate dimensions 0.16 x 0.17 x 0.55 mm^3 was secured on the tip of a glass fiber with silicone grease and cooled to –100 ± 1°C during data collection by using a cold nitrogen stream. The data were collected in a θ range of 0.99 to 21.72°. Successful refinement of the structure was carried out in the triclinic P-1 space group. Of the 21,397 reflections that were collected, 13,226 were determined to be unique (R(int) = 0.067) and 11,595 data were observed ($I > 2.00\sigma(I)$). The data were corrected absorption with transmission factors ranging from 0.63 to 0.99.

Table 8. Summary of crystal data for $[ReCl_2(o\text{-}P2)_2][Re_2Cl_6(o\text{-}P2)]\cdot 4CH_2Cl_2$ (**16·17**•$4CH_2Cl_2$).

	16·17•$4CH_2Cl_2$
Formula	$C_{100}H_{86}Cl_{16}P_6Re_3S_{12}$
Formula weight	2984.03
Space Group	P-1
a, Å	13.456 (1)
b, Å	20.402 (3)
c, Å	21.554 (1)
α, deg	88.26 (1)
β, deg	72.99 (1)
γ, deg	84.93 (1)
V, Å^3	5635.85 (10)
Z	2
Density (calc), Mg/cm^3	1.76
μ, mm^{-1}	3.95
Temp, °C	-100
Goodness-of-fit on F^2	1.29
R1[a]	0.075
wR2[b]	0.159

[a] $R1 = \Sigma||F_o| - |F_c||/\Sigma|F_o|$. [b] $wR2 = [\Sigma w(|F_o| - |F_c|)^2/\Sigma w|F_o|^2]^{1/2}$; $w = 1/\sigma^2(|F_o|)$.

Table 9. Summary of crystal data for $MoCl_2O_2$(*o*-$P2O_2$)•CH_2Cl_2 (**19**•CH_2Cl_2).

	19·CH_2Cl_2
Formula	$C_{37}H_{25}O_4Cl_4P_2MoS_4$
Formula weight	961.33
Space Group	P21/n
a, Å	10.747 (3)
b, Å	17.309 (4)
c, Å	21.101 (5)
α, deg	90.00
β, deg	100.36 (2)
γ, deg	90.00
V, Å^3	3862 (2)
Z	4
Density (calc), Mg/cm^3	1.58
μ, mm^{-1}	0.82
Temp, °C	-85
Goodness-of-fit on F^2	0.832
R1[a]	0.1028
wR2[b]	0.3521

[a] $R1 = \Sigma||F_o| - |F_c||/\Sigma|F_o|$. [b] $wR2 = [\Sigma w(|F_o| - |F_c|)^2/\Sigma w|F_o|^2]^{1/2}$ $w = 1/\sigma^2(|F_o|)$.

(ii) Structure Solution and Refinement. The asymmetric unit consists of one $[Re_2Cl_6(o\text{-}P2)]^-$ (**17**) moiety, two half $[ReCl_2(o\text{-}P2)_2]^+$ (**16**) cations residing on centers of inversion, and four solvent molecules. Solvent disorder and poor packing severely affected the scattering ability of the crystal at higher theta angles; data collection was therefore limited to θ less than 21.72°. The poor scattering and the high absorption led to a variety of issues during the refinement of the structure. The solvent disorder was completely resolved for only one of the solvent molecules (C(100), Cl(15), and Cl(16)). The atoms Cl(15), Cl(16), Cl(15B), and Cl(16B) were refined at 50% occupancy in alternate least squares cycles. There is also a possibility that the phenyl groups that involve C(15)-C(20) and C(21)-C(26) are undergoing a wagging motion (*i.e.* a rotational twist along the P-C bond). Atoms C(1), C(34), C(41), C(59), C(66), and C(67) were refined isotropically and hydrogen atoms were placed in calculated positions and allowed to ride on the bonded atom. The methyl hydrogen atoms were included as rigid groups with rotational freedom at the bonded carbon atom. Refinement of nonhydrogen atoms was carried out with anisotropic temperature factors except as noted above.

The structure was solved by direct methods and refined by full-matrix-block least squares refinement. The final refinement was based on 13,219 reflections that were used to fit 1,232 parameters to give R1 = 0.0751

and wR2 = 0.1594. The goodness-of-fit index was 1.291. After the last least squares cycle, the highest peak in the difference Fourier map was 2.398 $e^-/Å^3$.

(2) $MoCl_2O_2(o\text{-}P2O_2)$ (19).

(i) Data Collection and Reduction. Single crystals of **19** were grown by slow evaporation, in air, from a CH_2Cl_2 solution of the compound. A brown crystal of dimensions 0.23 x 0.34 x 0.47 mm^3 was secured on the tip of a glass fiber with Dow Corning silicone grease and placed in a cold N_2 (g) stream. Least-squares refinement using 24 well-centered reflections in the range $2 \leq 2\theta \leq 24°$ indicated that the crystal was consistent with an orthorhombic crystal system. The data were collected at - 85 ± 1 °C using the ω-2θ scan technique to a maximum 2θ value of 47°. Of the 6327 reflections that were collected, 358 were systematically absent. An empirical absorption correction based on azimuthal scans of three reflections with χ near 90° was applied which resulted in transmission factors ranging from 0.705 - 1.00. The data were corrected for Lorentz and polarization effects.

(ii) Structure Solution and Refinement. The structure was solved in the space group $P2_1/n$ using the MITHRIL[19] and SHELXL 93[20] structure solution programs and refined by full-matrix least-squares refinement on F^2.[21] The final full-matrix least-squares refinement was based on 5743 reflections that were used to fit 426 parameters with 4 restraints to give R1 = 0.1028 and wR2 = 0.3521. The goodness-of-fit index was 0.832, and the maximum shift in the final difference map was 0.175 Å associated with C105. After the last

least squares cycle, the mean shift/esd was 0.065 and the highest peak in the difference Fourier map was 1.22 $e^-/Å^3$ which is associated with Mo1 and O2.

The methyl group centered about atom C8 was found to be disordered, and was refined isotropically as twin methyl groups, A and B, with a combined occupancy of 1.0. Restraints were introduced to keep the C8A···S4 distance similar to C7···S3, and C8A···C5 similar to C7···C6 (0.01 Å deviation allowed). The phenyl ring carbon atoms C25 and C26 were found to be disordered and were refined isotopically as groups C25A, C25B and C26A, C26B, with combined occupancies of 1.0 for each set and restraints to keep C25A···C24, C25B···C24 and C26A···C21, C26B···C21 equivalent. All other non-hydrogen atoms were refined anisotropically, except for solvent molecules.

All hydrogen atoms except H24, and H26B were placed at calculated positions. Those hydrogen atoms which are exceptions to this were located in the difference map and refined with their temperature factors riding the atoms to which they are bonded. No hydrogen atoms were placed on C25A, C25B, or C26A. There is currently one unresolved area in the structure containing C104, C105, C106, and C107 which is contributing to the overall poor refinement level. It appears that this group may be two overlapping CH_2Cl_2 molecules. The highest peaks remaining in the difference map are currently located around the metal atom, and are near the terminal oxygen atoms in the current model.

3. Results and Discussion

A. Reactions with $[M_2(NCCH_3)_{10}][BF_4]_4$ (M= Rh, Re).

The reaction of $[Rh_2(NCCH_3)_{10}][BF_4]_4$ and P1 in a 1:4 ratio instantaneously produced an opaque green solution in acetonitrile. A dark green, nearly black, solid was obtained by precipitation with diethyl ether which left behind an orange solution. The solubility of P1 in diethyl ether is quite high, thus it is most likely the source of the color. Based on the recovery of 0.011 g of unreacted P1, the actual reaction stoichiometry is 1:1. Unfortunately, attempts to grow crystals suitable for a single crystal X-ray diffraction study have proven unsuccessful to date. The color change to green is indicative of TTF oxidation, most likely accompanied by partial reduction of the $Rh_2^{II,II}$ dinuclear precursor to $Rh_2^{I,II}$. Such a redox reaction has been observed in the reaction between $[Rh_2(NCCH_3)_{10}][BF_4]_4$ and *o*-P2 as well.[8b] The green color is also reminiscent of the powder samples of the paramagnetic material $\{[Rh(NCCH_3)_4][BF_4]_{1.5}\}_\alpha$, which is obtained from bulk electrolysis of reactions of $[Rh_2(NCCH_3)_{10}][BF_4]_4$.[22]

The ^1H NMR spectrum of the green product (**15**) is essentially featureless, exhibiting only broad resonances from 1.5 to 2.5 and 7.0 to 9.0 ppm. A ^{31}P NMR signal was not observed, further supporting its assignment as a paramagnetic species. An EPR spectrum of the product at 133 K in a 1:1 CH_3CN/toluene glass displays a sharp signal with anisotropic g values of g_1

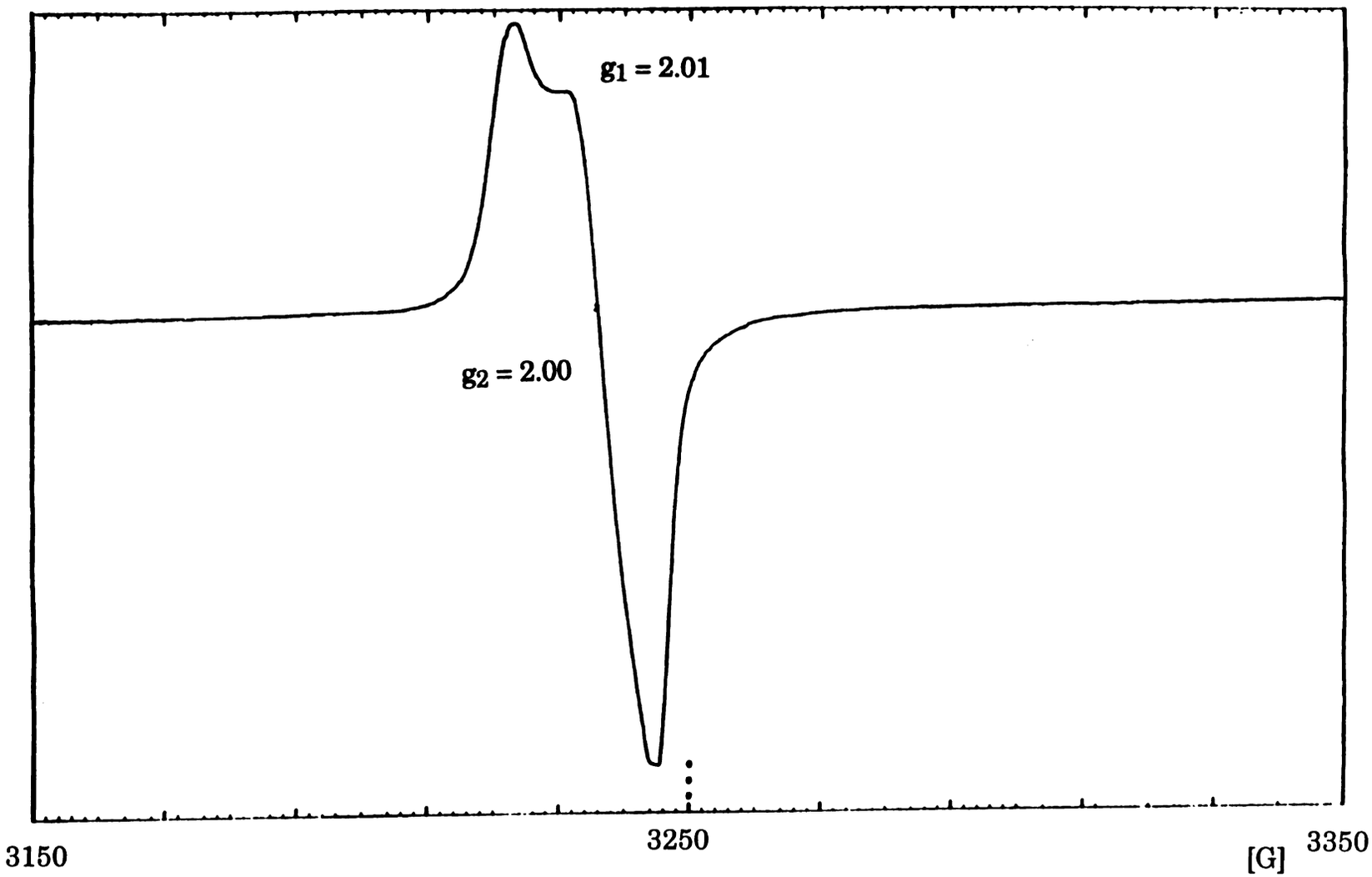

Figure 25. EPR spectrum of green paramagnetic solid from $[Rh_2(NCCH_3)_{10}][BF_4]_4$ + P1 in a toluene/CH_3CN glass at 133 K.

= 2.01 and g_2 = 2.00, as seen in Figure 25. This anisotropy is characteristic of $[TTF]^{\bullet+}$ (g_1 = 2.011, g_2 = 2.009, g_3 = 2.002).[23] The narrow signal spans 51 G, which is indicative of an organic rather than metal-based radical which supports the $[TTF]^{\bullet+}$ oxidation product mentioned previously.

The electronic absorption spectrum of **15** recorded in CH_2Cl_2 exhibits the characteristic phenyl and TTF chromophore absorption bands for an oxidized TTF at λ_{max} = 510 and 600 nm. The transition at 510 nm can be assigned as an intermolecular excitation of the $TTF^{\bullet+}$ radical by analogy to previous studies of TTF.[24] The infrared spectrum of the product displays bands assignable to the phenyl rings of the ligand at 695 and 530 cm^{-1}, as well as a broad feature at 1050 cm^{-1} which is indicative of the $[BF_4]^-$ counter-ion. A salient feature of the spectrum is the absence of any bands indicative of acetonitrile. It has been noted that the solvated Rh wire, $\{[Rh(NCCH_3)_4][BF_4]_{1.5}\}_\alpha$, exhibits very weak nitrile stretches in its IR spectrum.[25] Another possibility is that the orange product is actually a combination of unreacted ligand and $[Rh_2(NCCH_3)_{10}][BF_4]_4$, with the green product being [P1][BF_4]. If indeed the true stoichiometry of the reaction is 1:1 there must be acetonitrile to complete the coordination sphere. This would account for the absence of the typical absorbances associated with the expected Rh species in the electronic spectrum, as well as the lack of acetonitrile bands in the infrared spectrum. It does not, however, account for the small amount of solid which was recovered from the orange filtrate.

The reaction of $[Re_2(NCCH_3)_{10}][BF_4]_4$ with 4 equivalents of *o*-P2 produces similar results. Upon combination of both reactants in acetonitrile, the reaction solution becomes dark green in color. Precipitation with diethyl ether reveals a paramagnetic green solid as evidenced by its ^1H and $^{31}P\{^1H\}$ NMR spectra. An EPR spectrum of this product in a 1:1 CH_3CN/toluene glass at 133 K reveals a very sharp signal at g = 2.00. Based on this signal it can be surmised that the product is a radical resulting from oxidation of *o*-P2, possibly accompanied by reduction of the Re_2^{4+} core from $Re_2^{II,II}$ to $Re_2^{II,I}$.

B. Preparation, Characterization and Reactivity of $[ReCl_2(o\text{-}P2)_2][Re_2Cl_6(o\text{-}P2)]$ (16•17)

(1) Reactivity of $[(n\text{-}Bu)_4N]_2[Re_2Cl_8]$ with *o*-P2 (1).

The unusual salt $[ReCl_2(o\text{-}P2)_2]$ $[Re_2Cl_6(o\text{-}P2)]$ (**16•17**) is prepared in highest yields from the reaction of $[(n\text{-}Bu)_4N]_2[Re_2Cl_8]$ with 2.4 equivalents of *o*-P2 in refluxing ethanol. The reaction is extremely time and solvent dependent. The use of solvents other then ethanol, such as acetonitrile or acetone result in a different set of product(s) or in no reaction. Refluxing the mixture for longer than 1.5 h. results in a green product which is more soluble than **16•17** in acetone and acetonitrile. This type of solvent dependence has been documented in similar reactions.[26] The time dependence is most likely a result of **17** being an intermediate complex for another product, possibly $\alpha\text{-}Re_2Cl_4(o\text{-}P2)_2$ or $[ReCl_2(o\text{-}P2)_2]Cl$, where α refers to the chelating ligand, and β the bridging form.

The mononuclear cation [*trans*-$ReCl_2$(o-P2)$_2$]$^+$ (**16**) results from nonredox cleavage of the dimetal unit, which is not particularly surprising given the demonstrated ability of bidentate phosphines to cleave the quadruple bond of $[Re_2X_8]^{2-}$ species. Similar reactions involving other bidentate phosphine ligands with an ethene backbone, such as bis(diphenylphosphino)ethene (dppee)[27] and bis(diphenylphosphino)benzene (dppb)[26] performed in alcohols produce the analogous complexes [*trans*-$ReX_2(LL)_2$]X (LL = dppb, dppee; X = Cl, Br). Analogous behavior has also been noted with ligands such as bis(diphenylphosphino)ethane (dppe),[2,28a] bis(diphenylphosphino)amine (dppa),[28b] bis(diethylphosphino)ethane (depe),[28c] and bis(ditolylphosphino)ethane (dtpe).[28d]

The anion in the structure, [α-Re_2Cl_6(*o*-P2)]$^-$ (**17**), results from the substitution of two chlorides on $[Re_2Cl_8]^{2-}$ with concomitant reduction of the rhenium core from Re_2^{6+} to Re_2^{5+}. The reaction conditions are similar to those reported for the synthesis of α-Re_2X_4(dppee)$_2$ (X = Cl, Br),[29] but in the present case only one chelating diphosphine ligand enters the coordination sphere. It is interesting to note that the dppee reactions proceed with M-M cleavage to yield the mononuclear Re(III) cation $[ReX_2(dppee)_2]^+$ with no evidence of the more substituted products of the type encountered in this study. The dinuclear anion **17** appears to be a previously undetected intermediate in the conversion of $[Re_2X_8]^{2-}$ compounds to the bis-substituted Re_2Cl_4(P-P)$_2$ compunds.

(2) Crystal Structure of $[ReCl_2(o\text{-}P2)_2]$ $[Re_2Cl_6(o\text{-}P2)]$ (16•17).

Thermal ellipsoid plots drawings of the ions $[ReCl_2(o\text{-}P2)_2]^+$ (**16**) and $[Re_2Cl_6(o\text{-}P2)]^-$ (**17**) are depicted in Figures 26 and 27. Selected bond distances and angles are provided in Tables 10 and 11 respectively. The asymmetric unit consists of one $[Re_2Cl_6(o\text{-}P2)]^-$ (**17**) moiety, two half $[ReCl_2(o\text{-}P2)_2]^+$ (**16**) units, and four solvent molecules. The cations are six-coordinate with *trans* chelating phosphine ligands. The angles P(3)-Re(3)-P(4) and P(4)-Re(3)-Cl(7) are 80.62 (13)° and 92.50 (13)° for one cation, and P(5)-Re(4)-P(6) = 79.63 (14)° and P(6)-Re(4)-Cl(8) = 88.42 (14)° for the second independent cation. These values are comparable to those observed in similar cations.[26-28] The average Re-Cl and Re-P values of 2.31(1) Å and 2.459(3) Å respectively are similar to corresponding distances reported for analogous bis-diphosphine complexes, $[ReCl_2(P\text{-}P)_2]^+$ (P-P = dppee, dppbe, dppe, dppa, depe, dtpe). In the *o*-P2 ligand, representative distances *e.g.*, C(33)-C(34) = 1.33(2) Å and S(5/6)-C(33/34) = 1.74(2) Å are essentially unchanged relative to the bond lengths in the free phosphine ligand.[30] These data suggest that there is no pronounced electronic change in the dithiole system due to the electronic donation of the phosphorus to the metal center. The out-of-plane bend of 22° at the S(5) and S(6) positions is similar to those observed for $[Rh(o\text{-}P2)_2][BF_4]$,[8b] $[Ni(o\text{-}P2)_2][BF_4]_2$ (**8**), and $[Pt(o\text{-}P2)_2][BF_4]_2$ (**11**)[31] and is most likely due to packing influences. The corresponding bend in the cation containing Re(4) is much smaller, being only 11°. This difference in the out-

Table 10. Summary of bond distances (Å) and angles (deg) for the cation $[ReCl_2(o\text{-}P2)_2]^+$ (**16**) in **16•17**.

Bond Distances

A	B	A-B (Å)	A	B	A-B (Å)
Re(3)	P(3)	2.456 (4)	Re(3)	P(4)	2.457 (4)
Re(3)	Cl(7)	2.296 (4)	P(3)	C(33)	1.840 (14)
P(3)	C(41)	1.83 (2)	C(33)	C(34)	1.33 (2)
C(33)	S(5)	1.74 (2)	S(5)	C(35)	1.77 (2)
S(7)	C(37)	1.78 (2)	C(37)	C(38)	1.33 (3)

Bond Angles

A	B	C	A-B-C (°)	A	B	C	A-B-C (°)
P(3)	Re(3)	P(4)	80.62 (13)	P(3)	Re(3)	P(4A)	99.38 (13)
Cl(7)	Re(3)	P(4)	92.50 (13)	Re(3)	P(3)	C(33)	105.5 (5)
Re(3)	P(3)	C(41)	123.7 (5)	P(3)	C(33)	C(34)	120.3 (12)
C(33)	S(5)	C(35)	93.6 (7)	S(5)	C(35)	S(6)	114.2 (8)

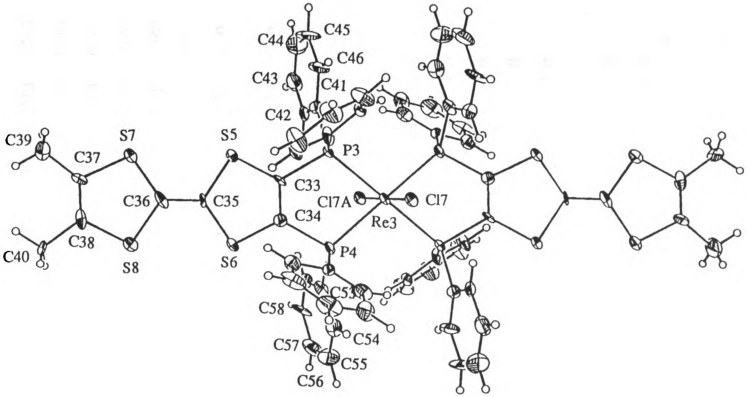

Figure 26. Thermal ellipsoid plot of the cation $[Re(o\text{-}P2)_2Cl_4]^+$ (**16**) with non-hydrogen atoms represented by their 50% probability ellipsoids.

Table 11. Summary of bond distances (Å) and angles (deg) for the anion $[Re_2Cl_6(o\text{-}P2)]^-$ (**17**) in **16•17**.

Bond Distances

A	B	A-B (Å)	A	B	A-B (Å)
Re(1)	Re(2)	2.2402 (2)	Re(1)	P(1)	2.335 (5)
Re(1)	P(2)	2.367 (5)	Re(1)	Cl(1)	2.380 (4)
Re(1)	Cl(2)	2.367 (4)	Re(2)	Cl(3)	2.315 (4)
Re(2)	Cl(4)	2.325 (4)	Re(2)	Cl(5)	2.351 (4)
Re(2)	Cl(6)	2.313 (5)	P(1)	C(9)	1.84 (2)
P(1)	C(1)	1.82 (2)	C(1)	C(2)	1.38 (2)
C(1)	S(1)	1.75 (2)	C(3)	C(4)	1.36 (2)
C(4)	S(4)	1.72 (2)	C(5)	C(6)	1.32 (3)

Bond Angles

A	B	C	A-B-C (°)	A	B	C	A-B-C (°)
Re(1)	Re(2)	Cl(4)	110.04	Re(1)	Re(2)	Cl(3)	100.2
Re(2)	Re(1)	Cl(1)	107.2	Re(2)	Re(1)	Cl(1)	111.3
Re(2)	Re(1)	P(1)	97.2	Cl(2)	Re(1)	Cl(1)	83.1
P(2)	Re(2)	Cl(1)	157.0	Cl(3)	Re(2)	Cl(6)	85.9
Cl(3)	Re(2)	Cl(5)	150.9	Re(1)	P(2)	C(2)	105.8
Cl(2)	Re(1)	P(2)	93.1	P(2)	C(2)	C(1)	116.7
C(1)	C(2)	S(2)	115.6	S(2)	C(3)	S(1)	114.3

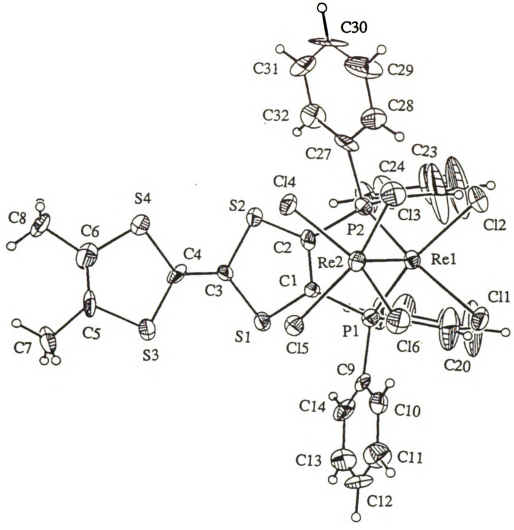

Figure 27. Thermal ellipsoid plot of the anion $[Re_2Cl_6(o\text{-}P2)]^-$ (**17**) with non-hydrogen atoms represented by their 50% probability ellipsoids.

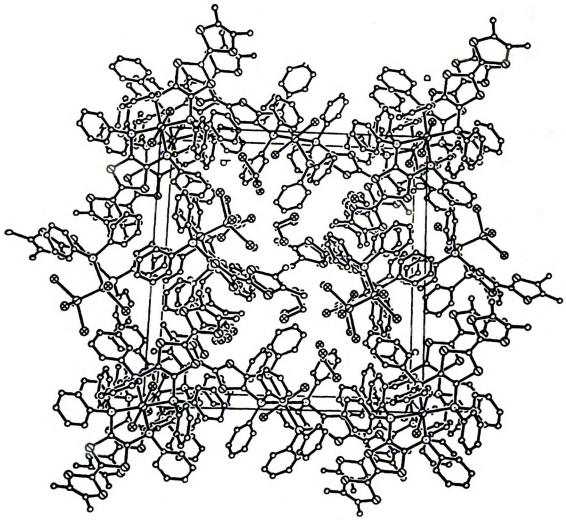

Figure 28. Packing diagram of $[ReCl_2(o\text{-}P2)_2][Re_2Cl_6(o\text{-}P2)]$ (**16•17**).

of-plane bend may account for the slight differences in the magnitude of the bonds and angles of the dithiole rings for the two cations.

The anion, **17**, is an unsymmetrical mixed-valence Re(II)-Re(III) molecule with four chloride ions residing on Re(2), and two chloride ions along with one chelating *o*-P2 ligand being coordinated to Re(1) in an eclipsed conformation when viewed down the Re-Re axis. The Re-Re distance is 2.2402(9) Å, which, based on the qualitative overlap scheme for the M_2L_8 geometry, represents a bond order of 3.5 ($\sigma^2\pi^4\delta^2\delta^{*1}$ electronic configuration). This is reasonable given that it is a little longer than the Re-Re quadruple bond in $[Bu_4N]_2[Re_2Cl_8]$ which is 2.222(2) Å,[2] but shorter than the metal-metal distance in the triply bonded compound $Re_2Cl_4(dth)_2$ (2.293(2) Å).[30] It should be noted that this distance is much longer than the those in the more symmetrical Re(II,III) phosphine cations $[Re_2Cl_4(PMe_3)_4]^+$ (2.205(1) Å) and $[Re_2Cl_4(PMe_2Ph)_4]^+$ (2.218(1) Å). This may be due to the fact that the orbitals are more contracted in the cations and therefore the metal ions are required to be closer in order to achieve good overlap.[32] The Re-Cl distances on the "formally" Re(III) center range from 2.313(5) to 2.351(4) Å, as compared to the average distance of ~2.29(2) Å in $[Re_2Cl_8]^{2-}$.[33] The Re-Cl distances to Re(1) are Re(1)-Cl(1) = 2.380(4) Å and Re(1)-Cl(2) = 2.367(4) Å. These are longer than corresponding values in $[Re_2Cl_4(PMe_2Ph)_4]^+$ (Re-Cl = 2.33 Å) and $[Re_2Cl_4(PMe_3)_4]^+$ (Re-Cl = 2.34 Å).[32] The only other dinuclear complexes with a single chelating ligand of which we are aware are $[Bu_4N][Re_2Cl_7(dto)]$ (dto =

3,6-dithiaoctane) and $[Bu_4N][Re_2Cl_7(dth)]$,[34] however in both of these cases the coordination mode for the bidentate ligand is axial-equatorial rather than equatorial-equatorial.

(3) Spectroscopic Characterization of $[ReCl_2(o\text{-}P2)_2][Re_2Cl_6(o\text{-}P2)]$ (16•17)

The paramagnetic nature of $[ReCl_2(o\text{-}P2)_2][Re_2Cl_6(o\text{-}P2)]$ leads to a broad, featureless ^1H NMR spectrum and the complete absence of $^{31}P\{^1H\}$ NMR signals. The IR spectrum confirms the presence of ν(Re-Cl) stretches at 329, 333 and 352 cm^{-1}. The electronic absorbance spectrum reveals the characteristic phenyl and TTF-based transitions that are attributable to the ligand at 276, 322, and 448 cm^{-1}. The extinction coefficients of the TTF bands are reliable indicators of the number of chromophores in the molecule.[8a] Thus based on the fact that free *o*-P2 with four phenyl groups exhibits a band at 276 nm with an ε value of 25,000 $M^{-1}cm^{-1}$ and $[ReCl_2(o\text{-}P2)_2][Re_2Cl_6(o\text{-}P2)]$ exhibits a transition at 276 with ε value of 74,600, one can ascertain that the compound contains three TTF phosphines (or 12 phenyl groups). The low-energy transition at 976 nm in the near-IR region signifies a $\delta \rightarrow \delta^*$ transition for a mixed-valence Re^{II}-Re^{III} complex.[2] The FAB mass spectrum of **16•17** displays the highest mass peak at m/z = +1457 which is consistent with the presence of the cation $[Re_2Cl_2(o\text{-}P2)_2]^+$. In the negative ion mode, the highest mass peak is at m/z = -1186 which is consistent with the anion, $[Re_2Cl_6(o\text{-}P2)]^-$.

(4) Isolation of $[ReCl_2(o\text{-}P2)_2]^+$ (16)

(i) Reduction of $[ReCl_2(o\text{-}P2)_2][Re_2(o\text{-}P2)Cl_6]$ (16•17). Reaction of **16•17** with a slight excess of the reducing agent $CoCp_2$ affords a yellow solid identified as $ReCl_2(o\text{-}P2)_2$ (**18**) on the basis of infrared, mass spectroscopic and magnetic susceptibility measurements. This reaction is similar to one reported by Walton *et. al.* for the reduction of $[ReCl_2(dppee)_2]Cl$ to $ReCl_2(dppee)_2$.[27] The neutral compound **18** is fairly insoluble, thereby allowing it to be separated from the by-product salt $[CoCp_2][Re_2Cl_6(o\text{-}P2)]$. The FAB mass spectrum of **18** contains a parent ion peak at m/z = 1457 for both positive and negative ion spectra which is consistent with $ReCl_2(o\text{-}P2)_2$. These results are in accord with **18** being neutral since both positive and negative ions were detected. The infrared spectrum of **18** exhibits modes due to *o*-P2 at 513 and 702 cm^{-1} and a characteristic ν(Re-Cl) feature at 330 cm^{-1}.

(ii) Oxidation of $ReCl_2(o\text{-}P2)_2$ (18). In order to further characterize the cation as found in the original compound, $ReCl_2(o\text{-}P2)_2$ was re-oxidized by gently refluxing the compound in CCl_4/CH_2Cl_2. It had been reported earlier that such conditions led to the oxidation of $ReCl_2(dppb)_2$ to $[ReCl_2(dppb)_2][Cl]$.[26] Mass spectroscopic analysis of **16**•[Cl] gives a parent ion peak at m/z = +1457, which is in accord with the presence of $[ReCl_2(o\text{-}P2)_2]^+$. Based on the chemistry of similar complexes, it is reasonable to assume that **16** retains the *trans* configuration throughout the redox reactions.[26,27] Alternatively one can treat **18** with $NOBF_4$ to yield $[ReCl_2(o\text{-}$

P2)$_2$][BF_4] (**16**•[BF_4]), but care must be taken not to add excess oxidant, as this will lead to oxidation of the TTF substituents as well. If this occurs, the solution assumes an intense green color.

(5) Electrochemical Studies

As Figure 29 shows, the electrochemistry of [$ReCl_2$(*o*-P2)$_2$][Re_2Cl_6(*o*-P2)] in 0.1 M TBABF_4/CH_2Cl_2 is complicated. This is due to the presence of three redox-active Re ions as well as three TTF phosphine ligands that are each capable of undergoing two one-electron oxidations. The most likely possibilities for redox processes based on the established electrochemistry of the *o*-P2 molecule and similar Re compounds whose electrochemical properties have been reported are provided in Table 12.;. The compound

Table 12. Possible redox reactions for the salt [$Re^{III}Cl_2$(*o*-P2)$_2$]-[$Re_2^{II,III}Cl_6$(*o*-P2)] (**16•17**).

[$Re^{III}Cl_2$(*o*-P2)$_2$]$^+$ (**16**)	[$Re_2^{II,III}Cl_6$(*o*-P2)]$^-$ (**17**)
oxidations	**oxidations**
Re(III) → Re(IV)	Re_2(II,III) → Re_2(III,III)
Re(*o*-P2)$_2^0$ → Re(*o*-P2)$_2^{2+}$ (2 e- total)	Re_2(*o*-P2)^0 → Re_2(*o*-P2)$^+$ (1 e-)
Re(*o*-P2)$_2^{2+}$ → Re(*o*-P2)$_2^{4+}$ (2 e- total)	Re_2(*o*-P2)$^+$ → Re_2(*o*-P2)$^{2+}$
reductions	**reductions**
Re(III) → Re(II)	Re_2(II,III) → Re_2(II,II)
Re(II) → Re(I)	

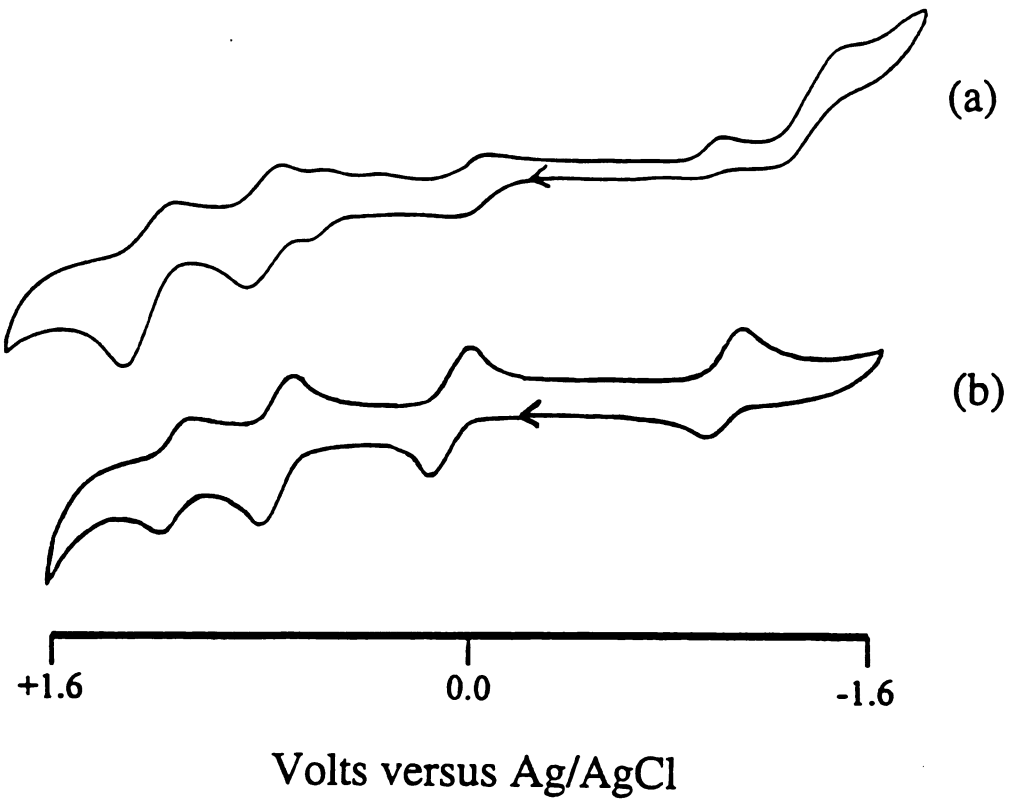

Figure 29. Cyclic voltammogram of (a) $[ReCl_2(o\text{-}P2)_2][Re_2Cl_6(o\text{-}P2)]$ (**16•17**) and (b) $[ReCl_2(o\text{-}P2)_2][BF_4]$ in 0.1 M $TBABF_4/CH_2Cl_2$ vs Ag/AgCl at a Pt disk electrode.

exhibits four TTF phosphine-based oxidation processes and three metal-based reductions, two of which would be expected to be fairly accessible, namely Re(III) → Re(II) and Re_2(II,III) → Re_2(II,II), and one of which would be much less accessible, namely Re(II) → Re(I). The two TTF phosphine ligands on the mononuclear cation, **16**, undergo oxidations at the same potential, therefore the coincidence of these processes leads to a total of 2 e^- being associated with these couples.

Obviously the only way one can assign the redox processes for the individual ions in **16•17** is to prepare at least one ion separately with an "innocent" counterion. In this vein, we have prepared and measured the electrochemistry for [$ReCl_2$(*o*-P2)$_2$][BF_4]) in a 0.2 M TBABF_4/CH_2Cl_2 solution at a Pt disk electrode (Figure 29. The salt (**16**•[BF_4]) exhibits couples at $E_{1/2}(ox)_1$ = +0.75 V, $E_{1/2}(ox)_2$ = +1.14 V and $E_{1/2}(red)_1$ = +0.07 V, with an irreversible reduction process located at $E_{(p,c)1}$ = -1.02 V. The published data for the related mononuclear Re(III) salt [$ReCl_2$(dppee)$_2$]Cl, recorded on 0.1 M TBAH/CH_2Cl_2 solutions using a Pt bead electrode, include an oxidation from Re(III) to Re(IV) at ca. +1.6 V and two reductions corresponding to Re(III)/Re(II) and Re(II)/Re(I) at -0.2 and ca. -1.4 respectively.[26] Based on these results, we can conclude that the mononuclear cation **16** is responsible for the oxidations at $E_{1/2}(ox)$ = +0.67 V and $E_{(p,a)}$ = +1.05, as well as reductions at $E_{1/2}(red)$ = +0.03 V and $E_{(p,c)}$ = -1.12 V in the c.v. of **16•17**. These are assigned to the two oxidations of the *o*-P2 ligands and reductions

from Re(III) → Re(II) and Re(II) → Re(I) respectively. The Re(III)/Re(IV) couple for *trans*-$[ReCl_2(dppbe)_2][Cl]$ was reported to occur at +1.51 V in a 0.1 M TBAH/CH_2Cl_2 solution,[26] which is beyond the 1.50 V scan range used for $[ReCl_2(o\text{-}P2)_2]^+$. The remaining features in the cyclic voltammogram of **16•17** are $E_{1/2}(ox)_2$ = +0.50 V, $E_{1/2}(ox)_2$ = +0.31 V and $E_{(p,c)2}$ = -0.79 V which are assigned as two *o*-P2 oxidations and a reduction from $Re_2(II,III)$ → $Re_2(II,II)$ in the dinuclear anion. The oxidation processes for the coordinated *o*-P2 ligands are shifted to more positive potentials relative to the free ligand ($E_{1/2}(ox)_1$ = +0.41 V, $E_{1/2}(ox)_2$ = +0.85 V), with those associated with the cation occurring at the highest values. This shift to higher potentials is indicative of strong metal-ligand interactions which leads to an electron-withdrawing effect on the TTF substituents.

(6) Magnetic Properties.

(i) $[ReCl_2(o\text{-}P2)_2][Re_2Cl_6(o\text{-}P2)]$ (16•17). (a) Magnetic susceptibility. The magnetic susceptibility measurements of **16•17** compound shown in Figure 30 reveal a Curie paramagnetic behavior for the salt with a Curie constant C = 0.395 and a temperature independent paramagnetism contribution (TIP) (χ_{TIP} = 9.64 x 10^{-3} emu/mol).[35] This TIP behavior was previously noted for a similar series of Re^{III} complexes, $ReX_3(PR_2Ph)_2$ (X = Cl, Br; R = Me, Et), although in these cases, χ_{TIP} was somewhat smaller (in the range 1.66 - 1.36 x 10^{-3} emu/mol).[36] The anion $[Re_2Cl_6(o\text{-}P2)]^-$ is a mixed-valence

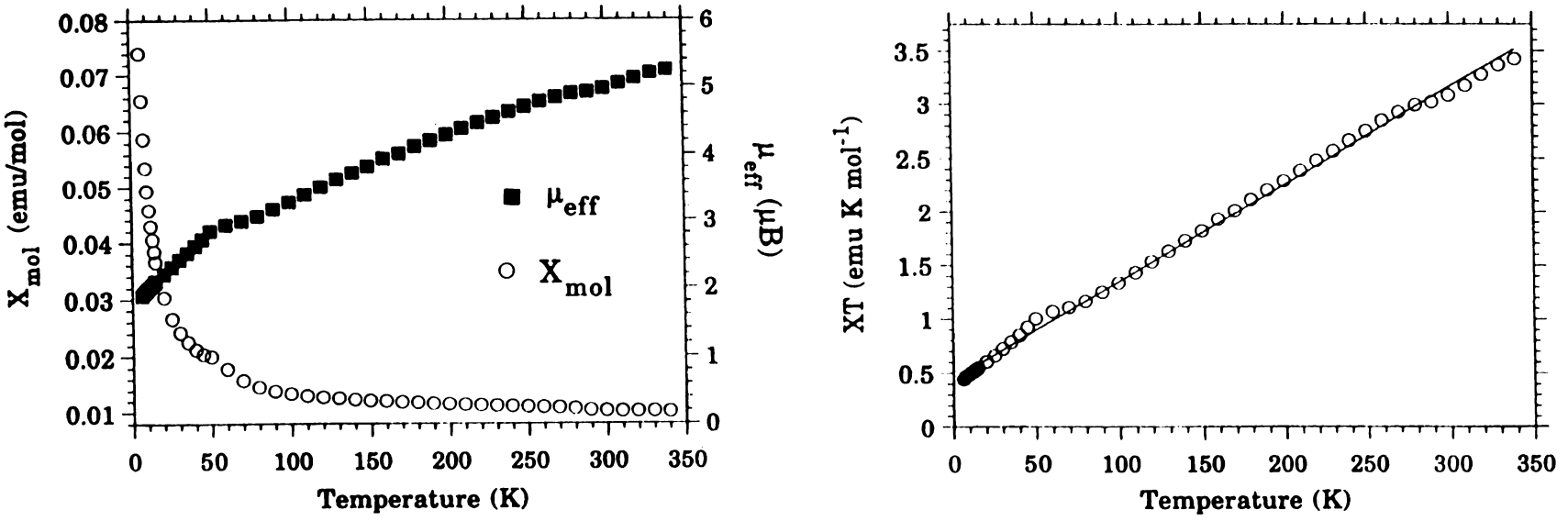

Figure 30. Magnetic data for $[ReCl_2(o\text{-}P2)_2][Re_2Cl_6(o\text{-}P2)]$ (**16•17**): (a) μ_{eff} (μB) and χ_{mol} (emu/mol) vs. temperature (K) and (b) χT (emu K mol^{-1}) vs. temperature (K) fit to the Curie-Weiss law with a slope of χ_{TIP}.

compound with an overall d^9 configuration and therefore should have an S = 1/2 ground state. Given that C = 0.395 for $[Re_2Cl_6(o\text{-}P2)]^-$ **17**, we can estimate μ_{eff} to be ~1.77 μ_B. This value is in good agreement with data obtained for similar compounds, such as $[Re_2Cl_4(PMe_2Ph)_4][PF_6]$, which exhibits a moment of ~1.8 μ_B at room temperature,[37] and $[Re_2X_4(dppm)_2][PF_6]$ (X = Cl, Br) which exhibit moments of ~1.5 μ_B.[38]

(b) EPR specroscopy. The EPR spectrum of $[ReCl_2(o\text{-}P2)_2][Re_2Cl_6(o\text{-}P2)]$ (**16•17**) in a 1:1 CH_2Cl_2/toluene glass at 4 K is shown in Figure 31. A complex pattern is observed that is indicative of hyperfine coupling to the ^{185}Re (I = 5/2) and ^{31}P (I = 1/2) nuclei. The spectrum is centered at 2833 G (g = 2.40). Given the complexity of the spectrum, exact $g_\perp$ and $g_{||}$ values were not able to be determined. Similar spectra have been reported for 1,3,6-$Re_2Cl_5(PMe_3)_3$ and 1,2,7-$Re_2Cl_5(PMe_3)_3$.[39]

(ii) $[ReCl_2(o\text{-}P2)_2][BF_4]$ (16•[BF_4]). The susceptibility measurements of the separate mononuclear cation, **16**, reveal a TIP (χ_{TIP} = 10.7x 10^{-3} emu/mol) with an extrinsic paramagnetic (Curie) contribution being observed at low temperatures. Assuming this impurity is an S=1/2 system, it can be estimated that it is 10% of one spin 1/2. The value for χ_{TIP} agrees quite well with the previously calculated value for **16•17**.

(iii) $ReCl_2(o\text{-}P2)_2$ (18). The d^5 compound, **18**, contains the same ligand system as **16** and is expected to possess one unpaired electron (S=1/2). The χ

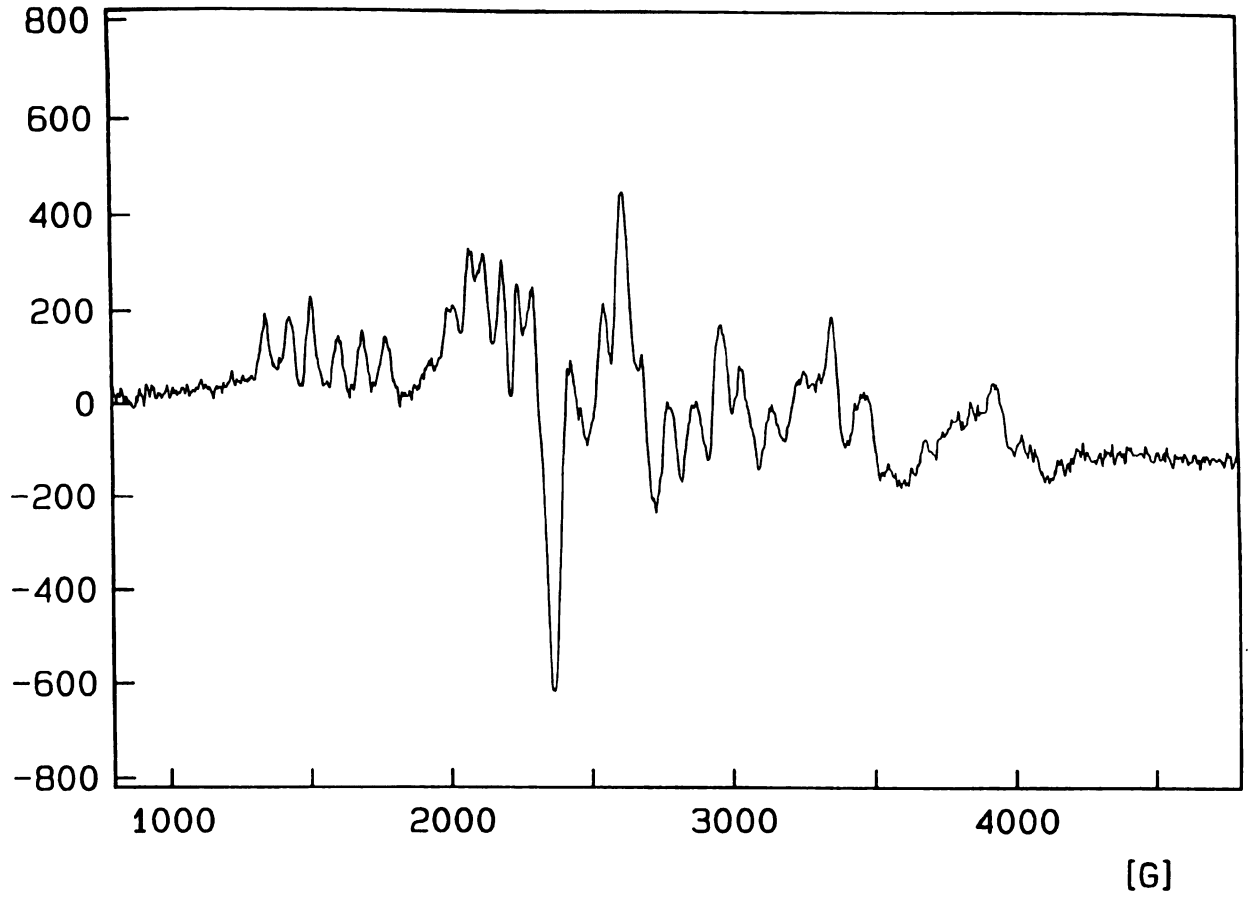

Figure 31. EPR spectrum of $[ReCl_2(o\text{-}P2)_2][Re_2Cl_6(o\text{-}P2)]$ (**16•17**) in a 1:1 toluene/CH_2Cl_2 glass at 4 K.

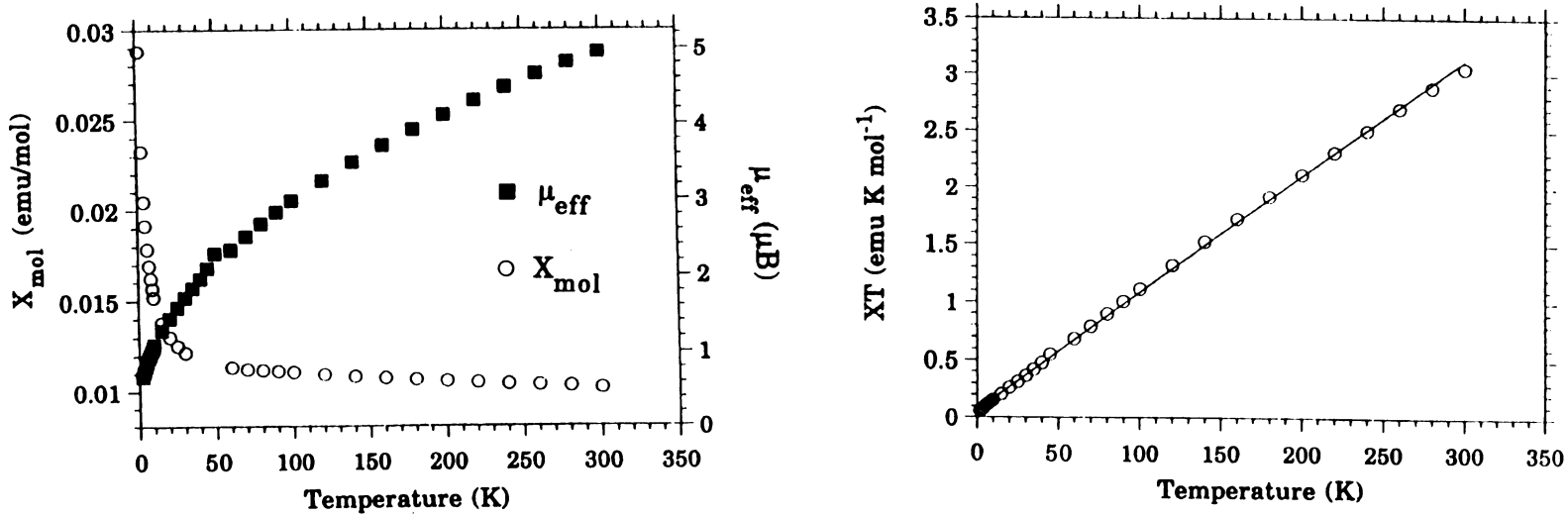

Figure 32. Plots of (a) μ_{eff} (μB) and χ_{mol} (emu/mol) vs. temperature (K) and (b) χT (emu K mol^{-1}) vs. temperature of $[Re(o\text{-}P2)_2Cl_2][BF_4]$ (**16**•$[BF_4]$).

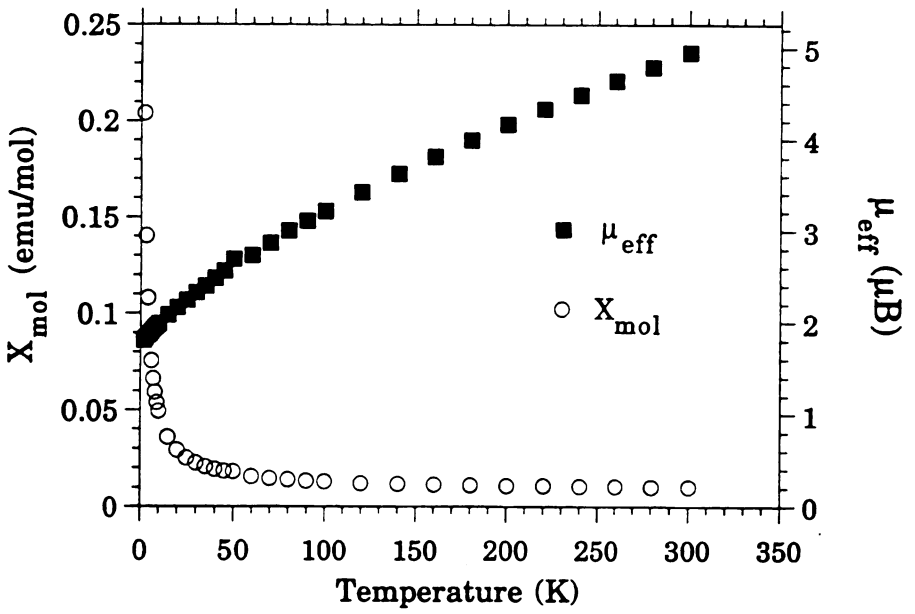

Figure 33. Plot of μ_{eff} (μB) and χ_{mol} (emu) vs. temperature (K) of $ReCl_2$(*o*-P2)$_2$ (18).

versus T data follow a Curie law with a C = 0.392 and a χ_{TIP} = 9.34 x 10^{-3} emu/mol. This is in agreement with the presence of non-interacting S=1/2 ions (C=0.375 for S=1/2 and g=2). The moment at r.t. is ~ 4.9 μ_B.

C. Reactions of $Mo_2[S(CH_3)_2]_4Cl_4$ with *o*-P2.

(1) Synthesis

Reactions to yield products of the type $Mo_2X_4L_4$ and $Mo_2X_4(LL)_2$ are well documented in the literature.[2] Given the existence of $Mo_2X_4(dppee)_2$ (X = Cl, Br, I)[41] and α-$Mo_2X_4(dppb)_2$ (X = Cl or Br),[42a] the possibility of forming $Mo_2X_4(o\text{-}P2)_2$ species would appear to be promising. To this end, the reaction of $Mo_2Cl_4[S(CH_3)_2]_4$ with two equivalents of *o*-P2 was undertaken, and it was discovered that the reaction is dependent on the solvent and the presence or absence of air.

The use of acetonitrile results in an emerald green solution which becomes dark brown over time and yields a green precipitate. When the reaction is performed in air with CH_2Cl_2 as the solvent, however, a homogeneous brown solution is obtained after stirring for approximately the same length of time. This brown solution is also observed to form under anaerobic conditions, but the reaction is slower and a precipitate forms. The addition of CH_2Cl_2 to the green precipitate from the reaction using acetonitrile causes an immediate color change to brown. The varied results obtained from differences in the solvent and reaction conditions are not surprising, given the previously documented reactions involving dppb, dppe,

and dpdt.[42] Solution studies and solid state properties of the α and β isomers of dpdt support the conclusion that the β-isomer is generally the thermodynamically favored form, but that the α-isomer can be obtained in solvents that take advantage of its low solubility. Similar behavior would be expected for reactions aimed at the synthesis of $Mo_2X_4(o\text{-}P2)_2$. The proposed mechanism for the occurrence of both isomers from a precursor that contains trans leaving groups (i.e. *trans*-$Mo_2X_4L_4$) involves internal rotation of the Mo_2 unit within the ligand framework.[42d,43]

Slow evaporation of solvent from the brown solution of CH_2Cl_2, in air, yielded brown crystals, identified as $MoCl_2O_2(o\text{-}P2O_2)$ (**19**) by X-ray crystallography. The formation of **19** is due to degradation of the *o*-P2 to the phosphine oxide, most likely caused by moisture. Oxidations of this nature are not uncommon with the tetrathiafulvalene phosphines, as the formation of $P4O_2$ from P4 has been observed to occur.[44] Oxygen adducts have also been commonly observed in the FAB-MS spectra of the homoleptic *o*-P2 complexes.[44] Furthermore, quadruply bonded Mo_2^{4+} complexes are subject to oxidative cleavage upon reaction with strong donor ligands.[2]

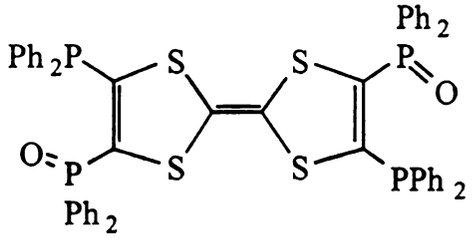

(2) Crystal Structure of $MoCl_2O_2$(*o*-P2O_2) (19)

A PLUTO drawing of $MoCl_2O_2$(*o*-P2O_2) (**19**) is provided in Figure 34, while selected bond distances and angles are provided in Table 13. The neutral compound is six-coordinate with axial chlorides and oxygen atoms *trans* to the bis-phosphine oxide, *o*-P2O_2, unit. The Mo-Cl distances of 2.412(6) and 2.360(6) Å are comparable to 2.410(1) Å, as found in $MoCl_2$(dppb)$_2$[42a] and 2.3903(3) for $MoCl_2O_2[OPCH_2(C_2H_4OCH_3)_2]_2$.[45] The angles around the metal center O(1)-Mo(1)-O(2) = 78.4(4)°, O(3)-Mo(1)-O(4) = 98.6(7)°, Cl(1)-Mo(1)-Cl(2) = 165.7(2)°, and O(1)-Mo(1)-Cl(1) = 87.4(4)°, indicate a highly distorted octahedral geometry, with the chlorides bent away from the phenyl rings of the *o*-P2O_2 ligand with Cl(1)-Mo(1)-Cl(2) = 165.7(2)°. Such a distortion from 180° is caused by repulsions from the bulky phenyl groups, and has been reported for the related compound $MoCl_2O_2[OPCH_2(C_2H_4OCH_3)_2]_2$, with a Cl(1)-Mo(1)-Cl(2) angle of 166.0(1)°. The Mo(1)-O(1) and Mo(1)-O(2) distances of 2.091(11) and 2.214(10) Å fall outside of the values observed for $MoCl_2O_2[OPCH_2(C_2H_4OCH_3)_2]_2$ (2.149(4) and 2.157(7) Å). The Mo(1)-O(3) distance of 1.67(2) Å is reasonable for a Mo-O(oxo) bond, which are typically in the range 1.68(3)-1.77(3) Å.[46] The elongation of Mo(1)-O(2) can be attributed to the strong *trans* influence of the terminal Mo-O(oxo) bond. The Mo(1)-O(4) distance is significantly longer at 2.114(9), and is closer to the terminal Mo-OH_2 interaction reported for (*p*-$CH_3C_6H_4NH)_2Mo_2I_6(H_2O)_2$ (2.188(11) = Mo-O) and (*p*-$CH_3C_6H_4N)_2Mo_2I_6(H_2O)_2$

Table 13. Summary of bond distances (Å) and angles (deg) for $MoCl_2O_2$(*o*-$P2O_2$)•CH_2Cl_2 (**19**•CH_2Cl_2).

Bond Distances

A	B	A-B (Å)	A	B	A-B (Å)
Mo(1)	O(1)	2.091 (11)	Mo(1)	Cl(1)	2.412 (6)
Mo(1)	O(2)	2.214 (10)	Mo(1)	Cl(2)	2.360 (6)
O(1)	P(1)	1.463 (12)	Mo(1)	O(3)	1.67 (2)
O(2)	P(2)	1.464 (11)	Mo(1)	O(4)	2.114 (9)
C(1)	C(2)	2.313 (5)	C(3)	C(4)	1.84 (2)
C(5)	C(6)	1.82 (2)	S(1)	C(2)	1.75 (2)
S(2)	C(1)	1.77 (2)	S(3)	C(5)	1.75 (2)
S(4)	C(6)	1.75 (2)	C(5)	C(7)	1.45 (2)

Bond Angles

A	B	C	A-B-C (°)	A	B	C	A-B-C (°)
O(1)	Mo(1)	O(2)	78.4 (4)	Cl(1)	Mo(1)	Cl(2)	165.7 (2)
O(3)	Mo(1)	O(4)	98.6 (7)	C(2)	S(1)	C(3)	93.2 (7)
O(1)	Mo(1)	Cl(1)	87.4 (4)	C(5)	S(3)	C(4)	96.8 (8)
Mo(1)	O(1)	P(1)	147.8 (8)	C(5)	C(6)	C(8A)	126.0 (14)
O(3)	Mo(1)	O(1)	90.7 (7)	C(5)	C(6)	C(8B)	124 (3)
O(1)	P(1)	C(2)	116.0 (7)	S(3)	C(4)	S(4)	112.4 (9)
P(2)	C(1)	C(2)	128.2 (13)	S(1)	C(3)	S(2)	112.1 (7)

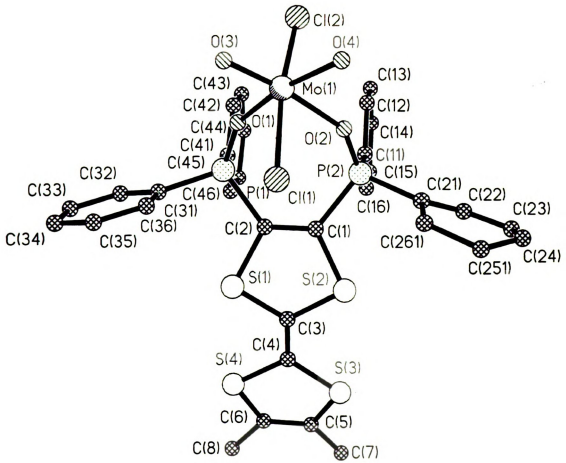

Figure 34. PLUTO representation of $MoCl_2O_2(o\text{-}P2O_2)$ (**19**).

(2.191(10) = Mo-O).[47] Although attempts to identify remaining peaks in the difference map have proven to be unsuccessful, the coordinated water molecule would account for the unusually close Mo(1)-O(2) distance and the O(3)-Mo(1)-O(4) angle being less than 102°. *Cis*-dioxomolybdenum complexes exhibit angle widening caused by strong repulsions of the strongly bonded terminal oxygen atoms.[45] As the structure currently stands, the metal is Mo^{VI} (d^0), however if O(4) is actually a water molecule, the oxidation state would be to Mo^{IV} (d^2).

The angle between the planes defined as O(1)-Mo(1)-O(2) and O(1)-P(1)-P(2)-O(2) is 24.0(6)°. With respect to the TTF core, all distances and angles are within normal ranges for the *o*-P2 unit, while the angles between the plane S(1)-S(2)-C(3)-C(4)-S(3)-S(4) and the planes defined as S(1)-C(2)-C(1)-S(1) and S(3)-C(5)-C(6)-S(4) are 28.7(4)° and 7.4(9)°, respectively. The larger of the two bends follows the trend observed for other M(o-P2) complexes such as $[Rh(o\text{-}P2)_2][BF_4]_2$, $[Ni(o\text{-}P2)_2][BF_4]_2$ (**8**), $[Pt(o\text{-}P2)_2][BF_4]_2$ (**11**), $[ReCl_2(o\text{-}P2)_2]^+$ (**16**), and $[Re_2Cl_6(o\text{-}P2)]^-$ (**17**), where the bend occurs at the sulfur positions closest to the phosphines.

(3) Spectrocscopic Characterization of $MoCl_2O_2(o\text{-}P2O_2)$ (19)

The ^1H NMR spectrum of the green solid obtained from the reaction of $Mo_2[S(CH_3)_2]_4Cl_4$ with *o*-P2 in acetonitrile shows resonances due to dimethyl sulfide and free *o*-P2. The singlet at 2.15 ppm is indicative of the methyl protons of bound dimethyl sulfide. Resonances at δ = 1.85 and 7.37 ppm are

due to the methyl and phenyl protons of the *o*-P2 ligand. The resonance at 1.95 ppm suggests the presence of an acetonitrile containing product, with fast exchange occurring with the deuterated solvent. The $^{31}P\{^{1}H\}$ NMR spectrum displays only a single signal, at -17.6, due to free *o*-P2. The presence of a band at 600 nm in the electronic absorption spectrum supports the presence of $Mo_2Cl_4(NCCH_3)_4$. Due to the close proximity of the characteristic absorption bands of the $\delta \rightarrow \delta^*$ transitions of $Mo_2Cl_4[S(CH_3)_2]_4$ (595 nm) and $Mo_2Cl_4(NCCH_3)_4$, (602 nm) it is not surprising that only a single broad band is observed. Such a conversion to the solvated complex should not be unexpected given the published synthesis of $Mo_2Cl_4(NCCH_3)_4$ involves the reaction of $Mo_2Cl_4[S(CH_3)_2]_4$ with acetonitrile at ambient conditions for 12 hours.[17]

Analysis of the brown solution obtained from the same reaction revealed very different results. The ^{1}H NMR spectrum displays resonances at 1.81, 1.84, and 2.13, with several broad signals between 7.2 and 7.6 ppm. The set of broad resonances at lower fields can be assigned to the phenyl protons of the *o*-P2 ligand. Likewise, the upfield resonances at 1.81 and 1.84 ppm are most likely due to two different environments for the methyl protons of *o*-P2. The resonance at 2.13 ppm can be assigned to the methyl protons of unreacted SMe_2 containing starting material. The $^{31}P\{^{1}H\}$ NMR spectrum indicates the presence of at least two different environments of bound phosphine. The resonance at 40.7 ppm is downfield shifted from the free

ligand by 59 ppm. This value is within the range observed for other Mo-P complexes, and is characteristic of five-membered rings formed by chelating phosphines.[41a] The other set of signals occurs further upfield as two sets of doublets centered at -1.39 ppm. A pattern such as this indicates two different phosphorus environments with P_A-P_B coupling. Assuming the two signals centered at -0.64 result from P_A coupling to P_B, and the signals centered at -2.71 ppm represent the coupling of P_B with P_A, the coupling constants are $^1J_{PA\text{-}PB}$ = 17.1 Hz, and $^1J_{PA\text{-}PB}$ = 19.5 Hz. If the pattern is viewed as two overlapping doublets, with the outer two (-0.57 and -2.63 ppm) signals originating from P_A, and the inner two signals (-0.71 and -2.80 ppm) originating from P_B, the coupling constants are $^1J_{PA\text{-}PB}$ = 249.4 Hz, and $^1J_{PA\text{-}PB}$ = 251.8 Hz. While neither calculation provides P_A-P_B coupling constants that are identical, the first interpretation is consistent with what is expected for *cis*-oriented phosphines.[48] The latter pattern produces coupling patterns which are to large for *cis*-oriented phosphines, are more characteristic of *trans*-oriented. Because of this ambiguity, a coordination mode cannot yet be assigned. The small downfield shift from the free ligand at -18.7 ppm,[8a] indicates that the phosphorus nuclei may not be directly bound to the metal but that they may be separated by a third atom as in the case of **19**. Another possibility is that they are not interacting with the metal at all.

The NMR spectra from the reaction with CH_2Cl_2 as the solvent display similar results. Reaction of $Mo_2[S(CH_3)_2]_4Cl_4$ with *o*-P2 in CH_2Cl_2 under

anaerobic conditions produced a green-brown precipitate and a brown solution. A ^{1}H NMR of the solid obtained from this brown solution contains resonances in two regions of the spectrum. The singlet at 1.85 ppm results from the methyl protons of the TTF ligand, while the broad set of signals between 6.9 and 7.3 ppm are due to the phenyl protons. The resonance occurring at 40.0 ppm in the $^{31}P\{^{1}H\}$ NMR spectrum is indicative of metal-bound phosphine, and is equivalent to the resonance observed in the spectrum of the brown solution from the reaction with acetonitrile. Addition of CH_2Cl_2 to the green solid eventually leads to this same brown solution as evidenced by ^{1}H and $^{31}P\{^{1}H\}$ NMR spectroscopy.

4. Concluding Remarks

Reactions of phosphine-fuctionalized tetrathiafulvalenes with metal-metal bonded complexes occur by several different reaction pathways, depending on the redox properties of the metal-containing complex, the solvent system, and the general reaction conditions. The TTF functionality is capable of reducing transition metals to mixed valence complexes, and effecting non-redox metal-metal bond cleavage. Although the backbone of the *o*-P2 ligand is similar to ligands such as dppbe and dppee, the β-bridging mode of *o*-P2 has not yet been observed. The lack of a β-isomer for $Mo_2X_4(dppbe)_2$ has been attributed to the rigidity of the ligand, which leads to an inability to bridge the dinuclear unit.[42a] This is was not the case for the dinuclear rhenium complexes, as both isomers were crystallograhically determined for X = Cl

and Br. Whether this same argument can be made for the expected chemistry for o-P2 remains to be seen. Reactions involving the starting material *trans*-$Mo_2Cl_4[S(CH_3)_2]_4$ may eventually provide evidence for the β-coordination mode. Given the tendency for the TTF phosphine ligands to form phosphine-oxides however, it will be necessary to study these reactions under much more stringent experimental conditions.

List of References

1. Cotton, F. A.; Hong, B. *Prog. Inorg. Chem.*, **1992**, *40*, 179.

2. Cotton, F. A.; Walton, R. A. *Multiple Bonds Between Metal Atoms, 2nd Ed.*, Clarendon Press: Oxford, **1993**, and references therein.

3. Puddephatt, R. J. *Chem. Soc. Rev.* **1983**, 99.

4. (a) Higgins, S. J.; Levanson, W. J. *J. Chem. Soc., Dalton Trans.* **1986**, 317. (b) Gray, L. R.; Higgins, S. J.; Levanson, W. J.; Webster, M. J. *J. Chem. Soc., Dalton Trans.* **1984**, 1433. (c) Fox, M. A.; Chaudler, D. A. *NATO ASI Ser. C.* **1987**, *214*, 405. (d) Gray, L. R.; Gulliver, D. J.; Levanson, W. J.; Webster, M. J. *J. Chem. Soc., Dalton Trans.* **1983**, 133. (e) Warren, L. F.; Bennett, M. A. *Inorg. Chem.* **1976**, *15*, 3126.

5. (a) Mahadevan, C.; Seshasayee, M.; Ramakrishna, B. L.; Manoharon, P. T. *Acta Crystallogr., Sect. C* **1985**, *41*, 38. (b) Bennett, M. A.; Robertson, G. B.; Rosalky, J. M.; Warren, L. F. *ActaCrystallogr. Sect. A* **1975**, *31*, S136.

6. (a) Campbell, F. L., III.; Cotton, F. A.; Powell, G. L. *Inorg. Chem.* **1984**, *23*, 4222. (b) Cotton, F. A.; Dunbar, K. R.; Poli, R. *Inorg. Chem.* **1986**, *25*, 3700. (c) Campbell, F. L., III.; Cotton, F. A.; Powell, G. L. *Inorg. Chem.* **1985**, *24*, 4384. (d) Cotton, F. A.; Dunbar, K. R.; Matusz, M. *Inorg. Chem.* **1986**, *25*, 3641.

7. (a) Agaskar, P. A.; Cotton, F. A.; Derringer, D. R.; Powell, G. L.; Root, D. R.; Smith, T. J. *Inorg. Chem.* **1985**, *24*, 2786. (b) Agaskar, P. A.; Cotton, F. A.; *Inorg. Chem.* **1986**, *25*, 15.

8. (a) Fourmigué, M.; Batail, P. *Bull. Soc. Chim. Fr.* **1992**, *129*, 829. (b) Fourmigué, M.; Uzelmeier, C. E.; Boubekeur, K.; Bartley, S. L.; Dunbar, K. R. *J. Organomet. Chem.*, **1997**, *529*, 343.

9. Dunbar, K. R. *J. Cluster Science* **1994**, *5*, 125-146.

10. (a) Nocera, D. G.; Gray, H. B. *J. Am. Chem. Soc.*, **1981**, *103*, 7349. (b) Nocera, D. G.; Gray, H. B. *Inorg. Chem.*, **1984**, *23*, 3686. (c) Trogler, W. C.; Erwin, G. L.; Geoffroy, G. L.; Gray, H. B. *J. Am. Chem. Soc.*, **1978**, *100*, 1160. (d) Chang, I.-J.; Nocera, D. G. *J. Am. Chem. Soc.*, **1987**, *109*, 4901. (e) Chang, I.-J.; Nocera, D. G. *Inorg. Chem.*, **1989**, *28*, 4309. (f) Partigianoni, C. M.; Chang, I.-J.; Nocera, D. G.

Coord. Chem. Rev., **1990**, *97*, 105. (g) Partigianoni, C. M.; Nocera, D. G. *Inorg. Chem.*, **1990**, *29*, 2033.

11. Matsubayashi, G.; Yokoyama, K.; Tanaka, T., *J. Chem. Soc. Dalton Trans.*, **1988**, 3060.

12. Munakata, M.; Kuroda-Sowa, T.; Masahiko, M.; Hirota, A; Kitagawa, S., *Inorg. Chem.*, **1995**, *34*, 2705.

13. Bousseau, M.; Valade, L.; Legros, J-P.; Cassoux, P; Garbauskas, M.; Interrante, L. V., *J. Am. Chem. Soc.*, **1986**, *108*, 1908.

14. (a) Dunbar, K. R. *J. Am. Chem. Soc.*, **1988**, *110*, 8247. (b) Dunbar, K. R.; Pence, L. E., *Inorg. Synth.* **1992**, *29*, 182.

15. Bernstein, S. N.; Dunbar, K.R., *Angew. Chem. Int. Ed. Engl.*, **1992**, *31*, 1360.

16. (a) Barder, T. J.; Walton, R. A. *Inorg. Chem.*, **1982**, *21*, 2510. (b) Barder, T. J.; Walton, R. A. *Inorg. Synth.*, **1985**, *23*, 116.

17. San Filippo, Jr., J.; Sniadoch, H. J.; Grayson, R. L., *Inorg. Chem.*, **1974**, *13*, 2121.

18. SHELXTL v. 5., G. M. Sheldrick and Siemens Analytical X-Ray Systems, Inc., **1995**, 6300 Enterprise Lane, Madison WI. 53719.

19. MITHRIL: Integrated Direct Methods Computer Program, Gilmore, C. J. *J. Appl. Cryst.* **1984**, *17*, 42.

20. Sheldrick, G.M. SHELXL93. Program for the Refinement of Crystal Structures. University of Gottingen, Germany, **1993**.

21. SHELXTL v. 5.04, G. M. Sheldrick and Siemens Analytical X-Ray Systems, Inc., **1997**, 6300 Enterprise Lane, Madison WI. 53719.

22. Finniss, G.M.; Canadell, E.; Campana, C.; Dunbar, K. R., *Angew. Chem. Int. ed. Engl.*, **1996**, *35*, 2771.

23. Clérac, R. Ph. D. Dissertation, Université Bordeaux, I., **1997**.

24. Torance, J. B.; Scott, B. A.; Weller, B.; Kaufman, F. B.; Seiden, P. E., *Phys. Rev. B.*, **1979**, *19*, 730.

25. Finniss, G.M.; Campagna, C.; Dunbar, K. R. manuscript in preparation.

26. Esjornson, D.; Bakir, M.; Fanwick P. E.; Jones, K. S.; Walton, R. A. *Inorg. Chem.*, **1990**, *29*, 2055.

27. Bakir, M.; Fanwick, P. E.; Walton, R. A. *Polyhedron*, **1987**, *6*, 907.

28. (a) Jaecker, J. A.; Murtha, D. P.; Walton, R. A. *Inorg. Chim. Acta.*, **1975**, *13*, 21. (c) Barder, T. J.; Cotton, F. A.; Lewis, D.; Schwoltzer, W.; Tetrick, S. M.; Walton, R. A. *J. Am. Chem. Soc.*, **1984**, *106*, 2882. (d) Cotton, F. A.; Daniels, L. M., *Inorg. Chim. Acta.*, **1988**, *142*, 255.

29. Anderson, L. B.; Bakir, M.; Walton, R. A. *Polyhedron*, **1987**, *6*, 1483.

30. (a) Bennett, M. J.; Cotton, F. A.; Walton, R. A. *J. Am. Chem. Soc.*, **1966**, *88*, 3 866. (b) Bennett, M. J.; Cotton, F. A.; Walton, R. A. *Proc. R. Soc., London*, **1968**, *A303*, 175.

31. Uzelmeier, C. E.; Fourmigué, M.; Grandinetti, G.; Dunbar, K. R. manuscript in peparation.

32. (a) Cotton, F. A.; Dunbar, K. R.; Falvello, L. R.; Tomas, M.; Walton, R. A. *J. Am. Chem. Soc.*, **1983**, *105*, 206. (b) Cotton, F. A.; Jennings, J. G.; Price, A. C.; Vidyasager, K. *Inorg. Chem.*, **1990**, *29*, 4138.

33. Cotton, F. A.; Frenz, B. A.; Stults, B. R.; Webb, T. R. *J. Am. Chem. Soc.* **1976**, *98*, 2768.

34. (a) Heyen, B. J.; Powell,G. L., *Polyhedron*, **1988**, *7*, 1207. (b) Heyen, B. J.; Jennings, J. G.; Powell, G. L., *Inorg. Chim. Acta.*, **1995**, *229*, 241.

35. Carlin, R. L.; *Magnetochemistry*, Springer: New York, **1986**.

36. Gunz, H. P.; Leigh, G. J. *J. Chem. Soc.*, **1971**, 2229.

37. Prater, M. E.; Dunbar, K. R. unpublished results.

38. Costello, M. T.; Derringer, D. R.; Fanwick, P. E.; Price, A. C.; Rivera, M. I.; Scheiber, E.; Siurek, III, E. W.; Walton, R. A., *Polyhedron*, **1990**, *9*, 573.

39. Cotton, F. A.; Price, A. C.; Vidyasagar, K. *Inorg. Chem.* **1990**, *29*, 5143.

40. Figis, B. N.; Lewis, J. *Progr.Inorg. Chem.*, **1965**, *6*, 37.

41. Bakir, M.; Cotton, F. A.; Falvello, L. R.; Simpson, C. Q.; Walton, R. A., *Inorg. Chem.*, **1988**, *27*, 4197.

42. (a) Bakir, M.; Cotton, F. A.; Cudahy, M.M.; Simpson, C. Q.; Smith, T. J.; Vogel, E. F.; Walton, R. A., *Inorg. Chem.*, **1988**, *27*, 2608. (b) Cotton, F. A.; Kitigawa, S., *Inorg. Chem.*, **1987**, *26*, 3463. (c) Cotton, F. A.; Kitagawa, S., *Polyhedron*, **1988**, *7*, 463. (d) Agaskar, P. A.; Fanwick, P. E.; Fitch, III, J. W., *Inorg. Chem.*, **1986**, *25*, 15.

43. Agaskar, P. A.; Cotton, F. A.; Deringer, D. R.; Powell, G. L.; Root, D. R.; Smith, T. J., *Inorg. Chem.*, **1985**, *24*, 2786.

44. (a) Fourmigue, M.; Jarshow, S.; Batail, P., *Phosphorus, Sulfur, and Silicon*, **1993**, *75*, 175. (b) Asara, J. M.; Uzelmeier, C. E.; Dunbar, K. R.; Allison, J., submitted to *Inorg. Chem.*, **1997**.

45. Herbowski, A; Lis, T.; Deutsch, E. A., *J. Organomet. Chem.*, **1993**, *460*, 25.

46. (a) Florian, L. R.; Corey, E. R., *Inorg. Chem.*, **1968**, *7*, 723. (b) Cotton, F. A.; Morehouse, S. M.; Wood, J. S., *Inorg. Chem.*, **1964**, *3*, 1603. (c) Cotton, F. A.; Wing, R. M., *Inorg. Chem.*, **1965**, *4*, 872. (d) Atovmyan, L. O.; Krasochka, O. N., *J. Chem. Soc., Chem. Commun.*, **1969**, *12*, 649.

47. Brencic, J. V.; Segedin, P., *Inorg. Chim. Acta*, **1978**, *29*, L281.

48. Pregosin, P. S.; Venanzi, L. M., *Chem. Br.*, **1978**, *14*, 276.

CHAPTER V

STEP-WISE SYNTHESIS OF METAL CONTAINING ARRAYS WITH BI- AND TETRADENTATE TETRATHIAFULVALENE-PHOSPHINE LIGANDS

1. Introduction

Our successful synthesis and isolation of the series $[M(o\text{-}P2)_2][BF_4]_2$ (M = Fe, Co, Ni, Pd, Pt) and $[Rh(o\text{-}P2)_2][BF_4]$ described in Chapter 2 illustrates the feasibility of incorporating TTF into transition metal complexes through the use of phosphine groups. Molecules such as these serve as models for high molecular weight arrays that contain the tetradentate ligand P4 (**2**).[1] In this vein, recent work by Fox and coworkers demonstrated that mononuclear complexes of the type $[MCl(dppb)_2][Cl]$ (M = Ni, Pd) could be used as models for the synthesis of coordination polymers with tetra(diphenylphosphino)benzene (tppb).[2] The incorporation of TTF rather than benzene as a substituent in such extended structures is an attractive alternative due to its redox activity. As a backdrop for the proposed studies it is important to note that functionalized TTF ligands have been used to bridge mononuclear metal centers in several instances. For example, McCullough and co-workers used the tetrathiolate ligand $[TTFS_4]^{4-}$ as a bridging ligand between mononuclear $[TiCp_2]^{2+}$, $[TiCp^*_2]^{2+}$, and $[Pt(PPh_3)_2]^{2+}$ groups.[5] In related work, Munakata *et. al.* demonstrated that tetrakis(ethylthio)tetrathia-fulvalene $[(EtS)_4TTF]$, can act as a bridging ligand between two CuX_2 (X = Cl, Br) centers to give one- and two-dimensional polymers.[6]

The rational design of arrays based on molecular precursors can be achieved by a variety of methods, the simplest of which are one-step self-assembly processes and stepwise bond formation.[3] The methods described in

this chapter fall into the category of "stepwise bond formation", and are related to what has been called the use of "complexes as metals/complexes as ligands."[3a,4] In this strategy, mononuclear or polynuclear metal-containing complexes that possess labile ligands are used as the central coordination "centers"; i.e. they become the transition metal, "M", in "ML_n" complexes. Labile ligands on these "building blocks" can be removed to form species with open metal coordination sites ("complex metals") which can be ligated by other metal complexes that possess donor sites ("complex ligands").[3a] Such a stepwise method allows for good control over the shape and size of the resulting "supermolecule." An advantage of this approach is the ability to introduce specific building blocks in different steps, thereby allowing for the placement of specific moieties at precise locations in the molecule.

In this chapter we describe the stepwise build-up of extended arrays from mononuclear and dinuclear building blocks with *o*-P2 or P4 ligands. A similar method was used by Fox *et al.*, to form homo- and heterometallic oligomers using MCl_2(dppb) (M = Ni, Pd, Pt) and [Ni(dppb)(tppb)][BF_4]$_2$ as molecular building blocks.[2] Herein we report the rational synthesis of a series of Pt, Pd, and Ni oligomers with *o*-P2 and P4 ligands, with the ultimate goal being to construct high molecular weight oligomeric materials by design.

2. Experimental

A. Synthesis

Starting Materials and Reaction Procedures. *Ortho*-$[P(C_6H_5)_2]_2(CH_3)_2TTF$,[7] $[P(C_6H_5)_2]_4TTF$,[8] and $PtCl_2(NCC_6H_5)_2$[9] were prepared according to published procedures. $PdCl_2(NCC_6H_5)_2$ was purchased from Aldrich Chemical Co., and $NiCl_2 \cdot 6H_2O$ was purchased from Fisher Scientific. Both reagents were used as received. Acetonitrile and methylene chloride were distilled over 3 Å molecular sieves, and ethanol was distilled over $Mg(OMe)_2$ under a nitrogen atmosphere. Diethyl ether was distilled over sodium-potassium/benzophenone. Unless otherwise specified, all reactions were carried out under an argon atmosphere by using standard Schlenk-line techniques.

(1) Preparation of $PtCl_2$(*o*-P2) (20)

Samples of $PtCl_2(NCC_6H_5)_2$ (0.103 g, 0.218 mmol) and *o*-P2 (0.139 g, 0.231 mmol) were loaded into separate flasks and dissolved in 5 mL of acetonitrile and dichloromethane respectively. The TTF solution was transferred into the flask containing the metal complex and stirred for 2 h, producing a color change to red. The solution volume was then reduced by one-half under reduced pressure, and copious amounts of Et_2O were added to precipitate an orange solid. The solid was washed three times with 5 mL of Et_2O and dried *in vacuo*; yield 0.147 g (78%). Single crystals were grown by slow evaporation of an acetonitrile solution of **20**. *Anal.* Calc'd for **20**,

$PtP_2S_4C_{32}H_{26}Cl_2$: C, 44.35; H, 3.02. Found: C, 45.21; H, 3.30. ^1H NMR (CD_2Cl_2) δ ppm: -CH_3, 1.90 (s); Ph-H, 7.58 (m), 7.86 (m). $^{31}P\{^1H\}$ NMR (CD_2Cl_2) δ ppm: 27.2 (s, $^1J_{Pt-P}$ = 3640 Hz). IR (Nujol, cm^{-1}): 693 (m, $\nu_{=C-H}$), 526 (s, $\nu_{C=C}$), 325 (m, ν_{Pt-Cl}), 303 (m, ν_{Pt-Cl}). C.V. (0.2 M CH_2Cl_2/$TBABF_4$, Pt electrode vs Ag/AgCl): $E_{(p,c)}$ = -0.49 V, $E_{1/2}(ox)_1$ = +0.70 V, $E_{1/2}(ox)_2$ = +1.14 V. UV/Visible (CH_3CN) λ_{max}, nm (ε, $M^{-1}cm^{-1}$): 458 ($1.6x10^3$), 315 ($2.5x10^4$), 248 ($2.8x10^4$). FAB-MS (m/z): 867 (M^+).

(2) Preparation of [Pt(*o*-P2)($NCCH_3$)$_2$][BF_4]$_2$ (21)

$PtCl_2$(*o*-P2) (**20**) (0.065 g, 0.075 mmol) and $AgBF_4$ (0.034 g, 0.175 mmol) were loaded into a 150 mL pear-shaped flask and treated with 10 mL of acetonitrile. The reaction mixture was refluxed for 2 h to give to a red solution and a white-gray precipitate. The mixture was allowed to cool, then filtered through Celite on a Shlenk-line and reduced in volume by 50% under vacuum. The red solution was treated with 30 mL of Et_2O to afford a red precipitate which was separated from the liquid, washed three times with 20 mL of Et_2O and dried *in vacuo*; yield 0.048 g (70%). ^1H NMR (CD_3CN) δ ppm: -CH_3, 1.90 (s); -$NCCH_3$, 1.96 (s), 2.18 (s); Ph-H, 7.37 (br), 7.79 (br). $^{31}P\{^1H\}$ NMR (CD_3CN) δ ppm: 28.96 (s, $^1J_{Pt-P}$ = 1646 Hz). IR (Nujol, cm^{-1}): 2327 (m, $\nu_{C\equiv N}$), 2298 (m, $\nu_{C\equiv N}$), 1053 (s, ν_{B-F}), 689 (m, $\nu_{=C-H}$).

(3) Preparation of Pt_2Cl_4(P4) (22)

P4 (**2**) (0.202 g, 0.224 mmol) and $PtCl_2(NCC_6H_5)_2$ (0.203 g, 0.430 mmol) were each dissolved separately in 5 mL of CH_2Cl_2 and the TTF solution was

added to the metal solution via cannula. After stirring for 24 h at r.t., a highly insoluble yellow-orange precipitate was collected by filtration in air, washed three times with 5 mL of Et_2O, and finally dried *in vacuo*; yield 0.256 g (81%). IR (Nujol, cm^{-1}): 1099 (s, ν_{B-F}), 688 (m, ν_{C-H}), 324 (m, ν_{Pt-Cl}), 304 (m, ν_{Pt-Cl}).

(4) Preparation of $[Pt_2(P4)(NCCH_3)_4][BF_4]_4$ (23)

Quantities of $AgBF_4$ (0.057 g, 0.293 mmol) and $Pt_2Cl_4(P4)$ (**20**) (0.102 g, 0.069 mmol) were treated with 12 mL of acetonitrile and stirred under refluxing conditions for 36 h. The mixture was allowed to cool, filtered through Celite to remove AgCl, and reduced in volume by 50%. The yellow-orange product was precipitated by the addition of Et_2O, filtered in air, washed three times with 10 mL portions of Et_2O, and dried *in vacuo*; yield 0.081 g (64%). ^1H NMR (CD_3CN) δ ppm: $NCCH_3$, 1.97 (s); Ph-H, 7.64 (br), 7.78 (br). $^{31}P\{^1H\}$ NMR (CD_3CN) δ ppm: 19.5 (s, $^1J_{Pt-P}$ = 3845 Hz), 26.3 (s, $^1J_{Pt-P}$ = 3421 Hz). IR (Nujol, cm^{-1}): 2328 (m, $\nu_{C\equiv N}$), 2286 (m, $\nu_{C\equiv N}$), 1055 (s, ν_{B-F}), 690 (m, $\nu_{=C-H}$). FAB-MS (m/z): CF_3SO_3H added, 1927 (M^+ = $[Pt_2(P4)(CF_3SO_3)_4]^+$).

(5) Preparation of $[Pt_2(P4)(o\text{-}P2)_2][BF_4]_4$ (24).

(i) Reaction of $[Pt(o\text{-}P2)(NCCH_3)_2][BF_4]_2$ (21) with P4 (2). A solution of P4 (**2**) (0.037 g, 0.039 mmol) in 5 mL of dichloromethane was added to a solution of $[Pt(o\text{-}P2)(NCCH_3)_2][BF_4]_2$ (**21**) (0.058 g, 0.055 mmol) dissolved in 10 mL of acetonitrile. The resulting solution was stirred for 12 h and reduced

to ca. one-half of its original volume by vacuum techniques. The tan product was isolated by the addition of 20 mL of Et_2O, washed repeatedly with Et_2O until the liquid was clear, and dried under reduced pressure; yield 0.059 g (75%). ^1H NMR (CD_3CN) δ ppm: -CH_3, 1.81 (s); Ph-H, 7.25 (m), 7.34 (m), 7.48 (m). $^{31}P\{^1H\}$ NMR (CD_3CN) δ ppm: 32.94 (s, $^1J_{Pt-P}$ = 2365 Hz). IR (Nujol, cm^{-1}): 1054 (ν_{B-F}), 689 ($\nu_{=C-H}$). C.V. (0.2 M CH_2Cl_2/$TBABF_4$, Pt electrode vs Ag/AgCl): $E_{(p,c)}$ = -0.89 V. UV/Visible (CH_3CN) λ_{max}, nm (ε, $M^{-1}cm^{-1}$): 248 ($1.1x10^5$), 289 sh, 345 sh, 502 ($3.5x10^3$).

(ii) Reaction of $[Pt_2(P4)(NCCH_3)_4][BF_4]_4$ (23) with *o*-P2 (1). Solid samples of $[Pt_2(P4)(NCCH_3)_4][BF_4]_4$ (**23**) (0.050 g, 0.027 mmol) and *o*-P2 (**1**) (0.036 g, 0.06 mmol) were treated with 10 mL of acetonitrile and stirred for 3 h at r.t. The resulting orange solution was decanted from any unreacted solid, reduced to 3-5 mL under reduced pressure, and treated with 20 mL of Et_2O to afford an orange precipitate. The liquid was decanted from the tan solid which was washed 3 times with 20 mL of Et_2O, and finally dried *in vacuo*; yield 0.047 g (61%). $^{31}P\{^1H\}$ NMR (CD_3CN) δ ppm: 32.94 (s, $^1J_{Pt-P}$ = 2365).

(6) Preparation of $PdCl_2$(*o*-P2) (25)

Samples of $PdCl_2(NCC_6H_5)_2$ (0.068 g, 0.178 mmol) and *o*-P2 (0.105 g, 0.175 mmol) were dissolved in 10 mL of CH_2Cl_2. The dark orange-red solution was stirred for 12 h, reduced to ~3 mL under reduced pressure, and treated with 20 mL of Et_2O to precipitate a red solid. The solid was collected

by filtration in air, washed with copious amounts of Et_2O, and dried under reduced pressure; yield 0.123 (91%). *Anal.* Calcd for **25**, $PdP_2S_4C_{32}H_{26}Cl_2$: C, 49.40; H, 3.37. Found: C, 49.86; H, 3.71. ^1H NMR ($CDCl_3$) δ ppm: -CH_3, 1.88 (s); Ph-H, 7.51 (m, 8H), 7.57 (br, 12H), 7.59 (d), 7.82 (m), 7.86 (m), 7.89 (m). $^{31}P\{^1H\}$ NMR ($CDCl_3$) δ ppm: 48.0 (s). IR (Nujol, cm^{-1}): 687 ($\nu_{=C-H}$), 515 ($\nu_{C=C}$), 324 (ν_{Pd-Cl}), 303 (ν_{Pd-Cl}). C.V. (0.2 M CH_2Cl_2/TBABF$_4$, Pt electrode vs Ag/AgCl): $E_{(p,c)}$ = -1.04 V, $E_{1/2}(ox)_1$ = +0.71 V, $E_{1/2}$ $(ox)_2$ = +1.10 V. FAB-MS (m/z): 778 (M^+).

(7) Preparation of [Pd(*o*-P2)(NCCH$_3$)$_2$][BF$_4$]$_2$ (26)

In a 100 mL Schlenk-flask covered in aluminum foil, 0.100 g of $PdCl_2$(*o*-P2) (**25**) (0.104 mmol) and 0.050 g of $AgBF_4$ (0.257 mmol) were treated with 10 mL of acetonitrile and stirred under refluxing conditions for 2 hours. The reaction mixture was allowed to cool to room temperature and the mixture was filtered through Celite to remove AgCl. The red-brown filtrate was reduced to 3-5 mL by vacuum techniques, and treated with 20 mL of Et_2O to produce a red-brown precipitate. The liquid was decanted from the solid which was washed 3 times with 20 mL of Et_2O and finally dried *in vacuo*; yield 0.090 g (90%). ^1H NMR (CD_3CN) δ ppm: -CH_3, 1.90 (s); -NCCH_3, 1.96 (s), 2.15 (s); Ph-H, 7.68 (br), 7.90 (br). $^{31}P\{^1H\}$ NMR (CD_3CN) δ ppm: 50.72 (s). IR (Nujol, cm^{-1}): 2322 ($\nu_{C\equiv N}$), 2294 ($\nu_{C\equiv N}$), 1055 (ν_{B-F}), 689 ($\nu_{=C-H}$), 513 ($\nu_{C=C}$).

(8) Preparation of Pd_2Cl_4(P4) (27)

Samples of $PdCl_2(NCC_6H_5)_2$ (0.0815 g, 0.213 mmol) and of P4 (**2**) (0.102 g, 0.109 mmol) were treated with 5 mL of CH_2Cl_2, to give a green-brown solution which was stirred for 24 h to give a brown precipitate. The solid was isolated by filtration, washed 3 times with 5 mL of Et_2O, and dried *in vacuo*; yield 0.119 g (87%). IR (Nujol, cm^{-1}): 687 (Ph), 322 (ν_{Pd-Cl}), 299 (ν_{Pd-Cl}). FAB-MS (m/z): 647 ($M^{2+}/2$).

(9) Preparation of $[Pd_2(P4)(NCCH_3)_4][BF_4]_3$ (28)

Solid samples of Pd_2Cl_4(P4) (**27**) (0.0602 g, 0.047 mmol) and $AgBF_4$ (0.0447 g, 0.230 mmol) were treated with 12 mL of CH_3CN and stirred under refluxing conditions for 36 h. The mixture was allowed to cool, concentrated to ~5 mL using vacuum techniques, and treated with 30 mL of Et_2O to afford a tan precipitate. The solid was collected by filtration in air, washed 3 times with 10 mL of Et_2O, and dried *in vacuo*; yield 0.045 g (47%). ^1H NMR (CD_3CN) δ ppm: $NCCH_3$, 1.96 (s); Ph-H, 7.62 (m), 7.77 (m). $^{31}P\{^1H\}$ NMR (CD_3CN) δ ppm: 50.9 (s). IR (Nujol, cm^{-1}): 2333 ($\nu_{C\equiv N}$), 2298 ($\nu_{C\equiv N}$), 688 ($\nu_{\doteq C-H}$). C.V. (0.2 M CH_2Cl_2/TBABF$_4$, Pt electrode vs Ag/AgCl): $E_{(p,c)}$ = -1.04, V $E_{1/2}(ox)_1$ = +0.71 V, $E_{1/2}(ox)_2$ = +1.10 V.

(10) Preparation of Ni_2Cl_4 (P4) (29)

Solutions of P4 (**2**) (0.203 g, 0.216 mmol in 7 mL of CH_2Cl_2) and $NiCl_2 \cdot 6H_2O$ (0.100 g, 0.421 mmol in 5 mL of EtOH) were gently refluxed in separate flasks. The flask containing the P4 solution was covered with

aluminum foil during the heating process to avoid light. While both solutions were still warm, the P4 solution was added to the $NiCl_2$/EtOH solution, and the mixture was refluxed for 30 min. The resulting insoluble orange solid was isolated by filtration in air, washed with *copious* amounts of Et_2O, and dried under reduced pressure; yield 0.190 g (78%). *Anal.* Calc'd for **30**, $Ni_2P_4S_4C_{54}H_{40}Cl_4$: C, 54.04; H, 3.34. Found: C, 53.45; H, 3.28. IR (Nujol, cm^{-1}): 689 (m, $\nu_{=C-H}$), 366 (m, ν_{Ni-Cl}), 338 (m, ν_{Ni-Cl}). FAB-MS (m/z): 599 ($M^{2+}/2$).

B. X-ray Crystallography

The structures of the compounds $PtCl_2$(*o*-P2) (**20**) and Pt_2Cl_4(P4) (**22**) were determined by application of general procedures that have been fully described elsewhere.[10] Crystal parameters and basic information pertaining to data collection and structure refinement are summarized in Table 14. Final full-matrix refinements on F^2 were carried out with the use of the SHELXTL version 5.0. structure solution package.[11]

(1) $PtCl_2$(*o*-P2)•CH_3CN (20•CH_3CN)

(i) Data Collection and Reduction. Single crystals of $PtCl_2$(*o*-P2)•CH_3CN (**20**•CH_3CN) were grown by slow evaporation of an acetonitrile solution of the compound. An orange parallelepiped of dimensions 0.20 x 0.20 x 0.14 mm^3 was mounted on the tip of a glass fiber and secured with epoxy. Data for **20** were collected on a Stoe IPDS diffractometer equipped with monochromated MoKα radiation at 293 ± 2 °C in a θ range of 1.9 to 25.8°.

Table 14. Summary of crystallographic data for $PtCl_2$(*o*-P2)•CH_3CN (**20**•CH_3CN) and Pt_2Cl_4(P4)•$3CH_3CN$ (**22**•$3CH_3CN$).

	20•CH_3CN	**22**•$3CH_3CN$
Formula	$PtCl_2S_4P_2NC_{34}H_{29}$	$Pt_2Cl_4S_4P_4N_2C_{58}H_{43}$
Formula weight	906.6	1586.2
Space group	C2/c	P2(1)/n
a, Å	20.667(4)	9.0311(5)
b, Å	20.008(4)	16.1894(9)
c, Å	17.017(3)	22.8868(13)
α, deg	90	90
β, deg	91.70(3)	96.1070(10)
γ, deg	90	90
V, Å^3	7033.5(24)	3327.2(3)
Z	8	4
d_{calc}, g/cm^3	1.714	1.599
μ, cm^{-1}	4.496	4.619
Temperature, °C	20 ± 2	-140 ± 2
R1[a]	0.027	0.053
wR2[b]	0.052	0.108
quality-of-fit[c]	0.886	1.055

[a] $R = \Sigma||F_o|-|F_c||/\Sigma|F_o|$, [b] $wR2 = [\Sigma w|F_o| - |F_c|)^2/\Sigma w|F_o|^2]^{1/2}$; $w = 1/\sigma^2(|F_o|)$.
[c] $\text{quality-of-fit} = [\Sigma w(|F_o| - |F_c|)^2/(N_{obs}-N_{parameter})]^{1/2}$

Initial data indicated that the crystal belonged to a monoclinic system; subsequent solution and successful refinement of the structure was carried out in the C2/c space group. Of the 27,300 reflections that were collected, 6803 were unique, and 5081 data were observed with $I > 2.00\sigma(I)$. The data were corrected for Lorentz polarization effects, and an empirical absorption correction based on azimuthal ψ-scans near $\chi = 90°$ was applied which resulted in transmission factors ranging from 0.02 to 0.05.

(ii) Structure Solution and Refinement. The structure was solved by direct methods and refined by full-matrix least squares refinement on F^2. All non-hydrogen atoms, except those associated with the solvent, were refined anisotropically. Hydrogen atoms were not included in refinement. The final refinement was based on 6803 reflections that were used to fit 400 parameters to give R1 = 0.0270 and wR2 = 0.0516. The goodness-of-fit index was 0.886, and the maximum shift in the final difference map was 0.000 Å associated with H(8C). After the last least squares cycle, the mean shift/esd was 0.000 and the highest peak in the difference Fourier map was 2.300 $e^-/Å^3$ which is associated with the metal center.

(2) Pt_2Cl_4(P4)•3CH_3CN•solvent (22•3CH_3CN)

(i) Data Collection and Reduction. Single crystals of Pt_2Cl_4(P4)•3CH_3CN (**22**•3CH_3CN) were obtained by loading a three-compartment, fritted, electrochemical cell with an acetonitrile solution of $PtCl_2(NCC_6H_5)_2$ in one outer chamber, an acetonitile solution of P4 in the second outer chamber

and acetonitrile in the center chamber. Over the period of 2 days, orange crystals formed in the center chamber and in the P4 chamber as the solutions diffused together. An orange needle of dimensions 0.44 x 0.30 x 0.21 mm^3 was immersed in perfluorinated ether, supplied by Prof. Larry Dahl of the University of Wisconsin, and secured on to the tip of a glass fiber. Data for **22** was collected on a Siemens SMART/CCD area detector diffractometer equipped with monochromated MoKα (λ_α = 0.71073) radiation. Initial data indicated that the crystal belonged to a monoclinic system; subsequent solution and successful refinement of the structure was carried out in the $P2_1/n$ space group. The data were collected at 13 ± 2 °C in a θ range of 1.9 to 25.8°. Of the 19,855 reflections that were collected, 7,711 were determined to be unique, and 5,923 data were observed with $I > 2.00\sigma(I)$. The data were corrected for Lorentz polarization effects and an empirical absorption correction based on azimuthal ψ-scans near $\chi = 90°$ was applied.

(ii) Structure Solution and Refinement. The structure was solved by direct methods and refined by full-matrix least squares refinement. The position of the unique Pt atom was located by the XS program in SHELXTL,[11] and the remaining non-hydrogen atoms were located by a series of alternating least-squares refinements on F^2. All other non-hydrogen atoms were refined anisotropically, with the exception of the solvent molecules. The solvent atoms defined by atoms C(80), C(81), N(82), C(91), and C(92) were defined as two disordered acetonitrile molecules

sharing a common nitrogen position; these were refined with a combined occupancy of 1.0. Hydrogen atoms were placed in calculated positions. The current refinement is based on 7,711 reflections that are being used to fit 318 parameters to give R1 = 0.0532 and wR2 = 0.1081. The goodness-of-fit index is 1.098, and the maximum shift in the final difference map is currently 0.138 Å associated with N(91). The highest peak in the difference Fourier map is 1.822 $e^-/Å^3$ which is associated with the metal center, Pt(1).

3. Results and Discussion

The mononuclear complexes $PdCl_2$(*o*-P2) and $PtCl_2$(*o*-P2) were prepared in relatively high yields from the reaction of *o*-P2 (**1**) with complexes of the type $MCl_2(NCC_6H_5)_2$ (M = Pt (**20**), Pd (**25**)). Both compounds exhibit redox chemistry involving the divalent metal center as well as the TTF group. Infrared and UV-visible spectroscopies verify the presence of bound chloride ion and the presence of a single *o*-P2 ligand. The reaction of two equivalents of $MCl_2(NCC_6H_5)_2$ with P4 (**2**) in CH_2Cl_2 or acetonitrile affords the insoluble products M_2Cl_4(P4) (M = Pt (**22**), Pd (**27**)). Infrared spectral analysis of **22** and **27** verify the presence of bound chloride ions and the presence of P4. The analogous dinuclear complex of Ni can be obtained under refluxing conditions from the reaction of a dichloromethane solution of **2** and an ethanol solution of $NiCl_2 \cdot 6H_2O$.

Reactions of **20**, **22**, **25**, and **27** with stoichiometric amounts of $AgBF_4$ lead to the precipitation of AgCl and the formation of soluble TTF-containing

products. The complexes $[M(NCCH_3)_2)(o\text{-}P2)][BF_4]_2$ [M = Pt (**21**), Pd (**26**)] and $[M_2(NCCH_3)_4(P4)][BF_4]_4$ [M = Pt (**23**), Pd (**28**)] were characterized by ^1H NMR, $^{31}P\{^1H\}$ NMR, and infrared spectroscopies. Subsequent reactions of two equivalents of **21** with P4 (**2**) or two equivalents of *o*-P2 (**1**) with **23** result in the formation of the dinuclear complex $[Pt_2(o\text{-}P2)_2(P4)][BF_4]_4$ (**24**).

The structures of $PtCl_2(o\text{-}P2)$ (**20**) and $Pt_2Cl_4(P4)$ (**22**) were determined by single crystal X-ray diffraction methods. Crystal parameters and basic information pertaining to data collection and structure refinement are summarized in Table 14. Selected bond distances and angles for each structure are listed in Table 17.

A. Preparation, Spectroscopy, and Redox Properties of MCl_2(*o*-P2) (M = Pt (20), Pd (25))

(1) Synthesis

The reaction of $MCl_2(NCC_6H_5)_2$ (M = Pt (**21**), Pd (**26**)) with o-P2 (**1**) results in the formation of the red complex $MCl_2(o\text{-}P2)$. The reaction is performed with both reactants dissolved in CH_2Cl_2 in the case of **25**, and with a CH_3CN solution of the metal precursor and a CH_2Cl_2 solution of **1** in the case of **20**. Displacement of benzonitrile for **1** is relatively sluggish, and the reaction requires longer reaction times to ensure complete substitution. These reaction procedures deviate from the typical method used to form MX_2(L-L) (M = Pt, Pd; L-L = dppee, dppb, dppe) compounds which usually involves the use of $[MX_4]^{2-}$. The presence of two labile ligands allows for the

clean synthesis of the desired product, MCl_2(L-L), without the formation of $[M^{II}(L\text{-}L)_2]^{n+}$ which often occurs if one begins with the tetrachloride.[2,14-16]

Both compounds are air stable and relatively insensitive to light in the solid state, but in solution they are prone to decomposition if exposed to light for extended periods of time (> 3 days). Such photochemical sensitivity has been documented for numerous complexes of both metals.[12] The decomposition of these compounds is accelerated in the presence of chlorinated solvents, most likely owing to the instability of the phosphine ligand.[13] Both complexes are soluble in nitriles, chlorinated solvents, and acetone.

(2) ^{1}H and ^{31}P{^{1}H} NMR Spectroscopic Studies

The ^{1}H NMR spectra of **20** and **25** in $CDCl_3$ exhibit a series of multiplets in the region δ 7.5 - 7.9 ppm due to the phenyl protons, and a singlet at δ ~1.9 ppm due to the methyl protons. The ^{31}P{^{1}H} NMR spectrum of **20** shows a Pt satellite doublet centered at 27.2 ppm ($^1J_{Pt\text{-}P}$ = 3640 Hz), in accord with magnetically equivalent phosphorus nuclei. The downfield shift of the signal from the free phosphine at -18.8 ppm[7] indicates that the phosphine is coordinated to the metal whereas the $J_{Pt\text{-}P}$ value is indicative of *trans*-disposed chlorides.[16b] Similar ^{31}P{^{1}H} NMR data were obtained for **25**, which exhibits only a single resonance at δ +48.0 ppm. These shifts are comparable to the reported values for other MCl_2(L-L) complexes of palladium and platinum where L-L is a diphosphine chelate.[16,17b] The

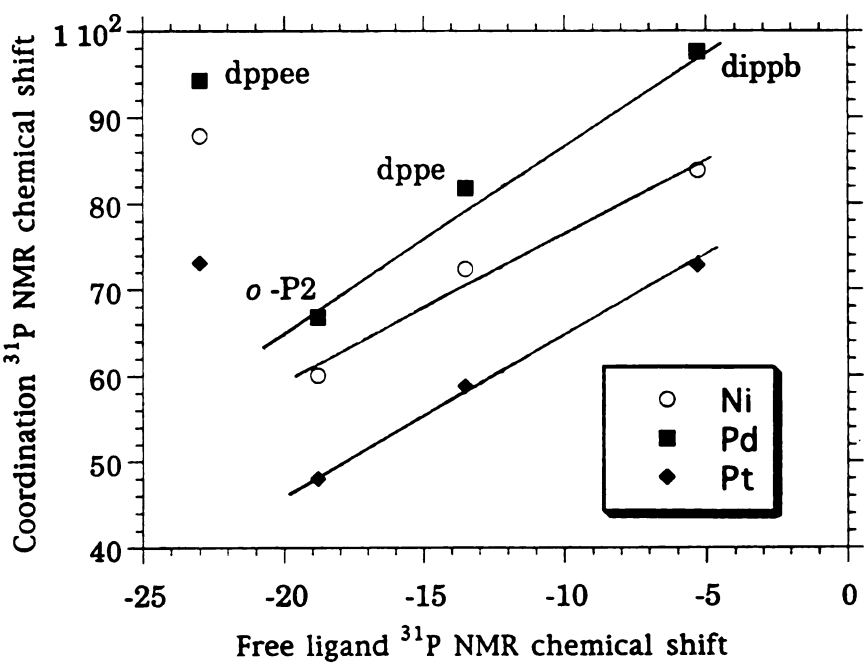

Figure 35. Correlation of ^{31}P NMR coordination chemical shift $\Delta\delta^{31}P$ in $MCl_2(L\text{-}L)$ (M = Ni, Pd, Pt) complexes with the free ligand ^{31}P NMR chemical shift $\delta^{31}P$.

increase in $\Delta\delta^{31}P$ [where $\Delta\delta^{31}P = \delta^{31}P(complex) - \delta^{31}P(ligand)$] for the series $PtCl_2$(*o*-P2) (**20**), $NiCl_2$(*o*-P2),[7] and $PdCl_2$(*o*-P2) (**25**) follows the previously observed trend for the chemical shifts of the compounds MCl_2(L-L) (M = Ni, Pd, Pt; L-L = dppe, dippb,[17] dppee[16]). A plot of the $\delta^{31}P$ chemical shifts of the free ligands against $\Delta\delta^{31}P$ for the MCl_2(L-L) series that includes *o*-P2 (**1**) reveals a linear relationship for **1**, dippb, and dppe (Figure 35). The rigidity of the ligand is thought to be the origin of the anomalous ^{31}P NMR chemical shifts for the dppee series of compounds.[16b]

(3) Infrared and Electronic Absorbance Spectroscopy

The infrared spectra of **20** and **25** display bands at ca. 690 and 520 cm^{-1} attributable to the ligand, **1**. Modes at 300 and 320 cm^{-1} are in the rangeexpected for the $A_1 + B_1$ $\nu_{M\text{-}Cl}$ stretching vibration, and agree well with literature values for other square-planar complexes with chelating ligands.[14] The electronic spectrum of **20** recorded in acetonitrile exhibits absorbances attributable to the phenyl groups at 248 nm and the TTF moiety at 315 and 428 nm. The extinction coefficient, ε, for the phenyl chromophores in TTF-phosphines is known to be approximately proportional to the number of phenyl groups in the molecule, thus the ε value of $2.8x10^4$ is indicative of one *o*-P2 (**1**) ligand (4 phenyl groups).[7] The bathochromic shift for each TTF absorption band in $PtCl_2$(*o*-P2) (**20**) relative to TTF indicates a weak interaction with the phosphine, while the shift from **1** indicates strong metal-phosphorus coordination, which serves to weaken the TTF-PR_2 interaction.

Table 15. Summary of ^{1}H and ^{31}P NMR spectrosopic data for compounds **20-20**.

compound	^{1}H NMR spectra,[a] ppm	^{31}P NMR spectra,[b] ppm	$^{31}P\{^{1}H\}$ NMR coupling constants, Hz
20, $PtCl_2(o\text{-}P2)_2$	1.90 (s, 6H), 7.58 (m, 13H), 7.86 (m, 7H)	27.2 (d)	$^{1}J_{Pt\text{-}P} = 3640$
21, $[Pt(o\text{-}P2)(NCCH_3)_2][BF_4]_2$	1.90 (s), 1.96 (s), 2.18 (s), 7.37 (br), 7.79 (br)	28.96 (d)	$^{1}J_{Pt\text{-}P} = 1646$
22, $Pt_2Cl_4(P4)$	none measured	none measured	none measured
23, $[Pt_2(P4)(NCCH_3)_4][BF_4]_4$	1.97 (s,), 7.64 (br), 0.78 (br)	19.5 (d)	$^{1}J_{Pt\text{-}P} = 3421$
		26.3 (d)	$^{1}J_{Pt\text{-}P} = 3845$
24, $[Pt_2(o\text{-}P2)_2(P4)][BF_4]_4$	1.81 (s), 7.25 (m), 7.34 (m), 7.48 (m)	32.94 (d)	$^{1}J_{Pt\text{-}P} = 2365$
25, $PdCl_2(o\text{-}P2)$	1.88 (s), 7.51 (m, 8H), 7.57 (br, 12H), 7.59 (d), 7.82 (m), 7.86 (m), 7.89 (m)	48.0	
26, $[Pd(o\text{-}P2)(NCCH_3)_2][BF_4]_2$	1.90 (s), 1.96 (s), 2.15 (s) 7.68 (br), 7.90 (br)	50.72	
27, $Pd_2Cl_4(P4)$	none measured	none measured	
28, $[Pd_2(P4)(NCCH_3)_4][BF_4]_4$	1.96 (s), 7.62 (m), 7.77 (m)	50.9	
29, $Ni_2Cl_4(P4)$	none measured	none measured	

[a] δ in CD_3CN, br = broad, m = multiplet. [b] δ in CD_3CN, relative to 85% H_3PO_4.

Table 16. Summary of cyclic voltammetry, electronic absorbance and infrared spectroscopy data for compounds **20-29**.

Compound	Cyclic Voltammetry,[a] V vs Ag/AgCl		UV-Vis Spectra λ_{max},[c] nm (ε x 10^4)	Infrared Spectra,[d] cm^{-1}
20, $PtCl_2(o\text{-}P2)_2$	$E_{1/2}(ox)_1$ = +0.70	$E_{(p,c)}$ = -0.49	458 (.16) 315(2.5)	693 (Ar), 526 (Ar)
	$E_{1/2}(ox)_2$ = +1.14		248 (2.8)	325 ($\nu_{Pt\text{-}Cl}$), 303 ($\nu_{Pt\text{-}Cl}$)
21, $[Pt(o\text{-}P2)(NCCH_3)_2][BF_4]_2$				2327 (ν_{C+N}),2298 ($\nu_{C\equiv N}$)
				1053 ($\nu_{B\text{-}F}$), 689 (Ar)
22, $Pt_2Cl_4(P4)$				1099 ($\nu_{B\text{-}F}$), 688 (Ar)
				324 ($\nu_{Pt\text{-}Cl}$), 304 ($\nu_{Pt\text{-}Cl}$)
23, $[Pt_2(P4)(NCCH_3)_4][BF_4]_4$				2328 ($\nu_{C\equiv N}$),2286 ($\nu_{C\equiv N}$)
				1055 ($\nu_{B\text{-}F}$), 690 (Ar)
24, $[Pt_2(o\text{-}P2)_2(P4)][BF_4]_4$		$E_{(p,c)}$ = -0.89[b]	248 (11), 289sh(9)	1054 ($\nu_{B\text{-}F}$) , 689 (Ar)
			345 sh(2.8),	
			502 (.35)	
25, $PdCl_2(o\text{-}P2)$	$E_{1/2}(ox)_1$ = +0.71	$E_{(p,c)}$ = -1.04		687 (Ar), 515 (Ar)
	$E_{1/2}(ox)_2$ = +1.10			324 ($\nu_{Pd\text{-}Cl}$), 303 ($\nu_{Pd\text{-}Cl}$)
26, $[Pd(o\text{-}P2)(NCCH_3)_2][BF_4]_2$				2322 ($\nu_{C\equiv N}$),2294 ($\nu_{C\equiv N}$)
				1055 ($\nu_{B\text{-}F}$), 689 (Ar) 513 (Ar)
27, $Pd_2Cl_4(P4)$				687 (Ar), 322 ($\nu_{Pd\text{-}Cl}$) 299 ($\nu_{Pd\text{-}Cl}$)
28, $[Pd_2(P4)(NCCH_3)_4][BF_4]_4$	$E_{1/2}(ox)_1$ = +0.71	$E_{(p,c)}$ = -1.04		2333 ($\nu_{C\equiv N}$), 2298 ($\nu_{C\equiv N}$),
	$E_{1/2}(ox)_2$ = +1.10			688 (Ar)
29, $Ni_2Cl_4(P4)$				689 (Ar), 366 ($\nu_{Ni\text{-}Cl}$) 338 ($\nu_{Ni\text{-}Cl}$).

[a] Electrochemical measurements in 0.2 M $TBABF_4/CH_2Cl_2$ solution at a Pt disk electrode referenced to Ag/AgCl. [b] measurements in 0.1 M $TBABF_4/CH_3CN$. [c] CH_2Cl_2 solution. [d] Nujol, CsI plates, Ar = aromatic.

(4) Electrochemistry

A cyclic voltammogram of $PtCl_2$(*o*-P2) (**20**) exhibits two accessible reversible oxidation couples and one irreversible reduction couple. The oxidations of the *o*-P2 (**1**) ligand are shifted to higher potentials relative to the free ligand as expected. The first oxidation is shifted by +360 mV, and the second oxidation is shifted by +426 mV. These values are similar to the cyclic voltammetric data obtained for $[Pt(o\text{-}P2)_2][BF_4]_2$ (**11**). The reduction couple at -0.49 V in **20** could be a one-electron reduction to Pt(I), or a two-electron process to Pt(0). The two-electron reduction is more commonly encountered, but this process generally occurs at more negative potentials, *e.g.* -1.71 V for $PtCl_2$(dppe).[18] Given the larger bite angle of dppe versus dppb and dppee,[19] it would be expected that a change to an ethylene backbone would result in a shift to more negative potentials for the metal reduction. Electrochemical data for **25** are quite similar to **20**, with reversible oxidations attributable to the ligand occuring at +0.71 and +1.10 V, and an irreversible reduction at -1.04 V (see Figure 36). Based on previous electrochemical studies of $[Pd(dppb)_2][BF_4]_2$, which exhibits a two-electron Pd(II)-Pd(0) reduction at -0.99 V, the reduction processes in both **20** and **25** appear to be more consistent with a one-electron reduction.[19]

B. Crystal Structure of $PtCl_2$(*o*-P2) (20)

Compound **20**, whose ORTEP figure is shown in Figure 37, is a slightly distorted square planar molecule with a Pt ion ligated by *cis* chlorides and one *o*-P2 ligand. The platinum atom and its four neighbors deviate from the

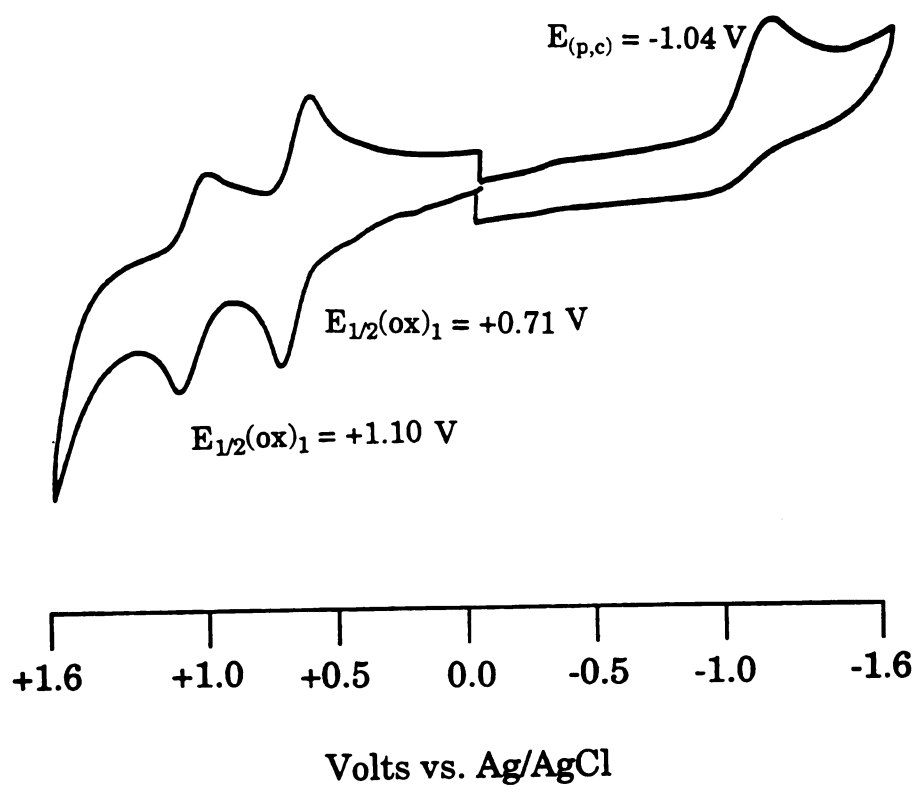

Figure 36. Cyclic voltammogram of $PdCl_2$(*o*-P2) (**25**) in 0.2 M $TBABF_4$ in CH_2Cl_2.

Table 17. Selected Bond Distances (Å) and Angles (deg) for $PtCl_2$(*o*-P2) (**20**) and Pt_2Cl_24(P4) (**22**).

Atom 1	Atom 2	20	22
Pt(1)	P(1)	2.2065(11)	2.219(2)
Pt(1)	P(2)	2.2235(11)	2.212(2)
Pt(1)	Cl(1)	2.3494(12)	2.356(2)
Pt(1)	Cl(2)	2.3476(12)	1.826(8)
P(1)	C(1)/C(2)	1.825(4)	1.312(12)
C(1)	C(2)	1.336(6)	1.757(8)
C(1)	S(1)	1.743(4)	1.321(17)
C(3)	C(4)/C(3)	1.339(6)	
C(5)	S(3)	1.755(5)	
C(5)	C(6)	1.319(7)	
C(5)	C(7)	1.505(7)	

Atom 1	Atom 2	Atom 3	20	22
P(1)	Pt(1)	P(2)	88.75(4)	88.85(8)
Cl(1)	Pt(1)	Cl(2)	90.40(4)	91.67(9)
P(1)	Pt(1)	Cl(2)/Cl(1)	176.33(4)	177.17(8)
P(1)	C(1)/C(2)	C(2)/C(1)	118.5(3)	119.3(6)
C(1)	S(1)	C(3)	94.4(2)	94.8(4)
C(4)	S(3)	C(5)	95.5(2)	
C(5)	C(6)	C(5)	128.0(5)	

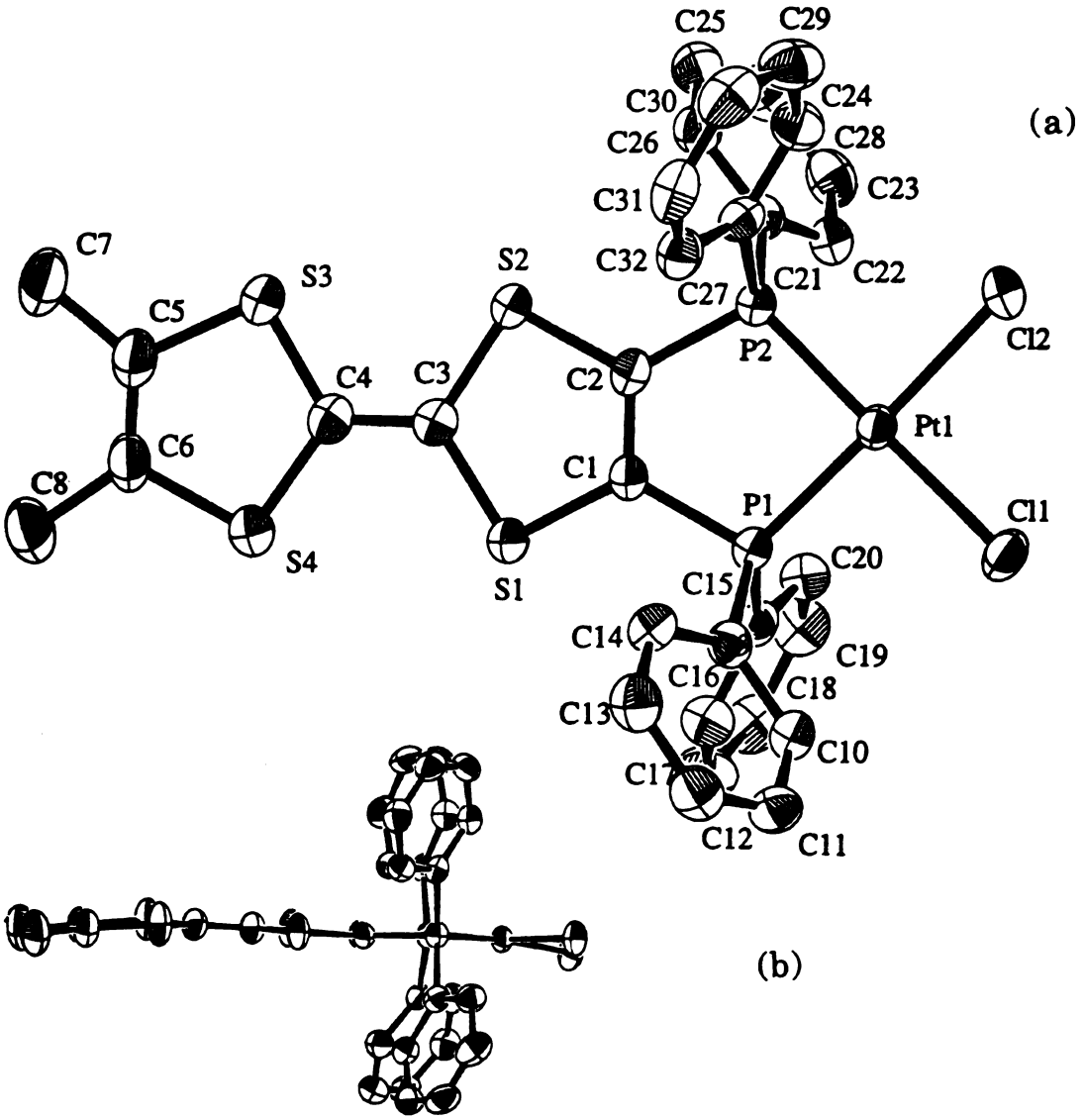

Figure 37. ORTEP representation of $PtCl_2$(*o*-P2) (**20**) with 50% ellipsoids viewed from the (a) top and (b) side.

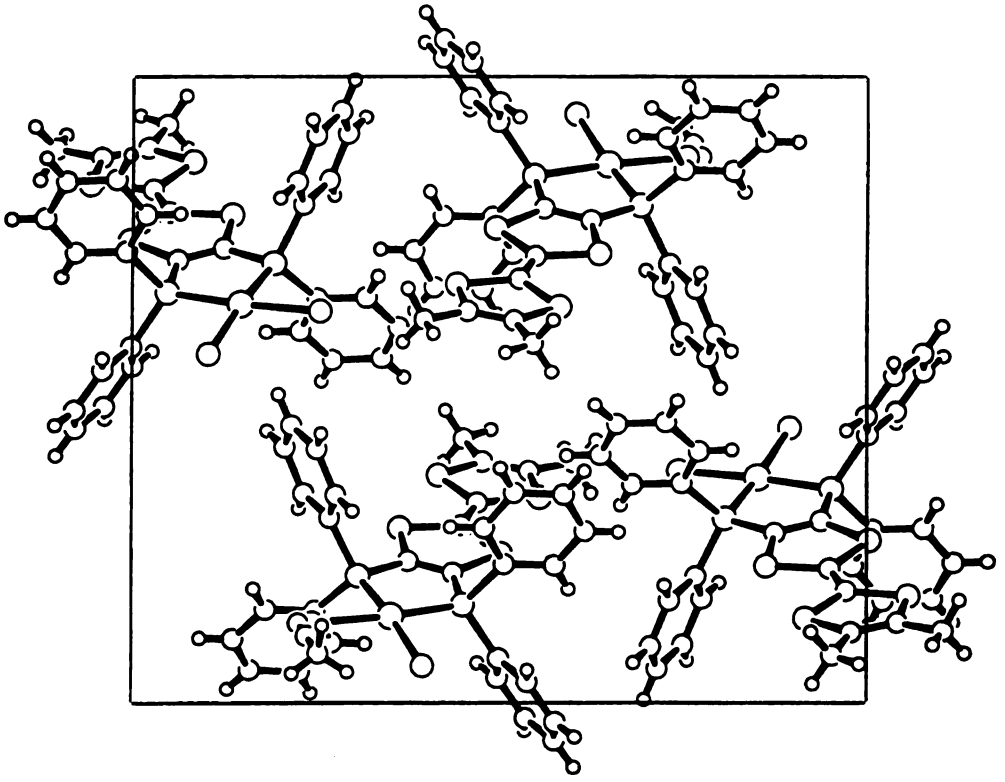

Figure 38. Packing diagram of $PtCl_2$(*o*-P2) (**20**).

best plane through the following atoms: Pt(1), 0.021(1); P(1), 0.069(1); P(2), -0.083(1); Cl(1), -0.075(1); Cl(2), 0.067(2). This results in a dihedral angle between planes P(1), P(2), Pt(1), and Cl(1), Cl(2), Pt(1) of 3.4°, which is nearly identical to the bonding arrangement observed for $NiBr_2$(*o*-P2),[7] but which differs from the planar geometry observed for $PtCl_2$(dppee),[16b] presumably due to the increased rigidity of dppee versus other di-phosphine ligands. Other angles in the molecule are within normal ranges, *e.g.* P(1)-Pt(1)-P(2) = 88.75(4)°, and Cl(1)-Pt(1)-Cl(2) = 90.40(4)°. The Pt-P bond distances of 2.2065(11) Å and 2.2235(11) Å are comparable to those found in the analogous dppee compound [2.211(2) Å], but significantly shorter than those found in $[Pt(o\text{-}P2)_2][BF_4]_2$ (**11**) (see Chapter 3). The Pt-Cl distances 2.3476(12) and 2.3494(12) Å are slightly shorter than the equivalent distances in the dppee complex 2.361(2) Å.[16b] The C(1)-C(2) double bond distance of 1.336(6) Å in **20** is similar to that in free *o*-P2 (**1**) (1.35(3) Å), and not statistically different than 1.337(6) Å, which is expected for a standard C=C double bond.[20] A shorter distance would be expected if Pt-to-P π-bonding is significant, as is the case with dppee.[16b,21] The π-bonding would also lead to complete coplanarity of Pt(1), P(1), P(2), C(1), and C(2), which is not the case for **20** (rms deviation = 0.022 Å).

The bond distances and angles within the TTF core are quite similar to those found in the Pt-(*o*-P2) complex, **11**. The largest difference is found in the C(1)-C(2) double bond distance of 1.336(6) Å for $PtCl_2$(*o*-P2) (**21**) and

1.354(14) Å for **11**. This distance is highly dependent on the identity of the metal, as can be seen from comparisons of the analogous distances in $NiBr_2$(*o*-P2) (1.25(1) Å), $[Ni(o\text{-}P2)_2][BF_4]_2$ (**8**) (1.328(12) Å) $[ReCl_2(o\text{-}P2)_2]^+$ (**16**) (1.34(2) Å average) and $[Re_2Cl_26(o\text{-}P2)]^-$ (**17**) (1.38(2) Å). Other notable differences between **20** and **11** are the wider C-S-C angles of 94.4(2)° and 94.8(2)° within the phosphine-fuctionalized ring of the TTF in **20** as compared to 92.6(4)° for the equivalent angles in **11**. Also of importance is the fact that the dithiole ring closest to the metal center is essentially planar with an out-of-plane bend of only 0.9(2)° between the planes C(1)-C(2)-S(2)-S(1) and S(1)-S(2)-C(3)-C(4)-S(3)-S(4). The methyl-substituted dithiole ring exhibits a bend of 7.3(2)° between the planes S(1)-S(2)-C(3)-C(4)-S(3)-S(4) and S(3)-S(4)-C(5)-C(6). This is quite different than the bis-(*o*-P2) complexes discussed in Chapter 3 which exhibit out-of-plane bends in the rings closest to the metal center, but which remain nearly planar at the outer dithiole ring that contains the methyl groups. The planar nature of the phosphine-fuctionalized fulvalene ring in **20** is believed to be partially due to electronic effects of the *trans*-halogens. This topic will be discussed in more detail in Chapter 6. Another obvious factor that may influence the conformation of the fulvalene rings is crystal packing forces. In $[M(o\text{-}P2)_2][BF_4]_2$ [M = Ni (**8**), Pt (**11**)] and $[Rh(o\text{-}P2)_2][BF_4]$ the tendency to form close S···S intermolecular interactions may facilitate the bending in the methyl-substituted dithiole ring.[8,22] It is obvious from the packing diagram for **20** (Figure 38), that there

are no such short intermolecular stacking interactions. The molecules of $PtCl_2$(*o*-P2) (**20**) pack in pairs, with adjacent molecules oriented in a head-to-tail fashion, a situation that serves to minimize repulsions between the phenyl rings. The closest distance between molecules is 11.08 Å.

C. Preparation and Spectroscopic Properties of M_2Cl_4(P4) [M = Pt (22), Pd (27), Ni (29)].

The reaction of two equivalents of $MCl_2(NCC_6H_5)_2$ (M = Pd, Pt) with P4 (**2**) in CH_2Cl_2, acetonitrile, or a mixture of the two solvents yields precipitates that are formulated as $Cl_2M(P4)MCl_2$. The P4 molecule is not particularly soluble in acetonitrile, thus the reaction is much slower in this solvent. The use of CH_2Cl_2 requires that the reaction be protected from light due to the instability of P4 (**2**) in chlorinated solvents over extended periods of time, and the known photochemical reactivity of Pt complexes.[12,13] The fact that the reaction appears to require one day to go to completion (shorter reaction times result in lower yields) may indicate a slow initial substitution of nitriles, but more reasonably reflects a slow coupling process to form the dimetal system.

The reaction of two equivalents of $NiCl_2 \cdot 6H_2O$ in EtOH with a CH_2Cl_2 solution of **2** at elevated temperatures results in the precipitation of $Cl_2Ni(P4)NiCl_2$ (**29**). Highest yields are obtained when the reaction is refluxed for an additional 30 min after combining the hot solutions. The hot ethanol solution increases the solubilities of $NiCl_2 \cdot 6H_2O$ and the hot CH_2Cl_2

solution of **2** prevents immediate precipitation of the reactants upon combining the respective solutions. This strategy was also used in the synthesis of NiX_2(*o*-P2) (X = Cl, Br).[7]

D. Crystal Structure of Pt_2Cl_4(P4) (22)

Compound **22**, shown in Figure 39, consists of two $PtCl_2$ fragments bridged by a P4 ligand. The geometry about the platinum centers is square planar with negligible deviations. This strictly coplanar arrangement was found for $PtCl_2$(dppee),[16b] but in **20** and $NiBr_2$(*o*-P2)[7] the molecules are slightly distorted. The P-Pt-P angles are 88.85(8)° and the Cl-Pt-Cl angles are 91.67(9)°. The *trans* relationships are P(1)-Pt(1)-Cl(1) = 177.17(8)°, and P(2)-Pt(1)-Cl(2) = 179.65(8)°. These metric parameters indicate a more ideal arrangement than that observed in either **11** or $PtCl_2$(*o*-P2) (**20**). The Pt-Cl distances (2.356(2) Å) are in the expected range, and are similar to analogous distances found in **20**. The Pt-P distances of Pt_2Cl_4(P4) (**22**) are also similar to those observed in **20**, but slightly longer than those in **11** presumably due to the different *trans*-influence of chlorides versus phosphines. The C(1)-C(2) distance of 1.312(17) Å is much shorter than the equivalent distance in both **11** and **20** as well as the free ligand **2**. This distance is also shorter than an idealized C=C double bond (1.337(6) Å),[20] but longer than the analogous bonds in $NiBr_2$(*o*-P2) and $PtCl_2$(dppee).[7,16b] This contraction of the bridging double bond suggests some degree of Pt-P π- bonding enhancement, which is

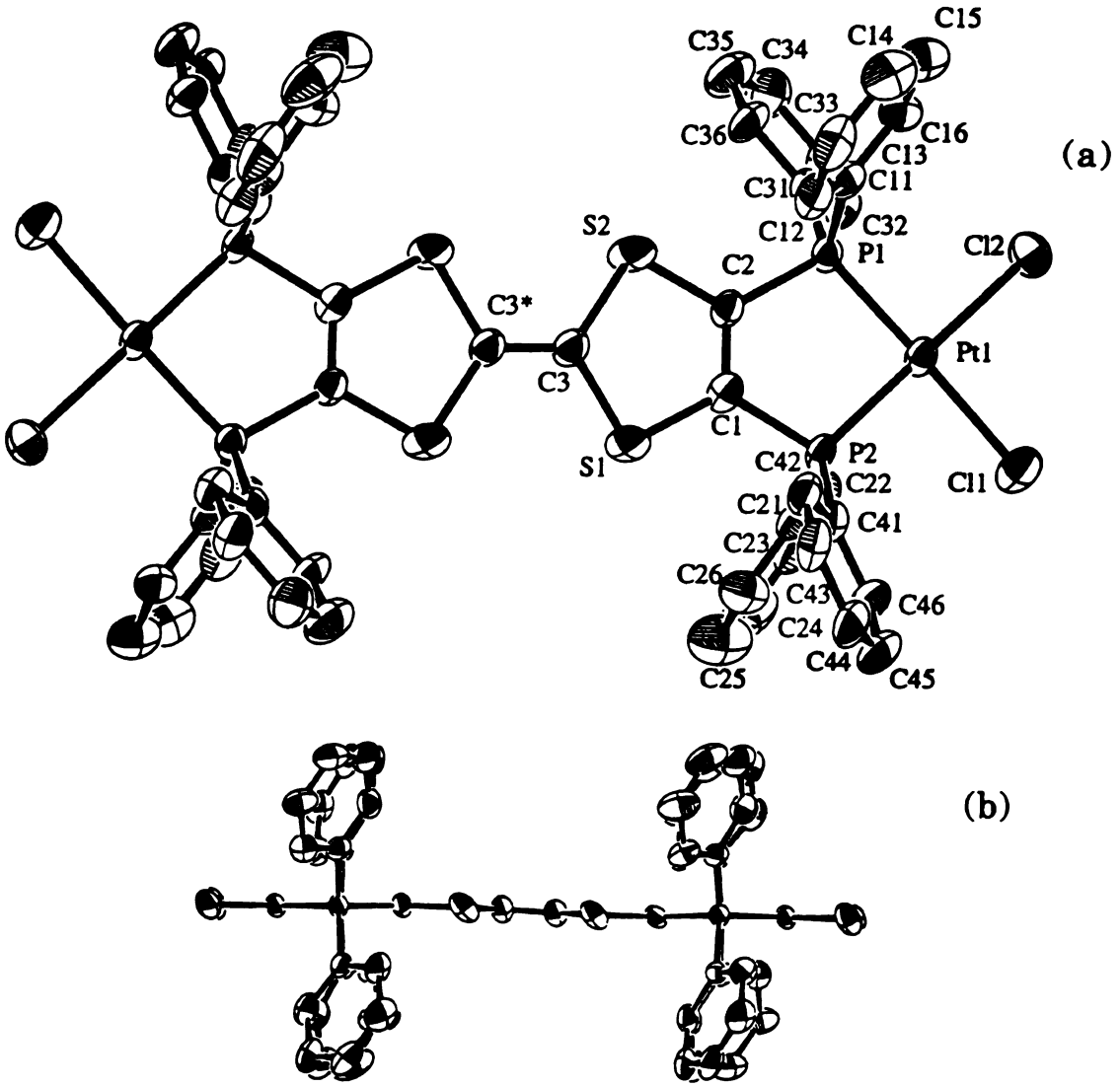

Figure 39. ORTEP representation of Pt_2Cl_4(P4) (**22**) with 50% ellipsoids viewed from the (a) top and (b) side.

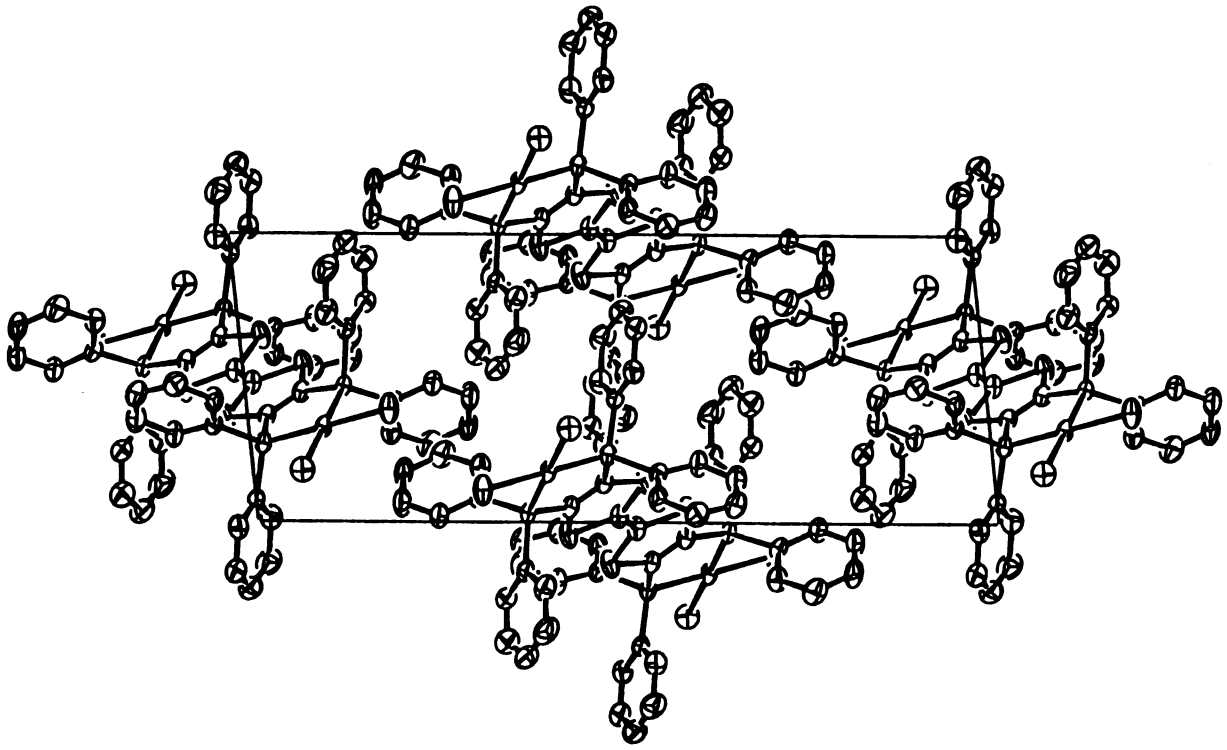

Figure 40. Packing diagram of Pt_2Cl_4(P4) (**22**) viewed down the a-axis.

supported by the coplanarity of the atoms involved (Pt(1), P(1), C(1), C(2), P(2)).[16b]

Bond distances and angles within the TTF core of **22** are similar to those observed for other TTF molecules. The S-C-S bond angles (94.8(4) and 95.0(4)°) are nearly identical to the equivalent bonds in the phosphine-fuctionalized ring of **20**. The C(3)-C(3)' double bond distance is slightly shorter, at 1.321(17) Å, than the analogous distances in **11** (1.338(13) Å) and **20** (1.339(6) Å), and considerably shorter than the distance in **2** (1.362(13) Å). These metric parameters suggest the operation of electronic effects on the TTF core for coordinated P4 molecules that are not operative for coordinated *o*-P2 molecules. Also of note is the strict planarity of the TTF unit in the P4 (2) bridged ligand. The structure of **22** is the only TTF-phosphine molecule, apart from $NiBr_2$(*o*-P2), that does not exhibit appreciable out-of-plane bending of the TTF core. Planar TTF substituents have been observed for all TTF-phosphines that are *trans* to halogens; this will be discussed in more detail in Chapter 6. The packing diagram for **22** is shown in Figure 40, where it can be observed that there are no stacking interactions. As a result of the bulky phenyl groups, the molecules are packed in a "staggered" arrangement.

E. Reactions of MCl_2(*o*-P2) and M_2Cl_4(P4) (M = Pt, Pd, Ni) with $AgBF_4$

(1) Synthesis

Reactions of MCl_2(*o*-P2) and M_2Cl_4(P4) (M = Pt (**21**),(**23**); Pd (**26**),(**28**)) with the appropriate quantities of $AgBF_4$ in refluxing acetonitrile results in abstraction of the halides and formation of $[M(NCCH_3)_2(o\text{-P2})][BF_4]_2$ and $[M_2(NCCH_3)_4(P4)][BF_4]_4$ (M = Pt (**21**),(**23**); Pd (**26**),(**28**)). The reactions are carried out under protection from light to prevent degradation of the reactants and/or products. Experiments performed at different reaction times and temperatures led to the conclusion that the highest yields are obtained when the mononuclear reactants are refluxed for 2 h, but that much longer reaction times are required for complete halide abstraction in the dinuclear compounds. In the case of $PtCl_2$(*o*-P2) (**20**) and $PdCl_2$(*o*-P2) (**25**), the reactants are soluble in chlorinated solvents, but only slightly soluble in nitriles, while the opposite is true for the products. The dinuclear compounds, **22** and **27**, are insoluble in most solvents, but the partially solvated products are highly soluble in acetonitrile. These solubility differences allow for ease of separation of reactants and products. It is important to note that while **23** and **28** are air-stable, **21** and **26** decompose in air, as signified by a color change from red and red-brown to green. The formation of a green solution is indicative of oxidation of the TTF core.

(2) Spectroscopic Studies

The infrared spectra of **21**, **23**, **26**, and **28** display characteristic modes at c.a. 690 and 520 cm^{-1} for the phosphine ligand. Bands at ca. 2325 and 2290 cm^{-1} are assigned to the C≡N stretch of coordinated acetonitrile. The

absence of ν(M-Cl) features supports the conclusion that the halide abstraction was successful. This is further supported by the presence of a ν(B-F) stretch at 1055 cm^{-1}.

FAB-MS experiments performed on $[Pt_2(NCCH_3)_4(P4)][BF_4]_4$ (**23**) reveals very little information due presumably to the high cationic charge on the metal complex. In order to introduce a counterion that might serve to reduce the cationic charge, triflic acid (HCF_3SO_3, or HOTf) was introduced to the matrix/analyte solution prior to analysis. The presence of triflate as a weakly coordinating counterion with high molecular weight "super-molecules" or "supramolecules" is well-documented in the independent work of Stang and Hupp. The triflates appear to assist in the FAB-MS analysis of cations with high charges.[23] With triflate as a counterion, the species $[Pt_2(P4)(OTf)_2]^+$, $[Pt_2(P4)(OTf)_2]^+$, and $[Pt^{2+}Pt^{2+n}(P4)^{n-1}](OTf)_4]^+$ (n = 0 or 1). are detectable. No peaks could be assigned to $Pt_2(P4)Cl_4$ (**22**) which further supports the conclusion that abstraction of halides to give $[Pt_2(P4)(NCCH_3)_4][BF_4]_4$ (**23**) was successful. Clearly, FAB-MS will be a useful tool in the characterization of multiply charged complexes such as **21**, **26**, and **28**.[1]

(3) ^1H and $^{31}P\{^1H\}$ NMR Spectroscopic Studies

The ^1H NMR spectra of **21**, **23**, **26**, and **28** in CD_3CN display a series of multiplets between δ 7.64 and 7.78 ppm due to the phenyl protons of the phosphine groups. All four compounds exhibit a sharp singlet at ca. 1.96 ppm

due to free acetonitrile which indicates some degree of lability of this ligand. Complexes $[Pt(o\text{-}P2)(NCCH_3)_2][BF_4]_2$ (**21**) and $[Pd(o\text{-}P2)(NCCH_3)_2][BF_4]_2$ (**23**) also display signals at δ = 2.18 and 2.15 ppm respectively, that are assigned to bound CH_3CN. The presence of residual water in the deuterated solvent used for the NMR spectra of **21** and $[Pd_2(P4)(NCCH_3)_4][BF_4]_4$ (**28**) may serve to mask this resonance in those cases. The singlet located at 1.90 ppm in the spectra of **21** and **26** is due to the methyl protons of the *o*-P2 ligand. The $^{31}P\{^1H\}$ NMR spectra of **21**, **23**, **26**, and **28** all display resonances that are shifted downfield relative to the free ligand values (-18.8 ppm for **1** and -18.2 ppm for **2**), which supports the formation of a five-membered ring through metal coordination of the phosphorus atoms. Both Pd complexes (**26** and **28**) display singlets at δ = 50.7 ppm for **26** and 50.9 ppm for **28**, indicating the presence of only one type of coordinated phosphorus nucleus. The ^{31}P NMR spectrum of **21** displays a singlet at 29.0 ppm with Pt satellites, supporting the presence of only one type of coordinated phosphorus nucleus with $^1J_{Pt\text{-}P}$ = 1646 Hz. The smaller $^1J_{Pt\text{-}P}$ coupling for **21** (1646 Hz) relative to **20** (3640 Hz) is indicative of the presence of *trans*- nitriles rather than chlorides, and follows the trend noted for $PtCl_2$(dppee) versus $[Pt(DMF)_2(dppee)][BPh_4]_2$ (DMF = dimethylformamide).[16b] The ^{31}P NMR spectrum of $[Pt_2(P4)(NCCH_3)_4][BF_4]_4$ (**23**) displays two singlets with Pt satellites at δ = 19.5 and 26.3 ppm. The larger magnitude of the $J_{Pt\text{-}P}$ coupling constants for both resonances (3845 and 3421 Hz) suggests that the halogen abstraction

was incomplete, and *trans*-chloride ligands are still present in some form. However, this is contradictory to the results of infrared and mass spectroscopic analysis. Refluxing times in excess of 2 days result in metal phosphorus bond cleavage and formation of $[Pt(P4)]_n[BF_4]_{2n}$ (**31**), as evidenced by a ^{31}P NMR resonance at δ 36.1 ppm (J_{Pt-P} = 2361 Hz). The larger coupling constant, relative to **21**, is indictative of the phosphorus groups being *trans* to each other.[8,22]

F. Synthesis and Characterization of $[Pt_2(o\text{-}P2)_2(P4)][BF_4]_4$ (24)

(1) Synthesis

The reaction of P4 (**2**) with two equivalents of $[Pt(NCCH_3)_2(o\text{-}P2)][BF_4]_2$ (**21**) yields the dinuclear complex $[Pt_2(o\text{-}P2)_2(P4)][BF_4]_4$ (**24**). The same product can be produced by substituting the CH_3CN ligands in the dinuclear complex $[Pt_2(NCCH_3)_4(P4)][BF_4]_4$ (**23**) with *o*-P2 (**1**). The product is very similar to the homo- and heterobimetallic complexes $[MM'(dppb)_2(tppb)][BF_4]_4$ (M, M' = Ni, Pd, Pt) reported by Fox *et al.*[1b] Complex **24** is stable in air, but demonstrates a tendency to decompose in solution with prolonged exposure to light.

(2) Spectroscopic Characterization

The infrared spectrum of **24** exhibits a strong ν(B-F) stretch for $[BF_4]^-$ at 1054 cm^{-1}. Bands at 689 and 517 cm^{-1} are due to the phosphine ligand. The absence of ν(C≡N) modes between 2200 and 2400 cm^{-1} suggests complete substitution of CH_3CN by the phosphine has occurred, but does not rule out

the possibility of residual coordinated CH_3CN since these modes can be very weak. Taube and Johnson have demonstrated that the frequency and intensity of the C≡N stretching vibration can be quite variable, and in some cases even absent when coordinated nitrile is present.[24]

The electronic spectrum of $[Pt_2(o\text{-}P2)_2(P4)][BF_4]_2$ (**24**) recorded in acetonitrile exhibits transitions at 248, 289 (sh), 345 and 502 nm. The feature at 248 nm is assignable to the phenyl chromophores, while those at 345 and 502 nm arise from the TTF unit. Using the extinction coefficient, ε, for the phenyl chromophores in TTF-phosphines as a gauge to calculate the number of phenyl groups in the molecule (*o*-P2 contains 4 phenyl groups and ε = 25,800), the ε value of $1.1x10^5$ is indicative of one P4 ligand (four PPh_2 groups) and two *o*-P2 ligands (two PPh_2 groups each).[7]

(3) ^1H and $^{31}P\{^1H\}$ NMR Spectroscopic Studies

The ^1H NMR spectrum of **25** contains the expected resonances in the range δ 7.32 - 7.48 ppm, assignable to the phenyl protons. The sharp singlet at 1.81 ppm is due to the methyl-protons of the *o*-P2 ligands. Integration of the signals results in a 20:3 ratio for the phenyl to methyl protons, supporting the presence of 16 phenyl and 4 methyl groups. The $^{31}P\{^1H\}$ NMR spectrum of **24** exhibits a singlet at δ = 32.9 ppm with Pt satellites ($J_{Pt\text{-}P}$ = 2365). The presence of only one signal shifted to lower fields relative to free *o*-P2 or P4 indicates that the environments of the coordinated *o*-P2 and P4 ligands are too similar to be distinguished from one another. Although the

coordinated phosphines of the P4 and *o*-P2 ligands in **24** are obviously not equivalent, the environments of the phosphines are sufficiently similar enough to render them magnetically equivalent. This is contradictory to what was observed in the ^{31}P NMR spectrum for $[Pt_2(dppb)_2(tppb)][BF_4]_4$, which shows the bi- and tetradentate ligands to possess inequivalent phosphines that exhibit a second order spectrum with one trans- and several cis-coupling constants.[2] The Pt-P coupling constant, $J_{Pt\text{-}P}$, is in the expected range for *trans*-phosphine ligands, and agrees well with $[Pt(o\text{-}P2)_2][BF_4]_2$ (**11**) and other $[Pt(L\text{-}L)_2]^{2+}$ complexes where L-L is a bis-phosphine ligand.[2,15,16]

(4) Electrochemistry

In the absence of electronic coupling, the electrochemistry of $[Pt_2(o\text{-}P2)_2(P4)][BF_4]_4$ (**24**) would be expected to display two accessible one-electron oxidation couples attributable to the P4 ligand and two superimposed one-electron oxidation couples due to each *o*-P2 ligand. No separation of the one-electron processes would be expected for the bidentate ligand, **1**, based on electrochemical data for the $[M(o\text{-}P2)_2]^{n+}$ series which revealed that the ligands behave as isolated redox centers. Based on the cyclic voltammetry of $PtCl_2(o\text{-}P2)$ (**20**) at least one reduction couple may be expected for the metal centers. The actual cyclic voltammogram of **24** is broad and relatively featureless in the anodic region. An irreversible reduction couple is evident at -0.89 V, which can be attributed to the previously described Pt(II)-Pt(I) reduction process. Coulometry experiments have not been performed, thus the exact nature of the process (one- or two-electrons) is undetermined. The

breadth of the signal may be a result of material depositing on the electrode surface, a problem that has been observed with other metal-P4 complexes (see Chapter 6). Another possibility is that communication between the TTF units results in the superposition of several oxidation couples. Given the results of the electrochemical studies for the $[M(o\text{-}P2)_2]^{n+}$ series however, no communication is expected between the phosphines of the *o*-P2 ligands. Perhaps the shorter bridging C-C double bond (C(1)-C(2)) in the structure of **22** versus **20** is an indication that the electronic nature of the coordinated P4 ligand might be altered as compared to the *o*-P2 species. Even if this is the case, the *o*-P2 ligands would still presumably act as isolated redox centers, and overlapping couples should not be expected.

4. Concluding Remarks

The use of systematic synthetic procedures involoving polydentate phosphine ligands to build extended materials with transition metal ions allows for greater control over the resulting structure than typical cluster synthesis methods. Fox and coworkers demonstrated that this methodology works quite well using bis- and tetraphosphines as the ligand base.[2] In the present study the typically innocent organic backbone of the ligand is replaced by TTF, which introduces added redox functionality and provides the possibility of obtaining materials with interesting magnetic and conducting properties. The syntheses of mononuclear and dinuclear metal complexes containing only phosphine and chloride ligands proceeds with relative ease and purity of product. The creation of vacant coordination sites

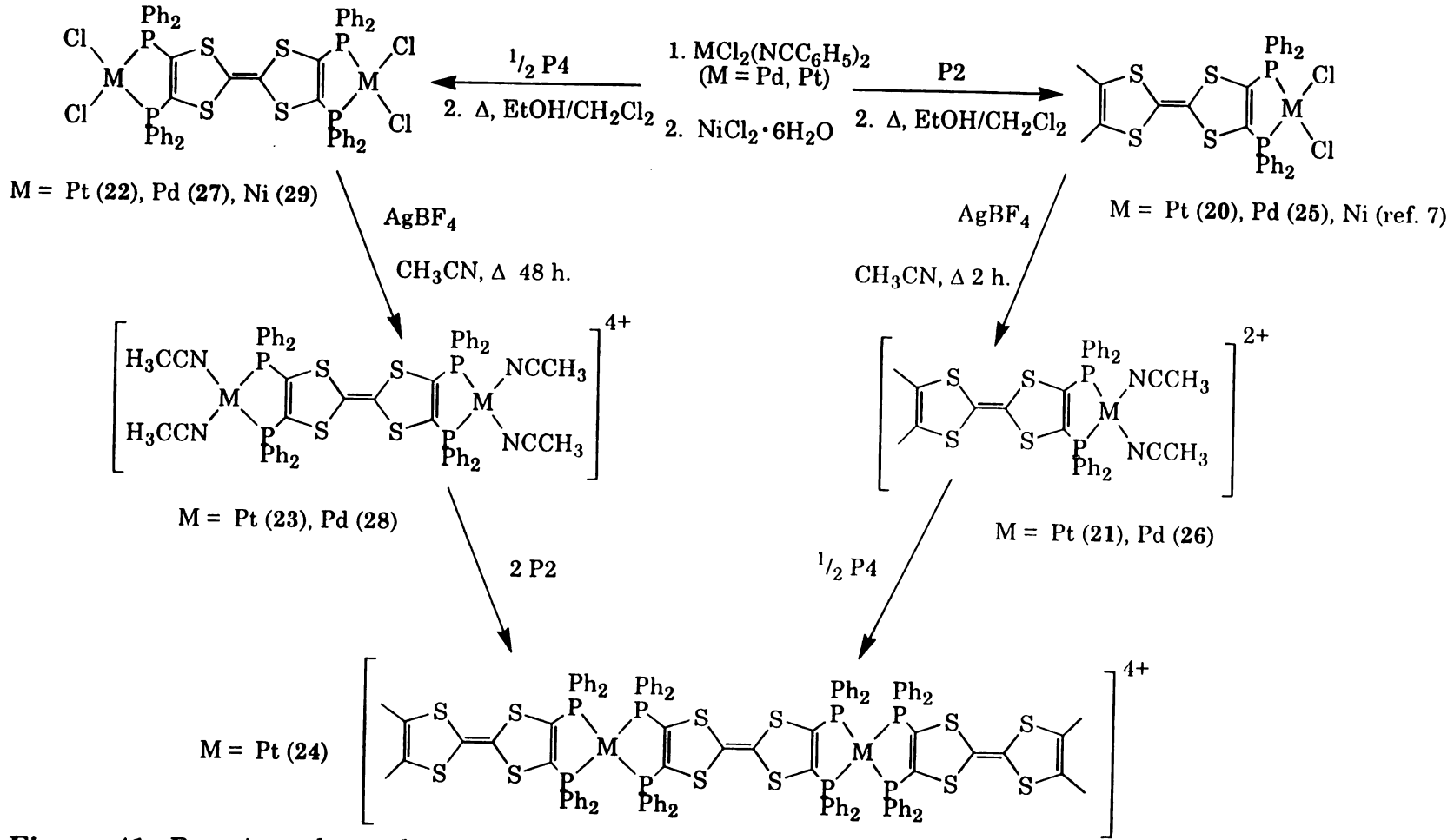

Figure 41. Reaction scheme depicting the step-wise synthesis of $[M_2(o\text{- P2})_2(P4)][BF_4]_4$ (M = Ni, Pd, Pt (24)).

by using reagents such as Ag^+ to abstract one or more halides is a well documented tool in synthetic chemistry, particularly in situations involving small molecule reactivity.[25] In the coordination polymers regime, such complexes have been referred to as "complex-metals" due to the presence of easily replaceable ligands which give rise to open coordination sites.[3a] These complexes can then be used as building blocks for the formation of higher nuclearity complexes with specifically engineered architectures. In the present chemistry the halide abstraction step appears to be sluggish in the case of the dinuclear complexes, and ^{31}P NMR data indicate that some partially halogenated impurities remain, especially in the platinum chemistry. This is not too surprising given that Pt(II) is fairly inert. The displacement of acetonitrile from partially solvated mononuclear-phosphine complexes with P4 results in a coupling of the two mononuclear species to form the dinuclear complex $[Pt(o\text{-}P2)_2(P4)][BF_4]_4$ (**22**). The same product can be obtained by reacting *o*-P2 with the partially solvated dinuclear complex, $[Pt_2(NCCH_3)_2(P4)][BF_4]_4$. The final step to form the all-phosphine product $[Pt_2(o\text{-}P2)_2(P4)]^{4+}$ has only been achieved with platinum, but it is reasonable to believe that this can be extended to any metal for which $MX_2(o\text{-}P2)$ or $M_2X_4(P4)$ can be prepared.

While this chemistry does not strictly fall into the category of "complexes as metals/complexes as ligands" due to the fact that thus far no two metal-containing complexes have been combined to form a single product, the potential for such chemistry exists. The complex

$[Ni_2(dppb)(tppb)][BF_4]_4$ can be formed by *in situ* halide abstraction from $NiCl_2(dppb)$ with HBF_4, followed by the addition of a stoichiometric amount of the tetradentate- phosphine tppb.[2] The fact that $Pt_2Cl_4(P4)$ (**20**) and $Pd_2Cl_4(P4)$ (**25**) do not begin to form until after the first 30 minutes suggests that the analogous product, $MCl_2(P4)$, might be possible to obtain. The formation could be rendered more favorable by the use of excess P4 and a dilute solution of metal reactant. The preparation of such a complex opens the possibility for the step-wise formation of highly extended structures with precise control over the identity of the metal units (scheme 3). Such control includes the formation of heterometallic complexes where more than one metal can be included whose properties can be specifically chosen to produce a desired outcome. This has been demonstrated by the use of $[Ni(dppb)(tppb)]^{2+}$ to form $[NiM'(dppb)_2(tppb)]^{4+}$, where M' = Pd or Pt.[2a]

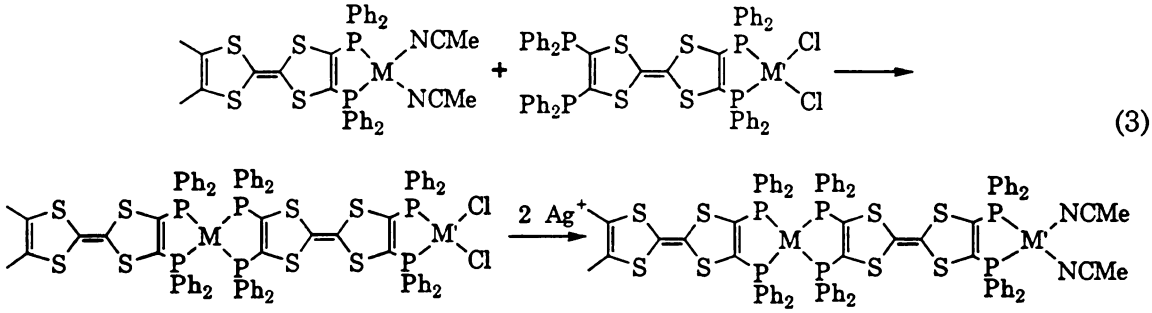

Another potential for this chemistry is the inclusion of magnetic metal centers to form extended structures with unpaired electrons. A preliminary report supports the successful synthesis of $CoCl_2(o\text{-}P2)$ by a method analogous to that used to prepare $NiX_2(o\text{-}P2)$.[26] Work in our laboratories supports this report, and indicates that $CoCl_4(P4)$ can be similarly prepared.

Using cobalt (II) (S = 3/2) as an example, $[Co_2(o\text{-}P2)_2(P4)][BF_4]_4$, would be expected to contain up to six unpaired electrons, barring strong antiferromagnetic coupling through the ligand. If the phosphine groups serve to restrict communication between metals in the chain, then molecules may result with a large number of unpaired electrons. If the redox properties of the TTF cores are exploited, the further possibility exists for adding three unpaired electrons by one-electron oxidations of each ligand. The spin total for the dimetal system could then be as high as nine unpaired electrons. The use of $[TCNQ]^-$ as the counteranion instead of $[BF_4]^-$ would introduce additional radical species and allow the possibility of conduction through stacked $[TCNQ]^{n-}$ (n = 0, 1) molecules. Given the potential for $[Co(o\text{-}P2)_2]^{2+}$ to bind two additional ligands, it may also be feasible to coordinate TCNQ directly to the metal center (Figure 42), thereby forming multidimensional arrays of metal and organic spins.

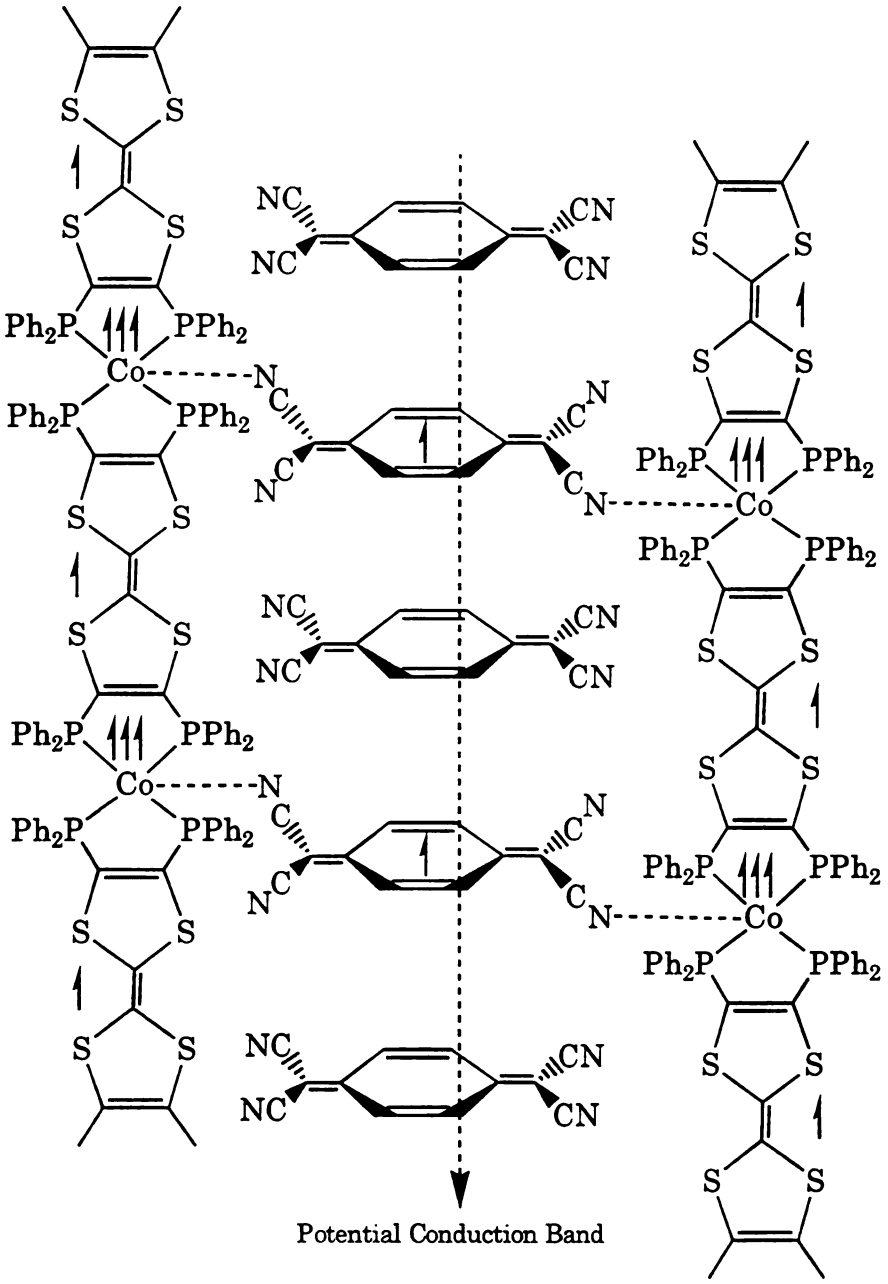

Figure 42. Schematic showing the potential coordination of $[TCNQ]^{n-}$ (n = 0, 1) to "$[Co_2(o\text{-}P2)_2(P4)]^{m+}$" (m = 4, 6, 7).

List of References

1. Asara, J. M.; Uzelmeier, C. E.; Dunbar, K. R.; Allison, J., *Inorg. Chem.*, **1998**, *37*, 1833.

2. (a) Fox, M. A.; Chandler, D. A. *Adv. Mater.* **1991**, *3*, 381-385. (b) Wang, P.-W.; Fox, M. A. *Inorg. Chem.*, **1994**, *33*, 2938-2945. (c) Fox, M.; Chandler, D. A., *NATO Adv. Studies Sers.*, **1987**, *214*, 405.

3. (a) Balzini, V.; Campagna, S.; Denti, G.; Juris, A.; Serroni, S.; Venturi, M. *Acc. Chem. Res.*, **1998**, *31*, 26. (b) Carter, F. L.; Siatkowski, R. E.; Wohltjen, H., Eds., *Molecular Electronics Devices*, North-Holland: AMsterdam, **1998**. (c) Lehn, J-M. *Supramolecular Chemistry*, VCH: Weinheim, Germany, **1995**. (d) Balzini, V.; De Cola, L., *Supramolecular Chemistry*, Kluwer: Dorecht, The Netherlands, **1992**. (e) Vögtle, F. *Supramolecular Chemistry*, Wiley: Chichester, U.K., **1993**. (f) Stang, P. J., Olenyuk, B. *Acc. Chem. Res.*, **1997**, *30*, 502. (g) Moore, J.S. *Acc. Chem. Res.*, **1997**, *30*, 402.

4. (a) Campagna, S.; Denti, G.; Serroni, S.; Ciano, M.; Balzini, V. *Inorg. Chem.*, **1992**, *31*, 4251. (b) Serroni, S.; Denti, G. *Inorg. Chem.*, **1992**, *31*, 4251.

5. McCullough, R. D.; Belot, J. A. *Chem. Mater.*, **1994**, *6*, 1396.

6. Gan, X.; Munakata, M.; Kuroda-Sowa, T.; Maekawa, M.; Misaki, Y. *Polyhedron*, **1995**, *14*, 1343.

7. Fourmigué, M.; Batail, P. *Bull. Soc. Chim. Fr.*, **1992**, *129*, 829.

8. Fourmigué, M.; Uzelmeier, C. E.; Boubekeur, K.; Bartley, S. L.; Dunbar, K. R. *J. Organomet. Chem.*, **1997**, *529*, 343.

9. Uchiyana, T. *Bull. Chem. Soc. Jap.*, **1981**, *54*, 181.

10. (a) Bino, A.; Cotton, F. A.; Fanwick, P. E. *Inorg. Chem.* **1979**, *18*, 3558. (b) Cotton, F. A.; Frenz, B. A.; Deganello, G.; Shaver, A. *J. Organomet. Chem.* **1973**, *50*, 227.

11. SHELXTL v. 5.04, G. M. Sheldrick and Siemens Analytical X-Ray Systems, Inc., **1997**, 6300 Enterprise Lane, Madison WI. 53719.

12. Cotton, F.A.; Wilkinon, G. *Advanced Inorganic Chemistry, 3rd Ed.*, Wiley & Sons, New York, **1972**.

13. Fourmigué, M., personal communication.

14. (a) Sanger, A. R. *J. Chem. Soc., Dalton Trans..*, **1977**, 1971. (b) Hudson, M. J.; Nyholm, R. S.; Stiddard, M. H. B. *J. Chem. Soc. (A)*, **1968**, 40.

15. Champness, N. R.; Levason, W.; Preece, S. R.; Webster, M.; Frampton, C. S. *Inorg. Chim. Acta*, **1996**, *244*, 65.

16. (a) Jarrett, P.S.; Sadler, P. J. *Inorg. Chem.*, **1991**, *30*, 2098. (b) Oberhauser, W.; Bachmann, C.; Brüggeller, P. *Inorg. Chim. Acta*, **1995**, *238*, 35.

17. Liu, S-T.; Chen, J-T.; Peng, S-M.; Hsiao, Y-L.; Cheng, M-C. *Inorg. Chem.*, **1990**, *29*, 1169.

18. Davies, J. A.; Staples, R. J. *Polyhedron*, **1991**, *10*, 899.

19. Miedaner, A.; Haltiwanger, R. C.; DuBois, D. L. *Inorg. Chem.*, **1991**, *30*, 417.

20. *Handbook of Chemistry and Physics, 63rd Ed.*, CRC, Clevelend Ohio, **1982-1983**, F-200.

21. Calligaris, M.; Carturan, G.; Nardin, G.; Scrivanti, A.; Wojcicki, A. *Organometallics*, **1983**, *2*, 865.

22. Uzelmeier, C. E.; Founigué, M.; Smucker, B.; Grandinetti, G.; Dunbar, K. R., manuscript in preparation.

23. (a) Whiteford, J. A.; Rachlin, E. M.; Stang, P. J. *Angew. Chem. Int. Engl.*, **1996**, *35*, 2524. (b) Slone, R. V.; Yoon, D. I.; Calhoun, R. M.; Hupp, J. T. *J. Am. Chem. Soc.*, **1995**, *117*, 11813.

24. Johnson, A.; Taube, H. *J. Indian. Chem. Soc.*, **1989**, *66*, 503.

25. (a) Schrock, R. R.; Osborn, J. A. *J. Am. Chem. Soc.*, **1971**, *93*, 2397. (b) Shapley, J. R. Schrock, R. R. *J. Am. Chem. Soc.*, **1969**, *91*, 2816. (c) Green, M.; Kuc, T. A.; Taylor, S. H. *J. Chem. Soc. (A)*, **1971**, 2334. (d) Haines, L. M.; Singleton, E. *J. Chem. Soc., Dalton Trans.*, **1972**, 1891. (e) Haines, L. M. *Inor. Nuc. Chem. Lett.*, **1969**, *5*, 399. (f) Haines, L. M. *Inorg. Chem.*, **1970**, *9*, 1517.

26. Fourmigué, M.; Jarchow, S.; Batail, P. *Phosphorus, Sulfur, Silicon*, **1993**, *75*, 175.

CHAPTER VI

ASSEMBLY OF OLIGOMERIC SYSTEMS FROM HOMOLEPTIC PLATINUM GROUP NITRILE COMPLEXES AND TETRAKIS(DIPHENYLPHOSPHINO)TETRATHIAFULVALENE (P4)

1. Introduction

The preparation of the mononuclear M-(*o*-P2) complexes described in Chapter III led us to become interested in the use of the tetradentate ligand $(PPh_2)_4TTF$ (P4) for the preparation of the analogous extended species. The presence of four phosphine groups on the TTF unit opens up the possibility for chelating metal centers on both sides, as observed in the molecular structure of Pt_2Cl_4(P4) (**22**). Based on the reactions of the *o*-P2 ligands it can be expected that P4 will react in a similar fashion, resulting in the preparation of coordination polymers.

It has been theorized that the introduction of transition metal ions into a conjugated polymer chain will create a partially-filled band, possibly leading to intrinsic conductivity.[1] The preparation of polymers requires two characteristics.[2] First, the redox-active centers (inorganic, organic, or a combination of the two) must be oriented to permit strong interactions, often requiring close spatial proximity and similar crystallographic and electronic environments for the units. Second, the polymers must be partially oxidized or reduced (forming mixed-valence species) to permit free charge transfer along the chain.[3]

Thus far, efforts to produce conducting or semiconducting coordination polymers have met with varied success. Some of these include metal coordination polymers of tetrathioxalate,[4] dihydroxybenzoquinone,[5] and benzodithiolene.[6] In considering our own approach, the molecule that bears the most resemblance to P4, from a coordination perspective, is

tetrakis(diphenylphosphino)benzene (tppb).[7] In this chapter, the chemistry of P4 with divalent metal ions is reported and the results discussed in light of the potential of these compounds to form oligomers/polymers.

A. Synthesis

Starting Materials and Reaction Procedures. The compounds $[P(C_6H_5)_2]_4TTF$,[8] $[Rh_2(NCCH_3)_{10}][BF_4]_4$,[9] $Ni(CF_3SO_3)_2$[10] and $[M(NCCH_3)_x][BF_4]_2$ (M = Ni, Co, Fe,[11] Pd,[12] x = 6; M = Pt,[13] x = 4) were prepared according to published procedures. Acetonitrile, and methylene chloride were distilled over 3 Å molecular sieves. Diethyl ether, hexanes and toluene were distilled over sodium-potassium/benzophenone. Unless otherwise specified, all reactions were carried out under an argon atmosphere by using standard Schlenk-line techniques.

(1) Reaction of $[Rh_2(NCCH_3)_{10}][BF_4]_4$ with P4: Formation of [Rh(P4)][BF4] (30)

3.8 mL of a stock solution P4 (0.2089 g, 0.222 mmol) in 11.5 mL of CH_2Cl_2 was added to an CH_3CN solution of $[Rh_2(NCCH_3)_{10}][BF_4]_4$ (0.308 g, 0.319 mmol, 10 mL), which led to an immediate darkening of the orange solution. After stirring for 24 h, the solvent was removed under vacuum and the residue redissolved in 3 mL of CH_3CN. The solution was treated with 30 mL of Et_2O and filtered in air, to yield a tan solid which was washed with additional Et_2O and dried *in vacuo*; yield 0.185 g (74% on [Rh(P4)][BF_4]). ^1H NMR (CD_2Cl_2) δ ppm: 25 °C: Ph-H, 7.28 (m, T1 = 0.72(2)s), 7.06 (m, T1 =

0.76(3)s); 0 °C: 7.24 (m), 7.05 (m); -35 °C: 7.07 (m). $^{31}P\{^{1}H\}$ NMR (CD_2Cl_2) δ ppm: 25 °C: 51.0 (d, $^{1}J_{Rh-P}$ = 34 Hz). C.V. (0.1 M $CH_3CN/TBAPF_6$, Pt electrode vs Ag/AgCl): $E_{1/2}(ox)_1$ = +0.76 V, $E_{1/2}(ox)_2$ = +1.12 V. UV/Visible (CH_3CN) λ_{max}, nm (ε, $M^{-1}cm^{-1}$): 387 ($8.1x10^3$), 310 ($3.4x10^4$), 266 ($3.8x10^4$). GPC (1.00 mL/min, THF, 254 nm): 20.65 min., 22.00 min retention.

(2) Reaction of $[M^{II}(NCCH_3)_n][BF_4]_2$ (M = Pt, n = 4; M = Pd, Co, Fe, Ni, n = 6) with P4.

(i) Formation of $[Pt(P4)]_n[BF_4]_{2n}$ (31). 5 mL of a stock solution of P4 (0.300 g, 0.319 mmol) in 15 mL of CH_2Cl_2 was added to an CH_3CN solution of $[Pt(NCCH_3)_4][BF_4]_2$ (0.057 g, 0.107 mmol, 10 mL) which caused a darkening of the orange solution. After stirring for 24 h, the solution was treated with 20 mL of Et_2O and filtered in air, to yield an orange solid which was washed with *copious* amounts Et_2O and dried *in vacuo*; yield 0.109 g (78% for $[Pt(P4)][BF_4]_2$). ^{1}H NMR (CD_3CN) δ ppm: 25 °C: Ph-H, 7.23 (br), 7.44 (br), 7.73 (br); 0 °C: 7.20 (br), 7.44 (br), 7.74; -15 °C: 7.20 (br), 7.43 (br), 7.73 (br); -35 °C: 7.20 (br), 7.40 (br), 7.71 (br). $^{31}P\{^{1}H\}$ NMR (CD_3CN) δ ppm: 36.1 (s, $^{1}J_{Pt-P}$ = 2361 Hz). IR (Nujol, cm^{-1}): 689 (m, $\nu_{=C-H}$), 1054 (br, ν_{B-F}). UV/Visible (CH_3CN) λ_{max}, nm (ε, $M^{-1}cm^{-1}$): 406 ($5.5x10^3$), 238 ($6.6x10^4$).

(ii) Formation of $[Pd(P4)]_n[BF_4]_{2n}$ (32). Solutions of 0.116 g of $[Pd(NCCH_3)_6]BF_4]_2$ (0.221mmol) in 6 mL of CH_3CN and 0.207 g (0.220 mmol) of P4 in 5 mL of CH_2Cl_2 were prepared in separate flasks. Upon addition of the phosphine solution to the metal complex, a color change from orange to

brown ensued. The solution was stirred for 12 h before being reduced to 5 mL and treated with 50 mL of Et_2O, which gave a brown precipitate. The mixture was filtered in air, and the solid was washed with *copious* amounts of Et_2O before being dried *in vacuo*; yield 0.243 g (90% for $[Pd(P4)][BF_4]_2$). *Anal.* Calcd for **32**, $PdP_4S_4C_{54}H_{40}$: C, 53.12; H, 3.31. Found: C, 53.67; H, 3.69. ^1H NMR (CD_3CN) δ ppm: 25 °C: Ph-H, 7.13 (m, T1 = 2.23(5)s), 7.20 (m, T1 = 1.99(3)s), 7.44 (br, T1 = 1.98(3)s); 0 °C: 7.13 (br), 7.19 (m), 7.43 (br); -15 °C: 7,14 (m), 7.17 (m), 7.42 (br); -35 °C: 7.16 (m), 7.42 (br). $^{31}P\{^1H\}$ NMR (CD_3CN) δ ppm: 44.2; (solid) δ ppm: 42.6. IR (Nujol, cm^{-1}): 525 (s, $\nu_{C=C}$), 670 (m, $\nu_{=C-H}$), 1049 (br, ν_{B-F}). UV/Visible (CH_3CN) λ_{max}, nm (ε, $M^{-1}cm^{-1}$): 337 ($4.1x10^4$). FAB-MS (in HCF_3SO_3, m/z): 1194 ($[Pd(P4)(CF_3SO_3)]^+$), 1601 ($[Pd_2(P4)(CF_3SO_3)_3]^+$), 2945 ($[Pd_3(P4)_2(CF_3SO_3)_5]^+$), 3890 ($[Pd_3(P4)_3(CF_3SO_3)_5]^+$), 4294 ($[Pd_4(P4)_3(CF_3SO_3)_7]^+$).

(iii) Formation of $[Co(P4)]_n[BF_4]_{2n}$ (33). 0.046 g (0.096 mmol) of $[Co^{II}(NCCH_3)_6][BF_4]_2$ and 0.101 g (0.107 mmol) of P4 were dissolved in 10 mL CH_3CN and 10 mL CH_2Cl_2, respectively. Upon addition of the phosphine solution to the cobalt complex, the reaction mixture immediately turned dark green. The reaction mixture was stirred overnight, concentrated to a volume of ~ 5 mL, and treated with Et_2O (20 mL) to give a green precipitate. The solid was isolated by decanting the solution, washed several times with Et_2O, and dried *in vacuo*; yield 0.056 g (51% for $[Co(P4)][BF_4]_2$) . ^1H NMR (CD_3CN) δ ppm: broad and unresolved. $^{31}P\{^1H\}$ NMR (CD_3CN) δ ppm: none observed.

EPR (1:1 toluene/acetonitrile, -140°C): g ≈ 2.21. magnetic moment, μ_{eff} (μ_B), 1T: 2.05 at 5 K, 5.00 at 340 K.

(iv) Formation of $[Fe(P4)]_n[BF_4]_{2n}$ (34). 0.051 g of $[Fe(NCCH_3)_6]BF_4]_2$ (0.107 mmol) and 0.105 g (0.112 mmol) of P4 were loaded into a Schlenk-flask and treated with a combination of 5 mL of CH_2Cl_2 and 10 mL of CH_3CN, which produced a red solution. The solution was stirred for 3 days before being treated with 40 mL of Et_2O to afford a red precipitate; the liquid was decanted, and the solid was washed 4 times with 5 mL portions of Et_2O. The solid was dried under vacuum; yield 0.094 g (75% for $[Fe(P4)][BF_4]_2$). ^1H NMR (CD_3CN) δ ppm: 6.90 (br), 7.27 (m), 7.34 (m), 7.59 (br). $^{31}P\{^1H\}$ NMR (CD_3CN) δ ppm: 53.6 (s), 73.8 (s).

(v) Formation of $[Ni(P4)]_n[BF_4]_{2n}$ (35). 0.051 g of $[Ni(NCCH_3)_6]BF_4]_2$ (0.107 mmol) and 0.104 g (0.111 mmol) of P4 were loaded into a Schlenk-flask and treated with a combination of 5 mL of CH_2Cl_2 and 10 mL of CH_3CN, to yield a green-brown solution. The solution was stirred for 1 week before being reduced to 5 mL under vacuum. The solution was treated with 50 mL of Et_2O to afford a green precipitate, the liquid was decanted, and the solid was washed 4 times with 10 mL portions of Et_2O. The solid was finally dried under vacuum; yield 0.050 g (41% for $[Ni(P4)][BF_4]_2$. ^1H NMR (CD_3N) δ ppm: $-CH_3$ 1.90 (s, 6H); Ph-H, 7.05 (br), 7.23 (m), 7.25 (br). $^{31}P\{^1H\}$ NMR (CD_3N) δ ppm: 41.7. IR (Nujol, cm^{-1}): 689 (m, $\nu_{\equiv C-H}$) 503 (s, $\nu_{C\equiv C}$), 1020 (br, ν_{B-F}).

(3) Reactions with excess P4

(i) $[Rh_2(NCCH_3)_{10}][BF_4]_4$. Solutions of 0.226 g of P4 (0.240 mmol) and 0.056 g of $[Rh_2(NCCH_3)_{10}][BF_4]_4$ (0.058 mmol) were prepared separately by dissolving the solids in 10 mL of CH_2Cl_2 and 10 mL CH_3CN respectively. The phosphine was then slowly added to the metal complex 5 mL at a time, causing the solution to change from orange to dark brown. After stirring for several hours, the volume of the solution was reduced by application of a vacuum to ~5 mL. An orange-brown solid precipitated from the solution following the addition of 50 mL of toluene. The product was recovered by decanting the orange liquid and washing the solid 5 times with 10 mL of toluene to remove unreacted ligand. Finally, the solid was collected by filtration in air and washed with *copius* quantities of Et_2O, and dried *in vacuo*. $^{31}P\{^1H\}$ NMR (CD_3CN) δ ppm: -18.2 (s), 50.3 (d)

(ii) $[Pd^{II}(NCCH_3)_6][BF_4]_2$. CH_2Cl_2 (15 mL) was added to a mixture of $[Pd^{II}(NCCH_3)_6][BF_4]_2$ (0.022 g (0.05 mmol) and $(Ph_2P)_4TTF$ (0.103 g 0.11 mmol), which dissolved the phosphine but left the palladium complex undissolved. After stirring for several minutes, an equal amount of acetonitrile was added which led to dissolution of the metal-complex and a color change from orange to dark red-orange. The solution was stirred overnight, reduced to dryness by vacuum, and washed several times with excess amounts of toluene to remove unreacted ligand. Due to the difficulty in preventing loss of solid, the washings were saved in a separate flask. Both

flasks were reduced to dryness by reduced pressure, washed with Et_2O, and dried *in vacuo*. ^1H NMR (CD_3CN) δ ppm: Ph-H, 7.23 (m), 7.70 (pentet). $^{31}P\{^1H\}$ NMR (CD_3CN) δ ppm: 44.0 (s), 43.7 (s), -17.1 (s).

3. Results and Discussion

A. Preparation and Characterization of $[M(P4)]_n[BF_4]_{xn}$ (M = Rh, x = 1; M = Pt, Pd, Co, Fe, Ni, x = 2) (30-35)

(1) Synthesis

The reaction of $[Rh_2(NCCH_3)_{10}][BF_4]_4$ with four equivalents of the tetradentate ligand P4 results in the formation of a product, formulated as $[Rh(P4)]_n[BF4]_n$ (**31**) based on the stoichiometry of the reaction. The reaction proceeds by sacrificing two equivalents of TTF-phosphine in order to reduce both d^7 metal centers. This is evidenced by the formation of a green solution, indicative of TTF cation formation. The reaction proceeds very similarly to the synthesis of $[Rh(o\text{-}P2)_2][BF_4]$,[14] with the exception of the use of CH_2Cl_2 as a solvent due to the low solubility of P4 in nitriles.

Similar reactions involving mononuclear metal precursors such as $[M(NCCH_3)_n][BF_4]_2$ (M = Pt, n = 4; M = Pt, Pd, Fe, Co, Ni, n = 6), proceed without the redox chemistry observed in the formation of **30**. The loss of nitriles appears to be quite rapid in mononuclear cases, as judged by the immediate color changes. The loss of acetonitrile is more difficult to gauge in the case of Rh due to the color changes caused by oxidation of the TTF moieties. The reaction conditions are quite similar to those used by Fox

and co-workers in the formation of long chain oligomers using tetrakis(diphenyl-phosphino)benzene (tppb).[7] In contrast to the insoluble products obtained by Fox, the products are highly soluble in most organic nitrile and chlorinated solvents, as well as acetone. Increased solubility may be a result of the high charge associated with complexes **30-35**, but given that the charges are the same for **31**, **32**, **35** and for complexes of Ni^{II}, Pd^{II}, and Pt^{II} with tppb, this does not explain the difference in solubilities. Unlike their mononuclear analogs, $[Ni(o\text{-}P2)_2][BF_4]_2$ (8) and $[Co(o\text{-}P2)_2][BF_4]_2$ (**9**) , **33** and **35** are air-sensitive, and decompose to an unidentified species. Complexes **31** and **32** are air stable and **32** is resistant to decomposition after heating at 80°C for 24 h. The complexes have been characterized by NMR, infrared, and electronic absorption spectroscopies. EPR and magnetic susceptibility studies of the paramagnetic Co^{II} complex have also been conducted. Elemental analysis of $[Pd(P4)]_n[BF_4]_{2n}$ (**32**) is in excellent agreement with a 1:1 formulation, while FAB-MS spectrometry contains mass ion peaks attributable to trinuclear species when triflic acid is used with the medium.[15]

(2) Spectrosopic Characterization

(i) NMR Spectroscopic Studies. The NMR spectral properties of **30-35** closely resemble those observed for their mononuclear, M-(*o*-P2), counterparts. The ^1H NMR spectra of **30-35** in CD_3CN exhibit a series of multiplets in the region δ = 7.2 - 7.7 ppm due to the phenyl protons. The

$^{31}P\{^{1}H\}$ NMR spectra of the Pd^{II} (**32**) and Ni^{II} (**35**) complexes each contain a single resonance at δ =44.2 and 41.7 ppm respectively. The downfield shift of the signal from the free phosphine at -18.2 ppm is a result of five-coordinate ring stabilization, and indicates that the phosphine is chelated to the metal center.[8,16] Compounds **30** and **31** each exhibit splitting patterns characteristic of coupling with an I = 1/2 nucleus. The ^{31}P spectra of $[Pt(P4)]_n[BF4]_{2n}$ (**31**) contain a singlet at δ = 36.1 ppm with satellites ($J_{Pt\text{-}P}$ = 2361 Hz) due to the 33% abundance ^{195}Pt. ^{103}Rh is 100% abundant, which explains the doublet observed in the ^{31}P NMR spectra of **30** at 51.0 ($J_{Rh\text{-}P}$ = 134 Hz). These data support that there is only one environment for the phosphorus nuclei in these complexes, and that they are metal-coordinated. $[Co(P4)]_n[BF_4]_{2n}$ (**33**) exhibits no observable resonances in its $^{31}P\{^{1}H\}$ NMR spectrum, and only broad signals in the ^{1}H spectrum, which indicates a paramagnetic complex.

The presence of an ^{31}P NMR signal for $[Fe(P4)]_n[BF_4]_{2n}$ (**33**) indicates that it is a diamagnetic product, with the metal behaving as a low-spin, d^6, Fe^{II} center similar to $[Fe(o\text{-}P2)_2][BF_4]_2$ (**12**). Compound **33** contains two signal patterns in its $^{31}P\{^{1}H\}$ NMR spectrum, both of which are downfield shifted relative to free ligand. The singlet at 53.6 ppm is in the same range as the other P4 complexes described above, indicating that it is a homoleptic phosphine. The second signal observed at δ = 73.8 ppm is at considerably lower fields than other complexes of *o*-P2, a fact that may indicate the

presence of coordinated fluoride in some form.[17] This has also been reported for **12** and confirmed by ^{19}F NMR spectroscopy. Similar experiments are warranted for **33**.

As stated previously, the above data support one environment of coordinated-phosphine in solution. If one considers the structures of the predicted long-chain products, this would is not be expected. In long chain oligomers, there must be both linking groups and end groups. These two different environments would be expected to exhibit very different chemical shifts in ^{31}P NMR spectra. For the reactions described here there are two different possibilities for end groups: phosphines and nitriles which would be *trans* to phosphines. In either case, two ^{31}P NMR signals would be expected, namely one in the region of the observed spectra for the internal phosphorus nuclei of the chain, and one for the phosphorus nuclei closest to chain termination. The latter signal would be expected to occur upfield from the internal phosphines, but downfield from the free ligand signal. This was the observation for the tppb coordination polymers mentioned previously. End-group analysis of these oligomers by ^{31}P NMR spectroscopy led to estimated chain lengths of 37±7 for Ni, 50±10 for Pd, and 23±5 for Pt.

Given the absence of of ^{31}P NMR resonances for **30-35** other than those predicted for internal phosphines (with the exception of $[Fe(P4)]_n[BF_4]_{2n}$) other options must be considered. One possibility is that a dynamic process occurs in solution causing the phosphines to reversibly coordinate to the metal. This would lead to an averaged signal and a broadening of the

terminal phosphines. To check for this, variable temperature ^{31}P NMR studies were performed on **30** and **32** in CD_2Cl_2 between 20 and -80 °C. The resulting spectra revealed no change with decreasing temperature. To further explore possible fluxionality, the solid state ^{31}P NMR spectra of $[Pd(P4)]_n[BF_4]_{2n}$ (**32**) were measured on a Varian-400 MHz spectrometer with the idea that end groups would be detected. The resulting spectrum exhibited a singlet at δ = 42.7 ppm, which supports the conclusion that a fluxional process is not present.

Another NMR method used to obtain a qualitative size comparison of two similar molecules is measuring the spin-lattice (T1) relaxation time. Nuclei in an NMR experiment are in a sample. The vibration and rotation of nuclei within a sample creates a complex magnetic field, called the lattice field. Some components of the lattice field can interact with nuclei in the higher energy state, and cause them to lose energy, returning to the lower state. T1 is the average lifetime of nuclei in the higher energy state. Larger molecules tend to undergo a greater degree of vibrations and rotations, thus causing a shorter T1 relaxation time. By comparing the T1 values of similar molecules, such as $[Pd(o\text{-}P2)_2][BF_4]_2$ (**10**) and $[Pd(P4)]_n[BF_4]_{2n}$ (**32**), or $[Rh(o\text{-}P2)_2][BF_4]$ and $[Rh(P4)]_n[BF_4]_n$ (**30**) we can obtain a qualitative estimation of the difference in size between the two molecules. Measurements of the T1 relaxation times of the phenyl protons of **10** and **32** showed both molecules to exhibit relaxation times on the order of 2 seconds. This indicates that there

is little size difference between the two molecules, supporting that **32** is not a long chain oligomer or polymer. Similar observations were made when comparing the Rh complexes, with both molecules exhibiting T1 values on the order of 0.7 seconds.

(ii) Infrared and UV-Visible Spectroscopy. The infrared spectra of **31**, **32**, and **35** display bands at ca. 690 and 520 cm^{-1} attributable to the C⎓C and H-C⎓C out-of-plane bends of the phenyl rings of the phosphine groups.[18] Strong bands at ca. 1050 cm^{-1} are due to the B-F stretch of the $[BF_4]^-$ groups. The absence of absorptions at higher wavenumbers (c.a. 2300 cm^{-1}) supports complete displacement of acetonitrile, but is not conclusive given that the frequency and intensity of the C≡N stretching vibration can be quite variable, and in some cases even be absent when coordinated nitrile is present.[18] The electronic spectra of **31** and **32** recorded in acetonitrile exhibit transitions attributable to the phenyl groups between 238 and 266 nm, and the TTF at 310-407. The overlap of certain features renders wavelength assignments difficult, and accounts for the absence of certain key transitions in **31** and **32**. Fourmigé and co-workers reported that the extinction coefficient, ε, for the phenyl chromophores in TTF-phosphines is approximately proportional to the number of phenyl groups in the molecule, where $\varepsilon = 2.5 \times 10^4$ is indicative of four phenyl rings.[8] Applying this value leads to an estimation of eight phenyl rings, or one P4 ligand for **30**, and two P4 units for **31**. In the case of **31**, such

a formulation would require dangling phosphines, but given the ^{31}P NMR spectrum this is not a possibility.

(iii) Magnetic Susceptibility and EPR Spectroscopic Studies of $[Co(P4)]_n[BF_4]_{2n}$ (33). Figure 43 shows the measured molar magnetic susceptibilities (χ), corrected for diamagnetisim, and the corresponding effective magnetic moment (μ_{eff}), from 5 to 320 K for $[Co(P4)]_n[BF_4]_{2n}$ (**33**). Studies revealed the magnetic susceptibility of **33** is similar to its mononuclear analog, $[Co(o\text{-}P2)_2][BF_4]_2$ (**9**). The μ_{eff} range of 5.00 μ_B at 320 K, to 2.05 μ_B at 5 K is in good agreement with a high-spin, S = 3/2 Co(II) molecule, with pseudo-octahedral geometry (see Chapter I).[19] The moment observed at higher temperatures is a result of the large spin-orbit coupling contribution to the expected μ_{eff} (spin-only) value of 3.87 μ_B. At temperatures below 20 K one populates the doubly-degenerate S = ½ ground.

EPR measurements of **33** were first carried out in CH_3CN/toluene (1:1) glasses at 121 K. Spectra of **33** display a broad signal at g = 2.21. This spectrum is similar to that observed for **9** in similar media, and suggests the metal center is a four-coordinate S = 1/2 molecule, a result that is in direct conflict with the observed magnetic moment in the solid state. In contrast to the spectra of **9**, compound **33** does not exhibit hyperfine splitting. These discrepancies between the solid state magnetic measurements and EPR spectra from solutions have yet to be resolved.

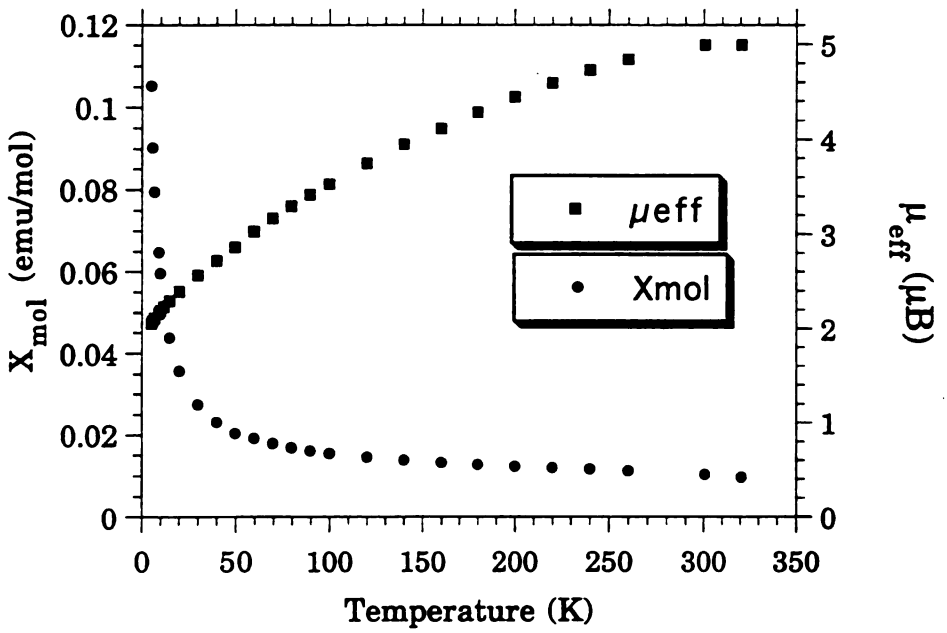

Figure 43. Plot of μ_{eff} (μ_B) and χ_{mol} (emu/mol) vs. temperature (K) of $[Co(P4)]_n[BF_4]_{2n}$ (**33**).

(iv) Electrochemistry of $[Rh(P4)]_n[BF_4]_n$ (30). Cyclic voltammetry data for **30** show two reversible oxidation couples at +0.76 and +1.12 V due to the accessible oxidations of the TTF moieties. Shifting of the couples by +0.30 and +0.21 V from the free P4 molcecule indicates strong interactions with the metal ions. These potentials are within the range that was found for $[Rh(o\text{-}P2)_2][BF_4]$ and $NiX_2(o\text{-}P2)$ (X = Cl, Br).[14,8] We note that the breadth of the signal may be a result of material depositing on the electrode surface. This problem has been observed for **31** and **32** also, and in those cases no well-defined couples were visible in the voltammograms. Another possibility is that communication between the TTF units results in the superposition of several oxidation couples. Electrochemical studies of the $[M(o\text{-}P2)_2]^{n+}$ series points to no communication of the phosphines through the metal, but the shorter bridging C-C double bond (C(1)-C(2)) in the structure of $Pt_2Cl_4(P4)$ (**22**) versus $PtCl_2(o\text{-}P2)$ (**20**) suggests that the electronic nature of the coordinated P4 ligand does not follow the same pattern.

(v) Fast Atom Bombardment Mass Spectrometry. Currently the most accurate method of determining molecular weight is Mass Spectrometry (MS). A problem which arises with MS is the high charge associated with these structures. For compounds such as **31-35** the charge is +2 for each metal center. In the gas phase, fragmentation occurs such that charges are generally minimized. Consequently, highly charged complexes are quite difficult to characterize.

Studies performed on $[Pd(P4)]_n[BF4]_{2n}$ (**32**) by Dr. John Allison and John Asara in conjunction with our laboratories reveal peaks attributable to the formation of polynuclear species.[15] The addition of triflic acid (HOTf) to the matrix/analyte allowed for the isolation of peaks representing $[Pd(P4)(OTf)]^+$ (m/z = 1194), $[Pd_2(P4)(OTf)_3]^+$ (m/z = 1601), $[Pd_3(P4)_3(OTf)_5]^+$ (m/z = 2945)]$^+$), $[Pd_3(P4)_3(CF_3\text{-}SO_3)_5]^+$ (m/z = 3890), and $[Pd_4(P4)_3(CF_3SO_3)_7]^+$ (m/z = 4294). Stang and coworkers are using triflate as a counterion for the FAB-MS characterization of a series of supermolecular inorganic structures with charges ranging from 4-8 by utilizing triflate as a counterion.[20] While the potential size of metal-P4 oligomers is too large to measure by standard FAB-MS techniques, new techniques such as Electrospray (ES) and Mass Assisted Laser Desorption Ionization (MALDI) MS may be useful for obtaining the parent ion peaks of extremely large inorganic species formed in solution by an extremely soft bombardment method.

(3) Proposed Cyclic Oligomers.

The appearance of only one signal in ^{31}P NMR spectra for **30-35** points to either a long chain polymer, where the number of bound phosphorus atoms outnumber the terminating phosphorus to such a high degree that the unbound signal is lost in spectrum baseline, or to the presence of a cyclic structure that renders all phosphorus environments equivalent. If one recalls the molecular structures of $[Rh(o\text{-}P2)_2][BF_4]$,[14] $[Ni(o\text{-}P2)_2][BF_4]_2$ (**8**), and $[Pt(o\text{-}P2)_2][BF_4]_2$ (**11**), all three contained out-of-plane bends between 27 and 32° at the bound dithiole ring of the TTF ligand. The bending occurs at

the sulfur positions closest to the metal bound phosphorus atoms. Given the angle of the deformations (~30°), and the extrapolation that bending occurs in both dithiole rings of the fully functionalized P4, the linking of six $[M(P4)]^{n+}$ units would result in a total bend for an "all-boat" conformation of 360°.

(i) Molecular Visualization. In order to visualize such a structure, the SPARTAN[21] program was used on a Silicon-Graphics workstation to minimize the "M(P4)" fragments using the SYBYL forcefield from Tripos, Inc.;[22] these were then used to build the $[Ni(P4)_6]^{12+}$ hexamer depicted in Figure 44. The resulting core measures an average distance of ~14 Å from hydrogen to hydrogen across the diameter. Although this is not a rigorous molecular mechanics analysis, the results suggest that the structure is possible on steric grounds.

(ii) Gel Permeation Chromatography. GPC is a common technique in organic polymer chemistry for establishing molecular weight distributions against a standard such as polystyrene.[23] The longer the retention time on the column, the smaller the size of the polymer chains. When the Rh compounds of *o*-P2 and P4 (**30**) were simultaneously passed down a GPC column, the elution time difference on the column was indiscernible (~ 20 min.). The low resolution indicated that the P4 complex is not in the range of the typical polymers that are separated on that column (>100,000 g/mole), and it also suggests that there is minimal difference between the *o*-P2 and P4 structures on a logometric scale of the column. In order to best utilize this

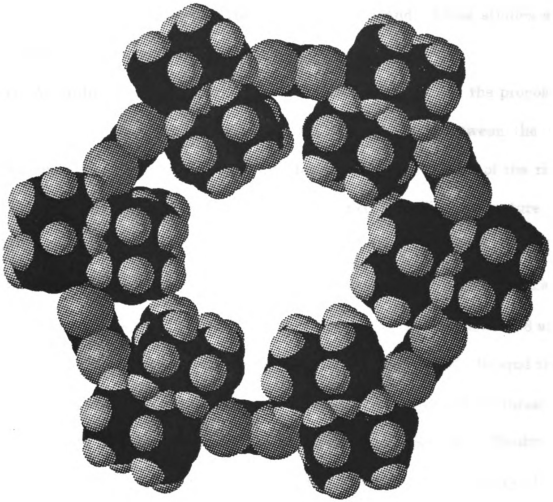

Figure 44. Molecular model of the proposed cyclic hexamer $[Ni(P4)_6]^{12+}$.

technique a column with greater resolution for low molecular weight polymers must be used. Although this will not give absolute molecular weights, the column can be calibrated with smaller arrays of known molecular weight that contain the P4 and/or P2 ligand. These studies are ongoing in our laboratories.

(iii) Variable Temperature ^{1}H NMR Spectrscopy. In the proposed cyclic oligomer structure, there is an expected difference between the ^{1}H NMR signals of the phenyl groups directed towards the interior of the ring and those on its exterior. To probe this diffference, variable temperature ^{1}H NMR measurements were made on $[Rh(P4)]_n[BF_4]_n$ (**30**), $[Pd(P4)]_n[BF_4]_{2n}$ (**32**), and $[Pt(P4)]_n[BF4]_{2n}$ (**31**). While **30** and **31** showed no significant changes to the spectra, **32** exhibited coalescence of two multiplets at 7.13 and 7.20 ppm (at 25 °C) to a broad resonance at 7.16 ppm at –35 °C. Beyond this change, the phenyl resonances remained broad and relatively featureless, limiting more detailed assignment of the spectra. Despite the difficulty in obtaining detailed information, the changes in the ^{1}H NMR spectra of **32** demonstrates that further studies are warranted.

B. Reactivity of $[Rh_2(NCCH_3)_{10}][BF_4]_4$ and $[Pd^{II}(NCCH_3)_6][BF_4]_2$ with excess P4.

In order to attempt end-group analysis on the $[BF_4]$- products, reactions were carried using excess P4 in the hopes that the additional ligands will cap metal terminated positions. This is the same procedure used

for the analysis of the tppb coordination polymers.[7] Reactions of $[Rh_2(NCCH_3)_{10}][BF_4]_4$ and $[Pd^{II}(NCCH_3)_6][BF_4]_2$ with excess P4 were carried out under identical conditions to the methods used for the synthesis of **30** and **32** in order to keep other experimental changes at a minimum. ^{31}P NMR spectral studies of the products reveal very different results for the two systems. The ^{31}P NMR spectrum of the product obtained from the reaction with Rh is identical to that of **30**, with the addition of a singlet at -18.2 due to free phosphine. This indicates that the use of a non-stoichiometric amount of ligand has no effect on the final product. Similar reactions with $Pd^{II}(NCCH_3)_6][BF_4]_2$ as the metal precursor produced a product(s) which exhibits three distinct singlets in its ^{31}P NMR spectrum. The signals at δ = 44.0 and 43.7 ppm are very near the observed signal in the spectrum of $[Pd(P4)]_n[BF_4]_{2n}$ (**32**) (44.2 ppm). The third signal is at much lower chemical shift values, near the expected position of free P4. This would indicate at least two different environments for coordinated phosphine, and supports the presence of end-capped phosphine at -17.1 ppm. Integration of the area under these peaks provides a roughly 2:1:2 ratio.

3. Concluding Remarks

Reactions between solvated precursors, such as $[Rh_2(NCCH_3)_{10}][BF_4]_4$ and $[M^{II}(NCCH_3)_n][BF_4]_2$ (M = Pt, n = 4; M = Pd, Co, Fe, Ni, n = 6), and the tetradentate TTF-phosphine ligand, P4 result in the formation of soluble products formulated as $[M(P4)]_n[BF_4]_{xn}$ (M = Rh, x = 1; M = Pt, Pd, Co, Fe,

Ni, x = 2). These complexes exhibit ^{31}P NMR spectra typical of a single environment for the phosphorus nuclei, with all phosphines being metal-bound. The appearance of one resonance at all temperatures points to either (1) the presence of an extremely high molecular weight polymer or (2) the adoption of a structure that places all of the P atoms in the same environment. One possible structure is the formation of cyclic oligiomers. Bends in the molecular structures of the mononuclear model compounds, $[M(o\text{-}P2)]_2[BF_4]_m$ (M = Rh, m = 1; M = Pt, Ni, m = 2), support this theory.

The preferred method for elucidating the molecular structure of the P4 complexes is single crystal X-ray diffraction. Unfortunately attempts to grow crystals of **30-35** have not been successful. Possible causes for this are the size of the cavity for the proposed hexamer, and the number of counterions associated with such a species. In order to grow crystals, a favorable packing situation must occur. The open cavity poses a problem due to the void space that must be filled in order to stabilize a the structure. The use of polyoxometallates such as $[TBA]_6[Mo_7O_{24}]$ could serve to pack this cavity, as well as to reduce the number of counterions required to balance the molecular cation. Preliminary studies indicate that addition of polyoxometallates to solutions of a typical P4 complex results in oxidation of the TTF unit. Such a reaction would be expected to lead to ring-opening due to forced planarity on at least one of the ligands. To circumvent this problem, other non-redox active anions are currently being investigated, including $[Fe(CN)_6]^{4-}$.

List of References

1. Gooding, R. D.; Lillya, C. P.; Chien, J. C. W. *J. Chem. Soc., Chem. Commun.* **1983**, 15.

2. Marks, T. J. *Angew. Chem., Int. Ed. Engl.* **1990**, *29*, 857.

3. Wang, P.-W.; Fox, M. A. *Inorg. Chem.* **1994**, *33*, 2938.

4. Reynolds, J. R.; Lillya, C. P.; Chien, J. C. W. *Macromolecules*, **1987**, *20*, 1184.

5. Wrobleski, J. T.; Brown, D. B. *Inorg. Chem.* **1979**, *18*, 2738.

6. Dirk, C. W.; Bousserau, M.; Barrett, P. H.; Moraes, F.; Wudl, F.; Heeger, A. J. *Macromolecules*, **1986**, *19*, 266.

7. Wang, P.-E.; Fox, M. A. *Inorg. Chem.* **1994**, *33*, 2945.

8. Fourmigué, M.; Batail, P. *Bull. Soc. Chim. Fr.* **1992**, *129*, 829.

9. Dunbar, K. R.; Pence, L. E. *Inorg. Synth.* **1992**, *29*, 182.

10. Dixon, N. E.; Lawrance, G. A.; Lay, P. A.; Sargeson, A. M.; Taube, H. *Inorg. Chem.* **1984** *23* 2940.

11. Hathaway, B. J.; Holah, D. G.; Underhill, A. E., *J. Chem. Soc.*, **1962**, 2444.

12. Thomas, R. R.; Sen, A., *Inorg. Synth.*, **1989**, *26*, 128.

13. DeRenzi, A.; Panunzi, A.; Vitagliano, A., *J. Chem. Soc., Chem. Commun.*, **1976**, 47.

14. Fourmigué, M.; Uzelmeier, C. E.; Boubekeur, K.; Bartley, S. L.; Dunbar, K. R., *J. Organomet. Chem.*, **1997**, *529*, 343.

15. Asara, J. M.; Uzelmeier, C. E.; Dunbar, K. R.; Allison, J. *Inorg. Chem.*, **1998**, *37*, 1833.

16. Carlin, R. L.; van Duyneveldt, A. J. *Magnetic Properties of Transition Metal Compounds*, Springer: New York, **1977**.

17. (a) Honeychuck, R. V.; Hersh, W. H. *Inorg. Chem.* **1987**, ***26***, 1826. (b) Honeychuck, R. V.; Hersh, W. H. *Inorg. Chem.* **1989**, *28*, 2869. (c) Lundquist, E. G.; Folting, K.; Hoffman, J. C.; Caulton, K. G. *Organometallics*, **1990**, *9*, 2254. (d) Fernandez, J. M.; Gladysz, J. A. *Inorg. Chem.*, **1986**, *25*, 2672.

18. Silverstein, R. M.; Bassler, G. C.; Morrill, T. C. *Spectrometric Identification of Organic Compounds, 4th Ed.* John Wiley & Sons: **1981.**

19. Johnson, A.; Taube, H., *J. Indian. Chem. Soc.*, **1989, *66***, 503.

20. Whteford, J. A.; Rachlin, E. M.; Stang, P. J. *Angew. Chem., Int. Ed. Engl.* **1996**, *35*, 2524.

21. SPARTAN 5.0, Wavefunction Inc., 18401 Von Karman Ave., Suite 370, Irvine, CA. 92612, USA.

22. SYBYL 6.4, Tripos Inc., 1699 South Hanley Road, St. Louis, MO, 63144, USA.

23. (a) Peckham, T. J.; Massey, J. A.; Edwards. M.; Manners, I.; Fousher, D. A. *Macromolecules*, **1996**, *29*, 2396. (b) Wood, B. R.; Semlya, J. A.; Hodge, P. *Polymer*, **1996**, *38*, 191

CHAPTER VII

CONCLUSION

The results presented in this dissertation establish the use of tris(2,4,6-trimethoxyphenyl)phosphine as an excellent supporting ligand for the stabilization of various metal complexes. The mononuclear Rh(I) complex, $[Rh(\eta^2\text{-TMPP})_2][BF_4]$ (**3**) was prepared from the reaction of the Rh(II) species $[Rh(\eta^3\text{-TMPP})_2][BF_4]_2$ with $CoCp_2$ in the presence of a methylating agent. The formation of **3** marks the first such series of homoleptic-phosphine complexes that spans three oxidation states, namely Rh (I, II, III). Dealkylation of **3** by addition of a nucleophile results in the formation of the unstable neutral species, Rh^I(TMPP)(TMPP-*O*) (**4**). Although considered sterically bulky, the TMPP ligand is quite flexible as evidenced by the variety of fluxional and isomerization processes that have been observed for its metal complexes.[1] The ability to change coordination modes makes it possible to access different oxidation states of a metal center while maintaining the same ligand set. At room temperature, solutions of **3** and **4** decompose to $[Rh^{III}$(TMPP)(TMPP-*O*)$][BF_4]_2$ and *ax,ax*-$[Rh^{III}$(TMPP-*O*$)_2][BF_4]$. The chemical relationship between the known rhodium-TMPP complexes studied in our laboratories is illustrated in Figure 14. Rather than forcing a particular geometry on the metal center, the ligand adjusts to the available coordination sites and the electronic requirements of the metal center. This ability is readily apparent when one examines geometry changes in going from Rh(I) to Rh(II) in the structure of $[Rh^I(\eta^2\text{-TMPP})_2][BF_4]\bullet[Rh^{II}(\eta^3\text{-TMPP}][BF_4]_2$ (**3**•$[Rh^{II}(\eta^3\text{-TMPP}][BF_4]_2$).

The combination of both hard and soft donor groups in a phosphine ligand leads to an ability to stabilize a metal atom in a variety of coordination geometries and oxidation states. The availability of *cis*-disposed phenoxide groups on Co(TMPP-*O*)$_2$ renders it able to act as an inorganic "ligand," as has been shown in the stabilization of the bimetallic complexes Cl_2Co(TMPP-*O*)$_2$ and Cl_2MnCo(TMPP-*O*)$_2$.[1d] The formation of the hexanuclear cluster, $[Co^{II}\mu^3OH)(\mu\text{-}OH)_3\{Co^{II}\text{-}\eta^3TMPP\text{-}O)_2\}_3][BF_4]_2$ serves as additional evidence for the use of Co(TMPP-*O*)$_2$ as a "synthon" for the preparation of polynuclear metallic complexes.

The functionalization of TTF with phosphine groups has been shown to be an excellent route into the synthesis of "hybrid" inorganic/organic compounds.[2] The preparation of $[M(o\text{-}P2)_2][BF_4]_2$ (Ni, Co, Pd, Pt, Fe), from the reaction of the appropriate fully-solvated precursor with *ortho*-$Me_2(PPh_2)_2TTF$ (*o*-P2) demonstrates the ability of these phosphines to coordinate to a host of different transition metals. Each of the complexes described in this study exhibit electrochemically accessible redox processes associated with both the TTF and the metal center. The molecular structures of members of this series show deformations in the TTF unit, which serves to allow for intermolecular interactions of ~3.5 Å between the TTF moieties of neighboring molecules. The result is a one-dimensional arrangement. The accessibility of the TTF oxidation pathway has been demonstrated by chemical oxidation of $[Rh^I(o\text{-}P2)_2][BF_4]$. The stabilization of $[Co^{II}(o$-

P2)$_2$][BF_4]$_2$ illustrates the potential for incorporating a paramagnetic center with the organic donor molecule. The salt, [$ReCl_2$(*o*-P2)$_2$][Re_2Cl_6(*o*-P2)] (**16•17**), contains the first documented dinuclear complex of the formula, α-M_2X_6(LL) (where LL is a chelating, bidentate ligand), and serves as evidence for an intermediate mixed-valence redox state in the formation of α-Re_2Cl_4(L-L)$_2$ compounds. Further study in the regime of metal-metal bonded chemistry is needed to determine whether a bridging mode (β) for *o*-P2 will be possible. The ethylene bridge of *o*-P2 renders it similar to the skeleton of the dppee and dppb ligands. The ethene derivative has been shown to engage in both α- and β- type coordination,[3] but to date the dppb has only been reported in the α- mode.[4] This may be a result of the restrictions placed on the ethene linkage by ring cyclization. If this is the case, similar problems would be expected for *o*-P2.

Systematic build-up of extended arrays has been achieved from reactions of *o*-P2 and (PPh_2)$_4$TTF (P4) with MCl_2(NCC_6H_5)$_2$ (M = Pt, Pd) and $NiCl_2$. The incorporation of halide atoms as terminating ligands allows for access to open coordination sites by abstraction of $[Cl]^-$ with $[Ag]^+$. The resulting solvated sites can then be replaced with additional phosphine groups to yield, for example, [Pt_2(P4)(*o*-P2)$_2$][BF_4]$_4$ (**24**). It is of interest to extend this series to Co and Mn analogs because incorporation of two paramagnetic metal centers with up to three TTF units leads to the possibility for forming complexes with 9 unpaired electrond for [(o-

P2)Co(P4)Co(o-P2)]$^{7+}$ and 13 unpaired electrons for the Mn^{II} derivative. The observation that the TTF cores in $[M(o\text{-}P2)_2][BF_4]_2$ act as isolated redox systems provides the basis for expecting molecules with a large number of unpaired electrons. The reaction of P4 with $[M(NCCH_3)_x][BF_4]_2$ (M = Pt, x = 4; M = Ni, Co, Pd, Fe, x = 6) or $[Rh_2(NCCH_3)_{10}][BF_4]_4$ results in the spontaneous assembly of compounds formulated as $[M(P4)]_n[BF_4]_{2n}$ or $[Rh(P4)]_n[BF_4]_n$. The $^{31}P\{^1H\}$ NMR spectral properties of these complexes are not in accord with straight chain oligomers. Resonances are observed for only metal-bound phosphorus environments with no end groups being detected. By using the *bis*-(*o*-P2) complexes as structural models for the analogous P4 compounds, it can be surmised that deformations in the neutral-TTF cores are also occurring in solution. Based on this hypothesis, one proposed structure type that is being considered is a cyclic oligomer. While the cyclized structure is a possibility for neutral TTF cores, oxidation of the units will result in strict planarity, thereby eliminating the potential for ring formation. If so, the reaction of $[P4]^{\cdot+}$ with the solvated precursors offers the potential for forming long chain polymers which may exhibit interesting magnetic properties by themselves, but with the additional possibility for conductive properties upon the incorporation of $[TCNQ]^{\cdot-}$ as the counterion.

List of References

1. (a) Dunbar, K. R.; Quillevéré, A.; Sun, J.-S. *Inorg. Chem.*, **1994**, *33*, 2598. (b) Dunbar, K. R.; Sun, J.-S. *J. Chem. Soc. Chem. Comm.*, **1994**, *2387*. (c) Sun, J.-J.; Uzelmeier, C. E.; Ward, D. L.; Dunbar, K. R. *Polyhedron*, **1998** in press. (d) Quillevéré, A.; Uzelmeier, C. E.; Sun, J.-J.; Dunbar, K. R. manuscript in preparation. (e) Haefner, S. C.; Uzelmeier, C. E.; Dunbar, K. R. manuscript in preparation.

2. (a) Fourmigué, M.; Batail, P. *Bull. Soc. Chim. Fr.* **1992**, *129*, 829. (b) Fourmigué, M.; Uzelmeier, C. E.; Boubekeur, K.; Bartley, S. L.; Dunbar, K. R. *J. Organomet. Chem.*, **1997**, *529*, 343. (c) Asara, J. M.; Uzelmeier, C. E.; Dunbar, K. R.; Allison, J., *Inorg. Chem.*, **1998**, in press.

3. Anderson, L. B.; Bakir, M.; Fanwick, P. E.; Walton, R. A. *Polyhedron*, **1987**, *6*, 1483.

4. Esjornson, D.; Bakir, M.; Fanwick, P. E.; Jone, K. S.; Walton, R. A. *Inorg. Chem.*, **1990**, *29*, 2055.

APPENDICES

APPENDIX A

PHYSICAL MEASUREMENTS

APPENDIX A

PHYSICAL MEASUREMENTS

1. Infrared Spectroscopy Infrared spectra in the 4800-400 cm^{-1} range were recorded on a Nicolet 740 FT-IR spectrophotometer. Spectra in the far-IR range (600-50 cm^{-1}) were recorded on a computer controlled Nicolet 750 FT-IR spectrophotometer equipped with a TGS/PE detector and silicon beam splitter at 2.0 or 4.0 cm^{-1} resolution. Solid state spectra were measured as Nujol mulls between CsI plates.

2. NMR Spectroscopy ^{1}H NMR spectra were measured on either a Gemini 300-MHz, Varian 300-MHz or Varian 500-MHz spectrometer. Chemical shifts were referenced relative to the residual proton impurity of the deuterated solvent: d_2-methylene chloride, 5.32 ppm; d_3-acetonitrile, 1.93 ppm; d_6-acetone, 2.04 ppm; d_1-chloroform, 7.24. $^{13}C\{^{1}H\}$ NMR spectra were recorded on a Varian 300-MHz spectrometer operating at 75.43 MHz or on a Varian 500-MHz spectrometer operating at 125.72 MHz. Signals were referenced relative to the ^{13}C solvent resonance. ^{19}F NMR spectra were recorded on a Varian 300-MHz spectrometer operating at 282.23 MHz. Signals were referenced relative to an external standard of trifluorotoluene. $^{31}P\{^{1}H\}$ NMR spectra were obtained on a Varian 300-MHz spectrometer operating at 121.42 MHz or on a Varian 500-MHz spectrometer operating at 202.37-MHz. Chemical shifts were referenced relative to an external

standard of 85% H_3PO_4. Positive chemical shifts are reported downfield relative to H_3PO_4.

3. EPR Spectroscopy X-band EPR spectra at temperatures above 90 K were obtained using a Varian E4 spectrometer. Spectra below 90 K were measured on a Bruker ES-300-E spectrometer equipped with an Oxford Instruments EPR-900 Continuous Flow Cryostat.

4. Electronic Absorption Spectroscopy Electronic absorption spectra were measured on a Hitachi U-2000 spectrophotometer.

5. Electrochemistry Electrochemical measurements were performed by using an EG&G Princeton Applied Research Model 362 scanning potentiostat in conjunction with a BAS Model RXY recorder. Cyclic voltammetric experiments were carried out at 22±2°C using 0.1 M tetra-*n*-butylammonium tetrafluoroborate ($TBABF_4$) as a supporting electrolyte, unless otherwise noted. Measurements were typically made at a scan rate of 200 mV/s using a platinum disk working electrode and a Ag/AgCl reference electrode. $E_{1/2}$ values, determined as $(E_{p,a}+E_{p,c})/2$, were referenced to a Ag/AgCl electrode and are uncorrected for junction potentials.

6. Magnetic Susceptibility Variable temperature and field magnetic susceptibility measurements were carried out on a Quantum Design model MPMS Superconducting Quantum Interference Device (SQUID) housed in the Physics and Astronomy Department at Michigan State University. The operating field was typically 1000 G and the temperature range 2 - 300 K.

7. **Mass Spectrometry** Fast Atom Bombardment (FAB) mass spectrometry studies were performed on a JEOL HX double-focusing mass spectrometer housed at the National Institutes of Health / Michigan State University Mass Spectrometry Facility.

8. **Elemental Analysis** Elemental analyses were performed at either Galbraith Laboratories, Inc., or Desert Analytics, Tucson, AZ.

APPENDIX B

STRUCTURAL ANALYSIS OF FUNCTIONALIZED TETRATHIAFULVALENES

APPENDIX B

STRUCTURAL ANALYSIS OF FUNCTIONALIZED TETRATHIAFULVALENES

1. Introduction

Organic molecules such as tetrathiafulvalene (TTF) and its derivatives are important precursors in the design of new conducting, optical and magnetic materials. These planar molecules can be readily oxidized to yield radical cations which, when associated with suitable electron acceptors such as 7,7,8,8-tetracyanoquinodimethane (TCNQ), form segregated stacks that allow for electrical conductivity due to the overlap of their π-orbitals.[1] These donor molecules have also been observed to form donor-acceptor salts with large metal-based cluster anions that exhibit remarkably variable properties, differences that are attributed to the size and shape of the organic donor and inorganic acceptors, as well as their redox properties. The magnetic and conductive properties of these salts are highly dependent on subtle changes in the packing of these structures in the solid state.[2] The discovery of a new, less stable, polymorph of TTF which crystallizes in what has been characterized as "chains", rather than stacks, indicates that interactions that are singled out as "important" or "dominant" may vary.[3] Recently, Fourmigué and Batail have shown that unsymmetrical methyl-TTF derivatives such as 3,4-dimethyltetrathiafulvalene can be used to prepare a

series of multidentate TTF-phosphine ligands, including 3,4-dimethyl-3'4'-bis(diphenylphosphino)tetrathiafulvalene (**1**).[4] The structures of **1**, **2**, and **36** have been undertaken in order to compare the geometrical features with those of related TTF derivatives and structures of the *ortho*-P2 ligand and its metal complexes.[5]

2. Experimental

A. X-ray Crystallography

(1) *ortho*-$(CH_3)_2$TTF (36)

(i) Preparation, Data Collection and Reduction. The synthesis of (**36**) was carried out according to methods previously published by Lerstrup, Johannsen and Jørgensen.[6] Crystals were obtained by dissolving the product in a minimum volume of hot toluene, allowing the solution to slowly cool to room temperature, followed by chilling at 258 K for 12 hours. An orange crystal of dimensions 0.68 x 0.60 x 0.29 mm^3 was secured on the tip of a glass fiber with Dow Corning silicone grease and placed in a cold N_2(g) stream. Least-squares refinement using 24 well-centered reflections in the range $4 \leq 2\theta \leq 24°$ indicated that the crystal was consistent with a monoclinic crystal system. The data were collected at -110 ± 1 °C using the ω-2θ scan technique to a maximum 2θ value of 47°. Of the 2950 measured reflections, 1481 were independent. An empirical absorption correction based on azimuthal scans of three reflections with χ near 90° was applied which resulted in transmission

factors ranging from 0.770 - 0.543. The data were corrected for Lorentz and polarization effects.

(ii) Structure Solution and Refinement. The structure was solved in the space group $P2_1/n$ using the MITHRIL[7] and SHELXL 93[8] structure solution programs and refined by full-matrix least-squares refinement on F^2.[9] The final full-matrix least-squares refinement was based on 1481 reflections that were used to fit 118 parameters to give R1 = 0.0354 and wR2 = 0.0851. The goodness-of-fit index was 1.068, and the maximum shift in the final difference map was 0.000 Å associated with H(7B). After the final least squares cycle, the mean shift/esd was 0.000 and the highest peak in the difference Fourier map was 0.32 $e^-/Å^3$ which is associated with C(3). All non-hydrogen atoms were refined with anisotropic displacement parameters. Methyl and aromatic hydrogen atoms were placed in calculated positions.

(2) *ortho*-$(CH_3)_2[(C_6H_5)_2P]_2TTF$ (1)

(i) Preparation, Data Collection and Reduction. Compound **1** was prepared by following the procedure outlined by Fourmigué and Batail *et al.*[2] Crystals were obtained by concentration, of a solution of **1** in a mixture of acetonitrile and toluene. An orange crystal of dimensions 0.12 x 0.12 x 0.23 mm^3 was secured on the tip of a glass fiber with Dow Corning silicone grease and placed in a cold $N_2(g)$ stream. Least-squares refinement using 12 well-centered reflections in the range $6 \leq 2\theta \leq 19°$ indicated that the crystal was consistent with a monoclinic crystal system. The data were collected at -110

± 1 °C using the ω-2θ scan technique to a maximum 2θ value of 50°. Of the 5477 measured reflections, 5201 were independent and 933 were found with I>2σ(I). An empirical absorption correction based on azimuthal scans of two reflections with χ near 90° was applied which resulted in transmission factors ranging from 1.00 - 0.412. The data were corrected for Lorentz and polarization effects.

(ii) Structure Solution and Refinement. The structure was solved in the space group $P2_1/c$ using the MITHRIL[7] and SHELXL 93[8] structure solution programs and refined by full-matrix least-squares refinement on F^2.[9] R(int) and R(σ) were determined to be 0.273 and 0.755, respectively. All non-hydrogen atoms were refined with anisotropic displacement parameters. Methyl and aromatic hydrogen atoms were placed in calculated positions and were not refined. Phenyl groups were restrained with C=C distances of 1.39 Å and C-C-C angles of 120.0°, and C(5)-C(7) and C(6-C(8) distances were refined to be equivalent, resulting in distances of 1.49(2) Å for C(5)-C(7) and 1.48(2) Å for C(6)-C(8). The final full-matrix least-squares refinement is based on 5183 reflections that are used to fit 297 parameters to give R1 = 0.0974 and wR2 = 0.2284. The goodness-of-fit index was 0.990, and the maximum shift in the final difference map was 0.070 Å, which is associated with H(7C). After the final least squares cycle, the mean shift/esd was 0.030 and the highest peak in the difference Fourier map was 0.58 $e^-/Å^3$ which is associated with S(4).

(3) [(C_6H_5)

(i) **Prepar**

was carried

al.[5b] Cryst

of hot tolu

temperatur

secured on

placed in

centered re

consistent

°C using th

measured

empirical a

with χ near

from 1.000

effects.

(ii) **Stru**

the space gr

programs a

and $R(\sigma)$ we

matrix leas

used to fit

(3) $[(C_6H_5)_2P]_4TTF$ (2)

(i) Preparation, Data Collection and Reduction. The preparation of 2 was carried out according to methods previously published by Fourmigué *et al.*[5b] Crystals were obtained by dissolving the product in a minimum volume of hot toluene and then allowing the solution to slowly cool to room temperature. An orange crystal of dimensions 0.42 x 0.39 x 0.29 mm^3 was secured on the tip of a glass fiber with Dow Corning silicone grease and placed in a cold N_2(g) stream. Least-squares refinement using 20 well-centered reflections in the range $6 \leq 2\theta \leq 16°$ indicated that the crystal was consistent with a triclinic crystal system. The data were collected at -110 ± 1 °C using the ω-2θ scan technique to a maximum 2θ value of 55°. Of the 4683 measured reflections, 2277 were found to be greater than $3\sigma(I)$. An empirical absorption correction based on azimuthal scans of three reflections with χ near 90° was applied which resulted in transmission factors ranging from 1.000 - 0.487. The data were corrected for Lorentz and polarization effects.

(ii) Structure Solution and Refinement. The structure was solved in the space group P-1 using the MITHRIL[7] and SHELXL 93[8] structure solution programs and refined by full-matrix least-squares refinement on F^2.[9] R(int) and R(σ) were determined to be 0.00 and 0.116, respectively. The final full-matrix least-squares refinement was based on 4683 reflections that were used to fit 438 parameters to give R1 = 0.0945 and wR2 = 0.2417. The

Table 18. Crystallographic Data for *ortho*-$(CH_3)_2$TTF (**36**), *ortho*-$(CH_3)_2[(C_6H_5)_2P]_2$TTF (**1**), and $[(C_6H_5)_2P]_4$TTF • toluene, (**2**) • toluene.

	36	**1**	**2 • C_7H_8**
Formula	$C_{85}H_8S_4$	$P_2C_{32}H_{26}S_4$	$P_4C_{68}H_{56}S_4$
Space group	P21/n	P21/n	P-1
a, Å	7.425(2)	11.387(15)	9552(8)
b, Å	9.568(3)	21.488(5)	12.077(11)
c, Å	14.035(4)	12.541(8)	12.442(9)
α, deg	90.00	90.10(4)	75.46(7)
β, deg	97.13(2)	105.42(7)	71.70(6)
γ, deg	90.00	90.11(6)	84.32(7)
V, Å^3	989.3(5)	2958(4)	1319(2)
Z	4	4	1
Data col. range, 2θ, deg.	4- 47	4 - 50	4 - 55
No. unique data,	1481	5201	4683
total with $F_o^2>3\sigma(F_o^2)$	1188	935	2716
R1[a]	0.035	0.097	0.095
wR2[b]	0.085	0.284	0.242
Quality-of-fit indicator	1.07	0.99	1.04

[a] $R = \Sigma||F_o| - |F_c||/\Sigma|F_o|$. ; [b] $wR2 = [\Sigma w|F_o| - |F_c|)^2/\Sigma w|F_o|^2]^{1/2}$; $w = 1/\sigma^2(|F_o|)$.

goodness-of-fit index was 1.037, and the maximum shift in the final difference map was 0.031 Å associated with H(52). After the final least squares cycle, the mean shift/esd was 0.019 and the highest peak in the difference Fourier map was 1.05 $e^-/Å^3$ which is associated with C(31). All non-hydrogen atoms were refined with anisotropic displacement parameters. Methyl and aromatic hydrogen atoms were placed in calculated positions. A molecule of toluene was found to reside on a center of inversion. The toluene was modeled with restraints on the C-C distances within the ring, as well as on the C···C distances between alternating C atoms of the ring (e.g. C(54)···C(52)). Occupancies were refined such that the two independent toluene fragments were assigned an occupancy of 0.5 for a total of 1.0.

2. Results and Discussion

A. Molecular Structure of *ortho*-$(CH_3)_2$TTF (36)

ORTEP drawings of *ortho*-$(CH_3)_2$TTF (**36**) are represented in Figure 45, while a packing diagram of **36** can be found in Figure 46. Selected bond distances and angles are provided in Table 19. The central core [S(1)-S(2)-C(3)-C(4)-S(4)-S(3)] of the title molecule is nearly planar with a maximum deviation of 0.016(2)° for C(3), and a RMS deviation of 0.001. The dihedral angles between planes C(5)-C(6)-S(4)-S(5) and S(3)-S(4)-C(4)-C(3)-S(1)-S(2) is 0.60(13)°, while the angle between planes C(1)-C(2)-S(2)-S(1) and S(1)-S(2)-C(3)-C(4)-S(4)-S(3) is 1.88(16)°. This is in contrast to the analogous dihedral angles in the neutral and cationic TTF crystal structures, where both

Table 19.

At
C
C
C
C
C
C
C
C
P
P

At
C(
S(
S(
C(
S(
P(
C(
P(

Table 19. Selected bond distances (Å) and Angles (deg.) for *ortho*-$(CH_3)_2$TTF (**36**) and *ortho*-$(CH_3)_2[(C_6H_5)_2P]_2$TTF (**1**).

Atom 1	Atom 2		36	1
C(1)	C(2)		1.308(5)	1.35(3)
C(3)	C(4)		1.340(4)	1.38(3)
C(5)	C(6)		1.338(4)	1.37(3)
C(5)	C(7)		1.500(5)	1.49(3)
C(1)	S(1)		1.743(4)	1.71(2)
C(3)	S(1)		1.765(3)	1.77(2)
C(5)	S(3)		1.755(3)	1.77(2)
C(4)	S(3)		1.753(3)	1.73(2)
P(1)	C(1)			1.88(2)
P(1)	C(11)			1.840(13)
Atom 1	**Atom 2**	**Atom 3**	**36**	**1**
C(1)	S(1)	C(3)	94.42(17)	94.8(10)
S(1)	C(3)	S(2)	114.27(17)	115.2(12)
S(3)	C(4)	S(4)	113.89(17)	114.1(15)
C(5)	S(3)	C(4)	96.14(15)	94.4(13)
S(3)	C(5)	C(6)	127.0(3)	114.0(15)
P(1)	C(1)	C(2)	119.0(15)	
C(1)	P(1)	C(11)	100.7(8)	
P(1)	C(11)	C(12)	122.7(9)	

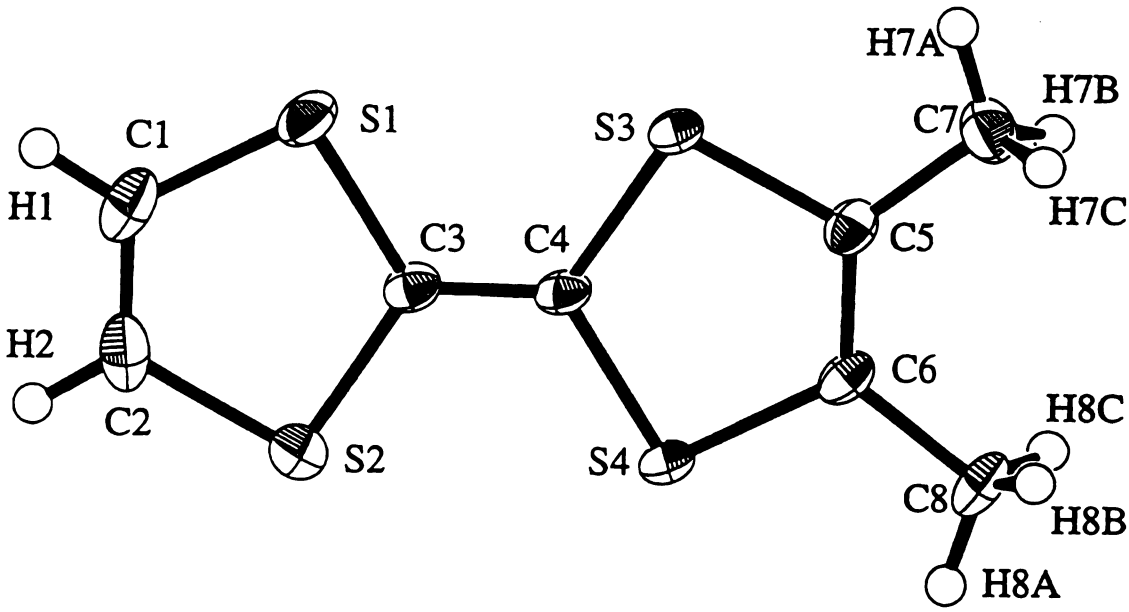

Figure 45. ORTEP representation of *ortho*-$(CH_3)_2$TTF **(36)** with 50% ellipsoids.

fulvalene rings exhibit the same out-of-plane-bend. For the neutral tetrathiafulvalene the value is 2.1° for both 5-membered rings,[10] whereas for cationic TTF the corresponding dihedral angles between the planes are 2.2°.[11] Bond distances and angles within the TTF-core of **36** are comparable to other TTF molecules. The C=C bond at the center of the molecule is 1.340(4) Å, and S···S distances within the molecule are 2.967(2) Å for S(1)···S(2) and 2.945(1) Å for S(3)···S(4). It should be noted that this value for the central C=C distance is equivalent to the neutral TTF (1.349(3) Å), but shorter than that found in the cationic TTF (1.369(4) Å). The bond lengths of the external carbons in **36** are 1.308(5) Å for C(1)=C(2) and 1.338(4) Å for C(5)=C(6). This lengthening of C(5)=C(6) renders it indistinguishable from C(3)=C(4). Another manifestation of the presence of methyl substituents is differences in the S···C distances. The 5-membered ring that contains the methyl groups exhibit S···C distances that are essentially all equivalent, but on the opposite side of the molecule, the sulfur to bridging-carbon distances are longer than the sulfur to exterior-carbon bond lengths by 0.024 (4) Å.

Typically, neutral TTF stacks in a parallel orientation to the b axis with intermolecular S···S contacts of 3.62 Å; the TTF cation in TTF-TCNQ also stacks parallel to the b axis, but with a much shorter TTF···TTF distance of 3.47 Å.[11] In contrast, **36** "dimerizes" into stacked pairs. These pairs (TTF-TTF'; symmetry code (') 1-x,-y,-z) pack with significantly longer intermolecular contacts of 3.932(2) Å, and furthermore align themselves in

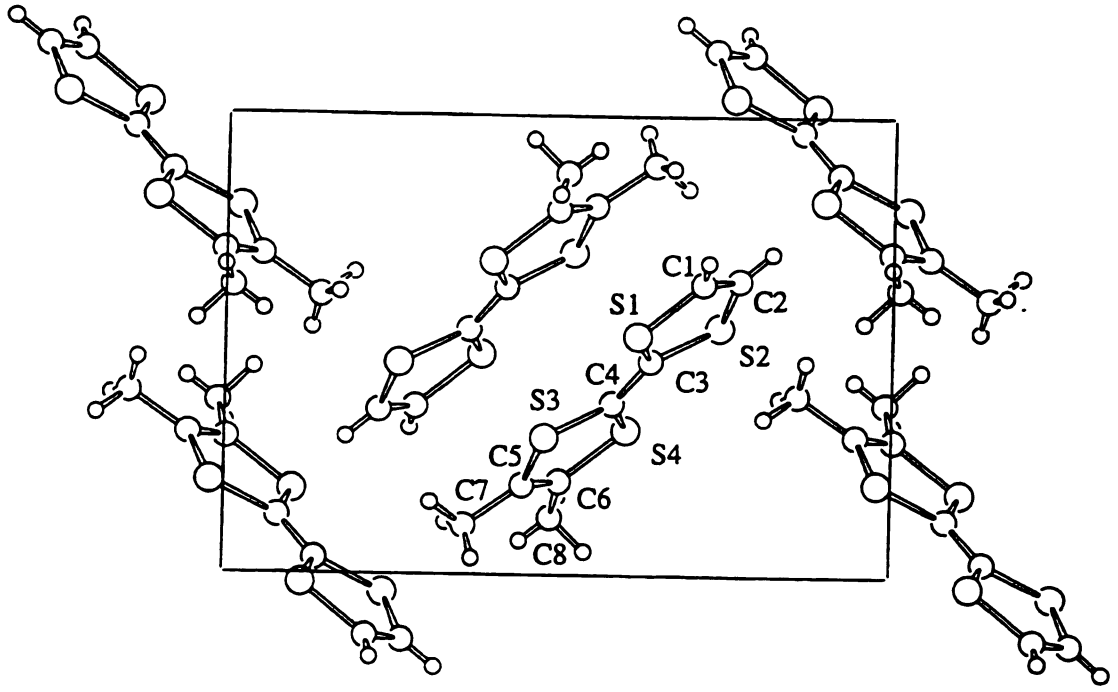

Figure 46. Packing diagram of *ortho*-$(CH_3)_2$TTF (**36**) viewed down the a-axis.

ahead-to-tail fashion, as clearly indicated in the packing diagram depicted in Figure 46. This distance is significantly greater than twice the van der Waals radius of sulfur (3.6 Å).[13] Adjacent pairs are approximately perpendicular to each other, with a dihedral angle of 83.03(4)° [between planes S(1)-S(2)-C(3)-C(4)-S(4)-S(3) and S(1)"-S(2)"-C(3)"-C(4)"-S(4)"-S(3)"; symmetry code (") 0.5-x,-0.5+y,-0.5-z]. This orientation results in one of the hydrogens, H(2), of the unsubstituted fulvalene ring system for each molecule pointing towards the $S(4)^{ii}$ p-orbital of a molecule in an adjacent pair. The C(2)···S(4)" intermolecular distance is 4.46(1) Å, which is greater than the sum of the van der Waals radii of carbon and sulfur (3.55 Å), indicating no significant interaction is present.

B. Molecular Structure of *ortho*-$(CH_3)_2[(C_6H_5)_2P]_2TTF$ (1)

A PLUTO drawing of *ortho*-$(CH_3)_2[(C_6H_5)_2P]_2TTF$ (**1**) is represented in Figure 47, and a packing diagram is in Figure 48. Selected bond distances and angles are provided in Table 19. Due to the poor refinement of **1**, high esd values associated with the bond distances and angles of the structure make accurate comparisons to **36** difficult. There are, however, certain differences that are worth pointing out. Bond distances and angles within the fulvalene rings of **1** remain similar to those observed in **36**.[12] Most notable is the lengthening of C(5)=C(6) [1.37(3) Å], making it nearly equal to C(3)=C(4) [1.38(3) Å]. This is the same effect caused by the addition of methyl rings in **36**. It is interesting to note that there appears to be very

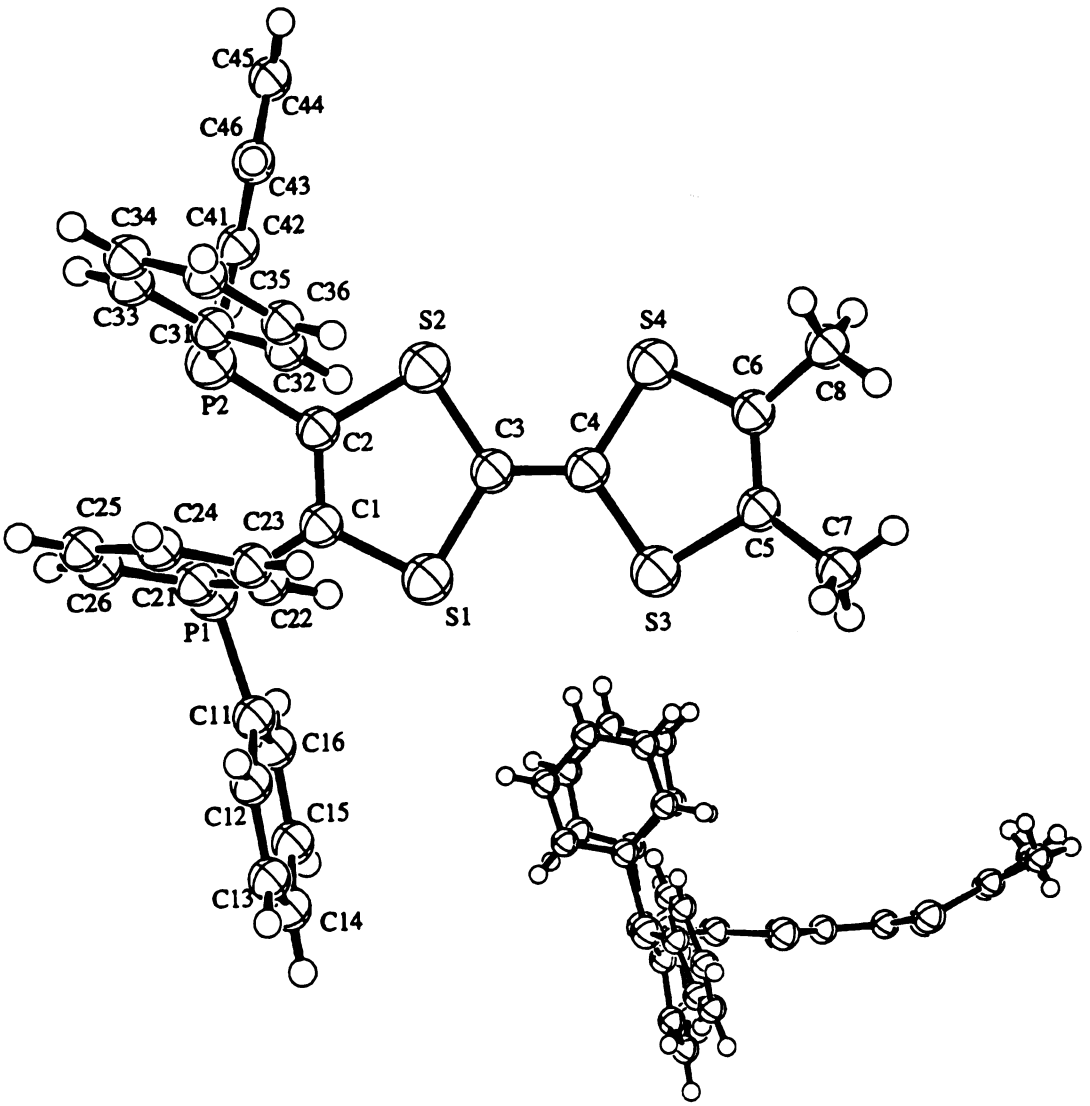

Figure 47. PLUTO diagram of *ortho*-$(CH_3)_2[(C_6H_5)_2P]_2TTF$ (1) with inset side view.

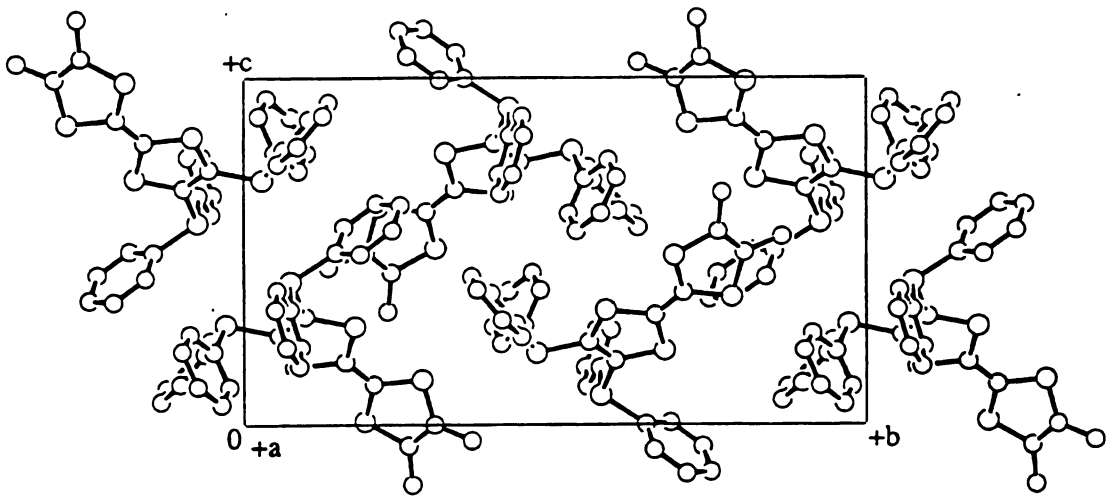

Figure 48. Packing diagram of *ortho*-$(CH_3)_2[(C_6H_5)_2P]_2TTF$ (**1**) viewed down the a-axis.

little affect on the other ring system due to the presence of the phosphine substituents. The C(1)=C(2) distance of 1.35(3) Å is ~.0.03 Å shorter than the other C=C bonds in **1**, just as the unsubstituted C=C bond in **36** is ~0.03 Å shorter than the central C=C bond and the C=C bond containing the methyl substituents. At first glance the C=C distances all appear to be elongated in **1** relative to **36**, but that may be an artifact of the poor refinement. The geometry about the phosphorus atoms is that of the unusual distorted tetrahedron, with angles of 100.7 (8) - 104.9(9)°, and average P-C distances of ~1.837 Å about P(1) and ~1.864 Å about P(2).

The most notable difference between the molecular structures of **1** and **36** is the out-of-plane bend located at S(3) and S(4) of the methylated dithiole ring. The dihedral angles between planes [C(5)-C(6)-S(4)-S(3)] and [S(1)-S(2)-C(3)-C(4)-S(3)-S(4)] is 23.0(7)°, while the angle between planes C(1)-C(2)-S(2)-S(1) and S(1)-S(2)-C(3)-C(4)-S(4)-S(3) is 7.9(6)°. While both these values are certainly larger than those observed in the precursor compound, **36**, the methylated ring is the more distinct in its deviation from planarity. Given the TTF core is neutral in the case of **1**, it is not surprising that the fulvalene rings are non-planar, but it is quite different than what has been seen in the previously structurally characterized metal complexes containing *trans*-phosphines. In all other bis-(*o*-P2) structures, the out-of-plane bend occurrs at the sulfur positions in the ring containing the phosphines, with the methylated ring exhibiting a much smaller bend. While the driving force for the bend in the metal complexes may be able to achieve the close

intermolecular S···S contacts, there are no such interactions in the structure of **1**. The packing diagram **1**, shown in Figure 48, reveals a motif where steric interactions serve to isolate the individual molecules from one another. The bend in the methyl-substituted dithiole ring appears to be due to its proximity to the phenyl rings of the adjacent *o*-P2 molecule. This packing arrangement results in the closest intermolecular S···S distance being 5.17 Å.

Apart from the location of the out-of-plane bend, the structure of **1** is very similar to the metal-ligand complexes previously discussed.[4,5] As expected, the P(1)-C(1) of **1** is longer in the free ligand than in the metal complexes by as much as ~0.11 Å {$[Rh(o\text{-}P2)_2][BF_4]$}.[5b] The C=C distances within the TTF core are all generally smaller than those in **1**, with the exception of the external C=C [equivalent to C(1)-C(2) in **1**] distance in the phosphine-funtionalized ring of $[Rh(o\text{-}P2)_2][BF_4]$.[5b] The most extreme case of this contraction is $NiBr_2$(*o*-P2), which has a C(50)-C(51) distance of 1.25(1) Å.[4] The angles within the methyl-substituted ring remain essentially unchanged between the free and coordinated ligand. The C-C-S and S-C-S angles within the phosphine-functionalized ring are slightly tighter in the coordinated ligand than in **1**, indicating some affect on the ring caused by the phosphorus donation.

C. Molecular Structure of $[(C_6H_5)_2P]_4TTF$ (2)

An ORTEP drawing of $[(C_6H_5)_2P]_4TTF$ **(2)** is represented in Figure 49, and a packing diagram is in Figure 50. Selected bond distances and angles

are provided in Table 20. Because the center of the molecule rests on a center of inversion, the two fulvalene rings are symmetry related. Bond distances and angles within the ring are similar to those reported in previous TTF structures. The C-S distances range from 1.744(7) Å for S(2)-C(3) to 1.782(7) Å for S(1)-C(1). These are slightly elongated relative to free TTF (1.729(2) - 1.756(2) Å),[10] and **36** (1.743(4) - 1.767(3) Å), but within errors for the phosphine-substituted ring of **1** (1.70(3) - 1.77(2) Å). The external and internal C=C distances are indistinguishable at 1.358(9) Å for C(1)=C(2), and 1.362(13) Å for C(3)=C(4). The geometry about the phosphorus continues to be distorted with C-P-C angles ranging from 101.5(3)° to 104.5(3)°. Unlike **1**, The fulvalene rings of **2** are nearly planar, with an out-of-plane bend of 3.65° between the dihedral planes C(1)-C(2)-S(1)-S(2) and S(1)-S(2)-C(3)-C(3)'-S(1)'-S(2)' (symmetry code (') = 2-x, 1-y, 1-z). The individual five-membered rings in question are planar with a maximum deviation of 0.007(4) for C(1), and 0.001(6) for C(3). The RMS deviation for the two planes are 0.005 and 0.000, respectively. The packing diagram in Figure 50 shows that **2** packs in slightly off-center "stacks", where only one fulvalene ring for each adjacent molecule overlaps with intermolecular S···S distances of 8.15 Such an extended distance precludes the presence of any significant interactions between molecules, as would be expected given the bulky phenyl groups.

Comparison of **2** with Pt_2Cl_4(P4) (**21**), shows differences reminiscent of what was observed for **1** and its own metal complexes. Due to the retention

Table 20. Selected bond distances (Å) and Angles (deg.) for $[(C_6H_5)_2P]_4TTF$ (**2**).

Atom 1	Atom 2		2
C(1)	C(2)		1.358(9)
C(1)	S(1)		1.782(7)
C(2)	S(2)		1.744(7)
C(3)	S(1)		1.752(6)
C(3)	S(2)		1.755(7)
C(3)	C(3)		'1.362(13)
P(1)	C(1)		1.804(7)
P(2)	C(2)		1.841(8)
P(1)	C(11)		1.842(8)
Atom 1	**Atom 2**	**Atom 3**	**2**
C(1)	S(1)	C(3)	95.5(3)
C(2)	S(2)	C(3)	95.6(3)
S(1)	C(3)	S(2)	114.8(4)
S(1)	C(3)	C(3)	'122.7(7)
P(1)	C(1)	C(2)	122.3(6)
P(2)	C(2)	C(1)	122.2(5)
C(1)	P(1)	C(11)	101.8(3)
P(1)	C(11)	C(12)	121.6(6)

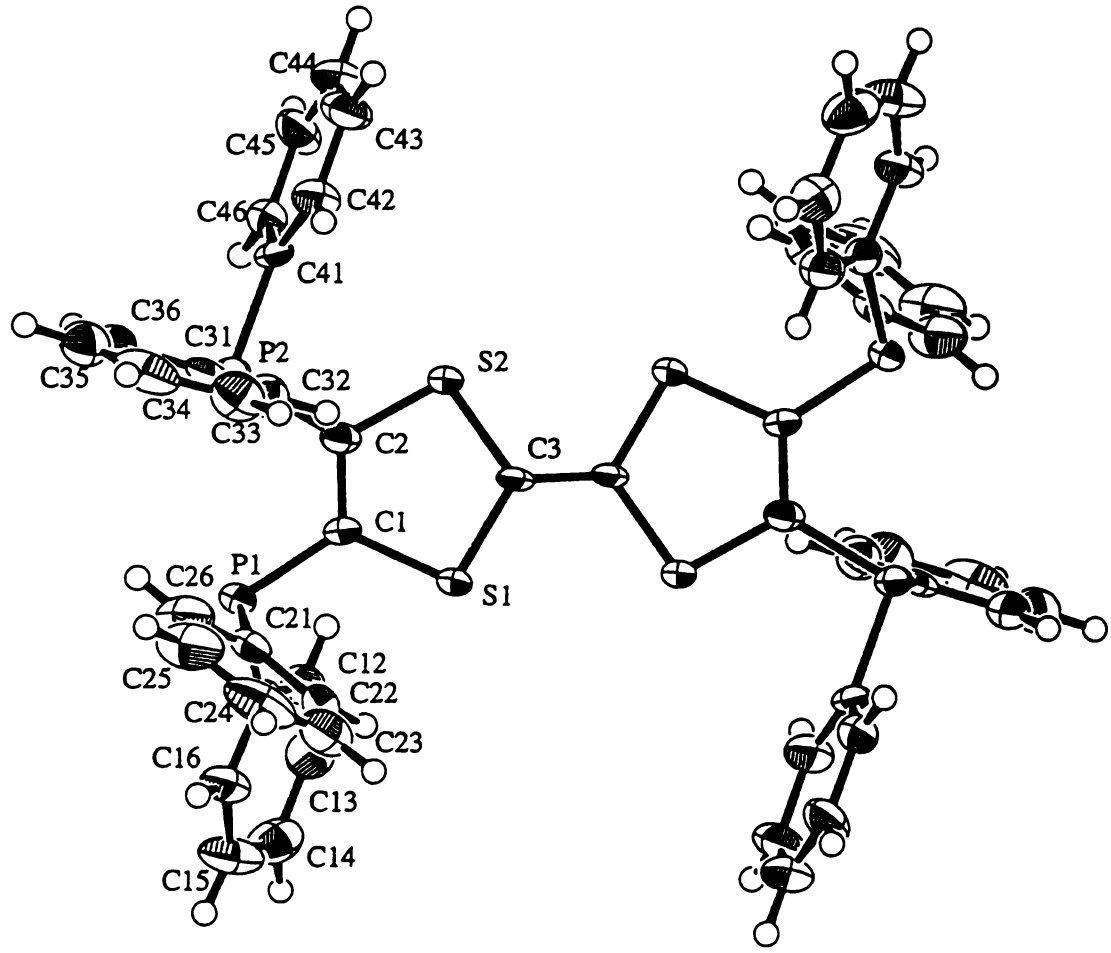

Figure 49. ORTEP representation of $[(C_6H_5)_2P]_4TTF$ (2) with 50% ellipsoids.

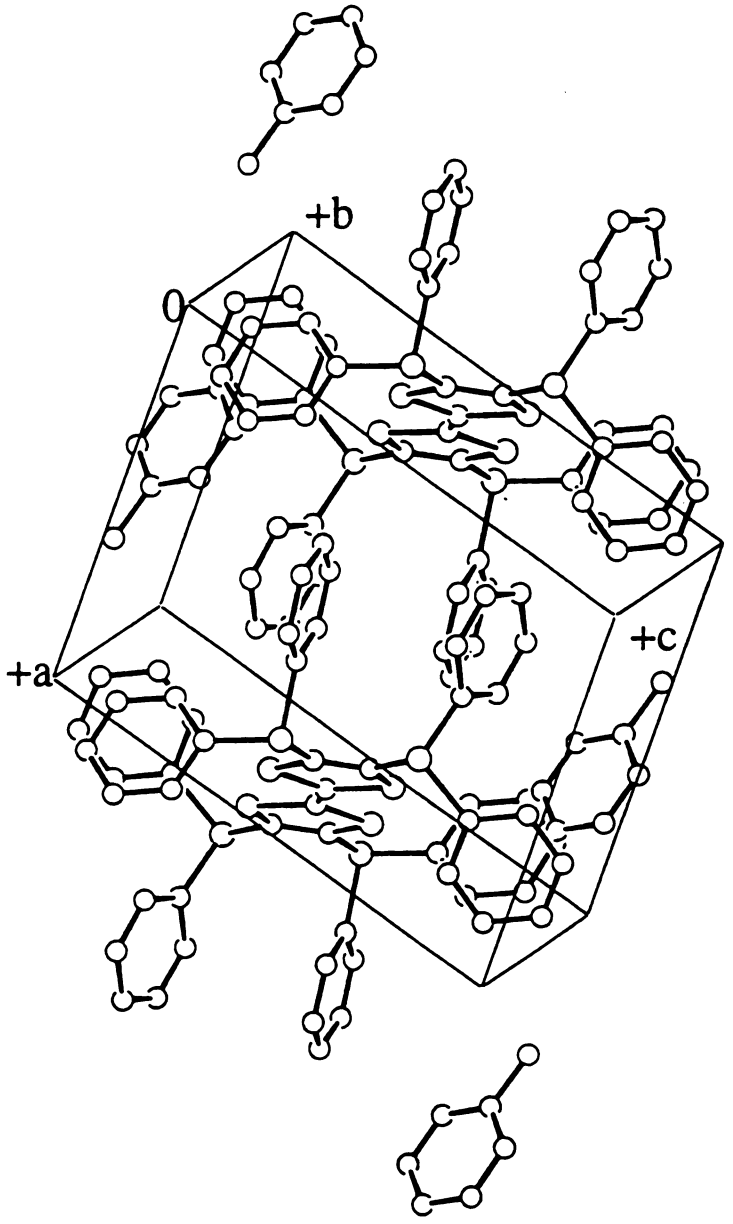

Figure 50. Packing diagram of $[(C_6H_5)_2P]_4TTF$ (**2**).

of symmetry from **1** to **21**, the fulvalene rings are equivalent, with C=C distances slightly elongated in the case of the free ligand. The P-C distances are longer in the free ligand, as expected, with no difference in the C-S-C angles. The C-C-S angles tighten by 1° upon coordination of the phosphine, indicating that while there may be some effect from the phosphorus donation, it does not seem as great as in the case of **1**.

3. Concluding Remarks

The series $(CH_3)_x[(C_6H_5)_2P]_{4-x}TTF$ represents a unique series of ligands capable of coordinating directly to metals centers to yield a variety of structural types. Single crystal X-ray studies of the free ligands and their methyl-substituted precursors indicate that the additional R groups have a pronounced effect on the orientation of the molecules within the crystal lattice. These steric effects also dictate elongated intermolecular S···S distances, which indicate that they will most likely not exhibit the typical conducting properties exhibited by most other TTF-based molecules. In the case of *o*-P2 (**2**), the steric effects of the phenyl groups appear to cause an out-of-plane bend in the methyl-substituted fulvalene ring not previously observed in this series of compounds. Comparisons between the free and bound ligands reveal small changes in the structure of the TTF core, possibly caused by the donation of the phosphorus atom to the metal center.

List of References

1. Ferraris, J.; Cowan, D. O.; Walatka, V.; Perlstein, J.H., *J. Am. Chem. Soc.*, **1973**, *95*, 948.

2. (a) Melby, L.R.; Harder, R.J.; Hertler, W.R.; Mahler, W.; Bensen, R.E.; Mochel, E.E., *J. Am. Chem. Soc.*, **1962**, *84*, 3374. (b) Kistenmacher, T.; Phillips, T. E.; Cowan, D.O., *Acta Cryst. C.*, **1974**, *B30*, 763.

3. Ellern, A.; Bernstein, J.; Becker, J.Y.; Zamir, S.; Shahal, L., *Chem. Mater.*, **1994**, *6*, 1378.

4. Fourmigué, M.; Batail, P., *Bull. Soc. Chim. Fr.*, **1992**, *129*, 29.

5. (a) Uzelmeier, C. E.; Fourmigué, M.; Grandinetti, G.; Dunbar, K. R., **1997** In preparation. (b) Fourmigué, M.; Uzelmeier, C. E.; Boubekeur, K.; Bartley, S. L.; Dunbar, K. R., *J. Organomet. Chem.*, **1997**, *529*, 343.

6. Lerstrup, K.; Johannsen, I. & Jørgensen, M. *Synth. Met.*, **1988**, *27*, B9.

7. Gilmore. C. J. MITHRIL. Computer Program for the Automatic Solution of Crystal Structures from X-ray Data. Department of Chemistry, University of Glaskow, Scotland., **1983**.

8. Sheldrick, G. M. SHELXL93. Program for the Refinement of Crystal Structures., **1993**, University of Gottingen, Germany.

9. North, A. C. T.; Phillips, D. C.; Mathews, F. S. *Acta Cryst.*, **1968**, *A24*, 351.

10. Cooper, L. B.; Kenney, N. C.; Edmonds, J. W.; Nagel, A.; Wudl, F.; Coppens, P., *J. Chem. Soc. Chem. Commun.*, **1971**, 889.

11. Bondi, A., *J. Phys. Chem.*, **1964**, *68*, 441.

12. Uzelmeier, C.E.; Fourmigué, M.; Dunbar, K.R., *Acta Cryst. C.*, **1998**,*C54*, in press.

APPENDIX C

SYNTHESIS OF $[Bu_4N]_2[Re_2Cl_8]$ FROM RHENIUM-CONTAINING LABORATORY RESIDUES.

APPENDIX C

SYNTHESIS OF $[Bu_4N]_2[Re_2Cl_8]$ FROM RHENIUM-CONTAINING LABORATORY RESIDUES.

1. Introduction

The precious metal content compounds used in our laboratories has sufficient value to make recovery an attractive prospect. Even though recovery, recycling, and reuse of laboratory chemicals may not be an economical option in many laboratories, hazardous waste regulations and economic incentives make it an option that should be continually assessed. In particular, the expense of many metals make this a useful process for use by inorganic chemists. Currently there are established methods for the recovery of silver and mercury from laboratory residues.[1] The metal values in spent catalysts or solutions that contain such noble metals as platinum, palladium, rhodium, and ruthenium are almost always worth recovering. While the recovery procedures for small quantities of platinum, palladium, and rhodium are reported in the literature, the chemistry of these metals is sufficiently distinct that no general procedure is applicable.[2]

Due to the extent of research being carried out with rhenium compounds in our laboratories, and our accumulation of a large quantity of rhenium-containing residues, it became useful to investigate a method for reclaiming rhenium in a form that could be used to prepare a common

starting material for dinuclear rhenium chemistry, namely $[Re_2Cl_8]^{2-}$. Currently, the only reported method for recovering rhenium residues involves the work-up of nitron hydrogen perrhenate precipitates and various solutions of rhenium-sulfur complexes which can be recovered as $K[ReO_4]$ and $[NH_4][ReO_4]$.[3] Described in this section is a new method for the recovery of rhenium residues, which ultimately results in the formation of $[(n\text{-}Bu)_4N]_2[Re_2Cl_8]$.

2. Experimental

A. Synthesis

All reactions were carried out in air unless otherwise stated. KCl was purchased from Columbus Chemical Industries, reagent grade nitric acid was purchased from Olin Corporation at 69% purity, and [TBA][Br] was purchased from Strem Chemicals. All starting materials were used as received. All rhenium-containing residues were kept isolated from all other metal waste, and was stored in clean, empty reagent bottles until time of use.

(1) Preparation of $KreO_4$ from Rhenium-Containing Residue.

Rhenium residues were combined into a 1 L round bottomed flask, such that the volume never exceeded 750 mL, and subsequently reduced in volume by roto-evaporation with heating at 60°C. This process was continued until the liquid volume had been sufficiently minimized. The remaining residue was washed into a 500 mL glass crystallizing dish using low boiling solvents such as acetone and hexanes to complete the transfer.

Once filled to half capacity, the dish was heated on a hot plate to boil off additional solvents and volatiles, which resulted in the formation of a sticky black residue. This process was repeated several times until all the residues were contained in the crystallizing dish. The dish was left to stand several days in a vacuum hood to further dry the residues, which left a crusted black solid on top, with some sticky residues beneath. This residue was scraped from the dish and transferred to a new container.

An amount of concentrated HNO_3 (~150-200 mL) was added to an empty 400-500 mL beaker, which was secured in an oil bath over a hot plate. Approximately 20 g of dried rhenium residues were carefully added to the acid. Upon introduction of the metal-containing solid, the acid began to bubble vigorously. The mixture was stirred occasionally with a spatula. When the bubbling appeared to subside, the mixture was heated to a temperature near 90°C. After 1-2 h, the hot liquid was separated from the undissolved black solid by filtration through a large fritted glass funnel. Care should be taken during the reaction of the residues with acid, and during the filtration of the hot mixture, as noxious NO_x fumes are produced. This liquid was returned to the oil bath, and 10-20 mL of a saturated aqueous solution of KCl was added to the acid.† The mixture was heated for an additional hour, with occasional stirring, and the hot liquid was carefully decanted into a new flask, using a minimum of hot water to complete the transfer. The solution was allowed to cool to room temperature, affording a

tan precipitate. This solid was isolated by decanting the liquid back into the previous flask, using cold water to wash the solid. The flask containing the liquid was returned to the oil bath, re-heated to ~90°C to reduce the volume, and additional black rhenium-residues were added to the solution. It may also be necessary to add additional HNO_3 (~75 mL total over the course of these procedures). The procedures were then carried out from the point following the addition of KCl (†). This was repeated numerous times until no additional black residues could be dissolved by the acid, or if no additional tan precipitate was formed upon cooling. In either case the liquid was transferred back to the crystallizing dish, heated to a black solid, and combined with the previously collected rhenium residue.

The tan solid that was collected was washed with acetone over a Buchner funnel, dried, transferred into a new flask, treated with deionized water, and finally heated to near boiling in an oil bath. A minimal amount of additional water was added with stirring to dissolve the solid. The hot solution was filtered through a Buchner funnel, and allowed to cool to room temperature, after which time an off-white crystalline solid was observed to form. The solid was isolated by filtration, and the recrystallization procedures were repeated 3 additional times, until the product appeared to be fairly pure by infrared spectroscopy. The final white microcrystalline solid was dried under reduced pressure. Recovery rate = ~ 2.0 - 3.0 g per hour. Total recovered quantity: ~13.0 g (with not all reactants being exhausted).

I.R. (Nujol, cm^{-1}): 914 ($\nu_{Re-O,}$ $[ReO_4]^-$), 316 , 304 ($[ReO_4]^-$); (Impurities): 1261, 1050, 723, 522, 482, 363.

(2) Metathesis of $KReO_4$ to form $[(n\text{-}Bu)_4N]_2ReO_4$

A sample of the impure $K[ReO_4]$ (10.00 g) was loaded into a 600 mL beaker and treated with 300 mL of millipore water.[4] The mixture was heated, with stirring, in order to fully dissolve the solid. To this hot solution was added an aqueous solution of [TBA][Br] (13.481 g, 0.042 mol; 100 mL), which led to the formation of a white precipitate. The mixture was cooled in an ice bath, and then filtered to collect the solid. The solid was washed with cold water, then a 2:1 Et_2O:EtOH solution followed by Et_2O, and finally dried under reduced pressure. Crude yield = 7.853 g. I.R. (Nujol, cm^{-1}): 904 (ν_{Re-O}), 801, 324 ($[ReO_4]^-$); (Impurities): 1055, 521, 480.

(3) Synthesis of $[(n\text{-}Bu)_4N]_2[Re_2Cl_8]$

The procedures for the preparation of $[(n\text{-}Bu)_4N]_2[Re_2Cl_8]$ were followed according to the method of Barder and Walton.[5] The synthesis was carried out using 3.028 g (9.310 mmol) of the $[Bu_4N][ReO_4]$ produced from the above procedures. Upon rotoevaporation of the final solution, a brownish-yellow residue was present along with the expected blue-green solid. This impurity was removed from the desired product by washing the product with EtOH and Et_2O. The final product was recrystallized from 300 mL of a 20:1 mixture of MeOH and HCl, collected by filtration, washed with Et_2O, and dried *in vacuo*. Yield = 1.657 g (47%).

3. Results and Discussion

A. Preparation and Characterization of $[(n\text{-Bu})_4N]_2[Re_2Cl_8]$ from Rhenium-Residues.

Rhenium-containing waste from our laboratories are typically combined and stored in various containers awithout contamination with other metal-containing wastes. Volatile organic solvents can be removed by rotoevaporation with mild heating. The application of further heat assists in the elimination of higher boiling volitiles, such as acids, and eventually yields a black solid. Reaction of this black solid in concentrated HNO_3 with aqueous KCl gives a tan solid upon cooling. This tan solid can be recrystallized from water to yield a crystalline solid identified as $K[ReO_4]$ contaminated with remaining miscellaneous impurities. The infrared spectrum of the solid (Fig. 51) reveals a strong band at 914 cm^{-1} which is due to the $\nu_{Re\text{-}O}$ stretch of $[ReO_4]^-$. The presence of additional bands in the spectrum indicate the presence of a mixture. In particular, the band at 363 cm^{-1} indicates the presence of a product which may contain Re-Cl groups. Reactions of rhenium compounds with HNO_3, H_2SO_4 and bromine water are known to result in the formation of "perrhenic" acids by oxidation of the metal to it's lowest oxidation state, namely Re^{VII} (d^0). The addition of KCl serves to introduce potassium as a cation, thus making the perrhenate anion insoluble and therefore easily extracted from water or acetone. This solubility

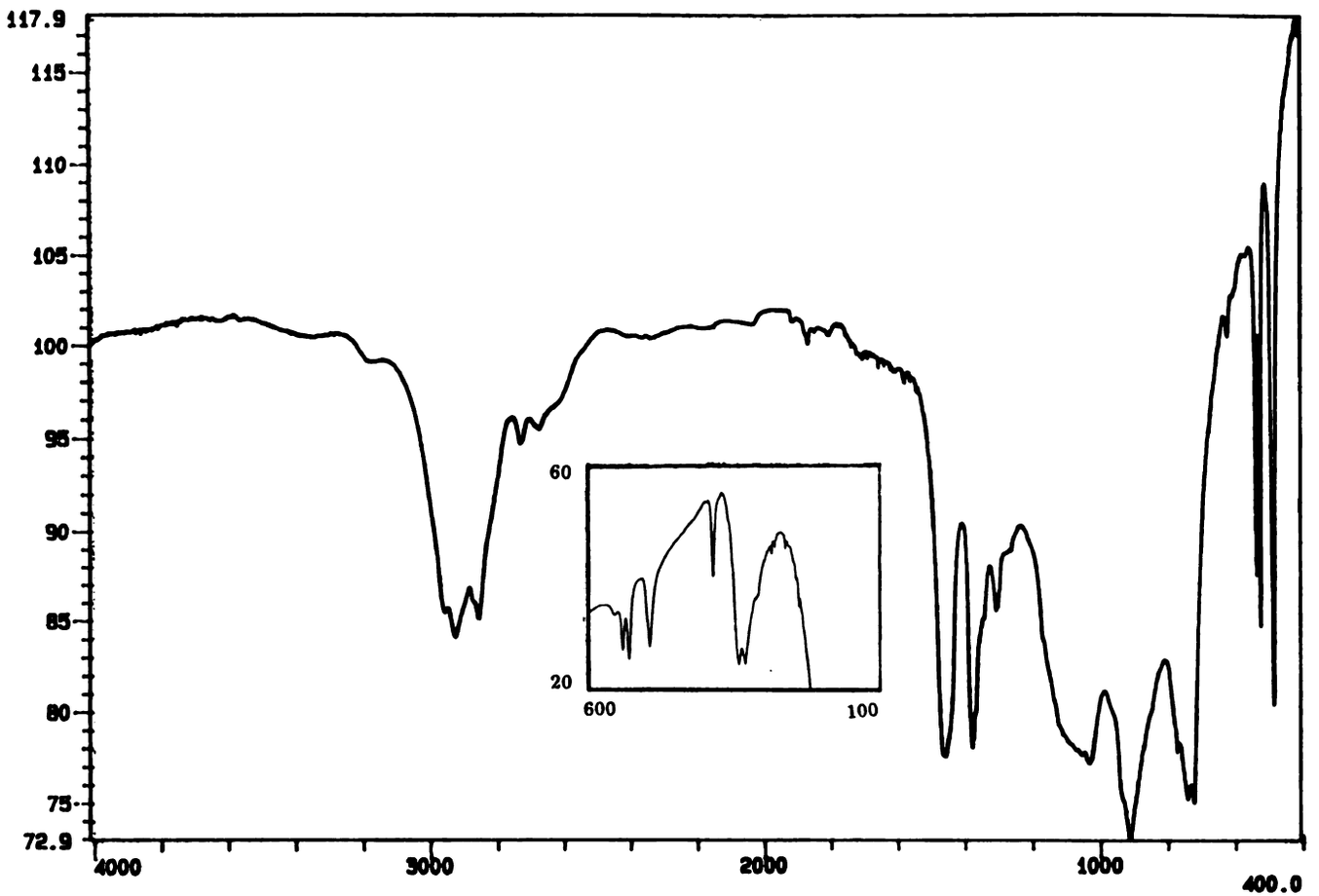

Figure 51. Infrared spectrum of impure K[ReO_4] obtained from the recovery of rhenium-containing residue. The far-infared region is shown in the inset.

differe

are mo

precipi

separa

52) re

feature

480 cm

have b

cm^{-1}, w

prepara

Walton

reporte

yellow-b

reaction

lead to b

4. Conc

laborato

the field

difference can be used to eliminate any polar impurities; those that remain are most likely neutral rhenium containing compounds such as Re_2O_7.

Metathesis of $KreO_4$ with aqueous $(n\text{-}Bu)_4NBr$ which leads to the precipitation of $[(n\text{-}Bu)_4N]ReO_4$ and serves as an additional step in the separation of impurities. An IR spectrum of the $[(n\text{-}Bu)_4N]ReO_4$ product (Fig. 52) reveals a much cleaner sample than the $K[ReO_4]$. Loss of the broad feature at 723 cm^{-1}, and a decrease in the intensity of the bands at 521 and 480 cm^{-1} (relative to $[ReO_4]^-$), provide evidence that some of the impurities have been removed. This is further demonstrated in the region below 400 cm^{-1}, where only the band associated with the ν_{as} of $[ReO_4]^-$ can be observed.

The use of the $[TBA][ReO_4]$ obtained from the rhenium waste in the preparation of $[(n\text{-}Bu)_4N]_2[Re_2Cl_8]$ by procedures published by Barder and Walton[5] results in a high-purity product, but in much lower yields than those reported in the literature. The greatest visible difference is the presence of a yellow-brown residue following concentration of the benzoyl chloride/ethanol reaction solution. This may be a result of Re-O containing impurities that lead to by-products.

4. Concluding Remarks

The preparation of salts containing $[Re_2Cl_8]^{2-}$ from rhenium-containing laboratory residue is a cost-effective process for research groups working in the field of. dirhenium metal-metal bonds. Aldrich lists $K[ReO_4]$ at

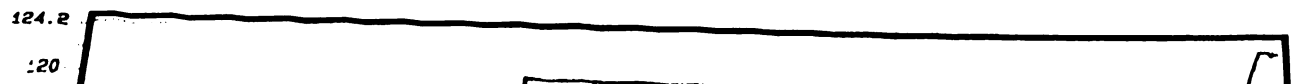
124.2
120

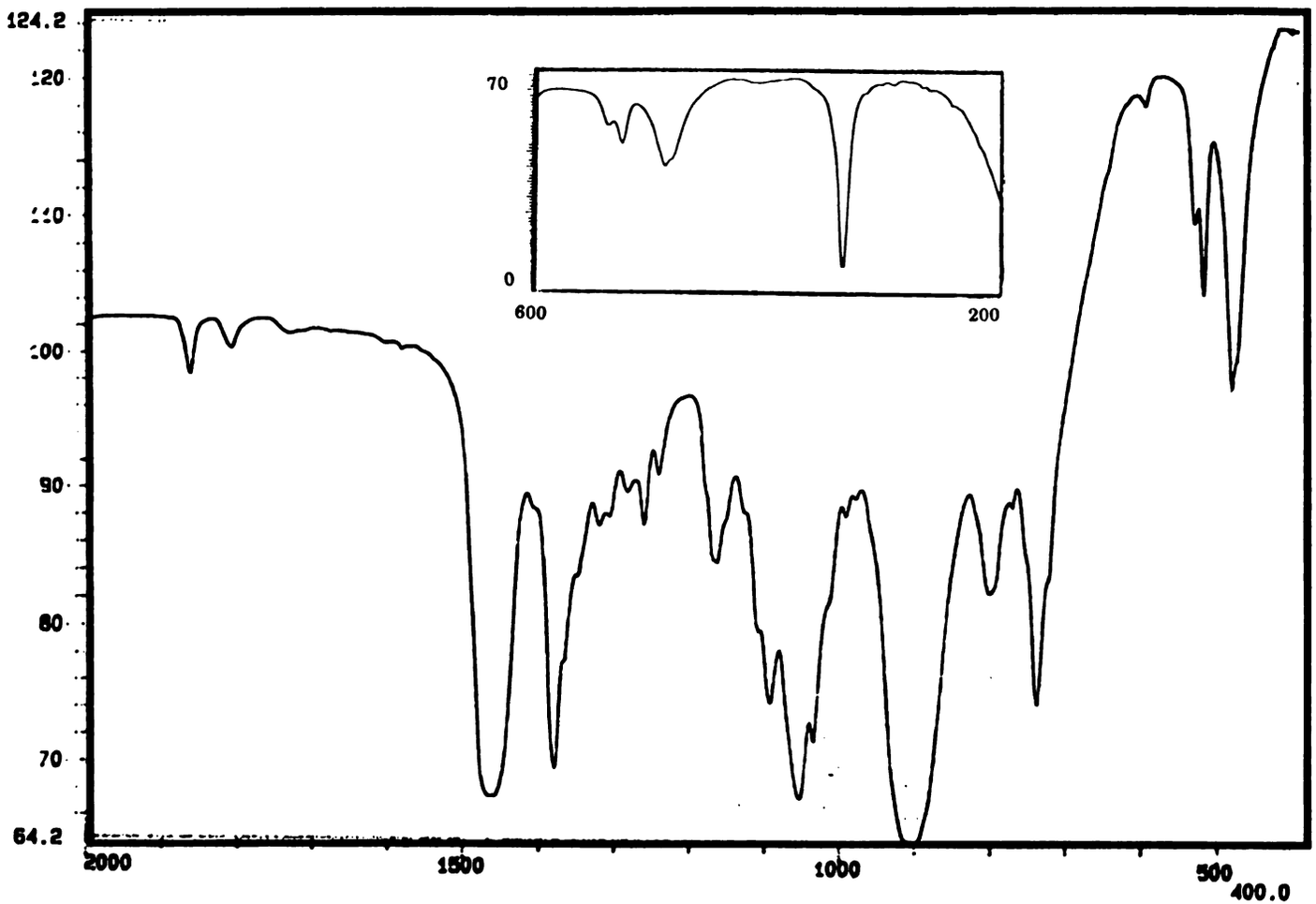

Figure 52. Infrared spectrum of impure [(n-Bu)$_4$N]ReO$_4$ obtained from the recovery of rhenium-containing residue. The far-infared region is shown in the inset.

approximately \$4.78/g for a 25g sample (the least expensive quantity available).[6] For the procedure outlined above the materials costs are as follows: \$4.70/500 g for KCl and \$9.00/7 lb for HNO_3. Given the approximate quantities of each material used, the final price is \$0.09/10 g of KCl and \$0.77/2.75 mL of HNO_3, or a total cost of \$0.86. Given the low yield of both the metathesis and $[Re_2Cl_8]^{2-}$ synthesis, it can be estimated that less than 25% of the "$K[ReO_4]$" was pure. Considering the cost of $K[ReO_4]$, as listed by Aldrich, it would cost ~\$15.54 to purchase 3.25 g of $K[ReO_4]$ whereas it cost \$0.86 to produce roughly the same amount using the described method

List of References

1. *Prudent Practices for Disposal of Chemicals from Laboratories*, 6th ed., National Academy Press, Washington, D.C., **1983**, 44.

2. *Handbook of Preparative Inorganic Chemistry, 2th ed.*, Brauer, G., Ed., Academic Press, New York, **1965**, 1560.

3. *Handbook of Preparative Inorganic Chemistry, 2th ed.*, Brauer, G., Ed., Academic Press, New York, **1965**, 1476.

4. Millipore water was obtained from the Biochemistry Department at Michigan State University.

5. Barder, T. J.; Walton, R. A., *Inorg. Synth.*, **19??**, *28*, 332.

6. *1996-1997 Aldrich Catalog*, Aldrich Chemical Company, Milwaukee, W.I., 1192.

APPENDIX D

$^{31}P\{^{1}H\}$ NMR ANALYSIS FOR PtCl(TMPP)(TMPP-*O*)

APPENDIX D

$^{31}P\{^{1}H\}$ NMR ANALYSIS FOR PtCl(TMPP(TMPP-*O*)

1. Introduction

Earlier work from our laboratories had shown that homoleptic TMPP compounds of Rh^{I}, Rh^{II} and Rh^{III} exhibit interesting redox chemistry and that they undergo reversible small molecule reactions based on the ability of the ether groups to dissociate.[1] Given these promising results, it was logical to extend these studies to Pd(II) and Pt(II)[2] which are known to be useful in catalytic applications when weakly bonded ligands are involved.[3j,k,4-6] In addition, polydentate ligands such as TMPP with steric requirements that favor octahedral coordination may enforce this geometry on metals for which six coordination is rarely observed.[7,8] In spite of the considerable interest, a fairly limited number of such compounds have been studied.[3]

^{31}P NMR spectroscopy has been used extensively as an important spectroscopic tool for the characterization of phosphine complexes due to the ^{31}P nucleus bearing a spin of 1/2 and being 100% abundant.[9] Although the specific theory pertaining to the chemical shift values for organometallic phosphine complexes is not well understood, ^{31}P NMR data are extremely useful for establishing spectroscopic "fingerprints" and trends which can be used for distinguishing related compounds. Coupling constants are particularly useful, owing to the fact that the $^{2}J(^{31}P, ^{31}P)$ for *trans* phosphines

are mu

metal

pattern

the geo

2. Exp

A. Syn

accordi

carried

softwar

3. Res

A. ^{31}P{

(TM

room te

are ind

33% ab

first si

satellit

These

intensi

= -26.3

are much larger than those for *cis* phosphines.[9c] The addition of a transition metal with I = 1/2, such as ^{195}Pt or ^{106}Rh introduces additional splitting patterns due to strong coupling with ^{31}P, which provides more information on the geometry of the complex.

2. Experimental

A. Synthesis and Physical Methods.

The preparation of PtCl(TMPP)(TMPP-*O*) (**37**) was carried out according to the literature procedure.[2] Spin-simulation experiments were carried out by using the LAME program which is included in the VNMR software package.

3. Results and Discussion

A. $^{31}P\{^{1}H\}$ NMR Simulation and Interpretation for PtCl(TMPP)-(TMPP-*O*) (37).

A $^{31}P\{^{1}H\}$ NMR spectrum of PtCl(TMPP)(TMPP-*O*) in acetonitrile-d_3 at room temperature exhibits an ABX second-order pattern with satellites that are indicative of two inequivalent phosphorus atoms coupled to ^{195}Pt (I = 1/2, 33% abundance).[10-11] Successful simulation of this spectrum was obtained by first simulating the ABX splitting pattern, thereby producing the expected satellite positions, followed by simulation of the AB P_A-P_B splitting pattern. These two spectra were overlayed with the approximate parent-to-satellite intensity ratio, which led to chemical shift values of P_A, δ = -20.48 ppm , P_B, δ = -26.39 ppm and coupling constants of $^{1}J(Pt\text{-}P_A)$ = 3212 Hz, $^{1}J(Pt\text{-}P_B)$ = 2993

Hz and $^2J(P_A\text{-}P_B)$ = 561 Hz (Figure 53); the large magnitude of $^2J(P_A\text{-}P_B)$ is common for *trans* phosphine ligands. These NMR data are in accord with the molecular geometry depicted in Figure 54 wherein one neutral TMPP ligand is coordinated in an η^1 fashion and a demethylated TMPP group is bound as an η^2- P,O ligand with *trans* P atoms, a phenoxide O and a Cl- ion in a square plane. These data are supported by the observed ^1H NMR spectrum.[2]

4. Concluding Remarks

Our identification of **37** as containing both an η^1-TMPP and a η^2-TMPP-*O* ligand indicates that, unlike most other P,O chelates reported in the literature, the TMPP ligand appears to be sufficiently flexible to adopt a myriad of bonding modes. This point is well-demonstrated by the observed hapticity changes of TMPP from monodentate in **37** to bidentate in Pd(TMPP-*O*)$_2$ (**7**), Pt(TMPP-*O*)$_2$,[2] and [Rh(TMPP)$_2$][BF$_4$] (**3**) to tridentate in [Pd(TMPP)$_2$][BF$_4$]$_2$,[2b] [Rh(TMPP)$_2$][BF$_4$]$_2$,[1b] and [Rh(TMPP)$_2$][BF$_4$]$_3$,[1a,b] and even μ^2-η^3 in [Co$_3$(μ^2-OH)$_3$(μ^3-OH){Co(TMPP-*O*)$_2$}$_3$][BF$_4$], (**8**).[12] The ability of TMPP to change hapticity in order to stabilize a given complex allows for reversibility of substitution reactions, which is generally not possible with complexes that undergo dissociative loss of a ligand such as phosphine. This attribute has been proven to be useful in the reversible reactions of [Rh(η^3-TMPP)$_2$]$^{2+}$ with small molecules such as CO and isocyanides.[2]

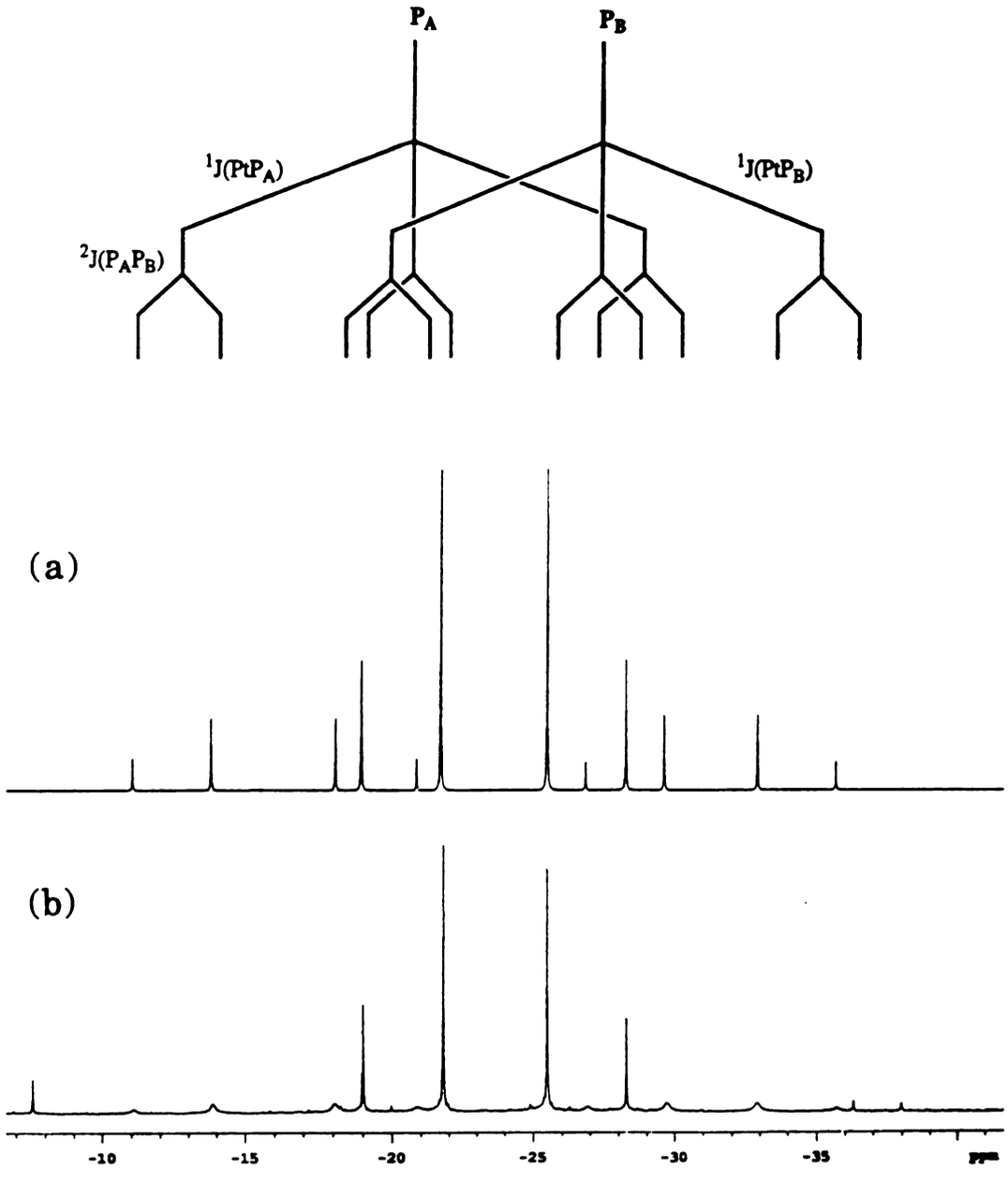

Figure 53. Calculated (a) and experimental (b) room temperature $^{31}P\{^1H\}$ NMR spectra of PtCl(TMPP)(TMPP-*O*) (**37**) in acetonitrile-d_3. The 1:3 satellite:parent intensity ratio resulting from the 33% abundance of ^{195}Pt is not drawn to scale in spectrum (a).

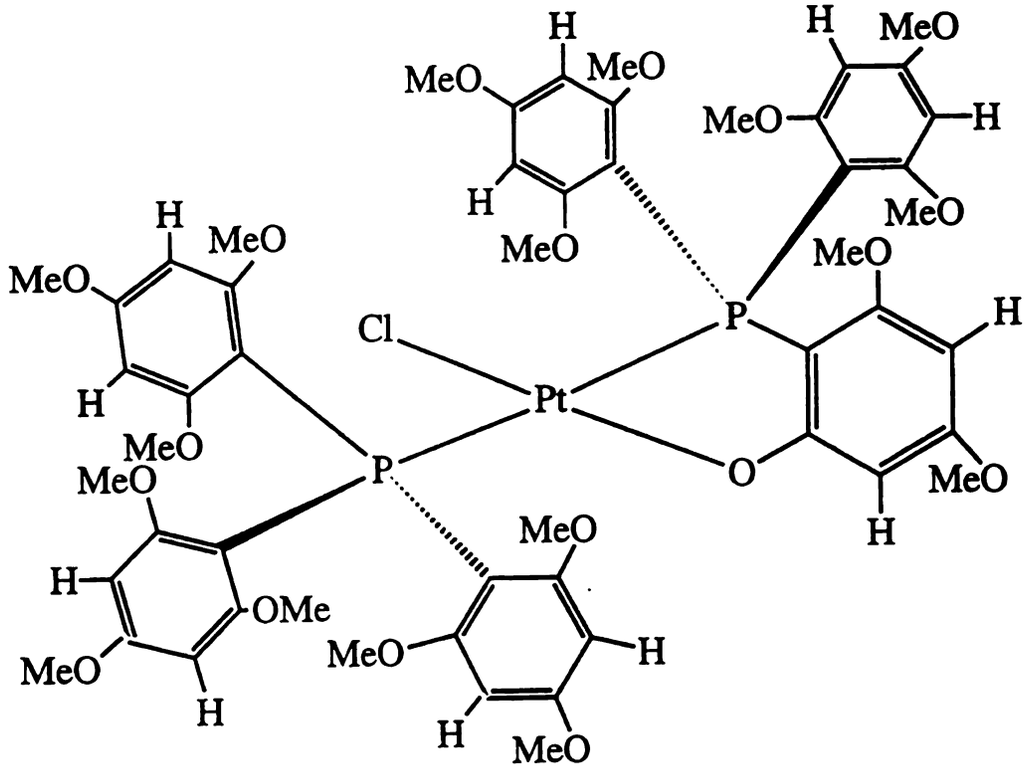

Figure 54. Illustration of PtCl(TMPP(TMPP-O) (**37**).

List of References

(1). (a) Dunbar, K. R.; Haefner, S. C.; Pence, L. E. *J. Am. Chem. Soc.* **1989**, *111*, 5504. (b) Dunbar, K. R.; Haefner, S. C.; Bender, C. *J. Am. Chem. Soc.* **1991**, *113*, 9540. (c) Dunbar, K. R.; Haefner, S. C.; Swepston, P. N. *J. Chem. Soc., Chem. Commun.* **1991**, 460. (d) Dunbar, K. R.; Haefner, S. C. *Organometallics* **1992**, *11*, 1431. (e) Haefner, S. C.; Uzelmeier, C. E.; Dunbar, K. R., manuscript in preparation.

(2). (a) Sun, J-S.; Uzelmeier, C.E.; Ward, D.L.; Dunbar, K.R., *Poyhedron*, **1998**, in press. (b) Dunbar, K. R.; Sun, J.-S. *J. Chem. Soc. Chem. Comm.*, **1994**, *2387*.

(3). (a) Anderson, G. K.; Kumar, R. *Inorg. Chem.* **1984**, *23*, 4064. (b) Braunstein, P.; Matt, D.; Dusausay, Y. *Inorg. Chem.* **1983**, *22*, 2043. (c) Podlahová, J.; Kratochvil, B.; Langer, V. *Inorg. Chem.* **1981**, *20*, 2160. (d) Empsall, H. D.; Johnson, S.; Shaw, B. L. *J. Chem. Soc., Dalton Trans.* **1980**, 302. (e) O'Flynn, K. H. P.; Mc Donald, W. S. *Acta Cryst.* **1977**, *B33*, 194. (f) Anderson, G. K.; Corey, E. R.; Kumar, R. *Inorg. Chem.*, **1987**, *26*, 97. (g) Alcock, N. W.; Platt, A. W. G.; Pringle, P. G. *J. Chem. Soc. Dalton Trans.*, **1989**, 2069. (h) Reddy, V. V. S.; Whitten, J. E.; Redmill, K. A.; Varshney, A.; Gray, G. M. *J. Organomet. Chem.*, **1989**, *372*, 207. (i) Braunstein, P.; Matt, D.; Dusausoy, Y.; Fischer, J.; Mitschler, A.; Ricard, L. *J. Am. Chem. Soc.*, **1981**, *103*, 5115. (j) Lindner, E.; Schrieber, R.; Kemmler, M.; Schneller, T.; Mayer, H. A. *Chem. Matter.* **1995**, *7*, 1951. (k) Lindner, E.; Schrieber, R.; Schneller, T.; Wegner, P.; Mayer, H. A. *Inorg. Chem.* **1996**, *35*, 514.

(4). (a) Peuckert, M.; Keim, W. *Organometalics* **1983**, *2*, 594.(b) Huang, Q.; Xu, M.; Qian, Y.; Xu, W.; Shao, M.; Tang, Y. *J. Organomet. Chem.* **1985**, *287*, 419. (c) Keim, W.; Behr, A.; Hoffmann, B.; Kowaldt, F. H.; Kürschner, U.; Limbäcker, B.; Sistig, F. *Organometalics* **1986**, *5*, 2356. (d) Klabunde, U.; Ittel, S. D. *J. Molec. Catal.* **1987**, *41*, 123.

(5). (a) Schrock, R. R.; Osborn, J. A. *J. Am. Chem. Soc.* **1976**, *98*, 2134. (b) Davies, J. A.; Hartley, F. R.; Murray, S. G. *Inorg. Chem.* **1980**, *19*, 2299. (c) Sen, A.; Lai, T. W. *Organometalics* **1982**, **1**, 415.

(6). Boeré, R. T.; Montgomery, C. D.; Payne, N. C.; Willis, C. J. *Inorg. Chem.* **1985**, *24*, 3680.

(7). (a) Blake, A. J.; Gould, R. O.; Lavery, A. J.; Schröder, M. *Angew. Chem. Int. Ed. Engl.* **1986**, *25*, 274. (b) Wieghardt, K.; Küppers, H. -J.; Raabe,

(8).

(9)

(10).

(11).

(12).

E.; Krüger, C. *Angew. Chem. Int. Ed. Engl.* **1986**, *25*, 1101. (c) Blake, A. J.; Holder, A. J.; Hyde, T. I.; Roberts, Y. V.; Lavery, A. J.; Schröder, M. *J. Organomet. Chem.* **1987**, *323*, 261. (d) Grant, G. T.; Sanders, K. A.; Setzer, W. N.; VanDerveer, D. G. *Inorg. Chem.* **1991**, *30*, 4053. (e) de Groot, B.; Hanan, G. S.; Loeb, S. J. *Inorg. Chem.* **1991**, *30*, 4644.

(8). Blake, A. J.; Crofts, R. D.; de Groot, B.; Schröder, M. *J. Chem. Soc. Dalton Trans.* **1993**, 485.

(9) (a) Davies, J.A., *The Chemistry of the Metal-Carbon Bond*, Hartley, F.R., Ed., Wiley-Interscience: New York, **1982**, 880. (b) Pregosin, P.S.; Kunz, R.W., *NMR Basic Principles and Progress*, Springer-Verlag, Heidelberg, **1979**, 55. (c) Collman, J.P.; Hegedus, L.S.; Norton, J.R.; Finke, R.G., *Principles and Applications of Organotransition Metal Chemistry*, Univ. Science Books, Mill-Valley, **1987**, 72.

(10). (a) *Comprehensive Coordination Chemistry*; Wilkinson, G.; Gillard, R. D.; McCleverty, J. A., Eds.; Pergamon Press: Oxford, England, **1987**; vol 5; chap. 52 and references therein.

(11). (a) Jones, C. E.; Shaw, B. L.; Turtle, B. L. *J. Chem. Soc., Dalton Trans.* **1974**, 992. (b) Empsall, H. D.; Shaw, B. L.; Turtle, B. L. *J. Chem. Soc., Dalton Trans.* **1976**, 1500. (c) Empsall, H. D.; Heys, P. N.; Shaw, B. L. *J. Chem. Soc., Dalton Trans.* **1978**, 257.

(12). Quillevéré, A.; Uzelmeier, C. E.; Sun, J.-S.; Dunbar, K. R., manuscript in preparation.

APPENDIX E

COMPILATION OF $^{31}P\{^{1}H\}$ NMR SPECTRAL DATA

APPENDIX E

Table 19. COMPILATION OF $^{31}P\{^{1}H\}$ NMR SPECTRAL DATA

	Compound	Chemical[a] Shift	$J_{M\text{-}P}$ Hz	$J_{PA\text{-}PB}$ Hz
(1)	*o*-P2	-18.8 (s)	–	–
(2)	P4	-18.2 (s)	–	–
(3)	$[Rh^{I}(TMPP)2][BF4]$	17.6 (d)[b]	158	–
(4)	$Rh^{I}(TMPP)(TMPP\text{-}O)$	20.0 (dd)[b]	162	22
		10.3 (dd)[b]	162	22
(5)	$ax,ax\text{-}[Rh^{III}(\eta^3\text{-}TMPP\text{-}O)_2][BF_4]$	35.5 (dd)[b]	153	–
(6)	$[Co_3(\mu^2\text{-}OH)_3(\mu^3\text{-}OH)(\mu^2\text{-}\eta^3\text{-}TMPP\text{-}O)_6[BF_4]_2$	not measured		
(8)	$[Ni^{II}(o\text{-}P2)_2][BF_4]_2$	42.1(d)	–	–
(9)	$[Co^{II}(o\text{-}P2)_2][BF_4]_2$	not observed		
(10)	$[Pd^{II}(o\text{-}P2)_2][BF_4]_2$	43.0 (s)	–	–
(11)	$[Pt^{II}(o\text{-}P2)_2][BF_4]_2$	35.8 (d)	2355 (Pt-P)	–
(12)	$[Fe^{II}(o\text{-}P2)_2][BF_4]_2$	56.1(s)	–	–
		75.5 (s)	–	–
(13)	$[Ni^{II}(o\text{-}P2)_2][O_3SCF_3]_2$	46.6(s)	–	–
(14)	$[Rh^{II}(o\text{-}P2)_2][BF_4]_3$	paramagnetic - not observed		
(15)	Product of $[Rh_2(NCCH_3)_{10}][BF_4]_4$ + 4 P1	paramagnetic - not observed		
(16)	$[Re^{III}Cl_2(o\text{-}P)_2]^+$	not observed		

	Compound	Chemical[a] Shift	J_{M-P} Hz	J_{PA-PB} Hz
(17)	$[Re_2^{II,III}Cl_6(o\text{-}P)]^-$	paramagnetic - not observed		
(18)	$Re^{II}Cl_2(o\text{-}P)_2$		not measured	
(19)	$Mo^{IV}Cl_2(o\text{-}P2O_2)(O)(H_2O)$	40.7 (s)[c]	19.7	–
(20)	$Pt^{II}Cl_2(o\text{-}P2)$	27.2 (d)[c]	3640.4	–
(21)	$[Pt^{I\ I}(o\text{-}P2)(NCCH_3)_2][BF_4]_2$	29.0 (d)	1646.0	–
(22)	$Pt_2^{II,II}Cl_4(P4)$		not measured	
(23)	$[Pt_2^{II,II}(P4)(NCCH_3)_4][BF_4]_4$	19.5 (d)	3845.5	–
		26.3 (d)	3420.9	–
(24)	$[Pt_2^{II,II}(P4)(o\text{-}P2)_2][BF_4]_4$	32.9 (d)	2365.8	–
(25)	$Pd^{II}Cl_2(o\text{-}P2)$	48.0 (s)[d]		
(26)	$[Pd(NCCH_3)_2(o\text{-}P2)][BF_4]_2$	50.7 (s)		
(27)	$Pd_2^{II,II}Cl_4(P4)$		not measured	
(28)	$[Pd_2^{II,II}(P4)(NCCH_3)_4][BF_4]_4$	50.9 (s)		
(29)	$Ni_2^{II,II}Cl_4(P4)$		not measured	
(30)	$[Rh^{I}(P4)]_n[BF_4]_n$	51.0 (d)	134	
(31)	$[Pt^{II}(P4)]_n[BF_4]_{2n}$	36.1 (d)	2361	–
(32)	$[Pd^{II}(P4)]_n[BF_4]_{2n}$	44.2 (s)	–	–
(33)	$[Co^{II}(P4)]_n[BF_4]_{2n}$	paramagnetic - not observed		
(34)	$[Fe^{II}(P4)]_n[BF_4]_{2n}$	53.6 (s)	–	–
		73.8 (s)	–	–
(35)	$[Ni^{II}(P4)]_n[BF_4]_{2n}$	41.7 (s)	–	–

	Compound	Chemical[a] Shift	$J_{M\text{-}P}$ Hz	$J_{P_A\text{-}P_B}$ Hz
(37)	PtCl(TMPP)(TMPP-*O*)	-20.5	3212	561
		-26.4	2993	561

[a] Chemical shift reported in CD_3CN relative to 85% H_3PO_4 unless noted otherwise.
[b] Chemical shift reported in d_6-acetone.
[c] Chemical shift reported in CD_2Cl_2.
[d] Chemical shift reported in $CDCl_3$.